UNIVERSITÉ DE STRASBOURG

ÉCOLE DOCTORALE MSII (ED n°269)

INSA de Strasbourg

Laboratoire des sciences de l'ingénieur, de l'informatique et de l'imagerie (ICUBE) – UMR 7357

Département Génie Civil Énergétique (GCE)

THÈSE présentée par :

Chong WANG

soutenue le : **13 Avril 2023**

pour obtenir le grade de : **Docteur de l'université de Strasbourg**

Discipline/ Spécialité : **Génie Civil**

Étude des propriétés de prise et du comportement mécanique des granulats de béton recyclé

THÈSE dirigée par :

M. CHAZALLON Cyrille	Professeur, INSA de Strasbourg
M. HORNYCH Pierre	IDTPE (HDR), Université Gustave Eiffel

RAPPORTEURS :

Mme. HATTAB Mahdia	Professeur, Université de Lorraine
M. CUI YuJun	Professeur, École des Ponts ParisTech

AUTRE MEMBRE DU JURY :

M. TORRENTI Jean-Michel	Professeur, École des Ponts ParisTech, Université Gustave Eiffel
Mme. BRAYMAND Sandrine	Maître de conférences, Université de Strasbourg

UNIVERSITY OF STRASBOURG

Investigation of the self-cementing properties and mechanical behaviour of recycled concrete aggregates

by

Chong WANG

A thesis submitted in partial fulfillment for

the degree of Doctor of Philosophy

in the

Doctoral School of MSII

April 2023

Acknowledgments

The work presented in this dissertation collected the research which is the result of my PhD at the National Institute of Applied Science of Strasbourg (INSA-Strasbourg) and the Laboratory ICube in the University of Strasbourg, France. This research was supported by the China Scholarship Council (CSC). I would like to take this opportunity to address my thanks to all persons who give me support to the accomplishment of this dissertation.

Here, I would like to address my deepest gratitude to my PhD supervisor, Prof. Cyrille CHAZALLON, for his guidance, assistance, encouragement and patience during my PhD studies. He encouraged me to be an independent thinker. It is my great honor to have such a responsible and outstanding supervisor. I also wish to acknowledge my co-supervisor Prof. Pierre HORNYCH, for his invaluable insights and guidance. He has taught me how to become a good writer. I am also grateful to Assoc Prof. Sandrine BRAYMAND and Assoc Prof. Peng JING. Thanks for their excellent guidance and constructive suggestions to help me finish the experimental tests.

I would like to thank my colleagues in the team of Civil Engineering and Energy at INSA Strasbourg, Assoc Prof. Saida MOUHOUBI, Assoc Prof. Juan Carlos QUEZADA, Assoc Prof. Georg KOVAL and Assoc Prof. Hossein NOWAMOOZ. Special thanks to the following PhD students, Fu Jiao TANG, Laura GAILLARD, Anicet DANSOU, Léo COULON, Lei MA, Xin NI, Jiang JIN, Qinglin DENG, Xiang ZHANG, Haitao GE, Ke ZHANG, Yuzhou SHUN, Oussama HAMMOUD, Marieh FATAHIZADEH, Renzhi WANG, Qianwen TAN and Victor DESLOGES, for all the great moments we have spent.

Finally, and most importantly, I wish to thank my parents and my sister, for their endless loves encouragements and supports. Especially I would like to thank my wife, for her support and understanding that made me complete my PhD research.

Contents

General introduction 1

Chapter I. Literature review 4

I.1 Unbound granular materials in pavement 4

I.1.1 Flexible pavement structure 4

I.1.2 Stress in unbound granular material layer 5

I.1.3 Deformation in unbound granular material layer 5

I.2 Repeated load triaxial test 7

I.2.1 Permanent deformation behavior of UGM 8

I.2.2 Resilient deformation behavior of UGM 15

I.3 Recycled concrete aggregates in unbound pavement 24

I.3.1 Physical properties of RCA 24

I.3.2 Mechanical behaviour of RCA 29

I.4 Self-cementing properties of RCA 30

I.4.1 The influence of self-cementing properties 30

I.4.2 Unhydrated cement content 33

I.5 Conclusion 38

Chapter II. Material study and laboratory testing 39

II.1 Materials and physical properties 39

II.2 Water absorption kinetics 44

II.3 Self-cementing properties 47

II.3.1 pH value measurement and calorimeter test 47

II.3.2 Thermogravimetric analysis 48

II.4 Microstructure analysis 51

II.5 Sample preparation and curing 51

II.6 Mechanical performance tests 53

II.7 Conclusions 57
Chapter III. Self-cementing properties of RCA 58
III.1 Chemical compositions 58
III.2 Calorimeter test 59
III.3 Thermogravimetric analysis (TGA) 61
III.3.1 Methods 61
III.3.2 Results 63
III.4 Hydration of unhydrated cement 65
III.5 Microstructural characteristics 69
III.5.1 Scanning electron microscopic analysis (SEM) 69
III.5.2 Mercury intrusion porosimetry (MIP) tests 73
III.6 Mechanism of self-cementing properties 75
III.7 Conclusions 76
Chapter IV. Mechanical behaviour of RCA in repeated load triaxial tests 78
IV.1 Methods 78
IV.2 Effect of RCA sources 81
IV.2.1 Permanent deformation behavior 81
IV.2.2 Resilient deformation behavior under CCP loading 85
IV.2.3 Resilient deformation behavior under VCP loading 89
IV.2.4 Discussion 94
IV.3 Effect of self-cementing properties 95
IV.3.1 Permanent deformation 96
IV.3.2 Resilient deformation behavior under CCP loading 104
IV.3.3 Resilient deformation behavior under VCP loading 115
IV.3.4 Discussion 122
IV.4 Conclusions 124

Chapter V. Mechanical behaviour of RCA in monotonic triaxial tests 126
V.1 Methods 126
V.2 Development of strength with curing time 126
V.3 Development of stiffness with curing time 131
V.4 Relationship between q_{max} and E_{50} 132
V.5 Development of strength parameters 134
V.6 Conclusions 137
Conclusions and perspectives 138
References 142
Résumé 154
Abstract 157
List of publications 159
APPENDIX A. Mathematical expressions for permanent deformation 160
APPENDIX B. Mathematical expressions for resilient deformation 161

List of Figures

Figure I.1. Flexible pavement structure. 4
Figure I.2. Stresses of unbound granular materials under the rolling wheel load (Lekarp et al., 2000a). 5
Figure I.3. Typical deformation of granular materials during one loading cycle (Lekarp et al., 2000a). 6
Figure I.4. Typical deformation of granular materials under cyclic loading. 7
Figure I.5. Typical failure mode of flexible pavement. 7
Figure I.6. Principle of typical repeated load triaxial test. 8
Figure I.7. Permanent deformation evolution of UGM with 6 different coarse aggregates content (f_v) at different deviator stress (Cui, 2018). 9
Figure I.8. Effect of stress history on permanent deformation (Brown & Hyde, 1975). 10
Figure I.9. Deformation behaviour of unbound granular materials (NF EN 13286-7, 2004). . 11
Figure I.10. Permanent deformation evolution of UGM with varying coarse aggregate contents (f_v) under different deviator stresses (Su et al., 2022a). 12
Figure I.11. Permanent strain values at 10,000 load cycles of the 5 UGM mixed with varying crushed aggregates content (Tutumluer & Pan, 2008). 13
Figure I.12. Influence of Drainage on Permanent Deformation Development (Lekarp et al., 2000b). 14
Figure I.13. Final permanent axial deformation of UGM with different fine content (4% and 15%) and water content (Jing et al., 2018). 14
Figure I.14. Resilient modulus of UGM compacted with vibration and impact methods under different water content (Stolle et al., 2009). 16
Figure I.15. Examples of resilient modulus with CCP and VCP (Allen & Thompson, 1974). 17
Figure I.16. Resilient modulus of UGM with varying coarse aggregates content (f_v) (Su et al. (2021)). 18
Figure I.17. Resilient volumetric deformation ε_v for Missillac sand with 8% water content: (a) 4% fine content and (b) 15.3% fine content (Jing et al., 2019). 19
Figure I.18. Resilient volumetric deformation ε_v for Missillac sand with 11% water content: (a) 4% fine content and (b) 15.3% fine content (Jing et al., 2019). 19
Figure I.19. Examples of fit using the improved Boyce model (Hornych et al., 1998). 22
Figure I.20. Experimental data and simulation data with DBGSP model of volumetric strain ε_v and the deviatoric strain ε_q (Ezaoui & Di Benedetto, 2008). 24

Figure I.21. Typical recycled concrete aggregates. 25
Figure I.22. Relationship between particle size and cement paste content for different RCA materials (Zhao et al., 2013). (Note: OC1, OC2 and OC3 are 3 different RCA) 26
Figure I.23. Relationship between cement paste content and density and water absorption of different RCA materials: (a) density and (b) water absorption (Zhao et al., 2013). 27
Figure I.24. Relationship between mortar content and Los Angeles coefficient of different RCA materials (Akbarnezhad et al., 2013). 28
Figure I.25. Permanent deformation of RCA, CB and WR at different water content (Arulrajah et al., 2013). 29
Figure I.26. Comparison of resilient modulus from repeated load triaxial tests on granite and RCA after curing 1 and 60 days (Arm, 2001). 31
Figure I.27. Back-calculated layer moduli for unbound layers of RCA and UGM (Arm, 2001). 31
Figure I.28. Relationship between UCS and pH value for 15 RCA materials (Paige-Green, 2010) 33
Figure I.29. X-ray diffraction patterns of different size fractions of fine RCA (Poon et al., 2006) (Note: C_2S is one of the compositions of cement, representing the presence of unhydrated cement in RCA). 34
Figure I.30. pH values of different size fractions of fine RCA (Poon et al., 2006). 34
Figure I.31. Rehydration temperatures of 6 different RCA (GR1-6) measured by semi-adiabatic calorimeter test (Deodonne, 2015). (Note that “s” is fine, “g” is the coarse aggregate) 36
Figure I.32. X-ray diffraction patterns of the Portland cement and recycled cement paste fine (RCPF) (Bordy et al., 2017). 37
Figure I.33. Treatment of SEM image (Oksri-Nelfia et al., 2016). 37
Figure II.1. Studied RCA materials: (a) NRCA; (b) ORCA; (c) RCAP 40
Figure II.2. Particle size distributions of RCA materials. 41
Figure II.3. Modified Proctor curves of RCA materials. 43
Figure II.4. Principle of the hydrostatic weighing method. 45
Figure II.5. Water absorption evolutions of RCA materials with different particle sizes: (a) 1-4 mm; (b) 4-10 mm and (c) 10-20 mm. 47
Figure II.6 Typical calorimeter. 48
Figure II.7. DTG curves of NRCA and ORCA without curing. 50
Figure II.8. TG curves of NRCA and ORCA without curing. 50

Figure II.9. Sample preparation equipment: (a) Mixer; (b) Vibrating hammer 52
Figure II.10. Curing conditions of RCA 52
Figure II.11. Triaxial apparatus and instrumented specimen. 54
Figure II.12. Stress paths for repeated load triaxial tests (CCP loading). 55
Figure II.13. Stress paths for repeated load triaxial tests (VCP loading). 56
Figure III.1. Hydration heat of NRCA and ORCA: (a) Total heat and (b) Rate of heat generation. 61
Figure III.2. Potential binder content and unhydrated binder content of NRCA calculated by non-evaporable water content (C_{water}) and $Ca(OH)_2$ (C_{CH}) with different w/c. 65
Figure III.3. Comparison of TG-DTG curves of NRCA without curing and curing for 360 and 720 days: (a) without curing; (b) 360 days and (c) 720 days. 66
Figure III.4 Comparison of TG-DTG curves of ORCA without curing and 360 days curing. 66
Figure III.5 The evolution of mass loss for NRCA in different temperature ranges. 68
Figure III.6. SEM images of NRCA curing for 1 and 360 days (300×): (a) 1 day (unbound); (b) 360 days (bound). 70
Figure III.7. SEM images of NRCA curing for 1 and 360 days (2400×): (a) 1 day (unbound); (b) 360 days (bound). 71
Figure III.8. SEM images of NRCA curing for 1 and 360 days (4000×): (a) 1 day (unbound); (b) 360 days (bound). 72
Figure III.9. Pore size distributions of fine NRCA soil curing 1 and 360 days. 74
Figure III.10. Cumulative intrusion void ratio e_M of fine NRCA soil curing 1 and 360 days. 74
Figure IV.1. Permanent axial deformations of all RCAs (curing for 1 day): (a) NRCA and ORCA; (b) RCAP. 82
Figure IV.2. Permanent radial deformations of all RCAs (curing for 1 day): (a) NRCA and ORCA; (b) RCAP. 83
Figure IV.3. Test results and k-θ model predictions of M_r for NRCA, ORCA, RCAP (curing for 1 day) and UGM (Corradini et al., 2021) under CCP loading. 86
Figure IV.4. Resilient deviatoric strain ε_q^r of RCA materials (curing for 1 day) under different constant confining pressures (σ_3=20/35/50/70/100/150 kPa): (a) NRCA; (b) ORCA and (c) RCAP. 87
Figure IV.5. Resilient volumetric strain ε_v^r of RCA materials (curing for 1 day) under different constant confining pressures (σ_3=20/35/50/70/100/150 kPa): (a) NRCA; (b) ORCA and (c) RCAP. 88

Figure IV.6. Resilient deviatoric strain ε_q^r of RCA materials (curing for 1 day) under different stress paths ($\Delta q/\Delta p$=0/1/1.5/2/2.5): (a) NRCA; (b) ORCA and (c) RCAP..... 90
Figure IV.7. Resilient volumetric strain ε_v^r of RCA materials (curing for 1 day) under different stress paths ($\Delta q/\Delta p$=0/1/1.5/2/2.5): (a) NRCA; (b) ORCA and (c) RCAP..... 91
Figure IV.8. Permanent axial deformation ε_1^p of NRCA and ORCA after varying curing times: (a) NRCA; (b) ORCA. 97
Figure IV.9. Final permanent axial deformation of NRCA and ORCA after 20000 cycles at different curing time. 98
Figure IV.10. Characteristic permanent strain ε_1^c of NRCA and ORCA after different curing times. 98
Figure IV.11. Average test results and the model prediction of ε_1^p for NRCA at different curing times. 101
Figure IV.12. Resilient modulus of NRCA and ORCA at different curing times: (a) NRCA; (b) ORCA. 102
Figure IV.13. Evolution of final resilient modulus M_r of NRCA and ORCA with curing time. 103
Figure IV.14. Test results and k-θ model predictions of M_r for NRCA and ORCA after varying curing times: (a) NRCA; (b) ORCA. 105
Figure IV.15. Evolution of k-θ model parameters K_1 and K_2 of NRCA with curing time. 108
Figure IV.16. Evolution of Uzan model parameters K_3, K_4 and K_5 of NRCA with curing time. 108
Figure IV.17. Resilient deviatoric strain ε_q^r of NRCA after different curing times under different constant confining pressures (σ_3=20/35/50/70/100/150 kPa): (a) curing 1 day; (b) curing 180 days; (c) curing 360 days and (d) curing 720 days. 110
Figure IV.18. Resilient volumetric strain ε_v^r of NRCA after different curing times under different constant confining pressures (σ_3=20/35/50/70/100/150 kPa): (a) curing 1 day; (b) curing 180 days; (c) curing 360 days and (d) curing 720 days. 111
Figure IV.19. Resilient deviatoric strain ε_q^r of ORCA after different curing times under different constant confining pressures (σ_3=20/35/50/70/100/150 kPa): (a) curing 1 day; (b) curing 28 days; (c) curing 360 days. 112
Figure IV.20. Resilient volumetric strain ε_v^r of ORCA after different curing times under different constant confining pressures (σ_3=20/35/50/70/100/150 kPa): (a) curing 1 day; (b) curing 28 days; (c) curing 360 days. 112

Figure IV.21. Evolution of parameters K_a, G_a and α of NRCA with curing time. 114
Figure IV.22. Evolution of n_1 and n_2 of NRCA with curing time. 115
Figure IV.23. Resilient deviatoric strain ε_q^r of NRCA after different curing times under different stress path ($\Delta q/\Delta p$=0/1/1.5/2/2.5): (a) curing 1 day; (b) curing 180 days; (c) curing 360 days and (d) curing 720 days..... 116
Figure IV.24. Resilient volumetric strain ε_v^r of NRCA after different curing times under different stress path ($\Delta q/\Delta p$=0/1/1.5/2/2.5): (a) curing 1 day; (b) curing 180 days; (c) curing 360 days and (d) curing 720 days. 117
Figure IV.25. Resilient deviatoric strain ε_q^r of ORCA after different curing times under different stress path ($\Delta q/\Delta p$=0/1/1.5/2/2.5): (a) curing 1 day; (b) curing 28 days; (c) curing 360 days..... 117
Figure IV.26. Resilient volumetric strain ε_v^r of ORCA after different curing times under different stress path ($\Delta q/\Delta p$=0/1/1.5/2/2.5): (a) curing 1 day; (b) curing 28 days; (c) curing 360 days. 118
Figure IV.27. Evolution of modified Boyce model parameters K_a and G_a of NRCA and ORCA with curing time. 120
Figure IV.28. Evolution of modified Boyce model parameters n_1 and γ of NRCA and ORCA with curing time. 121
Figure IV.29. Evolution of DBGSP model parameters α, β and n_2 of NRCA and ORCA with curing time..... 121
Figure V.1. Stress-strain curves of NRCA under different confining pressures after different curing times: (a) 20 kPa; (b) 40 kPa and (c) 70 kPa. 127
Figure V.2. Stress-strain curves of ORCA under different confining pressures after different curing times: (a) 20 kPa; (b) 40 kPa and (c) 70 kPa. 128
Figure V.3. Evolution of peak deviatoric stress q_{max}: (a) NRCA and (b) ORCA. 129
Figure V.4. Evolution of secant modulus E_{50}: (a) NRCA and (b) ORCA. 132
Figure V.5. Relationship between q_{max} and E_{50} for NRCA and ORCA, under different confining pressures (20/40/70 kPa) and curing times (1/28/360 days). 133
Figure V.6. Failure lines of RCA materials after curing for 1, 28 and 360 days: (a) NRCA and (b) ORCA. 135
Figure V.7. Evolution of peak friction angle at failure for NRCA and ORCA. 136
Figure V.8. Evolution of cohesion at failure for NRCA and ORCA 136

List of Tables

Table I.1. Typical density and water absorption of RCA and NA (Nwakaire et al., 2020). 25
Table I.2. Regression parameters for resilient modulus of HRCA and RBRCA (Jitsangiam et al., 2015). 32
Table II.1. Physical properties of all RCA materials. 41
Table II.2. Targeted water contents and dry densities. 53
Table II.3. Monotonic triaxial test and repeated load triaxial test program. 53
Table II.4. Stress paths for resilient behaviour tests (CCP loading). 56
Table II.5. Stress paths for resilient behaviour tests (VCP loading). 56
Table III.1. Initial chemical compositions of NRCA and ORCA. 59
Table III.2. *k* values for different types of supplementary cementing materials. 63
Table III.3. Selected components of NRCA and ORCA without curing. 64
Table III.4. Mass losses of NRCA and ORCA curing for different times. 67
Table IV.1. Average permanent deformation of NRCA, ORCA and RCAP. 83
Table IV.2. Summary of k-θ model and Uzan model parameters for NRCA, ORCA, RCAP and UGM. 86
Table IV.3. Modified Boyce model parameters of NRCA, ORCA and RCAP, under constant confining pressure. 89
Table IV.4. DBGSP model parameters of NRCA, ORCA and RCAP, under constant confining pressure. 89
Table IV.5. Modified Boyce model parameters of NRCA, ORCA and RCAP, under variable confining pressure. 92
Table IV.6. Testing parameters of UGM and RCAP. 92
Table IV.7. DBGSP model parameters of NRCA, ORCA and RCAP, under variable confining pressure. 93
Table IV.8. Characteristic resilient modulus E_c of RCA materials (NRCA, ORCA and RCAP), UGM and RAP. 94
Table IV.9. Classification of unbound granular materials based on E_c and ε_1^c 94
Table IV.10. Classification of RCA materials. 94
Table IV.11. RLTT results of NRCA and ORCA after different curing times. 98
Table IV.12. Parameters of the proposed model for NRCA based on curing times. 100
Table IV.13. Average and standard error of final resilient modulus M_r of NRCA and ORCA. 102

Table IV.14. Average M_r of NRCA and ORCA at different curing times. 106
Table IV.15. Summary of k-θ model parameters for NRCA and ORCA. 106
Table IV.16. Summary of Uzan model parameters for NRCA and ORCA. 107
Table IV.17. Synthesis of model parameters for bound and unbound materials. 109
Table IV.18. Modified Boyce model parameters of NRCA and ORCA after different curing times (CCP loading). 113
Table IV.19. DBGSP model parameters of NRCA and ORCA after different curing times (CCP loading). 113
Table IV.20. Modified Boyce model parameters of NRCA and ORCA after different curing times (VCP loading). 119
Table IV.21. DBGSP model parameters of NRCA and ORCA after different curing times (VCP loading). 119
Table IV.22. Classification of RCA materials after different curing times. 122

General introduction

In 2018, over 800 million tonnes of construction and demolition wastes (CDW) were generated in Europe, in which concrete wastes are the main components and represent up to 75% of the total CDW by weight. As a consequence, the use of recycled crushed concrete aggregates (RCA) as a substitution of natural aggregates (NA) in pavement base and subbase layers has become more popular in recent years.

Recycled concrete aggregates (RCA) are produced by crushing concrete wastes, containing both original natural aggregates and attached mortar which could retain very low amount of residual unhydrated cement. The residual unhydrated cement in RCA can react with water and cause the secondary hydration of RCA, increasing strength and stiffness of unbound pavement layers built with RCA, known as self-cementing properties of RCA.

Besides, the engineering properties of RCA from different sources could be totally different due to the different strength and quality of concrete structures. Thus, it is also important to study the influence of the RCA source and engineering properties on the performance of RCA in unbound pavement base and subbase layers.

Many studies have been conducted to study the performance of RCA as an unbound granular material (UGM) in pavements over the past years. In general, the overall conclusions are that the performance of most RCA materials is comparable to that of NA. However, it is also found that there are relatively few studies, and experimental data, in the literature about the effect of self-cementing properties and RCA source on the mechanical behaviour of RCA.

Objectives and scope

The objective of this study is to investigate the effect of self-cementing properties and RCA source on the mechanical behaviour of RCA, by conducting repeated load triaxial tests and monotonic triaxial tests. The main objectives include:

1. Evaluating the self-cementing properties of RCA materials and developing a calculation method to evaluate the potential unhydrated cement content.
2. Studying the hydration of unhydrated cement during the curing stage and the effect of self-cementing properties on microstructure of RCA specimen.
3. Investigating the effect of self-cementing properties on the permanent deformation of RCA under repeated loading.

4. Investigating the effect of self-cementing properties on the resilient deformation behaviour of RCA under repeated loading, such as resilient modulus, resilient deviatoric strain and volumetric strain.
5. Investigating the effect of self-cementing properties on the shear behaviour of RCA, such as shear strength, stiffness, cohesion and friction angle.
6. Investigating the effect of RCA source on the permanent deformation and resilient deformation behaviours of RCA under repeated loading.

Outline

This thesis is organized into five chapters.

The first chapter is the literature review. First, the role and mechanical behaviour of UGM under repeated loading were presented. The factors affecting permanent deformation and resilient deformation behaviour are introduced. Some mathematical models to predict resilient deformation behaviour were also summarized. Then, the physical properties and mechanical behaviours of RCA are presented. At the end, the methods to evaluate self-cementing properties and their influence on mechanical behaviour of RCA were reported.

The second chapter, firstly, presents the basic physical properties of three studied RCA materials: grading, density, water absorption, fine content, rounded particle content, Los Angeles coefficient, Micro-Deval coefficient, water-soluble sulfate content, compaction, and water absorption kinetic. Subsequently, the methods to evaluate self-cementing properties, by pH value, calorimeter test and thermogravimetric analysis (TGA), and microstructure observation, by scanning electron microscopic analysis (SEM) and mercury intrusion porosimetry (MIP) tests, were introduced. In the end, the monotonic triaxial test and the repeated load triaxial tests were presented, including specimen preparation, experimental device and test procedures.

In the third chapter, self-cementing properties of RCA materials were evaluated by the pH value and calorimeter test. To calculate the unhydrated cement content, a method based on TGA was developed. The hydration of unhydrated cement after pavement construction and the evolution of microstructure were studied by TGA, SEM and MIP. At the end, the mechanism of self-cementing properties was analysed based on these observations.

In the fourth chapter, the effects of self-cementing properties and RCA source on the permanent deformation and resilient deformation behaviour were investigated. For the modelling analysis,

the k-θ model and Uzan model were used to predict the resilient modulus, while the modified Boyce model and DBGSP model were used to predict resilient volumetric and deviatoric strains. Finally, a classification of these RCA materials, considering or not self-cementing properties, was obtained, based on repeated load triaxial test results.

In the fifth chapter, the effect of self-cementing properties on the shear behaviour of RCA under monotonic triaxial tests was presented. The development of strength, stiffness, cohesion and friction angle with curing time were analysed.

Finally, the general conclusions and some perspectives for future studies were presented.

Chapter I. Literature review

The main objective of this chapter is to present a literature review of the physical properties and self-cementing properties of recycled concrete aggregates (RCA). The mechanical behaviours of unbound granular materials (UGM) and RCA under repeated load triaxial tests are also introduced. Firstly, a brief description of flexible pavement structure and mechanical behaviour of UGM under repeated load triaxial tests is introduced (Sections I.1 and I.2) to understand the important role of UGM. Then, the physical property, mechanical behavior and self-cementing properties of RCA (Sections I.3 and I.4), a substitution of UGM, are summarized in detail.

I.1 Unbound granular materials in pavement

I.1.1 Flexible pavement structure

Approximately 60% of the road network in France or Europe is flexible pavement structure (Jing et al., 2018): a relatively thin bituminous surface layer is supported by unbound or bound granular material base and/or subbase layers located on subgrade, as shown in Figure I.1.

In this pavement structure, especially when the upper bituminous surface layer is thin, granular base and subbase layers play an important role in the overall performance of pavement, improving the distribution of traffic stress applied on the upper surface layer and transmitting traffic loads to the subgrade. Consequently, it is essential to thoroughly understand the response of granular materials under traffic loads.

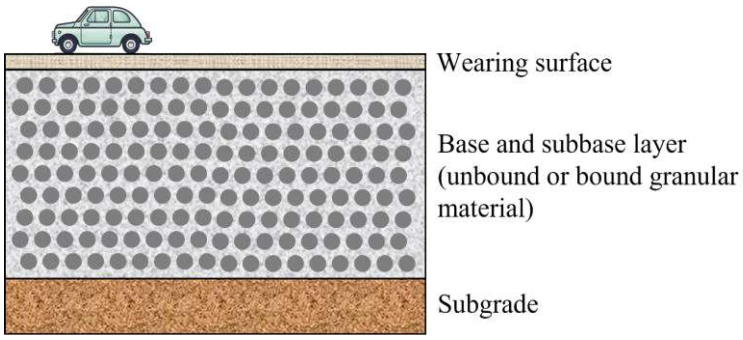

Figure I.1. Flexible pavement structure.

I.1.2 Stress in unbound granular material layer

The stress of unbound granular materials under traffic loads is quite complex due to the rolling wheel, consisting of vertical, horizontal and shear stresses, as illustrated in Figure I.2. In unbound granular material layers, the vertical and horizontal stresses are positive, while the shear stress is reversed with the movement of wheel across the pavement, resulting in a rotation of the principal stress axes. Repeated load triaxial test is the most representative method to study the mechanical behavior of UGM under the traffic loads as it can stimulate the rotation of the principal stress.

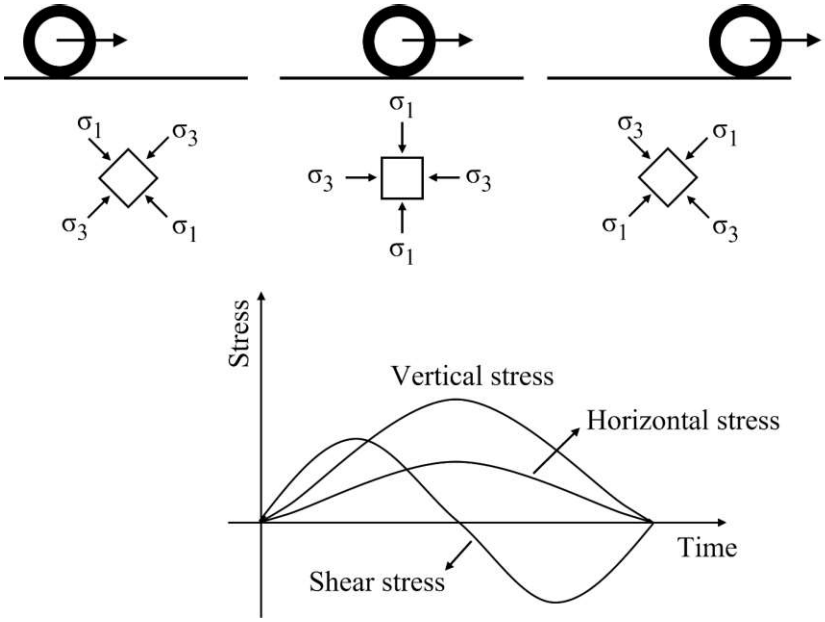

Figure I.2. Stresses of unbound granular materials under the rolling wheel load (Lekarp et al., 2000a).

I.1.3 Deformation in unbound granular material layer

Granular materials are made with a large number of individual particles which has different particle shapes and sizes. It has been postulated (Chan, 1990; Lekarp et al., 2000a; Luong, 1982) that the deformation of granular soils under loading is the result of three main mechanisms: consolidation, distortion, and attrition. The consolidation mechanism is the change in shape and compressibility of particle assemblies, showing as densification or dilation of granular materials. The distortion mechanism is characterized by bending, sliding and rolling of individual particles, related to the shape and morphology of coarse aggregates. The attrition mechanism is the crushing and breakage of the particles when the applied load exceeds the strength of particles.

The deformational response of granular layers during one traffic loading cycle is characterized by a permanent (residual) deformation, residual strain after the load is removed, and resilient (recoverable) deformation, which are recovered after each loading cycle, as illustrated in Figure I.3. It should be noted that only when the permanent deformation is stable, the recoverable deformation can be treated as resilient deformation.

During the service life of pavement, granular layers bear a large number of cyclic traffic loadings. Figure I.4 shows the typical deformation of granular materials under cyclic loading. The permanent deformation increases quickly during the first loading cycles and then reaches a stable value (plastic shakedown state). However, if the pavement was not designed properly, the permanent deformation increases with loading cycle continuously (plastic creep state or incremental collapse state). With the accumulation of traffic loadings, the permanent deformation increases until the failure of pavement: the large-radius rutting and the fatigue crack of the upper bituminous surface layer as shown in Figure I.5.

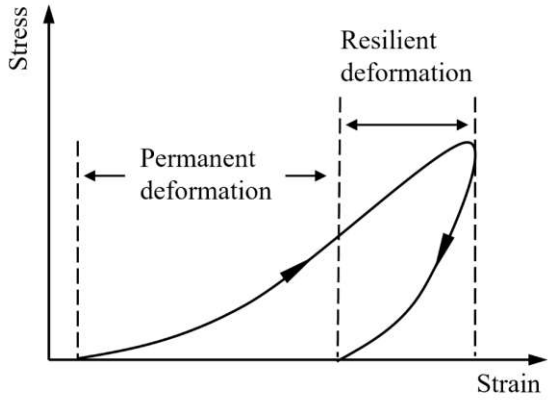

Figure I.3. Typical deformation of granular materials during one loading cycle (Lekarp et al., 2000a).

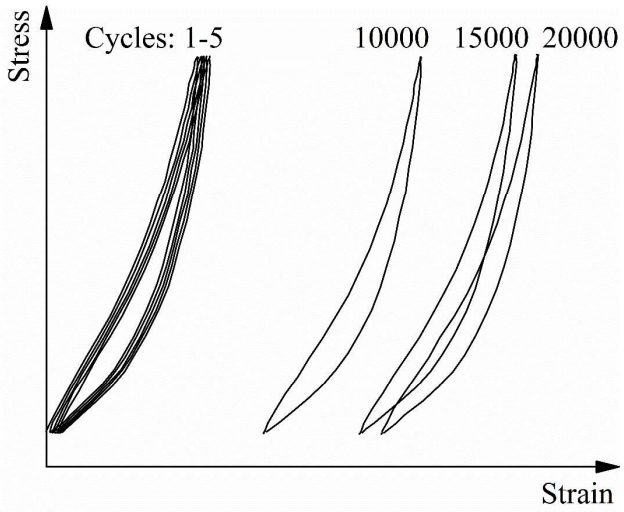

Figure I.4. Typical deformation of granular materials under cyclic loading.

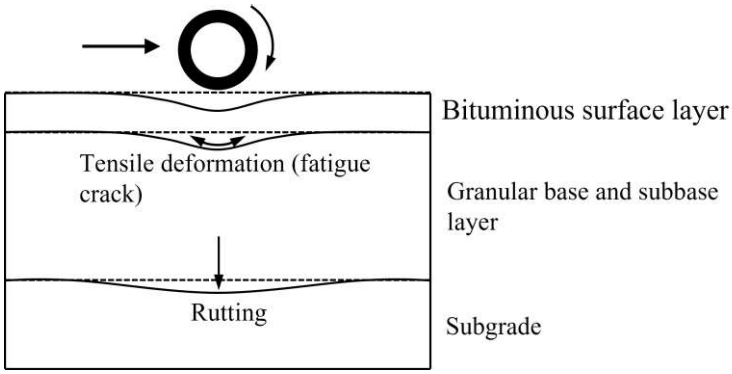

Figure I.5. Typical failure mode of flexible pavement.

I.2 Repeated load triaxial test

As illustrated in section I.1, permanent deformation and resilient deformation behaviours of unbound granular materials (UGM), under traffic loads, are essential for pavement design, avoiding the failure of pavement. The response of UGM under cyclic traffic loads can be obtained by pavement loading tests or laboratory techniques.

Repeated load triaxial test (RLTT) is widely used and is the most representative laboratory test to study the response of granular materials in pavement, with permanent deformation and resilient deformation behaviours, as it can simulate the pavement loading conditions. Figure I.6 shows the principle of a typical repeated load triaxial test: a variable axial deviatoric stress q and a confining pressure σ_3, constant or variable, were applied on the cylindrical specimen in a

triaxial cell with a large number of loading cycles. Then, the permanent deformation and resilient deformation behaviours under traffic loads can be obtained.

Different stress paths ($\Delta q/\Delta p$) can be applied on the samples, simulating the traffic loadings on the pavement. According to the applied σ_3, two different loading methods can be used to study the permanent deformation and resilient deformation behaviours: constant confining pressure σ_3 (CCP loading) and variable confining pressure σ_3 (VCP loading), where q and σ_3 were cycled in phase, as shown in Figure I.6.

The stress invariants, mean normal stress p and the deviator stress q, can be defined as:

$$p = \frac{\sigma_1 + 2\sigma_3}{3} \tag{I.1}$$

$$q = \sigma_1 - \sigma_3 \tag{I.2}$$

where σ_1 is the vertical stress and σ_3 is the confining pressure.

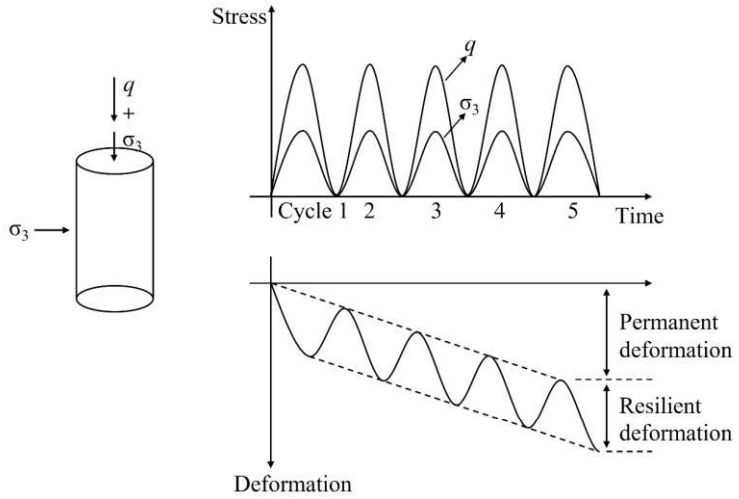

Figure I.6. Principle of typical repeated load triaxial test.

I.2.1 Permanent deformation behavior of UGM

The gradual accumulation of permanent deformation could lead to rutting, resulting in the failure of the pavement. As a result, permanent deformation determined by repeated load triaxial tests (RLTT) is one of the most important parameters for pavement design. Several factors can influence the permanent deformation behaviour of granular materials: type of granular materials, stress level and history, principal stress rotation, number of loading cycles,

density, fine content, particle size distribution, water content and suction (Ho et al., 2014; Jing et al., 2018; Lekarp et al., 2000b).

Stress level, history and principal stress rotation

Stress level is one of the most important factors affecting the development of permanent deformation in UGM. In the early RLTT, reported by Morgan (1966), results showed that the permanent axial deformation increases with deviator stress level, while decreases with confining pressure. Cui (2018) conducted repeated load triaxial tests on UGM with 6 different coarse aggregates content (from 0 to 45% by volume) at 5 different deviator stress level (q=10, 15, 20, 25 and 30 kPa), and also found that the permanent deformation increases with the deviator stress level, as shown in Figure I.7. A similar behavior has been reported by Lekarp et al. (2000b), Yang et al. (2008), Jing et al. (2018) and Xiao et al. (2018).

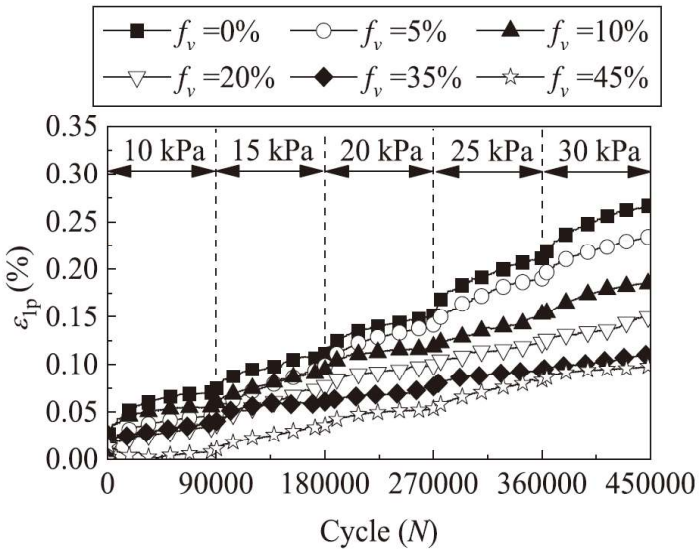

Figure I.7. Permanent deformation evolution of UGM with 6 different coarse aggregates content (f_v) at different deviator stress (Cui, 2018).

Permanent deformation behaviour of UGM also relates to the stress history. Brown and Hyde (1975) investigated the effect of stress history on permanent deformation behaviour by conducting a series of RLTT under successive stress levels and a direct highest stress level. The results show that the permanent deformation under a direct highest stress level was significantly larger than that under successive stress levels, as indicated in Figure I.8. When repetitive loads are applied, the gradual material stiffening reduces the permanent deformation during the subsequent loading cycles. However, a multi-stage loading procedure was still used by many researchers to study the effect of stress level on permanent deformation, although the stress

history has an influence on the RLTT results (Cui, 2018; Gidel et al., 2001; Jing et al., 2018; Senanayake et al., 2022).

As illustrated in Figure I.2, the movement of wheel across the pavement, resulting in a rotation of the principal stress axes. However, the effect of principal stress reorientation on permanent deformation is not yet fully understood, as RLTT, the most common method to simulate traffic loads, fails to change the direction of principal stresses continuously.

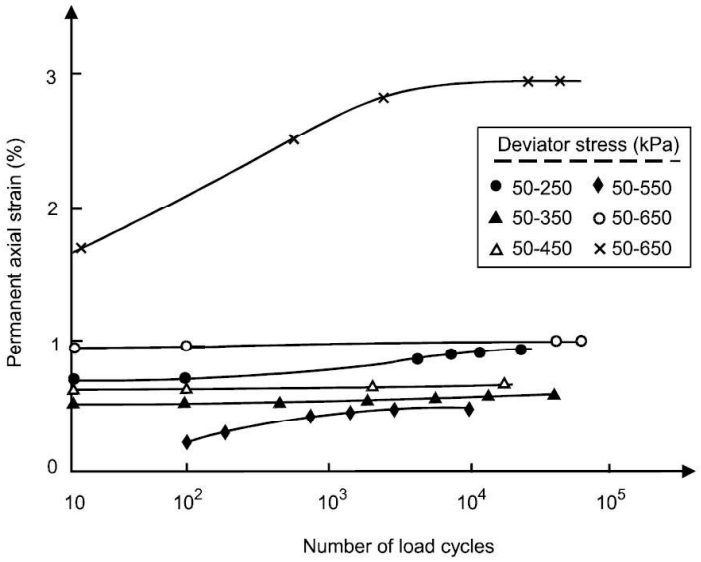

Figure I.8. Effect of stress history on permanent deformation (Brown & Hyde, 1975).

Number of loading cycles

As illustrated above, the deformational response of UGM during one traffic loading cycle is characterized by a permanent (residual) deformation and resilient (recoverable) deformation. As the number of traffic loads increase, the accumulation of permanent deformation with each loading cycle contributes to the growth of permanent deformation in UGM with repeated loadings. Therefore, the number of loading cycles is another important factors affecting the development of permanent deformation in granular materials.

According to the shakedown theory (Werkmeister et al., 2001), permanent deformation tests can lead to three ranges of UGM behavior: plastic shakedown, plastic creep and incremental collapse, as shown in Figure I.9. With the increase of deviator stress level, the UGM turns plastic shakedown state gradually to the incremental collapse, leading to the failure of pavement. Thus, the pavement design method demands the UGM is in the plastic shakedown state during the service life of pavement. Under plastic shakedown state, the permanent deformation

increases fast in the first loading cycles, and then reaches a stable and constant value (Gaillard et al., 2019; Jing et al., 2018). Under plastic creep state, the permanent deformation increases fast in the first loading cycles, and then increases sequentially with a certain permanent deformation rate, which could lead to the rutting of pavement after long term service. While for incremental collapse state, failure will occur at low number of loading cycles.

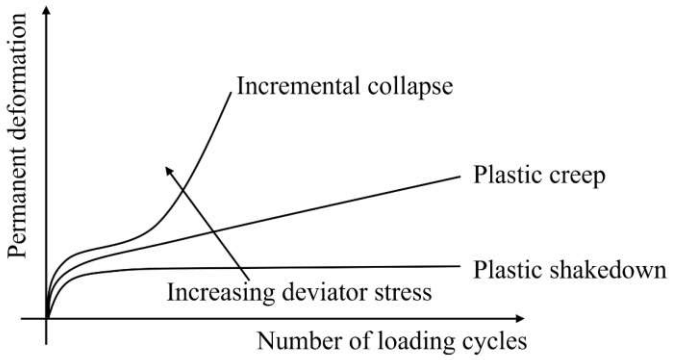

Figure I.9. Deformation behaviour of unbound granular materials (NF EN 13286-7, 2004).

Fine content

The effect of fine content on permanent deformation behaviour is studied by many researchers (Cui, 2018; Duong et al., 2013; Jing et al., 2018; Su et al., 2022a). It can be stated that the resistance to permanent deformation is governed by the skeleton of coarse grains, if the fine content is not too large. Instead, the fine particles isolate the coarse grains and take the main role if the fine content is large (Jing et al., 2018; Su et al., 2022a). Figure I.10 depicts the permanent deformation of UGM with 6 different coarse aggregate contents (from 0 to 45% by volume), under 5 different deviator stress levels (q=10, 15, 20, 25 and 30 kPa), reported by Su et al. (2022a). It was found that the permanent deformation increases with the increasing fine content, which is attributed to the reinforcement effect of coarse aggregates.

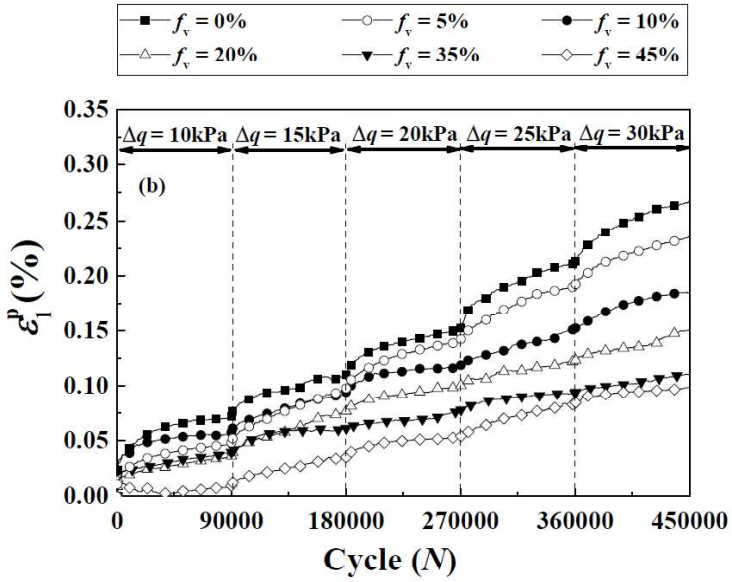

Figure I.10. Permanent deformation evolution of UGM with varying coarse aggregate contents (f_v) under different deviator stresses (Su et al., 2022a).

Aggregate type

A significant number of researches have been conducted to investigate the effect of aggregates type on the permanent deformation (Cook et al., 2017; Janoo et al., 2004; Mishra & Tutumluer, 2012; Tutumluer & Pan, 2008). It was proved that the crushed, angular aggregates have a better performance on the resistance to permanent deformation than cube-shaped, rounded aggregates due to the better particle interlock. Figure I.11 depicts the permanent deformation values at 10,000 load cycles of 5 different UGM, mixed with different percentages of crushed aggregates (from 50% to 100%). It can be observed that for both UGM, the permanent deformation decreases with the increasing crushed aggregates content.

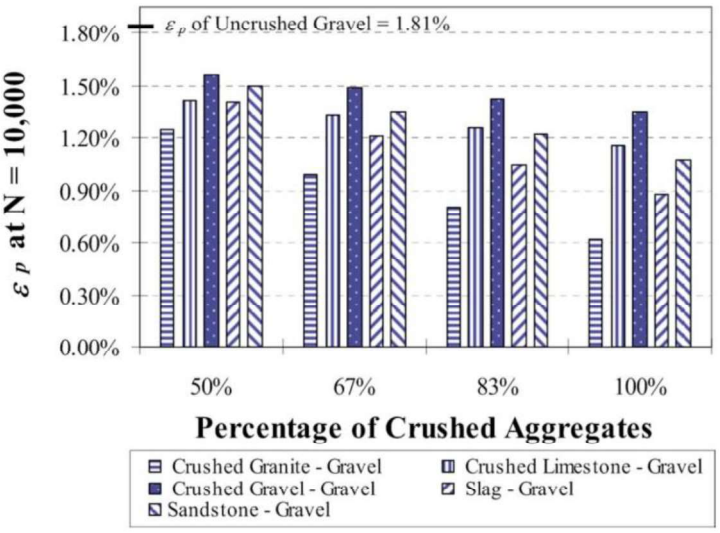

Figure I.11. Permanent strain values at 10,000 load cycles of the 5 UGM mixed with varying crushed aggregates content (Tutumluer & Pan, 2008).

Water content

The effect of water content is significantly important for the long-term behaviour of granular materials. In fact, an adequate amount of water has a positive influence on the mechanical behavior of UGM due to the lubricating effect of water in a granular assembly. In the past several decades, the effect of water content on permanent deformation has been reported in many studies (Barksdale, 1972; Dawson et al., 1996; Jing et al., 2019; Su et al., 2022a). Under saturated and unsaturated state, the increase of water content led to an increase of permanent deformation. Lekarp et al. (2000b) presented an example of the positive effect of drainage on permanent deformation, decreasing pore pressure and increasing effective stress, resulting in improvement of permanent deformation resistance of the material, as shown in Figure I.12.

Jing et al. (2018) studied the effect of fine content and water content on permanent deformation of UGM. They found with high fine content, a relatively small increase in water content can dramatically increase the permanent deformation, as illustrated in Figure I.13.

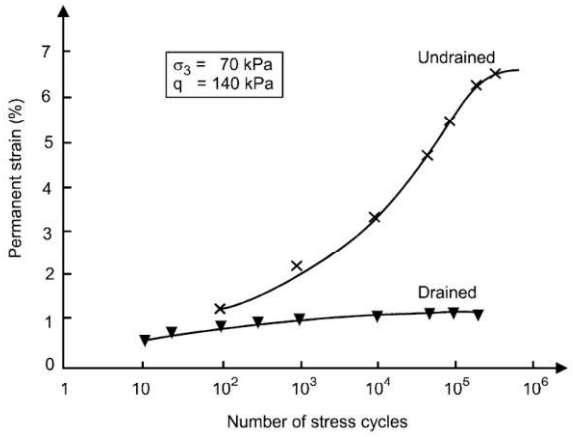

Figure I.12. Influence of Drainage on Permanent Deformation Development (Lekarp et al., 2000b).

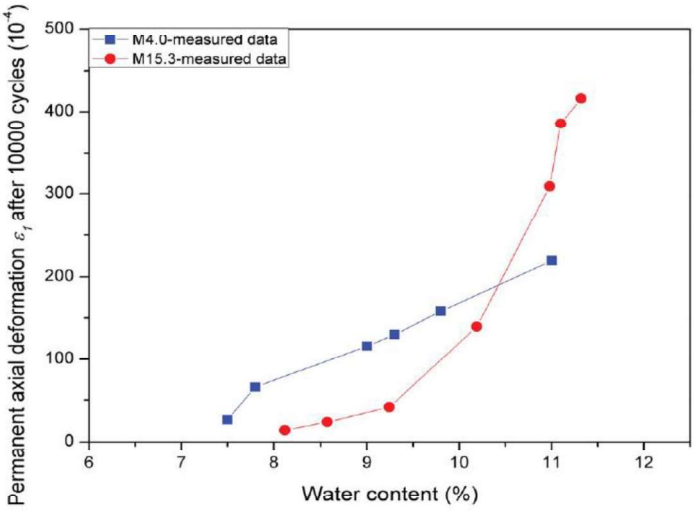

Figure I.13. Final permanent axial deformation of UGM with different fine content (4% and 15%) and water content (Jing et al., 2018).

Density

The effect of density, as described by degree of compaction, is important for the long-term behavior of granular materials. Barksdale (1972) observed that the permanent deformations of several UGM compacted at 95% maximum dry density (MDD) are average 185% higher than these compacted at 100% MDD. Van Niekerk (2002) reported that the effect of compaction on the mechanical behaviour was more significant than the effect of grading, composition and loading stress.

Models predicting permanent deformation

Many mechanistic-empirical models are derived from the repeated load triaxial tests, since they are very easy to use and can predict permanent deformation very well. Those models often describe a relationship between the accumulation of permanent deformation and the number of load cycles. Among those models, Hornych (1993) proposed an empirical model to describe the effect of the number of load cycles and was adopted in French standard (AFNOR, 1995):

$$\varepsilon_1^p = A(1-(\frac{N}{N_0})^B) \tag{I.3}$$

where ε_1^p is the permanent strain (10^{-4}) after N_0 cycles, N_0 is the number of cycles before the first measurement (N_0=100 in this study), parameter A represents the final permanent axial deformation and parameter B controls the evolution of permanent deformation with increasing N.

Besides, the effect of stress level and stress history on permanent deformation have been considered also and many other models were proposed, as summarized in Appendix A.

I.2.2 Resilient deformation behavior of UGM

Resilient deformation is another one of the most important parameters for pavement design, leading to fatigue cracking of the overlying bound layers.

It is well known that unbound granular materials show a nonlinear and time-dependent elastic-plastic response under traffic loading, as shown in Figure I.4. To study this nonlinear and time-dependent elastic-plastic behaviour, the resilient deformation behaviour is generally presented in terms of resilient modulus M_r, resilient volumetric strain ε_v and resilient deviatoric strain ε_q, which can be defined as (NF EN 13286-7, 2004):

$$M_r = \frac{\sigma_1^r}{\varepsilon_1^r} \text{ (CCP loading)} \tag{I.4}$$

$$\text{or } M_r = \frac{\sigma_1^{r2} + \sigma_1^r\sigma_3^r - 2\sigma_3^{r2}}{\sigma_1^r\varepsilon_1^r + \sigma_3^r\varepsilon_1^r - 2\sigma_3^r\varepsilon_3^r} \text{ (VCP loading)} \tag{I.5}$$

$$\varepsilon_v = \varepsilon_1^r + 2\varepsilon_3^r \tag{I.6}$$

$$\varepsilon_q = \frac{2(\varepsilon_1^r - \varepsilon_3^r)}{3} \tag{I.7}$$

where σ_1^r and σ_3^r are resilient axial and radial stress, ε_1^r and ε_3^r are resilient axial and radial strain.

As permanent deformation, the resilient deformation behavior is also influenced by some factors, such as stress, fine content, water content, density, and type of aggregates.

Stress

It is well known that the stress level has the most significant impact on resilient deformation behaviour of UGM. Many studies (Han-Cheng et al., 2020; Lekarp et al., 2000a; Stolle et al., 2009; Sweere, 1992; Uzan, 1985) have shown that the resilient modulus of UGM highly depends on the confining pressure σ_3 and the sum of principal stresses θ, as shown in Figure I.14.

Besides, the loading method, constant confining pressure (CCP loading) and variable confining pressure (VCP loading), also has an influence on resilient deformation behaviour of UGM. Allen and Thompson (1974) compared the resilient modulus under both two loading methods (CCP and VCP), as shown in Figure I.15. Results show CCP method generally has higher resilient modulus compared to that under VCP method.

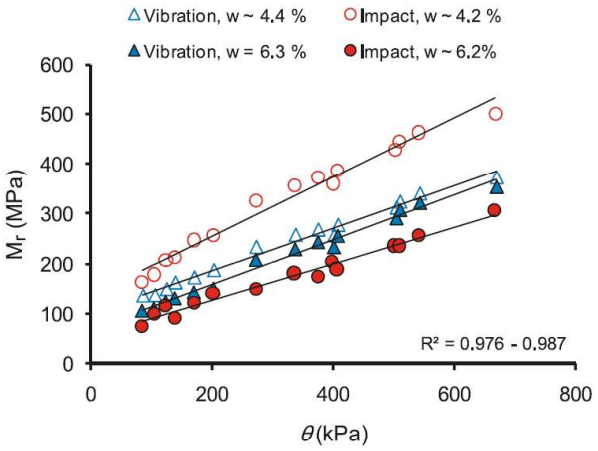

Figure I.14. Resilient modulus of UGM compacted with vibration and impact methods under different water content (Stolle et al., 2009).

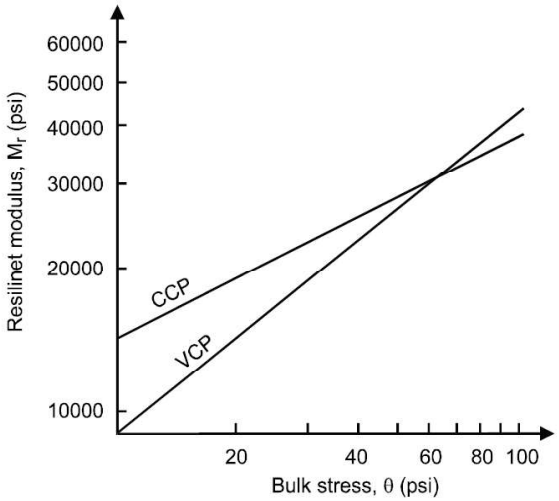

Figure I.15. Examples of resilient modulus with CCP and VCP (Allen & Thompson, 1974).

Fine content

The effect of fine content on the resilient response of UGM is very important, while the effect of fine content on resilient behaviour is not fully understood. Some researchers (Thom & Brown, 1987) have reported that resilient modulus generally increases with the decrease of fine content. Su et al. (2021) reported that the resilient modulus increases with the increasing coarse aggregates content, as shown in Figure I.16. However, other researchers (Jing et al., 2019; Jorenby & Hicks, 1986) also observed that the stiffness increases initially and then decreases with the increase of fine content. The initial improvement in resilient deformation behaviour is attributed to the filling effect of fines into pore space. Gradually, excess fines displace the coarse particles so that the mechanical performance relies mainly on the fines, and stiffness decreases.

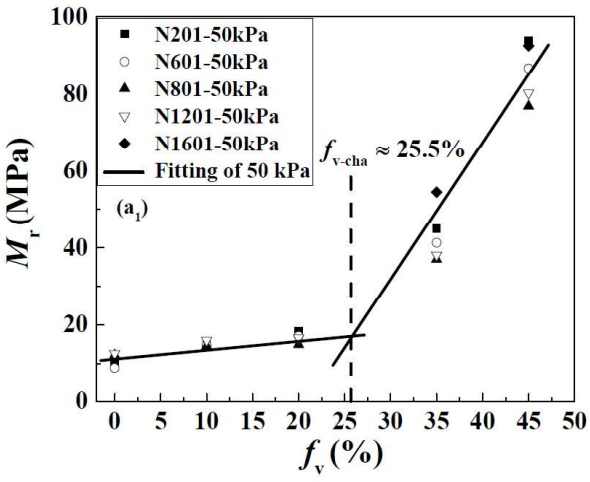

Figure I.16. Resilient modulus of UGM with varying coarse aggregates content (f_v) (Su et al. (2021)).

Water content

Water content has a significant influence on resilient deformation behaviour of UGM. Generally, the increase of water content could lead to the decrease of resilient modulus and increase of resilient volumetric strain ε_v and resilient deviatoric strain ε_q (Dawson et al., 1996; Hicks, 1970; Ho et al., 2014; Jing et al., 2019). However, it is generally agreed that for partially saturated state, the resilient deformation behavior of UGM is less influenced by water content. While when complete saturation is approached, the resilient deformation behavior could be affected significantly. Jing et al. (2019) reported that only when the fine content is high, the resilient deformation behavior of UGM is sensitive to high water content, as shown in Figure I.17 and Figure I.18.

More recently, the influence of water content on resilient response has been investigated with fine content, as the fine content can influence the effect of water content. It is believed that the coupling effect of water content and fine content can be better determined by suction. Many researchers have shown the strong correlations between suction value and resilient response of granular materials (Ho et al., 2014; Jing et al., 2019; Nowamooz et al., 2011).

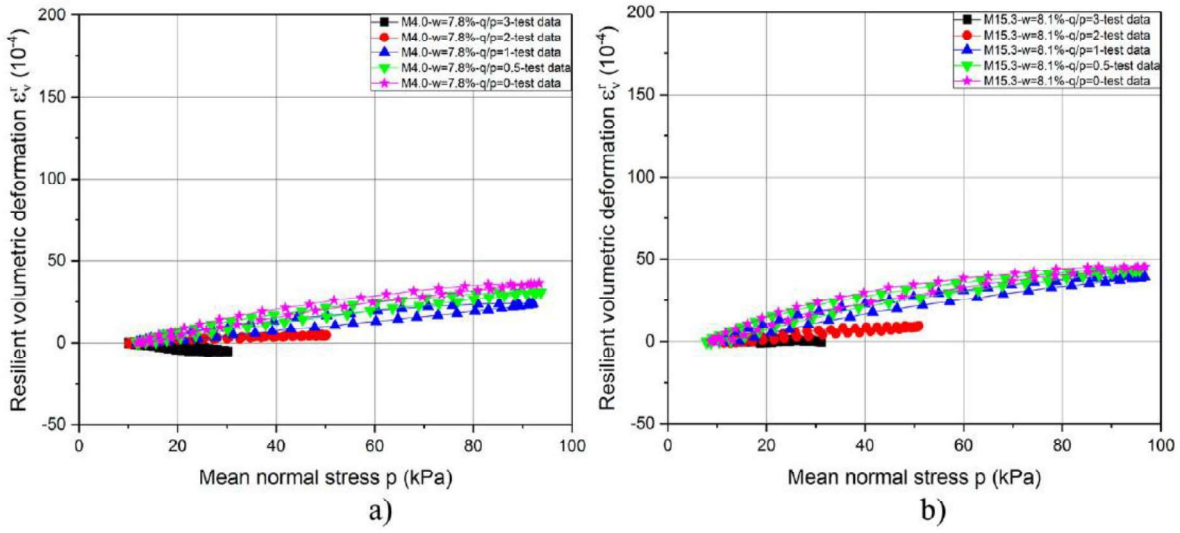

Figure I.17. Resilient volumetric deformation ε_v for Missillac sand with 8% water content: (a) 4% fine content and (b) 15.3% fine content (Jing et al., 2019).

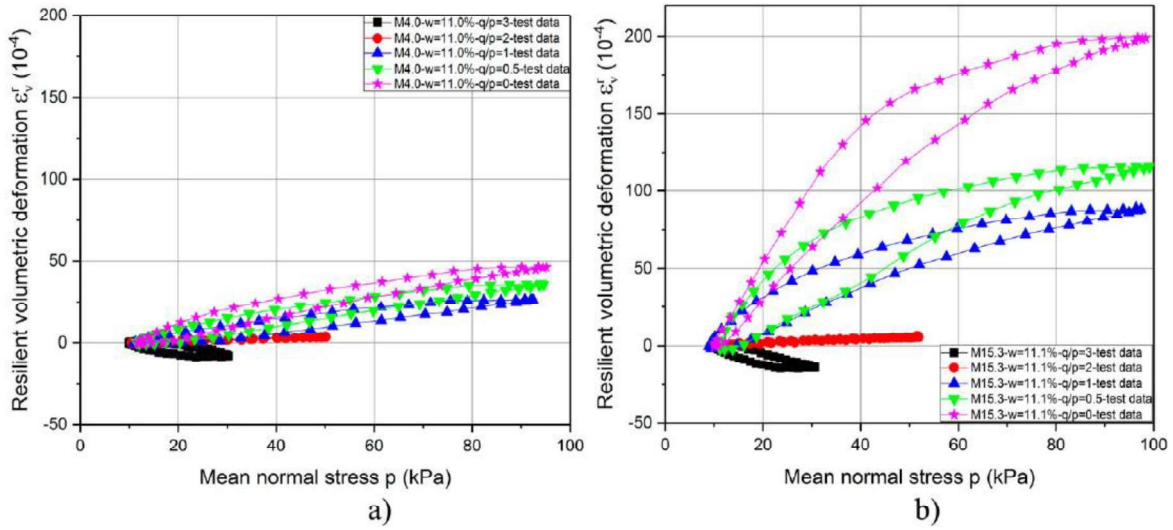

Figure I.18. Resilient volumetric deformation ε_v for Missillac sand with 11% water content: (a) 4% fine content and (b) 15.3% fine content (Jing et al., 2019).

Effect of aggregate type and particle shape

Similar to the permanent deformation behaviour, type of aggregates is an important factor on resilient deformation behaviour of UGM. Allen and Thompson (1974) reported that crushed aggregate which have angular shape, provides better load spreading properties and a higher resilient modulus than that of uncrushed gravel with rounded particles. Similar observation was

reported by other researchers (Cook et al., 2017; Janoo et al., 2004; Kwon et al., 2017; Pan et al., 2006).

Density

Numerous researches (Brown & Selig, 1991; Hicks, 1970; Trollope et al., 1962) have been carried out to study the effect of density on resilient deformation behavior. Since the number of particle contacts per particle increases greatly with increased density, the average contact stress induced by the traffic loads decreases. Hence, the resilient deformation in particle decreases and the resilient modulus increases with the increasing density. Results reported by Trollope et al. (1962) show that the resilient modulus increased by up to 50% between loose and dense specimens. However, compared with stress, the effect of density on resilient deformation is less pronounced (Brown & Selig, 1991; Lekarp et al., 2000a).

Models predicting resilient modulus

UGM exhibits a complex non-linear and time-dependent resilient response under repeated loading, and the traditional experimental methods to describe the resilient behaviour are time consuming. Hence, various empirical-analytical models have been proposed to predict the resilient deformation behaviour of UGM, such as resilient modulus M_r, resilient volumetric and deviatoric strain.

Biarez (1962) described the stress-dependent stress-strain behaviour of granular materials subjected to repeated loading. Independently, similar works were performed in the United States (Hick & Monismith, 1971; Seed et al., 1967). Both results presented the k-θ model to describe the relationship between M_r and sum of principal stresses θ:

$$M_r = k_1 \left(\frac{\theta}{p_a}\right)^{k_2} \tag{I.8}$$

where, k_1 and k_2 are parameters, p_a is the atmospheric pressure (100 kPa).

To consider the effect of deviator stress q, Uzan (1985) improved the k-θ model, known as Uzan model:

$$M_r = k_3 \left(\frac{\theta}{p_a}\right)^{k_4} \left(\frac{q}{p_a}\right)^{k_5} \tag{I.9}$$

where, k_3 k_4 and k_5 are parameters, p_a is the atmospheric pressure (100 kPa).

Lekarp et al. (2000a) have summarized many other computational models for resilient modulus, as summarized in Appendix B.

Models predicting volumetric strain and deviatoric strains

A different approach can be used in characterizing the resilient deformation behaviour of UGM by resilient volumetric strain ε_v and deviatoric strain ε_q. ε_v and ε_q can be expressed by bulk moduli K and shear moduli G as:

$$\varepsilon_v = \frac{p}{K} \tag{I.10}$$

$$\varepsilon_q = \frac{q}{3G} \tag{I.11}$$

where p and q are mean normal stress (p=(σ_1+σ_2+σ_3)/3) and deviatoric stress (q=σ_1-σ_3).

According to Boyce (1980), bulk moduli K and shear moduli G can be expressed as following:

$$K = K_a \bullet p^{1-n} / (1 - \beta \frac{q^2}{p^2}) \tag{I.12}$$

$$G = G_a \bullet p^{1-n} \tag{I.13}$$

where β=(1-n)K_a/(6G_a), K_a, G_a and n are parameters, related to K, G and nonlinear coefficient. As a result, the volumetric strain and deviatoric strain could be expressed as:

$$\varepsilon_v = \frac{p^n}{K_a}\left[1 + \frac{(n-1)\bullet K_a}{6G_a}\left(\frac{q}{p}\right)^2\right] \tag{I.14}$$

$$\varepsilon_q = \frac{p^n}{3G_a} \bullet \frac{q}{p} \tag{I.15}$$

In the Boyce model, given by Equations (I.14) and (I.15), the resilient behaviour of UGM is assumed to be isotropic and non-linear. However, due to the initial compaction and conditioning, a higher stiffness is usually obtained in vertical direction, known as anisotropy behaviour. To consider the effect of anisotropy behaviour, Hornych et al. (1998) has improved the Boyce model by introducing a coefficient of anisotropy γ, multiplying the major principal stress σ_1. Thus, the new mean normal stress p^* and the new deviatoric stress q^* can be redefined as follows:

$$p^* = \frac{\gamma\sigma_1 + 2\sigma_3}{3} \tag{I.16}$$

$$q^* = \gamma\sigma_1 - \sigma_3,\ 0 < \gamma < 1 \tag{I.17}$$

Then, based on the expression of the initial Boyce model, the volumetric strain ε_v and the deviatoric strain ε_q can be expressed by the following equations:

$$\varepsilon_v = \frac{p^{*n}}{p_a^{n-1}}\left[\frac{\gamma+2}{3K_a} + \frac{n-1}{18G_a}(\gamma+2)\left(\frac{q^*}{p^*}\right)^2 + \frac{\gamma-1}{3G_a} * \frac{q^*}{p^*}\right] \tag{I.18}$$

$$\varepsilon_q = \frac{2}{3} * \frac{p^{*n}}{p_a^{n-1}}\left[\frac{\gamma-1}{3K_a} + \frac{n-1}{18G_a}(\gamma-1)\left(\frac{q^*}{p^*}\right)^2 + \frac{2\gamma+1}{6G_a} * \frac{q^*}{p^*}\right] \tag{I.19}$$

where p_a is the atmospheric pressure (p_a=100 kPa), K_a, G_a, γ and n are model parameters. K_a and G_a are related to the bulk and shear moduli, γ is the anisotropy coefficient and n is the non-linear coefficient. The new model showed a good agreement between the measured and modelling results, as shown in Figure I.19.

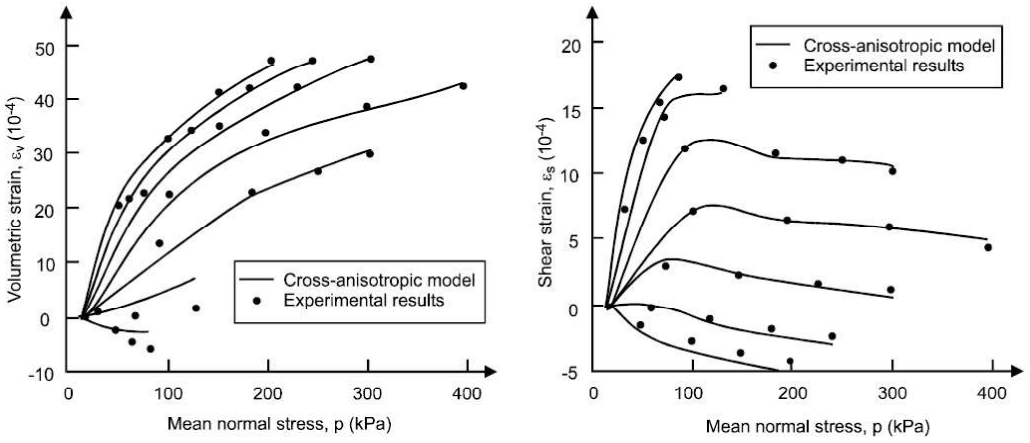

Figure I.19. Examples of fit using the improved Boyce model (Hornych et al., 1998).

Recently, Ezaoui et al. (2006) and Ezaoui and Di Benedetto (2008) have proposed another anisotropic model, the DBGSP model, to describe the anisotropic resilient behavior of UGM. According to the assumption of a transverse isotropic elastic behaviour, the strain increment and stress increment can be linked by the symmetric tensor $\underline{\boldsymbol{M}}$:

$$\underline{\Delta\varepsilon} = \underline{M} \cdot \underline{\Delta\sigma} \text{ <or> } \begin{pmatrix} \Delta\varepsilon_r \\ \Delta\varepsilon_r \\ \Delta\varepsilon_z \\ \sqrt{2}\cdot\Delta\varepsilon_{rz} \end{pmatrix} = \begin{pmatrix} \frac{1}{E_r} & \frac{-\nu_{rr}}{E_r} & \frac{-\nu_{rz}}{E_z} & 0 \\ \frac{-\nu_{rr}}{E_r} & \frac{1}{E_r} & \frac{-\nu_{rz}}{E_z} & 0 \\ \frac{-\nu_{rz}}{E_z} & \frac{-\nu_{rz}}{E_z} & \frac{1}{E_z} & 0 \\ 0 & 0 & 0 & \frac{1}{2G} \end{pmatrix} \cdot \begin{pmatrix} \Delta\sigma_r \\ \Delta\sigma_r \\ \Delta\sigma_z \\ \sqrt{2}\cdot\Delta\sigma_{rz} \end{pmatrix} \tag{I.20}$$

According to the theory proposed by Ezaoui et al. (2006) and Ezaoui and Di Benedetto (2008), the elastic parameters E_z, E_r and ν_{rz} can be expressed as:

$$E_z = \frac{\alpha}{P_{ref}^{\ n}} \cdot \sigma_z^{\ n} \tag{I.21}$$

$$E_r = \frac{1}{P_{ref}^{\ n}} \cdot \frac{\alpha}{\beta} \cdot \sigma_r^{\ n} \tag{I.22}$$

$$\nu_{rz} = \frac{\nu_0}{2} \cdot \left(1 + \beta \cdot \frac{\sigma_z^{\ n}}{\sigma_r^{\ n}}\right) \tag{I.23}$$

where P_{ref} is a constant equal to 1MPa, α, β, n, v_0 are model parameters. α is related to the Young modulus, β is the anisotropy coefficient, v_0 is related to the Poisson ratio. Then, axial strain increment $\Delta\varepsilon_1$ and the radial strain increment $\Delta\varepsilon_3$ can be expressed by the parameters α, β, n, v_0 and v_{rr} as following equations:

$$\Delta\varepsilon_1 = \frac{P_{ref}^{\ n}}{\alpha \cdot \sigma_z^{\ n}} \left(\Delta\sigma_z - \nu_0 \left(1 + \beta \frac{\sigma_z^{\ n}}{\sigma_r^{\ n}} \right) \Delta\sigma_r \right) \tag{I.24}$$

$$\Delta\varepsilon_3 = \frac{P_{ref}^{\ n}}{\alpha} \left(\frac{\beta(1-\nu_{rr})}{\sigma_r^{\ n}} \Delta\sigma_r - \frac{\nu_0 \left(1 + \beta \frac{\sigma_z^{\ n}}{\sigma_r^{\ n}} \right)}{2\sigma_z^{\ n}} \Delta\sigma_z \right) \tag{I.25}$$

Consequently, volumetric strain ε_v and the deviatoric strain ε_q can be obtained from $\Delta\varepsilon_1$ and $\Delta\varepsilon_3$. Figure I.20 shows an example fitted by DBGSP model, a good agreement between experimental data and simulation data can be obtained.

Appendix B also summaries other computational models summarized by Lekarp et al. (2000a). The modified Boyce model and DBGSP model will be discussed in detail in Chapter IV.

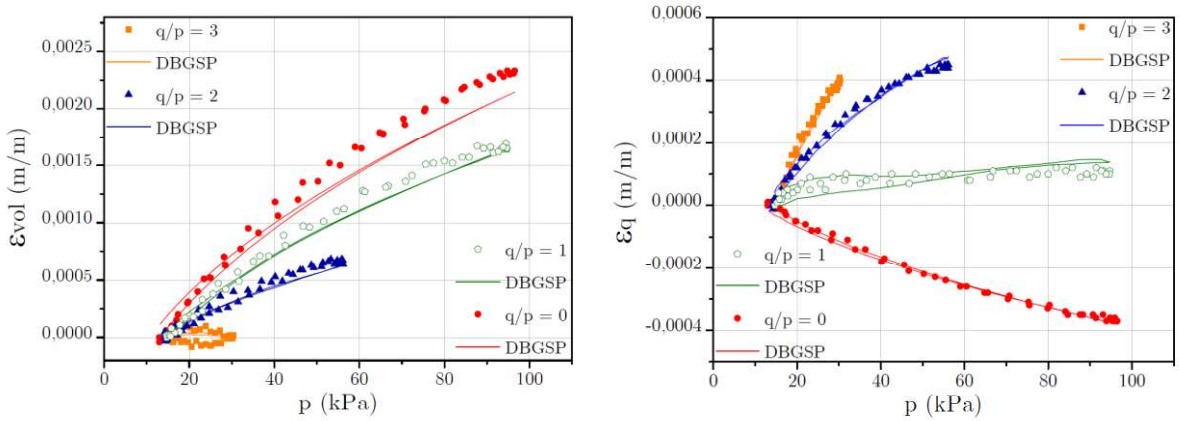

Figure I.20. Experimental data and simulation data with DBGSP model of volumetric strain ε_v and the deviatoric strain ε_q (Ezaoui & Di Benedetto, 2008).

I.3 Recycled concrete aggregates in unbound pavement

In Europe, over one third of the total wastes are construction and demolition wastes (CDW) (over 800 million tonnes in 2018) (Eurostat, 2018), in which concrete wastes are the main components and represent up to 75% of total CDW by weight (Nwakaire et al., 2020). Deposing CDW in landfills not only occupy a large land space, but also impose huge pressures on the environment. To overcome these problems, recycling and reuse of concrete wastes into pavement base and subbase layers has become a topic of global concerns in recent years (Lu et al., 2021; Saberian et al., 2018; Sobhan et al., 2016; Yaghoubi et al., 2018).

I.3.1 Physical properties of RCA

Recycled concrete aggregates (RCA) are produced by crushing demolition concrete wastes in recycling plant, composed of original natural aggregate (NA) ranging from 65% to 70% and mortar surrounding the natural particles ranging from 30% to 35% (Nwakaire et al., 2020), as shown in Figure I.21. Compared with the natural aggregate, the use of RCA has several social, environmental, and economic advantages. Consequently, the use of RCA for concrete production and pavement construction is quite popular in recent years (Cardoso et al., 2016).

Due to the presence of attached mortar, the porosity and water absorption of RCA are higher, while the density, strength and resistance to abrasion and fragmentation are lower, compared to that of NA (Belin et al., 2014; Deodonne, 2015), mainly depending on the properties of original concrete and the crushing method.

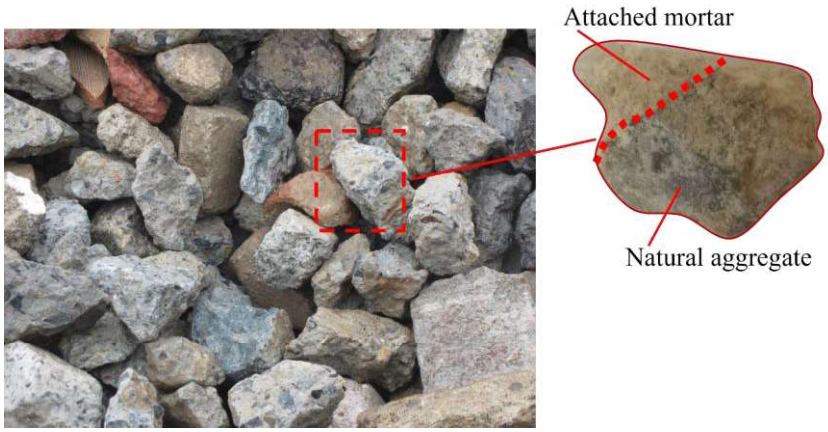

Figure I.21. Typical recycled concrete aggregates.

Porosity, density and water absorption

It was known that the attached mortar has a higher porosity, from 10% to 16%, than that of natural aggregates (NA), from 0% to 4% (Deodonne, 2015), as the mixing water reacted with cement and evaporated after the hardening of concrete. While the higher porosity results in a higher water absorption and lower density of RCA. As a result, porosity, density and water absorption of RCA are generally believed to be related with the mortar content (Deodonne, 2015). Table I.1 summaries the typical apparent density and water absorption of RCA and NA with different particle size (coarse and fine aggregate). It confirms that the density of RCA aggregate is generally lower than that of NA. However, it also depends on the quality of original concrete.

Table I.1. Typical density and water absorption of RCA and NA (Nwakaire et al., 2020).

Aggregate	Apparent density ρ_a/ (Mg/m^3)	Water absorption/%
Coarse RCA	2.54, 2.55, 2.67	3.2, 4.9, 5.6, 6.3
Coarse NA	2.29, 2.65, 2.71	0.2, 0.4, 0.46, 1.64
Fine RCA	2.64, 2.65, 2.68	3.4, 7.0, 11.63
Fine NA	2.57, 2.70, 2.72	0.4, 0.6, 2.06

As for the water absorption, the value of RCA (from 3.2% to 11.63%) is much higher than that of NA (from 0.2% to 2.06%) due to the attached mortar. It is reported that the water absorption of RCA ranges from 3% to 12%, while it is generally lower than 3% for NA (Belin et al., 2014;

Deodonne, 2015), which is in good agreement with Table I.1. The water absorption of calcareous or quartzitic aggregates can reach 3%, whereas it is close to 0.5% for granitic and basaltic aggregates (Pereira et al., 2009; Zega et al., 2010).

Since these properties of RCA, such as porosity, density and water absorption, are related to the mortar content, many researchers (Deodonne, 2015; Mefteh et al., 2013; Zhao et al., 2013) try to establish the relationship between attached mortar content with these properties. It was found that the cement paste content increases with the decreasing particle size (Zhao et al., 2013), as illustrated in Figure I.22, which was reported also by other researchers (Juan & Gutierrez, 2009). Figure I.23 depicts the relationship between cement paste content and the density and water absorption of three different RCA materials, showing density of RCA decreases, while water absorption increases with the increasing cement paste content. However, this conclusion is only suitable for the same RCA as these properties also highly depend on the property of original concrete. Thus, the water absorption of fine RCA aggregates was higher than the coarse aggregates, as can be seen in Table I.1.

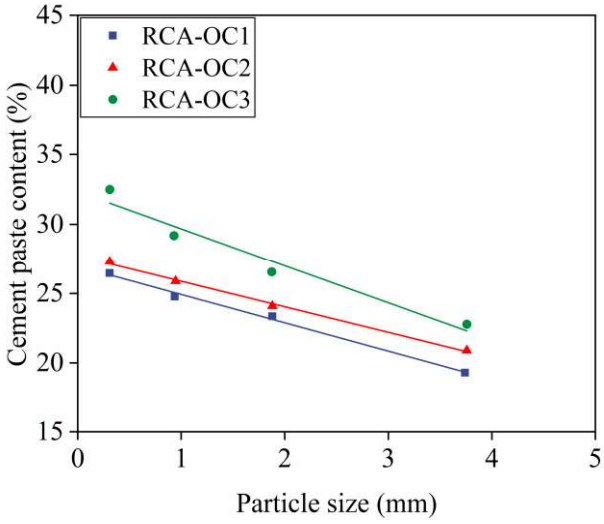

Figure I.22. Relationship between particle size and cement paste content for different RCA materials (Zhao et al., 2013). (Note: OC1, OC2 and OC3 are 3 different RCA)

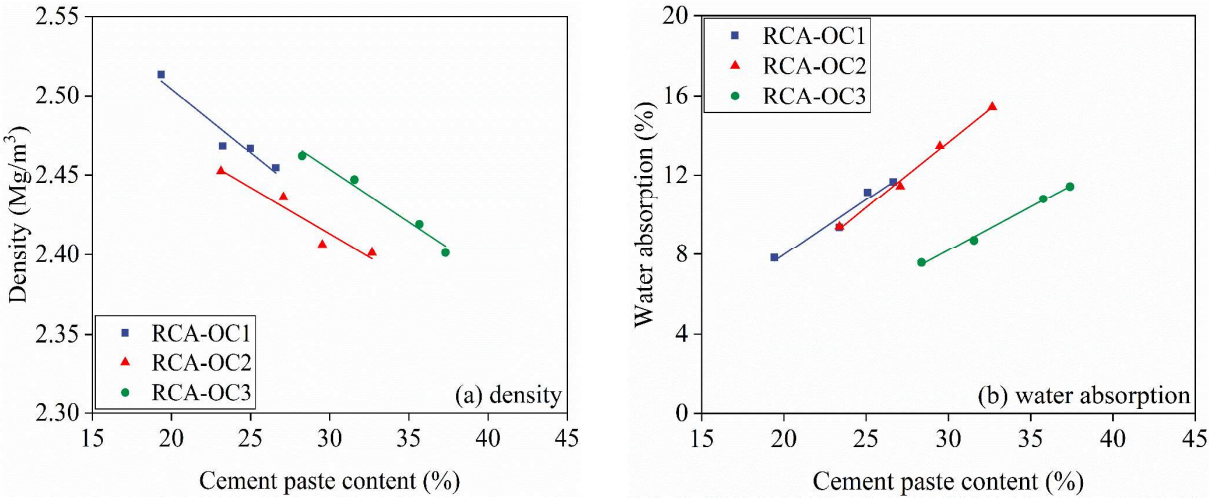

Figure I.23. Relationship between cement paste content and density and water absorption of different RCA materials: (a) density and (b) water absorption (Zhao et al., 2013).

Resistance to abrasion and fragmentation

Micro-Deval coefficient (NF EN 1097-1, 2011) and Los Angeles coefficient (NF EN 1097-2, 2020) are frequently used to determine the resistance of aggregates to abrasion and fragmentation. As other physical properties, such as density and water absorption, the resistance of RCA aggregates to abrasion and fragmentation are also influenced by the attached mortar content. Figure I.24. depicts the relationship between mortar content and Los Angeles coefficient of different RCA materials (Akbarnezhad et al., 2013). It shows that the Los Angeles coefficient increases with the attached mortar content as the resistance of mortar to fragmentation is weaker than that of natural aggregates (NA). However, these properties are also strongly influenced by the properties of original concrete and the crushing method. Generally, the resistance of RCA aggregates to abrasion and fragmentation are weaker than these of NA due to the presence of attach mortar and the interfacial transition zone (ITZ) between the attached mortar and original NA (Deodonne, 2015; Zhao, 2014).

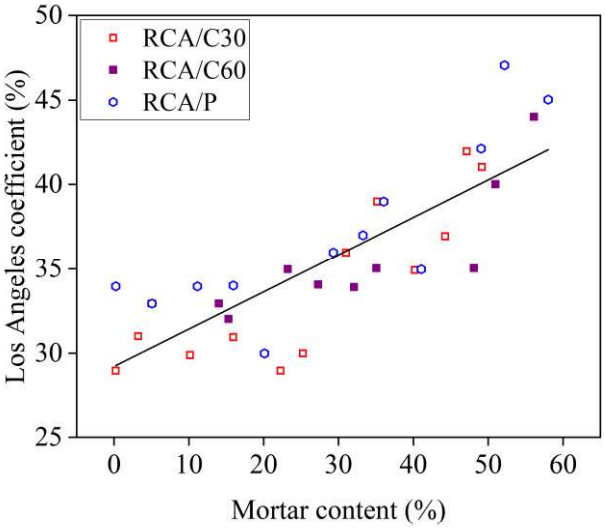

Figure I.24. Relationship between mortar content and Los Angeles coefficient of different RCA materials (Akbarnezhad et al., 2013).

Water absorption kinetics

It was known that the water absorption of RCA ranges from 3% to 12%, while it is generally lower than 3% for natural aggregates (NA). Many researchers (Deodonne, 2015; Tegguer, 2012) observed that the saturation time of RCA to reach a saturation state is generally longer, may be higher than 24 hours, than that of NA. Deodonne (2015) concluded that the water absorption of RCA after soaked 24 h ranges from 60% to 95%, depending on the attached mortar content and particle size. Solyman (2005) observed that RCA absorbs most of water , around 80%, in first 10 minutes when RCA were immersed in the water, in agreement with Tegguer (2012). As a consequence, the amount of water absorbed during mixing or compaction of RCA specimen shall be strongly different and depends on the water absorption kinetics of RCA. If the RCA were not saturated before mixing or compaction, aggregates could absorb free water during RLTT, which could influence the mechanical behaviour of RCA as water content has a big influence on RLTT result.

Many studies have been conducted to study the influence of water absorption on the workability of concrete prepared with RCA (Mefteh et al., 2013; Poon et al., 2004). However, little studies could be found on the influence of water absorption on the pavement constructed with RCA (Wang et al., 2022).

I.3.2 Mechanical behaviour of RCA

Although the physical properties of most RCA are not so good as those of natural aggregates, numerous studies have been conducted to study the mechanical behaviour of RCA as an unbound granular material (UGM) in pavements over the past years (Arm, 2001; Bestgen et al., 2016; Gabr & Cameron, 2012; Lu et al., 2021; Soleimanbeigi et al., 2015; Yaghoubi et al., 2018). In general, the overall conclusions are that the performance of most RCA materials is comparable to that of natural aggregates (NA).

Arulrajah et al. (2013) studied the effect of water content on permanent deformation and resilient modulus of RCA, crushed brick (CB) and waste excavation rock (WR). The results show that the permanent deformation increases while resilient modulus decreases with the increase of water content, in agreement with the UGM. However, for RCA under dry state, the permanent deformation and resilient modulus are less influenced by water content due to the high water absorption of RCA, as shown in Figure I.25. Besides, the performance of RCA was found to be superior to other recycled materials and even NA since RCA presents the lowest permanent deformation than that of other recycled materials. Similar observation was observed by other researchers (Azam & Cameron, 2013; Gabr et al., 2013; Gabr & Cameron, 2012; Jayakody et al., 2019).

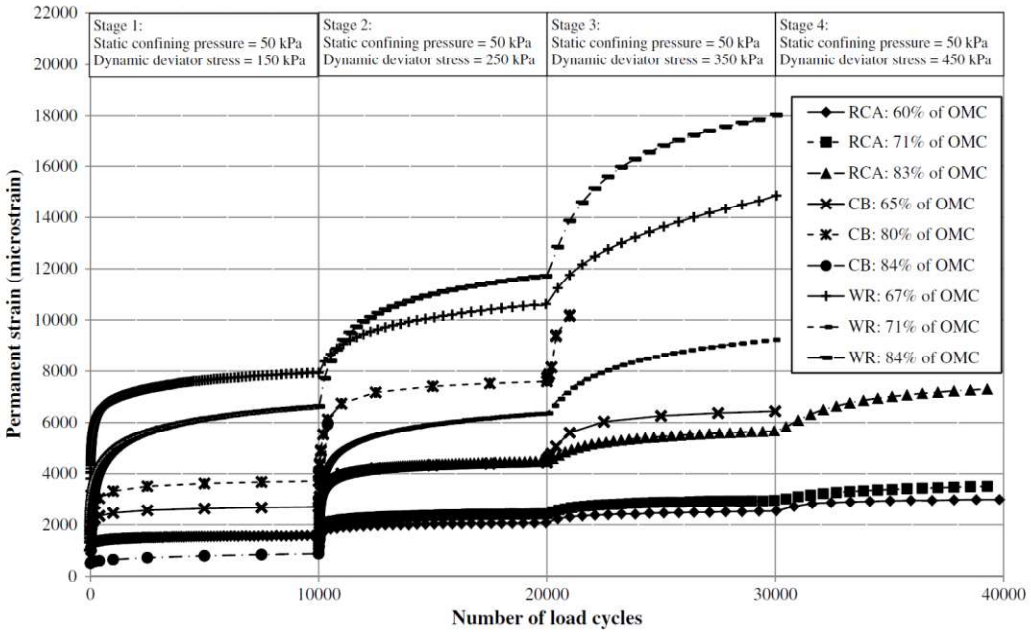

Figure I.25. Permanent deformation of RCA, CB and WR at different water content (Arulrajah et al., 2013).

Gabr and Cameron (2012) studied the permanent deformation and resilient modulus of two RCA materials and one quartzite aggregates. Results indicate that RCA materials obtained from different sources have different permanent deformation and resilient modulus. However, their performance were both superior to that of quartzite aggregates.

Arulrajah et al. (2014) has studied the shear behaviour of RCA by monotonic triaxial tests. Results show that RCA materials exhibit strain-softening behaviour, whose shear stress decreases after peak shear strength, which is a typical shear response for UGM. Besides, the effective friction angles at the peak state of RCA are 53°, while the peak apparent cohesion is very low.

In recent years, it is quite popular to mix RCA with other waste materials (Azam & Cameron, 2013; Lu et al., 2021; Saberian et al., 2018), such as recycled clay masonry (RCM), recycled asphalt pavement (RAP), crushed brick (CB), crushed rock (CR) and even crumb rubber. However, the performance of these mixtures highly depends on the type and amount of additives.

I.4 Self-cementing properties of RCA

I.4.1 The influence of self-cementing properties

It is well known that concrete structures contain partial unhydrated cement even after long term service (Lin & Meyer, 2009; Mills, 1966). However, the crushing process to produce recycled concrete aggregates (RCA) can expose these unhydrated cement particles (Amin et al., 2016). Subsequently, when RCA are used in pavement unbound base and subbase layers, these unhydrated cement could hydrate with moisture and create bonds between particles, increasing the strength and stiffness of pavement and gradually turning unbound layers to the partially bound layers, known as self-cementing properties of RCA. However, this behaviour is not observed with unbound granular materials (UGM).

Arm (2001) conducted repeated load triaxial tests on both RCA and UGM (crushed granite) after curing 1 and 60 days. It was found that the resilient modulus of RCA increases with curing time, while that of UGM (crushed granite) is constant, as seen in Figure I.26. Furthermore, field tests (Falling Weight Deflectometer test) on three different pavement sites prepared by RCA were also conducted, as shown in Figure I.27. FWD results reveal that the stiffness growth of

unbound RCA layer is largest in the first months and then diminishes, the continuous growth of stiffness can be observed even after 2 years.

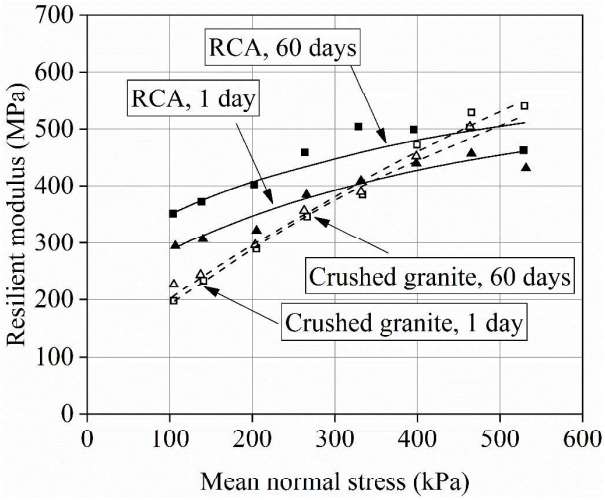

Figure I.26. Comparison of resilient modulus from repeated load triaxial tests on granite and RCA after curing 1 and 60 days (Arm, 2001).

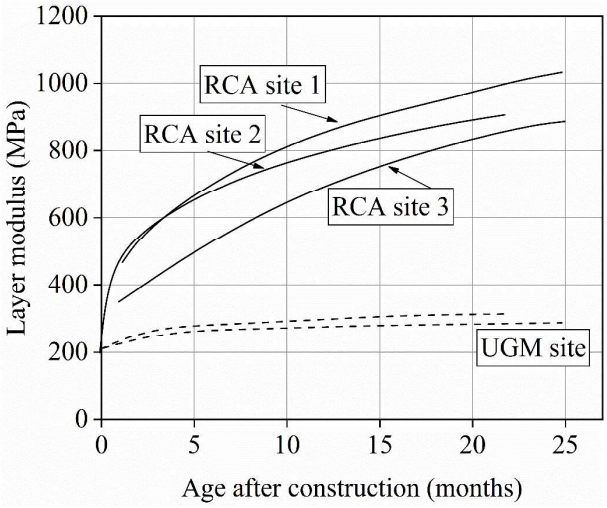

Figure I.27. Back-calculated layer moduli for unbound layers of RCA and UGM (Arm, 2001).

Jitsangiam et al. (2015) studied the resilient modulus of two RCA materials both sourced from same high strength concrete structure: 100% RCA (HRCA) and the mixture of 95% HRCA and 5% brick (RBRCA), after curing 1, 90 and 180 days. They observed that the resilient modulus of HRCA increases steadily till the studied curing time (180 days), while that of RCA mixed with brick (RBRCA) increases until 90 days. The resilient modulus was also modelled by k-θ model (Seed et al., 1967), with the parameters summarized in Table I.2. The results show that the self-cementing properties increase resilient modulus while decrease the stress dependency

of both two RCA materials, since parameter k_1 increases while k_2 decreases with curing time. The scattered data of HRCA curing 180 days, indicated by high R^2, revealing the unbound HRCA specimen would transform into bound specimen, as the stress dependency was not the property of bound materials. Similar results were also observed by Batmunkh et al. (2010).

Paige-Green (2010) measured the unconfined compressive strength (UCS) and pH value of 15 different RCA materials, sourced from different locations, after curing 28 and 56 days. Figure I.28 depicts UCS, after curing 28 and 56 days, and pH values of these 15 different RCA materials. He pointed out that the RCA with high pH value (above 9.5), showing self-cementing properties as UCS increases with curing time. Blankenagel et al. (2006) also found the UCS of RCA increases with curing time. In fact, pH value can not be related to the self-cementing properties of RCA directly. High pH value implies more soluble alkaline hydration products, suggesting that the RCA were not completely carbonated and may contain some unhydrated cement. Still, many scholars use pH value to evaluate the self-cementing properties as it can be measured easily and quickly (Bestgen et al., 2016; Kim et al., 2014; Poon et al., 2006; Rudman, 2019).

Table I.2. Regression parameters for resilient modulus of HRCA and RBRCA (Jitsangiam et al., 2015).

Materials	Curing days	Regression parameters		
		k_1	k_2	R^2
HRCA	1	6.9	0.792	0.982
	90	98.5	0.399	0.975
	180	305.6	0.265	0.560
RBRCA	1	3.0	0.934	0.982
	90	61.2	0.464	0.977
	180	69.2	0.462	0.935

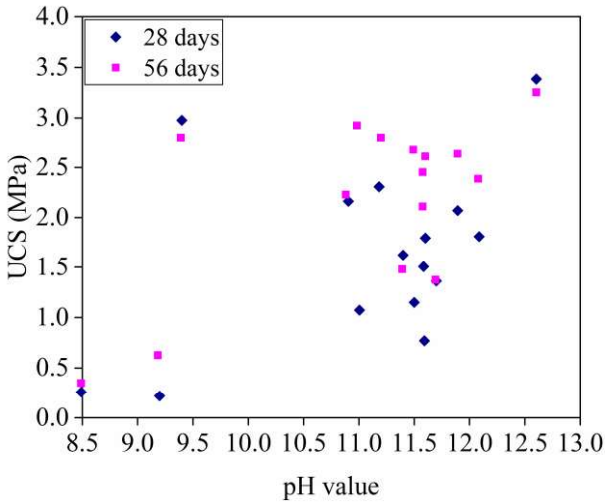

Figure I.28. Relationship between UCS and pH value for 15 RCA materials (Paige-Green, 2010).

I.4.2 Unhydrated cement content

Self-cementing properties of RCA can be ignored for cementitious matrix in new concrete, while it is important when used as unbound granular materials in pavement. Many methods were adopted to evaluate the self-cementing properties of RCA in the past years, such as pH value, thermogravimetric analysis (TGA), X-ray diffraction (XRD) analysis, semi-adiabatic calorimeter tests and scanning electron microscope (SEM) (Amin et al., 2016; Bestgen et al., 2016; Bordy et al., 2017; Kim et al., 2014; Oksri-Nelfia et al., 2016; Poon et al., 2006; Prosek et al., 2020), while the assessment of residual unhydrated cement content, the cause of self-cementing properties, has been rarely studied.

As the attached mortar content increases with the decreasing particle size, Poon et al. (2006) pointed out that the unhydrated cement in fine aggregates (0-0.6 mm) are most likely the principal cause of self-cementing properties, since these aggregates show higher pH value and the unhydrated cement was detected by X-ray diffraction analysis (XRD), as shown in Figure I.29 and Figure I.30. Besides, fine aggregates could play a more important role, like cement powder, forming bonds between particles, turning unbound specimens to bound specimens. Furthermore, the unhydrated cement in fine aggregates are early hydrated since fine aggregates has a larger specific surface area, suggesting that long-term storage of RCA could reduce self-cementing properties. This was confirmed by Kim et al. (2014), by conducting pH value measurement test and semi-adiabatic calorimeter test on the RCA after long term storage in an open stockpile with high relative humidity.

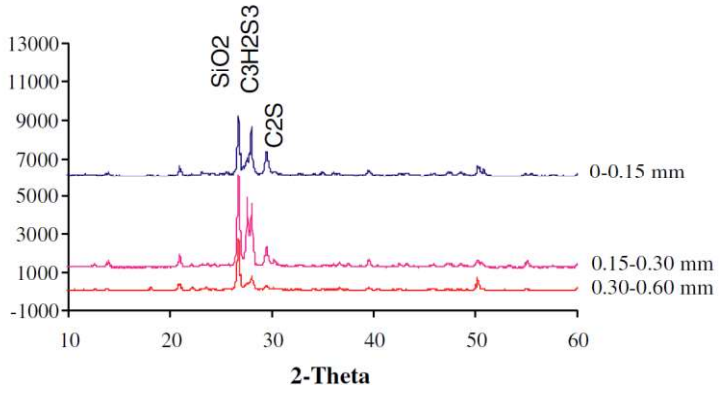

Figure I.29. X-ray diffraction patterns of different size fractions of fine RCA (Poon et al., 2006) (Note: C_2S is one of the compositions of cement, representing the presence of unhydrated cement in RCA).

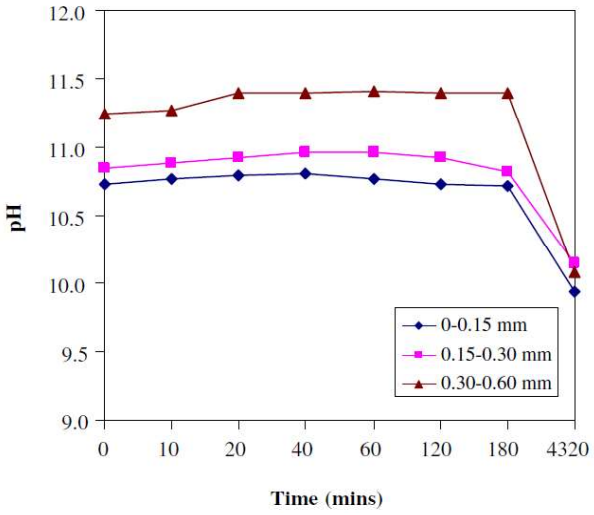

Figure I.30. pH values of different size fractions of fine RCA (Poon et al., 2006).

As mentioned above, several methods, such as pH value, thermogravimetric analysis (TGA), X-ray diffraction (XRD) analysis, semi-adiabatic calorimeter tests and scanning electron microscope (SEM) were adopted to evaluate the self-cementing properties of RCA in the past years. Among these methods, pH value was used frequently as it can be measured easily and quickly (Bestgen et al., 2016; Kim et al., 2014; Paige-Green, 2010; Poon et al., 2006; Prosek et al., 2020; Rudman, 2019). In fact, high pH value implies more soluble alkaline hydration products, suggesting that the RCA were not completely carbonated and may contain some unhydrated cement. Paige-Green (2010) revealed that the RCA with pH value higher than 11 exhibits self-cementing properties, while RCA with lower pH value show negligible self-cementing properties.

Thermogravimetric analysis (TGA) is favored by some researchers to evaluate the self-cementing properties since it can do the quantitative analysis (Bordy et al., 2017; Oksri-Nelfia et al., 2016). According to the TGA results, some cement hydration products, such as portlandite ($Ca(OH)_2$), calcite ($CaCO_3$) and bound water, can be determined. Then, the unhydrated cement content can be calculated according to the stoichiometry of cement hydration. Oksri-Nelfia et al. (2016) measured the $Ca(OH)_2$ content of RCA crushed from a 5 years old concrete, by TGA. Afterwards, the unhydrated cement content, 2.3%, was calculated from the $Ca(OH)_2$ content. Bordy et al. (2017) proposed another calculation method based on bound water which was obtained also from TGA results. The results show that the unhydrated cement content of a laboratory-made cement paste is 24%, much higher than the value of RCA (2.3%) reported by Oksri-Nelfia et al. (2016). Note that the unhydrated cement content in concrete depends on several factors, such as cement paste content, age, service environment and composition of concrete.

Semi-adiabatic calorimeter test is another frequently used method to evaluate self-cementing properties of RCA (Amin et al., 2016; Bordy et al., 2017; Deodonne, 2015; Kalinowska-Wichrowska et al., 2020; Kim et al., 2014; Oksri-Nelfia et al., 2016; Prosek et al., 2020; Wang et al., 2018), by measuring the released heat or temperature due to the hydration of unhydrated cement. Deodonne (2015) measured the hydration temperature of 6 different RCA materials (GR1-6), with full particle size (s+g) and coarse aggregates (g), depicted in Figure I.31. It shows that the increased temperatures, depending on the self-cementing properties of RCA, are lower than 3 °C for these RCA materials. Furthermore, he also found that both fine and coarse RCA can release heat and hydrated with water, as the temperature of coarse RCA (GR5 (g)) also increases. Bordy et al. (2017) also measured the temperature of RCA crushed from a fresh laboratory-made concrete (curing 90 days). Results also show that the increased temperatures are around 3 °C.

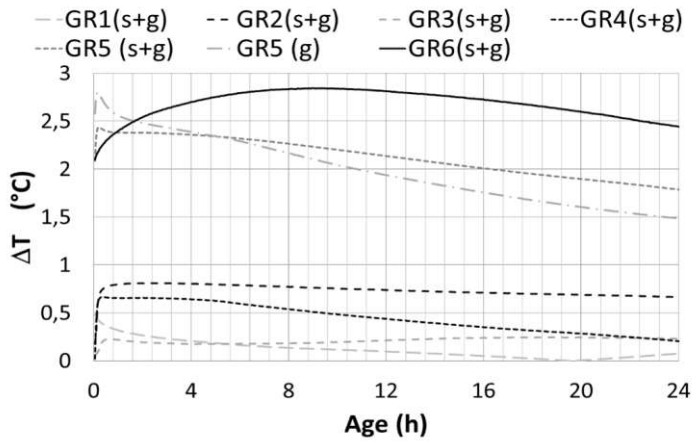

Figure I.31. Rehydration temperatures of 6 different RCA (GR1-6) measured by semi-adiabatic calorimeter test (Deodonne, 2015). (Note that "s" is fine, "g" is the coarse aggregate)

X-ray diffraction (XRD) analysis was also used to detect the existence of unhydrated cement (Bordy et al., 2017; Kim et al., 2014; Poon et al., 2006). Figure I.32 depicts the comparison of X-ray diffraction patterns between cement and a laboratory-made recycled cement paste fines (RCPF), crushed from a 89 days old fresh cement paste, reported by Bordy et al. (2017). It shows the unhydrated cement, composed by dicalcium silicate (C_2S), tricalcium silicate (C_3S) and tricalcium aluminate (C_3A), was observed by XRD analysis. However, unlike cement paste, RCA was crushed from the demolition concrete waste after long term service, whose cement paste content was much lower that of pure cement paste, resulting in a much lower unhydrated cement content than that of pure cement paste. Thus, it could be difficult to detect the existence of unhydrated cement in RCA (Jitsangiam et al., 2015; Kim et al., 2014; Poon et al., 2006).

Among these methods, scanning electron microscope (SEM) analysis was rarely adopted for RCA. The polishing process means that this method is more suitable for concrete, instead of crushed RCA whose surface is not flat and difficult to be polished. Besides, the hydration of unhydrated cement during polishing and the accuracy of this method is another drawback. Figure I.33 shows the treatment process of SEM image to quantify the unhydrated cement content, by calculating the area of unhydrated cement, presented as white in Figure I.33 (c).

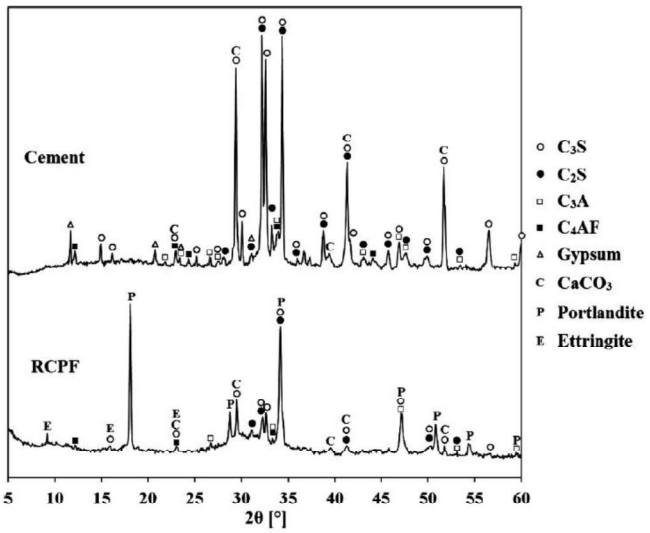

Figure I.32. X-ray diffraction patterns of the Portland cement and recycled cement paste fine (RCPF) (Bordy et al., 2017).

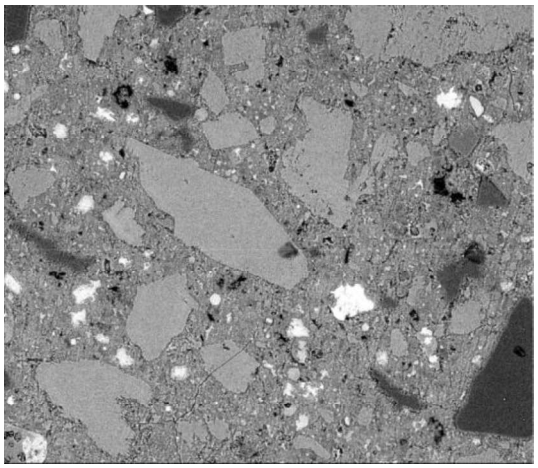

(a) SEM of concrete

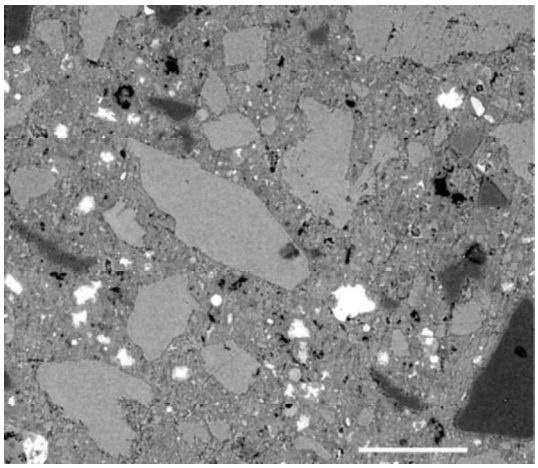

(b) Filtered image of concrete

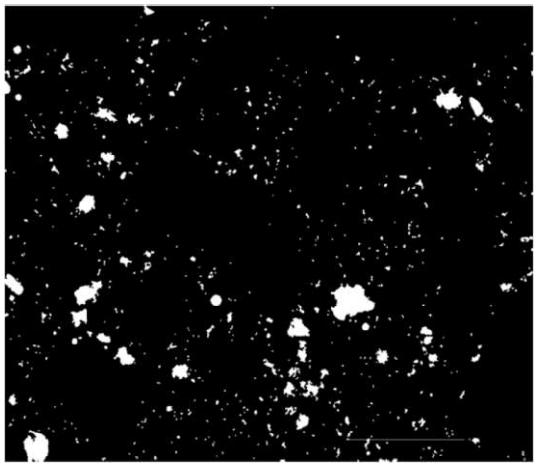

(c) Binary image of unhydrated cement

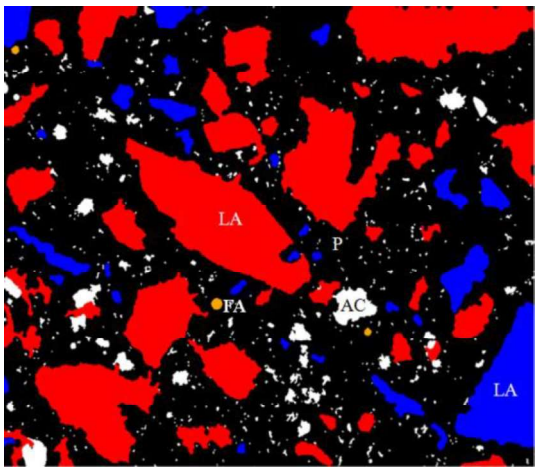

(d) Reconstructed image of concrete

Figure I.33. Treatment of SEM image (Oksri-Nelfia et al., 2016).

I.5 Conclusion

In this chapter, we introduced the important role of unbound granular materials (UGM) in flexible pavement. The mechanical behavior of UGM under repeated loading was presented. Based on the literature review, it can be concluded that the permanent deformation behaviour of UGM is influenced by many factors, such as stress level, stress history, principal stress rotation, number of loading cycles, density, fine content, particle size distribution, aggregate type, water content and suction.

Similarly, the resilient deformation behaviour of UGM is influenced by some factors such as stress, fine content and water content, density, type of aggregates. Other factors such as stress history, number of loading cycles and particle size distribution are generally considered to be minor significance. Some models based on resilient modulus, resilient volumetric strain and resilient deviatoric strain are summarized. As a substitution of UGM, the permanent deformation and resilient deformation behaviours of recycled concrete aggregates (RCA) are also influenced by these factors.

The physical and mechanical behaviour of RCA were also introduced. From the literature review, it can be observed that RCA have higher porosity and water absorption, while lower density, strength and resistance to abrasion and fragmentation, compared to these of natural UGM due to the attached mortar, which limits the application of RCA in pavements. However, RCA generally has an angular shape and rough surface due to the crushing process and attached mortar. As a result, the performance of most RCA materials is comparable to that of natural UGM.

An increase of strength and stiffness of unbound pavement layers built with RCA can be observed, known as self-cementing properties of RCA, which is not observed on UGM. Self-cementing properties is believed to be primarily caused by the unhydrated cement in RCA. Many methods can be used to evaluate self-cementing properties of RCA, such as pH value, thermogravimetric analysis (TGA), X-ray diffraction (XRD) analysis, semi-adiabatic calorimeter tests and scanning electron microscope (SEM).

In the following chapter, the physical properties of our studied materials are studied. The process to study self-cementing properties, microstructure and mechanical behaviour under monotonic and repeated load triaxial test after curing are introduced.

Chapter II. Material study and laboratory testing

This chapter first presents the sources and physical properties of the three studied RCA materials, namely NRCA, ORCA and RCAP. The water absorption kinetic of RCA was also studied. Then, three methods to evaluate the self-cementing properties of RCA by pH value measurement, calorimeter tests and thermogravimetric analysis (TGA) were introduced. After that, scanning electron microscopic analysis (SEM) and mercury intrusion porosimetry (MIP) tests were presented to study the influence of self-cementing properties on the microstructure of RCA. In the end, monotonic triaxial tests and repeated load triaxial tests (RLTT) were presented to study the short and long-term mechanical behaviour of RCA, including sample preparation and curing, experimental device and experimental procedures.

II.1 Materials and physical properties

Materials

As the aim of this study is to work with RCA issued from real industrial recycling plants, it was not chosen to use RCA casting and curing in the laboratory with a known component. Thus, three RCA materials, sourced from concrete buildings and concrete pavement, were obtained from three different recycling plants in France, to represent different type of RCA materials, as shown in Figure II.1.

- NRCA and ORCA were both sourced from demolished buildings, obtained from different recycling plants. NRCA was crushed at the beginning of the study in 2020 (New RCA) at a recycling plant in Strasbourg, France, while ORCA was crushed in 2012 (Old RCA) at a recycling plant in Gonesse, France, and stored outdoor in big plastic bags to prevent humidity variations and carbonation. The long-term storage was expected to largely reduce the self-cementing properties of ORCA (Kim et al., 2014), as the unhydrated cement can hydrate during storage. Thus, the self-cementing properties of the two RCA (NRCA and ORCA) can be better compared.
- RCAP was sourced from a demolished concrete highway pavement (RCAP), located in the region of Alsace, France. RCAP was also crushed at the beginning of the study in 2020 at another recycling plant in Strasbourg, France.

Since those concrete wastes come from different recycling plants and are a mix of wastes from different old structures, any details such as strength and composition of the initial concrete are

unknown. Therefore, these materials can represent a general condition of RCA materials. The unknown concrete wastes were crushed by impact crushers in recycling plants. Only one crushing cycle was carried out for each type of concrete waste. Note that the original natural aggregates (NA) of all concrete wastes were all sourced from Alsace, France, where aggregates generally have the same mineralogical compositions (silicic-calcareous aggregates).

Figure II.1. Studied RCA materials: (a) NRCA; (b) ORCA; (c) RCAP

Particle size distribution

After crushing, RCA materials were sieved and divided into three particle size fractions (<4 mm, 4-10 mm and 10-20 mm) in these recycling plants, and then stored in the laboratory with plastic bags to protect them from carbonation. A well-graded granular materials can provide more points of contact and thus improve the mechanical properties and cementation effect of residual unhydrated cement in RCA (Consoli et al., 2012). To increase the effectiveness of cementation effect and to represent the standard 0-20mm unbound granular materials, three RCA were reconstituted to a same grading curve close to the mean value of the upper and lower limits of the specifications of European Standard NF EN 13285 (2018), as shown in Figure II.2.

The particle size distributions of the three RCA materials before and after compaction, for sample preparation, are also shown in Figure II.2. The "after compaction" grading curves show that weak particle breakage has occurred during the mixing and compaction, and thus increases the fines content. Before compaction, the fines (passing 63 μm sieve) content were 2.1%, 2.2% and 5.3% for NRCA, ORCA and RCAP, respectively. After compaction, the fines content increased to 4.6%, 5.2% and 6.4%, respectively, as presented in Table II.1. However, a lower increase of fines content of RCAP was observed in comparison to NRCA and ORCA, indicating a smaller mortar content of RCAP since the strength of mortar is lower than that of natural aggregates. Note that the breakage of weak particles can also release more effective unhydrated

cement as self-cementing properties are mainly influenced by the fine portions (Poon et al., 2006).

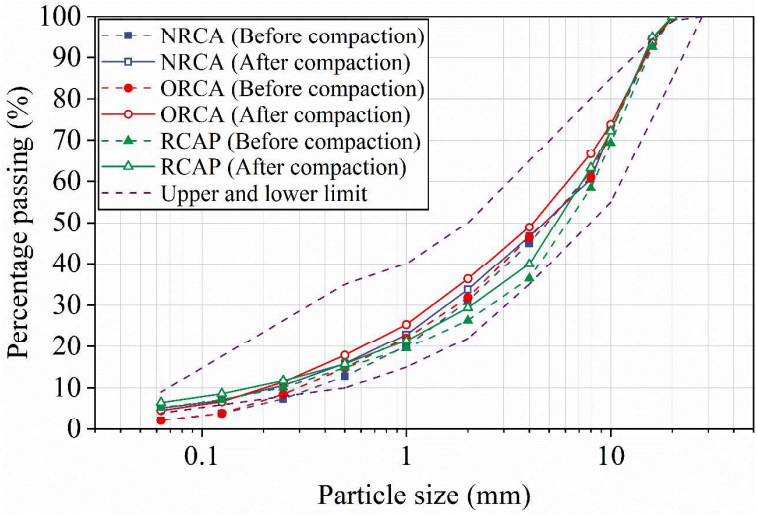

Figure II.2. Particle size distributions of RCA materials.

Table II.1. Physical properties of all RCA materials.

Properties		NRCA	ORCA	RCAP	Standard
Apparent density	coarse (10-20 mm)	2.65	2.57	2.69	NF EN 1097-6 (2014)
ρ_a (Mg/m^3)	sand (4-10 mm)	2.66	2.61	2.66	
	fine (1-4 mm)	2.60	2.66	2.59	
Water absorption	coarse (10-20 mm)	4.64	4.30	2.56	NF EN 1097-6 (2014)
WA_{24} (%)	sand (4-10 mm)	5.81	5.19	3.21	
	fine (1-4 mm)	10.86	8.65	7.00	
Fines content before compaction (< 63 µm) (%)		2.1	2.2	5.3	NF EN 933-1 (2012)
Fines content after compaction (< 63 µm) (%)		4.6	5.2	6.4	
Rounded particles content (%)		4.1	1.1	15.1	NF EN 933-5 (1998)
Crushed particles content (%)		95.9	98.9	84.9	
Los Angeles coefficient (%)		30.8	32.2	24.5	NF EN 1097-2 (2020)
Micro-Deval coefficient (%)		21.6	21.3	17.9	NF EN 1097-1 (2011)
Water-soluble sulfate content (%)		0.23	0.13	0.08	NF EN 1744-1 (2014)

Apparent density

As any properties of parent concrete of RCA, such as strength and composition, are unknown, the physical properties of RCA after crushing were carefully studied. Table II.1 summarizes the main physical properties of these RCA materials. It appears that the apparent particle density

of these RCA materials is similar to that of natural aggregates (NA), as observed also by other researchers (Nwakaire et al., 2020). Generally, NA have a higher density than that of RCA due to the attached mortar. However, that also depends on the properties of original concrete wastes and on the crushing method.

Water absorption

The water absorptions of NRCA and ORCA, saturated for 24 h (WA_{24}), are larger than those of RCAP and natural aggregates (NA), for all tested fractions (1-4 mm, 4-10 mm, 10-20 mm). It is reported that the water absorption of RCA is strongly influenced by the particle size and attached mortar content, ranging from 3% to 12%, while it is generally lower than 3% for NA (Belin et al., 2014; Deodonne, 2015), which is in good agreement with this study. The water absorption of calcareous or quartzitic aggregates can reach 3%, whereas it is close to 0.5% for granitic and basaltic aggregates (Pereira et al., 2009; Zega et al., 2010). The difference of water absorption between RCA and NA is mainly due to the presence of attached mortar, showing that RCAP has a lower attached mortar content.

Resistance to abrasion and fragmentation

The Los Angeles coefficient (LA) and Micro-Deval coefficient (MDE), defined as the percentage of the mass of the test portion (coarse aggregates between 10 mm and 14 mm) passing the 1.6 mm sieve after the test, were used to determine the resistance of aggregates to fragmentation and wear. It can be observed that LA and MDE of RCAP are smaller than those of NRCA and ORCA, revealing a better resistance to fragmentation and wear of RCAP. These results could be related again to the low mortar content of RCAP, because the mortar has a lower resistance to crushing than the rock particles. This is also in accordance with water absorption. In addition, LA, MDE and water-soluble sulfate content (SS) were compared with European Standard NF EN 13285 (2018) and the French national and regional technical guides (CETE de l'Est, 2009; UNICEM IDF, 2003) used for RCA in pavements. The main properties of these RCA materials were found within the specified limits (LA≤40, MDE≤35 and SS≤0.7%). The grading curves after compaction also fulfil the requirements of RCA for a pavement base course. As a result, these RCA materials can be used in pavement base and subbase layers.

Modified Proctor compaction curves

The Modified Proctor compaction curves of the three RCAs are presented in Figure II.3. The optimum moisture contents (OMC) of all RCA materials are significantly higher than most of

NA, which are typically in the range of 4 % to 6 %, as observed also by other researchers (Arulrajah et al., 2012; Bestgen et al., 2016; Gabr & Cameron, 2012). Besides, the OMC of NRCA and ORCA are higher than that of RCAP. The compaction curves of NRCA and ORCA are flatter, implying that NRCA and ORCA are less sensitive to water in comparison to RCAP. This higher OMC and less sensitive behavior can be attributed to their higher water absorption as shown in Table II.1.

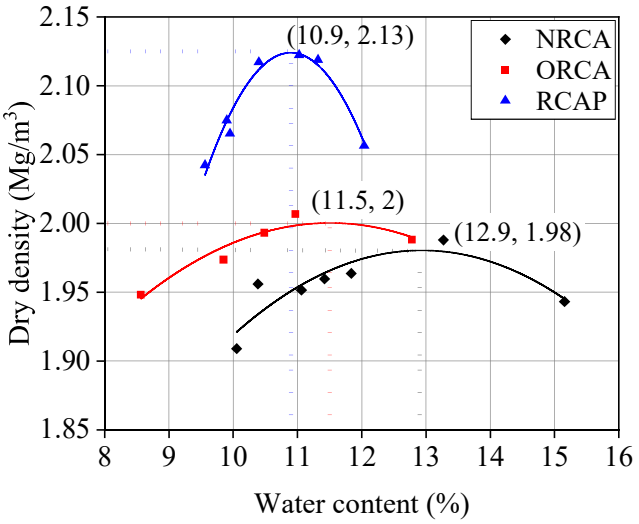

Figure II.3. Modified Proctor curves of RCA materials.

Particle shape

Coarse RCA typically have a more angular shape and rougher surface texture than NA, as a result of the crushing process and attached mortar on the surface of RCA (Bestgen et al., 2016; Kuo et al., 2002). According to European standard NF EN 933-5 (1998), the rounded particles are defined as particles with more than 50 % of rounded surface, which can be sorted out by hand. However, as presented in Table II.1, RCAP presented a much higher percentage of rounded particles (15.1%) than those of NRCA (4.1%) and ORCA (1.1%). It should be noted that the attached mortar content and RCA shape are influenced by the crushing process and the properties of concrete wastes (strength and rounded aggregates content). In the case of concrete structures with a high amount of original rounded particles and low strength, the attached mortar can separate from the rounded particles during the crushing process, leading to a smaller mortar content and a lower water absorption. Since the crushing process for the three RCA was similar, the higher percentage of rounded particles of RCAP can be attributed to the low strength of the parent concrete and high amount of rounded aggregates.

To conclude, RCAP has a higher fine content before compaction, and the compaction has no significant influence on increasing fine content, compared with that of NRCA and ORCA. Besides, the water absorption, optimum moisture content, LA and MDE of RCAP are also lower, while rounded particle content is higher, than those of NRCA and ORCA. These results both indicate that the parent concrete of RCAP has a lower strength and high amount of rounded aggregates, and RCAP contains less attached mortar on the aggregates after crushing.

In general, the design compressive strength of concrete for pavements in France is smaller than that for buildings. In addition, the compressive strength of concrete for pavements varies more largely than that for buildings. For example, the recommend compressive strength of roller compacted concrete which is widely used in concrete pavements in France is 20 MPa (Mathias et al., 2009; Selvam et al., 2022), and the compressive strength of pervious concrete which is increasingly used in pavements in urban areas ranges from 3.4 to 27.5 MPa, while it varies between 24 to 34 MPa for typical concrete used for buildings (Debnath & Sarkar, 2020). As a result, the strength of parent concrete of RCAP could be smaller than that of NRCA and ORCA, leading to a smaller mortar content, higher fines content and higher percentage of rounded particles of RCAP after the crushing process, which is in good agreement with the physical properties of the three RCA materials. However, we must mention that these properties fulfil the requirements of RCA for a pavement base course (CETE de l'Est, 2009; NF EN 13285, 2018; UNICEM IDF, 2003).

II.2 Water absorption kinetics

For the repeated load triaxial test, European Standard NF EN 13286-7 (2004) demands to store the mixture of unbound granular materials for 24 h before compaction to achieve a uniform water content. Whereas previous studies revealed that more than 24 h are required to saturate coarse RCA due to the larger water absorption and the presence of mortar (Deodonne, 2015; Tam et al., 2008; Tegguer, 2012). If coarse RCA aggregates are not fully saturated during storage, some of the free water could be absorbed by the aggregates during the test and this could influence the experimental results. To assess whether the standard procedure for specimen preparation (NF EN 13286-7, 2004), storing the mixture for 24 h for moisture homogenization, is appropriate for RCA, the hydrostatic weighing method was used to measure the water absorption kinetics (Belin et al., 2014; Tegguer, 2012), as shown in Figure II.4.

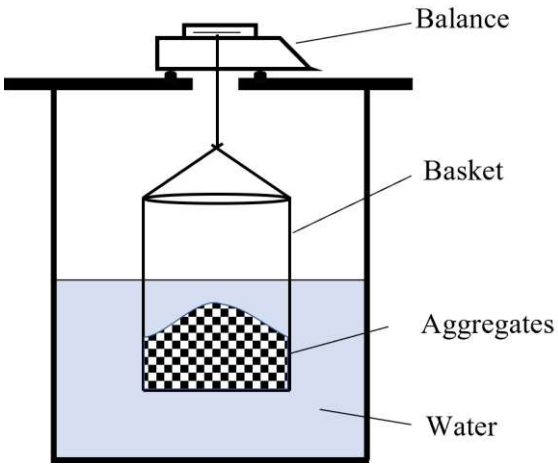

Figure II.4. Principle of the hydrostatic weighing method.

For each RCA material, three fractions (1-4 mm, 4-10 mm and 10-20 mm) were first dried in an oven to a constant mass m_0 at a temperature of 110°C (Tegguer, 2012). Then, aggregates cooled to room temperature were placed in a basket (mesh perforation: 1 mm) and immersed in distilled water at the time t=0. Note that the height of distilled water should be the same during all tests to keep the same buoyancy force exerted on the basket. The aggregates were then agitated to remove any trapped air bubbles. The recording of the balance $M(t)$ at time t was started approximately after 1 minute and ended after 120 h. At the end of the test, aggregates were extracted from water and the surface of the aggregates was dried gently with dry cloths following the European Standard NF EN 1097-6 (2014). Then, the mass of the aggregates m_{120} at saturated surface dry state after 120 h of immersion was measured. The water absorption ($W(t)$) of aggregates at time t (h) is defined as:

$$W(t)=\frac{m_{120}-m_0-(M_{120}-M(t))}{m_0} \quad \text{(II.1)}$$

where m_0 is the dry mass and m_{120} is the mass of aggregates at saturated surface dry state after 120 h of immersion; M_{120} and $M(t)$ are the balance recordings at 120 h and at time t.

The evolutions of water absorption for all RCA materials and for the three fractions (1-4 mm, 4-10 mm and 10-20 mm) are shown in Figure II.5. The results indicate that the water absorption of RCA decreases with increasing particle size, because attached mortar content decreases as particle size increases (Juan & Gutierrez, 2009). Besides, water absorption increases very fast during the first hour and then tends to become constant.

After 24 h, the aggregates with 1-4 mm fractions of all three RCA materials are fully saturated, while the degrees of saturation range from 90% to 95% for the other fractions (4-10 mm and 10-20 mm) and more than 48 h are required for saturating these fractions, as observed in Figure II.5.

As the content of 1-4 mm, 4-10 mm and 10-20 mm fractions before compaction in NRCA, ORCA and RCAP and their degree of saturation after 24 h of immersion can be obtained from Figure II.2 and Figure II.5, the degrees of saturation of the 0-20 mm mixtures after 24 h of immersion can be calculated, and they reach 96.1%, 96.8% and 94.9% for NRCA, ORCA and RCAP, respectively, indicating that the mixtures are close to saturation after 24 h. As a result, the standard method (NF EN 13286-7, 2004) that demands to store the mixture for 24 h is suitable for RCA.

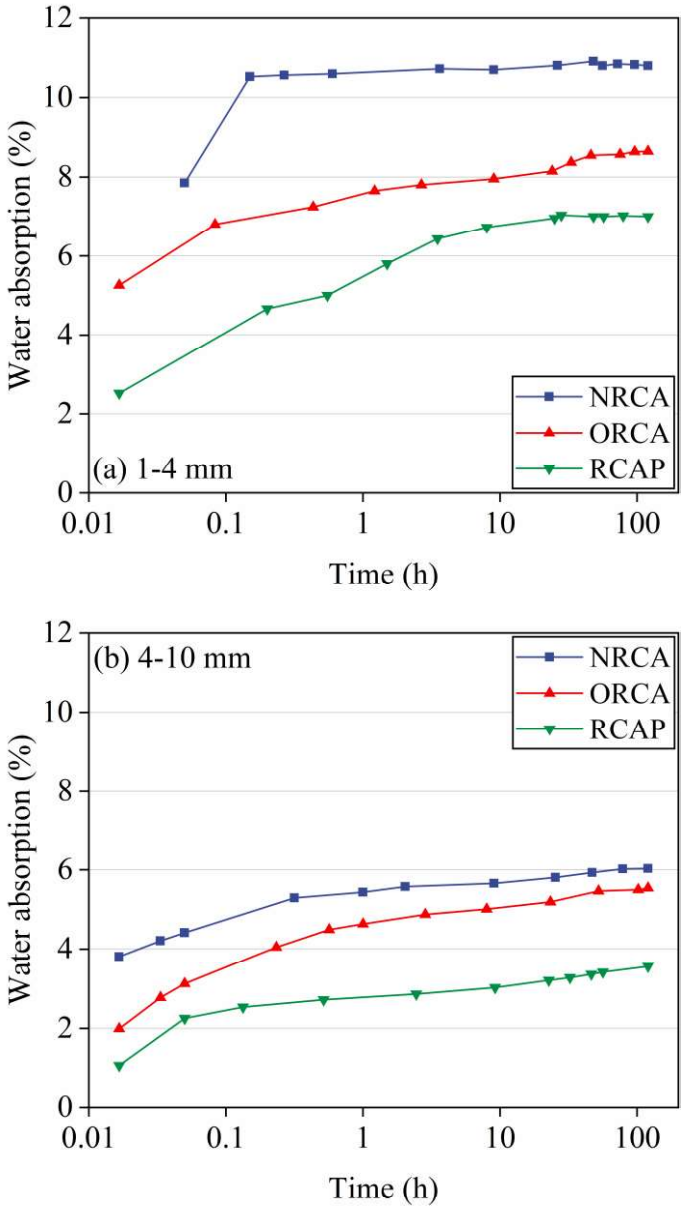

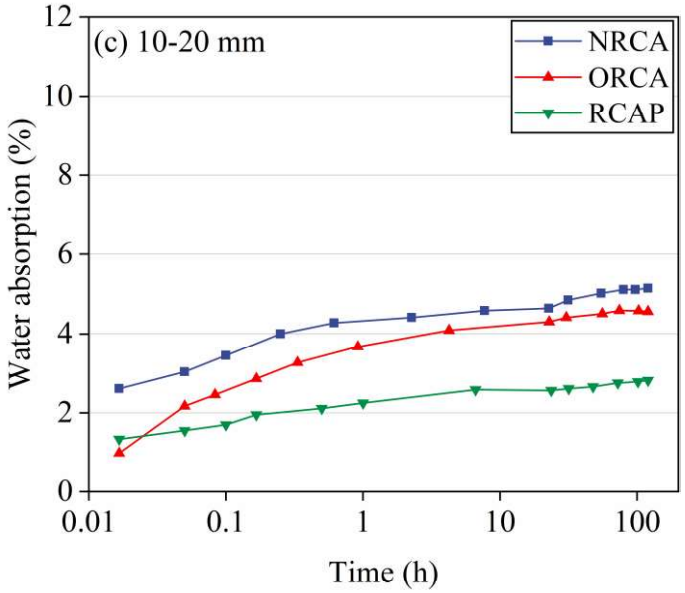

Figure II.5. Water absorption evolutions of RCA materials with different particle sizes: (a) 1-4 mm; (b) 4-10 mm and (c) 10-20 mm.

II.3 Self-cementing properties

II.3.1 pH value measurement and calorimeter test

pH value measurement, calorimeter test and thermogravimetric analysis (TGA) were methods widely used by other researchers to evaluate self-cementing properties of RCA (Bordy et al., 2017; Kim et al., 2014; Paige-Green, 2010; Poon et al., 2006). Only 0-2 mm fine aggregates, previously dried in the oven at 60 °C, were used to evaluate self-cementing properties of RCA as self-cementing properties are mainly influenced by fine particles (Poon et al., 2006). For pH value measurement, 30 g of RCA fine aggregates (0-2 mm) and 75 g of distilled water were mixed and stirred for 2 minutes (BS 1377-3, 2018). Then, the pH value of each suspension, stored for 24 h, was measured by a pH meter.

The heat of hydration were measured by the semi-adiabatic method (NF EN 196-9, 2010). To reach an equilibrium temperature, the mixing water, RCA fine aggregates and the calorimeter device (Figure II.6) were stored in the test room at a temperature of 20±5 °C for at least 24 hours prior to the test. Then, the previously weighted 360 g of RCA and 180 g of water were mixed quickly and placed in the calorimeter device to measure the heat of hydration of RCA for 24 hours. Another calorimeter, containing the same mass of water (180 g), was considered as the reference calorimeter.

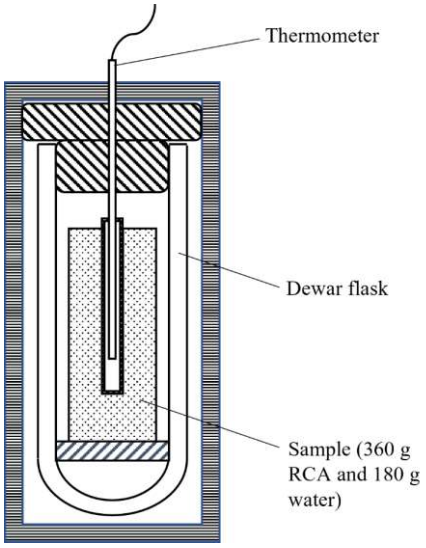

Figure II.6 Typical calorimeter.

To better understand the self-cementing properties of RCA materials, their chemical properties, such as water-soluble sulfate content and calcite content, were also measured. Water-soluble sulfate content of RCA was measured in accordance with the European standard NF EN 1744-1 (2014). 1 kg of previously heated (60 °C) distilled water was added to the 25 g of fine aggregates, stirring the mixture for 15 minutes while maintaining the temperature of 60 °C. Then, the solution was extracted through a filter paper and the water-soluble sulfate content was measured by a photometer.

Calcite content was measured by the calcimeter method (NF ISO 10693, 1995) to assess the degree of carbonation of two RCA before use, especially for ORCA after long-term storage. 0.5-2 g of powder ground from fine aggregates were firstly added to 10 ml of chlorhydric acid and the volume of released carbon dioxide was measured. Then, the calcite content can be calculated according to the measured volume of carbon dioxide.

II.3.2 Thermogravimetric analysis

To quantify unhydrated cement content and to investigate the hydration of unhydrated cement during curing, NRCA and ORCA fine aggregates (0-2 mm), without curing and after curing for 360 and 720 days, were subjected to thermogravimetric analysis (TGA). TGA was performed at Institut Jean Lamour laboratory of Lorraine university, with 50-100 mg air-dry fine aggregates (0-2 mm) heating at a constant heating rate of 10 °C/min from 25 °C to 1000 °C under N_2 atmosphere. Then, the phases content of RCA, such as non-evaporable water content,

$Ca(OH)_2$ and $CaCO_3$ content can be calculated by the weight loss from the TG curve. Potential self-cementing properties of RCA can be deduced from these values.

Figure II.7 and Figure II.8 show an example of derivative thermogravimetry (DTG) and thermogravimetry (TG) curves of NRCA and ORCA after crushing (without curing). According to the endothermic peaks on the DTG curve of NRCA (Figure II.7), 4 main peaks can be observed in DTG curve. The first peak, around 100 °C, is due to the decomposition of ettringite and C-S-H. In fact, they cannot clearly be identified in TGA since their peaks are partially overlapped (Qoku et al., 2017; Ramachandran et al., 2002). The peak of gypsum ($CaSO_4 \cdot 2H_2O$) is around 150 °C. $Ca(OH)_2$ can be found in the third peak between 430 and 490 °C. The last peak, between 550 to 850 °C, is caused by the decomposition of calcite ($CaCO_3$). The decomposition of CH and $CaCO_3$ can be expressed as:

$$Ca(OH)_2 \rightarrow CaO + H_2O \tag{II.2}$$

$$CaCO_3 \rightarrow CaO + CO_2 \tag{II.3}$$

Then, the non-evaporable water content C_{water}, $Ca(OH)_2$ content C_{CH} and calcite content C_{CaCO3} of NRCA and ORCA can be determined from their TG curves. Note that the non-evaporable water, defined as the water retained on the specimen at the boiling temperature (105 °C), has often been wrongly identified with chemically bound water which exhibits in a wider temperature range (probably start losing chemically bound water from 60 °C) (Taylor, 1997). To further study the hydration of unhydrated cement content during curing phase, the mass loss in different temperature ranges, due to the decomposition of ettringite (between 70/90 and 120 °C), gypsum $CaSO_4 \cdot 2H_2O$ (between 140 and 170 °C) and portlandite $Ca(OH)_2$ (between 430 and 490 °C), were also calculated from TG curves. It should be mentioned that different materials may have a slightly different decomposition temperature instead of a fixed temperature range. Thus, the corresponding decomposition temperatures are chosen carefully according to the slope of the DTG curves. Then, C_{CH}, C_{water} and C_{CaCO3} can be determined from the TG curves (Figure II.8) as:

$$C_{CH} = \frac{74.09}{18.01} \bullet (M_{430\ °C} - M_{490\ °C}) \tag{II.4}$$

$$C_{water} = M_{105\ °C} - M_{550\ °C} \tag{II.5}$$

$$C_{CaCO_3} = \frac{100.09}{44.01} \bullet (M_{550\ °C} - M_{850\ °C}) \tag{II.6}$$

where the ratio 74.09/18.01 and 100.09/44.01 correspond to the molar mass ratio of $Ca(OH)_2/H_2O$ and $CaCO_3/CO_2$, while $M_{T\,°C}$ is the sample weight (%) obtained from TG curve at temperature T °C (T=105, 550 and 850). C_{CH}, C_{water} and C_{CaCO3} are the $Ca(OH)_2$ content, non-evaporable water content and calcite content.

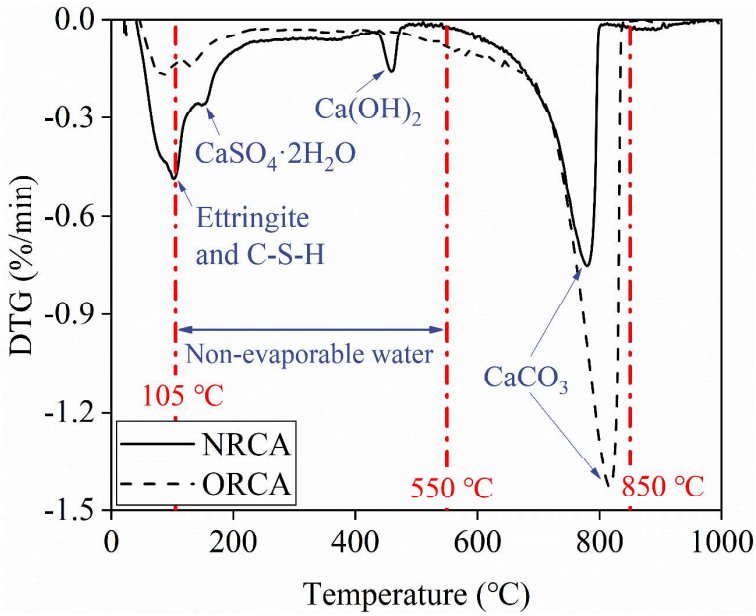

Figure II.7. DTG curves of NRCA and ORCA without curing.

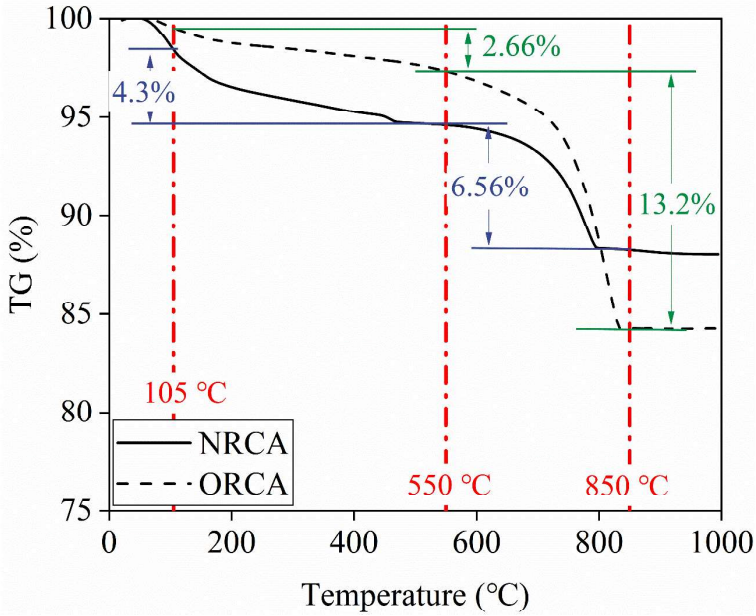

Figure II.8. TG curves of NRCA and ORCA without curing.

II.4 Microstructure analysis

Scanning electron microscopic analysis (SEM) was conducted to inspect the microstructures, while mercury intrusion porosimetry (MIP) technique was used to measure the pore size distribution of NRCA before and after curing for 360 days. Both SEM and MIP tests were performed at GeoRessources laboratory of Lorraine university. For SEM tests, small SEM samples (length*width*height=15*15*5 mm) were collected from the specimen after repeated load triaxial test and coated with gold prior to SEM analysis.

For MIP tests, the largest specimen was limited to 15 cm^3 in the MIP tests, while the coarse aggregates will increase the nonuniformity of RCA specimen. Besides, it is believed that the fine aggregates contain more unhydrated cement and are the main cause of self-cementing properties of RCA. Thus, only small piece of fine soil (diameter between 2 mm and 4 mm) collected from the specimen after repeated load triaxial test were used for MIP tests. Then, the fine piece soils were dried in the oven at 60 °C, to avoid shrinkage due to the high temperature.

II.5 Sample preparation and curing

For monotonic and repeated load triaxial tests, all the samples were prepared using a standard procedure (NF EN 13286-7, 2004). Firstly, the mixtures were prepared at a water content equal to OMC-1%. As the degree of saturation of the mixture after 24 h is higher than 95% (Chapter II.2), as mentioned before, the standard specimen preparation method (NF EN 13286-7, 2004) is suitable for RCA. Therefore, the mixtures were sealed in plastic bags for 24 h for moisture homogenization. After that, each sample, with a diameter of 150mm and a height of 285mm, was compacted in a split mould to the targeted dry density, which is the optimum dry density at the targeted water content, by vibrating hammer in 7 layers. The surface of each layer was slightly scarified before compacting the next layer for a better bonding. The mixer and vibrating hammer are shown in Figure II.9.

It is worth noting that many factors affect permanent and resilient deformation behavior of UGM, such as water content, dry density, gradation and stress state (Lekarp et al., 2000a, 2000b). In this study, to minimize the influence of these factors and to compare the performance of these RCA materials, all the specimens are prepared with the same testing parameters, such as particle size distribution, water content (OMC-1%) and dry density (maximum dry density at the targeted water content), selected from the Modified Proctor curves (Figure II.3) for the

three RCA mixtures, as summarized in Table II.2, to improve the comparison of their short and long-term mechanical behavior.

Finally, the specimens were demolded and wrapped with plastic bags and stored indoors for different periods, as shown in Figure II.10, to study the influence of self-cementing properties on the short- and long-term mechanical behaviour of RCA by monotonic and repeated load triaxial test. The monotonic triaxial test and repeated load triaxial test programs are summarized in Table II.3.

Figure II.9. Sample preparation equipment: (a) Mixer; (b) Vibrating hammer

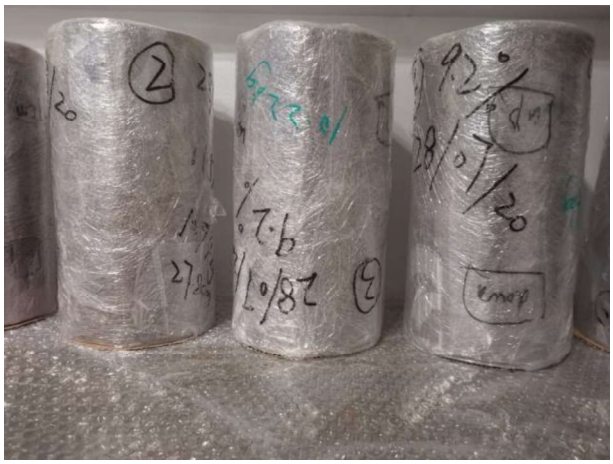

Figure II.10. Curing conditions of RCA

Table II.2. Targeted water contents and dry densities.

Materials	Optimum moisture content (%)	Maximum dry density (Mg/m^3)	Targeted water content (%)	Targeted dry density (Mg/m^3)
NRCA	12.93	1.98	11.9	1.97
ORCA	11.51	2	10.5	1.99
RCAP	10.90	2.13	9.9	2.07

Table II.3. Monotonic triaxial test and repeated load triaxial test program.

Test	Curing time/ days		
	NRCA	ORCA	RCAP
Monotonic triaxial test	1/28/360	1/360	None
Repeated load triaxial test	1/180/360/720	1/28/360	1

II.6 Mechanical performance tests

After curing for different periods, the specimen weight was first measured to make sure that no water evaporated during the curing stage. Subsequently, the specimen were subjected to monotonic triaxial test and repeated load triaxial tests (RLTT) to study the shear strength, permanent deformations and resilient deformations.

The triaxial tests were carried out with a triaxial apparatus (Wykeham Farrance), as shown in Figure II.11. The axial displacement was measured with an external LVDT (used for monotonic triaxial tests) and two Hall-Effect transducers (used for repeated load triaxial tests), and the radial strain was measured with a ring equipped with a Hall-Effect transducer. The Hall-Effect sensors were anchored in the specimen and passing through the membrane, which requires the waterproofing of the connection with the resin.

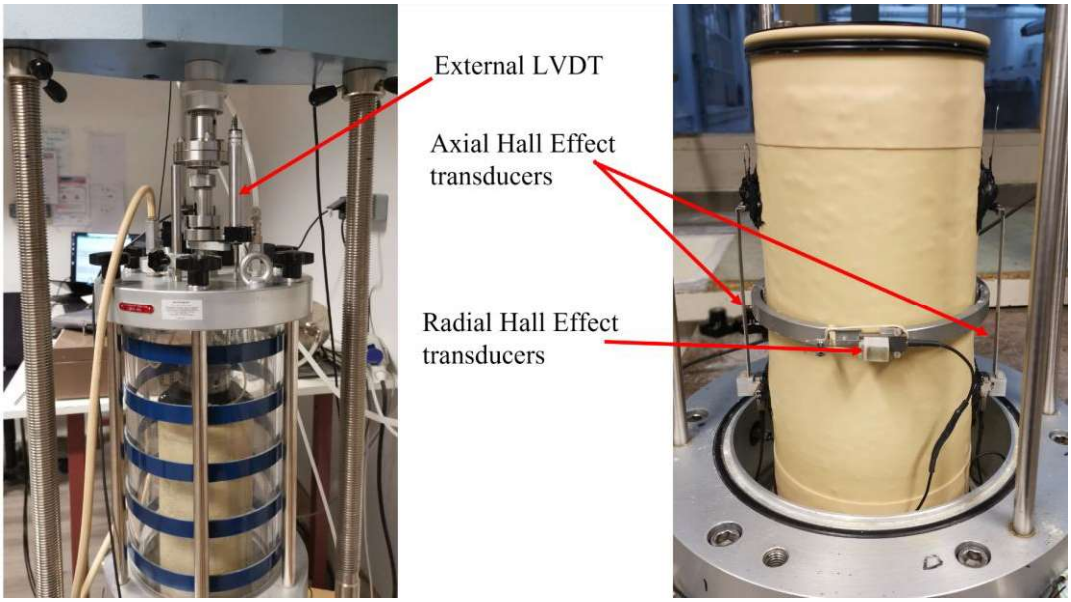

Figure II.11. Triaxial apparatus and instrumented specimen.

Monotonic triaxial tests

Monotonic triaxial tests were used to study the shear behaviour of RCA, after different curing times. In monotonic triaxial tests, three different confining pressures (20 kPa, 40 kPa and 70 kPa) were applied to the samples to determine the failure line. The tests were performed under drained conditions at a displacement rate of 0.3 mm/min until failure. The results of monotonic triaxial tests allow to determine the failure line (maximum strength line) in the p, q stress space and to calculate the friction angle φ and cohesion c for each material. The deviatoric stress q and mean normal stress p are defined by:

$$q = \sigma_1 - \sigma_3 \tag{II.7}$$

$$p = \frac{\sigma_1 + 2\sigma_3}{3} \tag{II.8}$$

where σ_1 is the vertical stress and σ_3 is the confining pressure.

Repeated load triaxial tests

The repeated load triaxial test (RLTT) is the most representative method to investigate permanent and resilient deformation behavior of unbound granular materials under traffic loadings. In this study, RLTTs were carried out following the procedure of the European Standard NF EN 13286-7 (2004), which consists of a conditioning phase (permanent deformation test) followed by a phase of study of the resilient behaviour (resilient deformation test).

In the conditioning phase, the sample was subjected to a constant confining pressure (CCP, σ_3=70 kPa) and a cyclic axial load ($\Delta q/\Delta p$=3, Δq=340 kPa) at the frequency of 1 Hz for 20000 loading cycles. The objective of this phase is to stabilize the permanent deformations.

In the resilient phase, after the conditioning phase, the tests were conducted successively under constant confining pressure (CCP) and variable confining pressure (VCP), where both confining pressure and axial load are cycled in phase. For CCP loading, six different confining pressures, 20 kPa, 35 kPa, 50 kPa, 70 kPa, 100 kPa and 150 kPa, and two different cyclic deviatoric stresses q (low stress level and high stress level) for each confining pressure, were applied on the specimen to study resilient deformation behavior under CCP loading. A total of 12 stress paths, as shown in Figure II.12, were applied on the same specimen. To synchronize the cyclic confining pressure with the cyclic deviatoric stress, these loads were applied at a lower frequency, 0.1 Hz, for 100 cycles. The last five cycles of each stress path were used to calculate the resilient strains. Note that the rupture line was obtained from the monotonic triaxial tests.

VCP loading is considered to better simulate the stress paths in pavements subjected to traffic loading than CCP loading. Five stress paths ($\Delta q/\Delta p$=0, 1, 1.5, 2, 2.5), with a high stress level, were applied on the same sample after CCP loading, as shown in Figure II.13. The loading frequency and cycles under VCP loading were the same as under CCP loading. Table II.4 and Table II.5 summarize the stress paths applied in the resilient tests under CCP and VCP loading. The stress paths for RLTT were obtained from European Standard NF EN 13286-7 (2004).

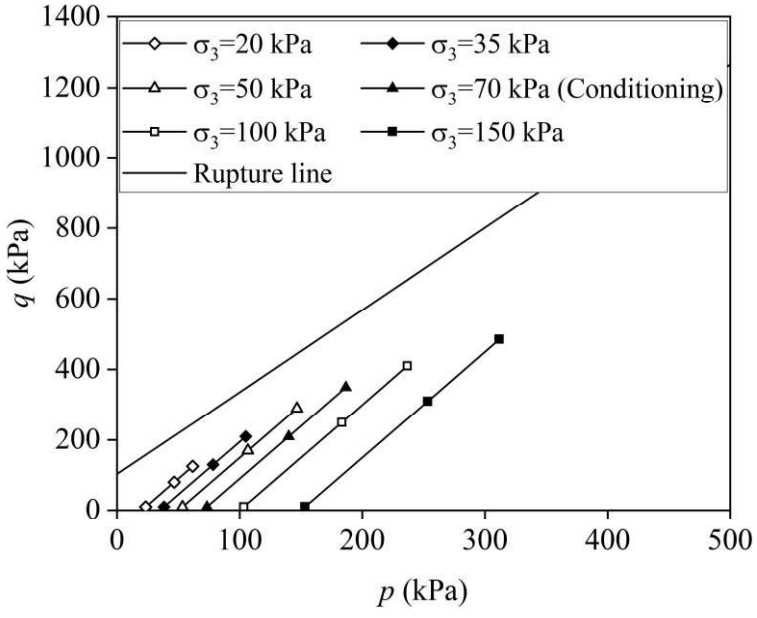

Figure II.12. Stress paths for repeated load triaxial tests (CCP loading).

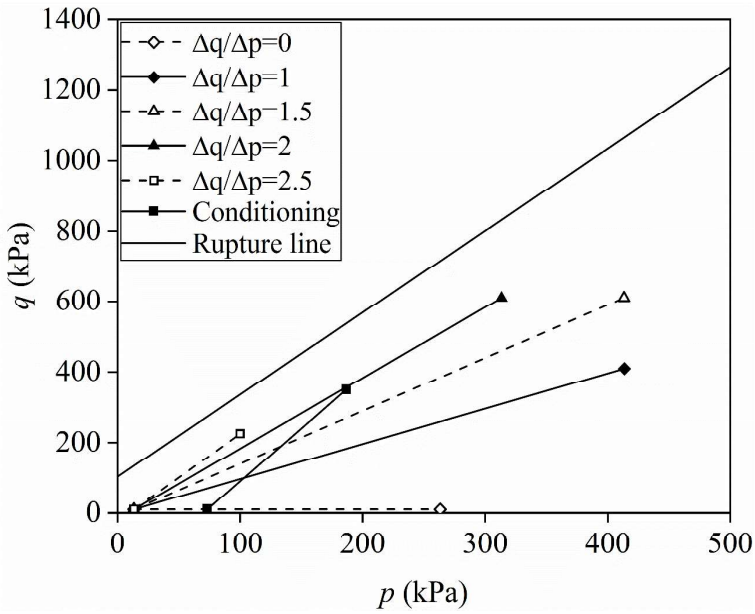

Figure II.13. Stress paths for repeated load triaxial tests (VCP loading).

Table II.4. Stress paths for resilient behaviour tests (CCP loading).

Confining pressure (kPa)	Stress level	Initial stress state		Cyclic stress paths	
		p_0 (kPa)	q_0 (kPa)	Δp (kPa)	Δq (kPa)
20	Low	23	10	23	70
	High	23	10	38	115
35	Low	38	10	40	120
	High	38	10	67	200
50	Low	53	10	53	160
	High	53	10	93	280
70	Low	73	10	67	200
	High	73	10	113	340
100	Low	103	10	80	240
	High	103	10	133	400
150	Low	153	10	100	300
	High	153	10	158	475

Table II.5. Stress paths for resilient behaviour tests (VCP loading).

$\Delta q/\Delta p$	Initial stress state		Cyclic stress paths	
	p_0 (kPa)	q_0 (kPa)	Δp (kPa)	Δq (kPa)
0	13	10	250	0
1	13	10	400	400
1.5	13	10	400	600
2	13	10	300	600
2.5	13	10	87	215

II.7 Conclusions

This chapter presents the physical properties and water absorption kinetics of the three studied RCA materials from different sources (NRCA, ORCA and RCAP). Besides, the procedures to evaluate self-cementing properties and microstructure, including pH value measurement, calorimeter test, thermogravimetric analysis (TGA), scanning electron microscopic analysis (SEM) and mercury intrusion porosimetry (MIP) were presented. Finally, monotonic and repeated load triaxial tests, used to characterize the mechanical behaviour, by conducting were also described.

The physical properties of the three RCA materials show that RCAP has a higher fine content before compaction and rounded particle content than NRCA and ORCA. RCAP also has a lower water absorption, optimum moisture content, LA and MDE. This indicates the high amount of rounded aggregates and low strength of the parent concrete of RCAP. However, these properties fulfil the requirements of RCA for a pavement base course.

The water absorption kinetics of the three RCA materials show that a degree of saturation higher than 95% is attained for all three RCA mixtures, after 24h, confirming the suitability of the standard specimen preparation method for RCA.

In the following chapter, the self-cementing properties of these RCA will be discussed and a new method will be proposed to calculate potential unhydrated cement content of RCA, which is responsible for the self-cementing properties. Furthermore, the hydration of unhydrated cement and the effect of self-cementing properties on the microstructure will be studied.

Chapter III. Self-cementing properties of RCA

In this chapter, the self-cementing properties of NRCA and ORCA were evaluated by pH value and released heat measured by calorimeter test. To obtain the unhydrated cement content, the cause of self-cementing properties, two methods, based on the portlandite ($Ca(OH)_2$) content and the non-evaporable water content, were developed. The other chemical properties, such as sulfate content and calcite content, were also measured and compared with TGA results. The hydration of unhydrated cement was investigated by subjecting RCA materials after curing to TGA. The development of microstructure due to the hydration of unhydrated cement was also studied by scanning electron microscopic analysis (SEM) and mercury intrusion porosimetry (MIP) test. At the end, the mechanism of self-cementing properties was demonstrated based on these observations.

III.1 Chemical compositions

Table III.1 shows the pH value, water-soluble sulfate content and calcite content of NRCA, ORCA and RCAP. Although pH value can not be related to the self-cementing properties of RCA directly, many scholars still use it to evaluate the self-cementing properties as it can be measured easily and quickly (Bestgen et al., 2016; Paige-Green, 2010; Poon et al., 2006). In fact, high pH value implies more soluble alkaline hydration products, suggesting that the RCA were not completely carbonated and may contain some unhydrated cement. The results show that the pH value of NRCA (13.07) is much higher than that of ORCA (10.53) and RCAP (9.48). Paige-Green (2010) revealed that the RCA with pH value higher than 11 exhibits self-cementing properties, indicating that NRCA shows self-cementing properties while those of ORCA and RCAP are negligible. For ORCA, the low pH value is mainly due to the long-term storage after crushing, unhydrated cement was hydrated already and carbonated. This is consistent with the observation of Kim et al. (2014) who concluded that the self-cementing properties of RCA fines, stored in open stockpiles at high temperature and humidity, are negligible. For RCAP, the negligible self-cementing properties is mainly due to the low strength of its parent concrete as mentioned above. Besides, Chang and Chen (2006) indicated that the concrete is not carbonated when pH value (solid/water=1:10) is higher than 11.5, suggesting that carbonation of NRCA is negligible while ORCA and RCAP is highly carbonated due to the long-term storage.

Table III.1. Initial chemical compositions of NRCA and ORCA.

Properties	NRCA	ORCA	RCAP	Limitation
pH value	13.07	10.53	9.48	No
Water-soluble sulfate content/%	0.23	0.13	0.08	0.7
Calcite content/%	14.7	29.97	11.67	No

Sulfate attack is a non-ignorable disease for hydraulically bound materials, which leads to an expansion in solid volume by forming gypsum or ettringite (Hewlett & Liska, 2019; Kampala et al., 2021). According to the European standard NF EN 13285 (2018) and the French national and regional technical guides (CETE de l'Est, 2009; UNICEM IDF, 2003), the water-soluble sulfate content of RCA, used in pavement base and subbase layers, should be less than 0.7%. It appears that the water-soluble sulfate content of both NRCA, ORCA and RCAP are under the limitation, although the water-soluble sulfate content of NRCA (0.23%) is higher than that of ORCA (0.13%) and RCAP (0.08%).

Table III.1 also shows that the calcite content of NRCA (14.7%) and RCAP (11.67%), measured by calcimeter method, is only half of ORCA (29.97%). This can be attributed to the long-term storage of ORCA and a large specific surface area after crushing, increasing the degree of carbonation while decreasing the pH value of ORCA, although ORCA was stored in plastic bags to prevent humidity and carbonation. However, partial $CaCO_3$ could also come from the original natural aggregates (NA), especially for ORCA, although an effort was made to eliminate the influence of original NA by limiting the maximum particle size (2mm).

III.2 Calorimeter test

As the self-cementing properties of RCAP is negligible indicated by the very low pH value (9.48), only NRCA and ORCA were subjected to the calorimeter test and thermogravimetric analysis (TGA). Figure III.1 shows the rate of heat generation and the total released heat of NRCA and ORCA, due to the hydration of unhydrated cement. It appears that the hydration of unhydrated cement takes place immediately after the RCA were mixed with water, even for ORCA, with a maximum rate of heat generation at the beginning and then decreases quickly in the next few hours (Figure III.1 (b)). For NRCA, the initial rate of heat generation is 2.3 mW/g and gradually decreases to a stable value till 24 hours. By contrast, ORCA has a much less rate of heat generation (0.48 mW/g) and heat releasing time (1 hour) than those of NRCA. As a

result, after 24 hours, the average heat released by NRCA is 14.7 J, in good agreement with the result (lower than 15 J) reported by Oksri-Nelfia et al. (2016), which is much higher than that released by ORCA (1.97 J).

It is pointed out that there are two main peaks in the rate of heat generation curves for the typical Portland cement (Hewlett & Liska, 2019). The first peak, within a few minutes after mixing, as observed for both NRCA and ORCA in Figure III.1, is due to the initial rapid hydration of tricalcium aluminate phases (C_3A) and alite (C_3S). Then, after a few hours until a few days (Hewlett & Liska, 2019; Kim et al., 2014), the hydration of C_3S and the formation of calcium silicate hydrate (C-S-H) phase develops strength and stiffness of cement paste and lead to the second, main exothermic peak (around 10 hours). Although the second peak was not detected on both NRCA and ORCA (Figure III.1), in which the strength and stiffness develop, the longer heat releasing time of NRCA (till 24 hours) suggests that a small amount of calcium silicate hydrate (C-S-H) phase is formed. While for ORCA, although the first peak was also detected, no potential self-cementing properties were observed as the heat releasing time is very short (1 hours), which is in good agreement with pH value. It also indicates that long-term storage can decrease self-cementing properties of RCA, as observed also by Kim et al. (2014).

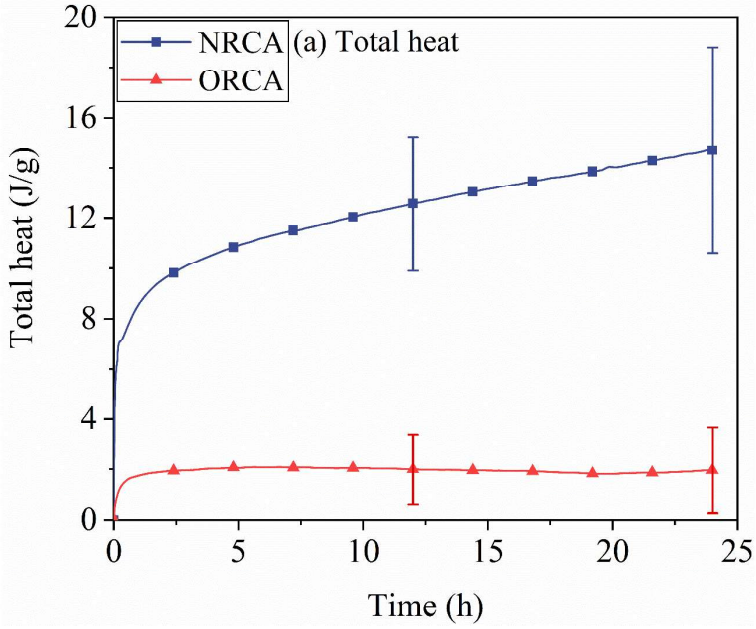

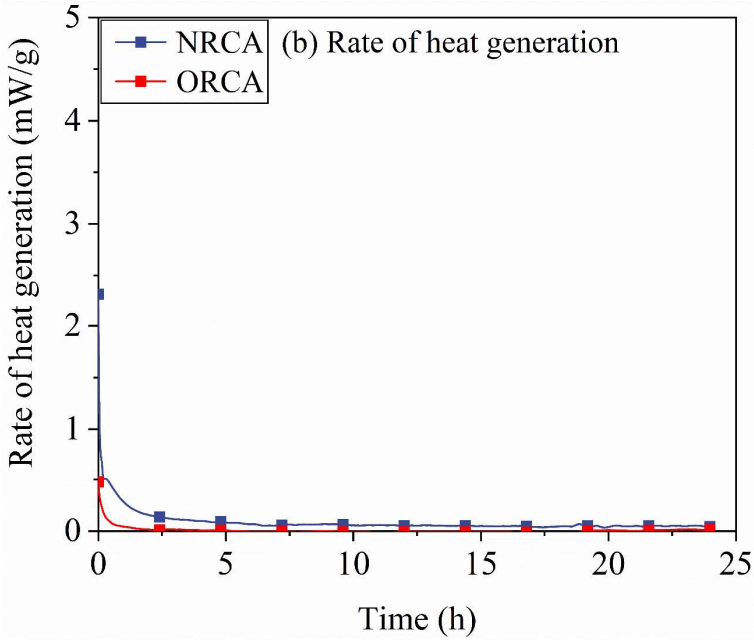

Figure III.1. Hydration heat of NRCA and ORCA: (a) Total heat and (b) Rate of heat generation.

III.3 Thermogravimetric analysis (TGA)

Since the chemical properties (sulfate content and calcite content) and self-cementing properties, evaluated by pH value and calorimeter test, were studied, TGA was performed on NRCA and ORCA fine aggregates (0-2 mm) to calculate unhydrated cement content, the cause of self-cementing properties.

III.3.1 Methods

Non-evaporable water and portlandite ($Ca(OH)_2$), corresponding to the hydration of cement, are usually considered as the useful indicator of the cement hydration (Taylor, 1997). It is reported that a complete hydration of unit Portland cement, without any supplementary cementing materials (SCMs), such as fly ash, silica fume, etc., will release 0.29 unit of $Ca(OH)_2$ (Oksri-Nelfia et al., 2016; Papadakis, 1999b, 2000) and 0.23-0.25 unit of non-evaporable water (taken as 0.24 in this study) (Bhatty, 1986; Mounanga et al., 2004; Pane & Hansen, 2005). Note that the non-evaporable water, defined as the water retained on the specimen at the boiling temperature (105 °C), has often been wrongly identified with chemically bound water that present in interlayer spaces, whose determination is complicated (Taylor, 1997). Then, the

relationship between C_{CH}, C_{water} and cement content (C_{cement}) of RCA made by Portland cement can be expressed as:

$$C_{CH} = 0.29 \times \alpha \times C_{cement} \quad \text{(III.1)}$$

$$C_{water} = 0.24 \times \alpha \times C_{cement} \quad \text{(III.2)}$$

where C_{CH}, C_{water} and C_{cement} are $Ca(OH)_2$ content, non-evaporable water content and Portland cement content in RCA, respectively. α is the degree of cement hydration. For concrete after long term of service life, the ultimate degree of cement hydration is mainly influenced by the initial water cement ratio (w/c), and can be calculated by the following equation developed by Mills (1966) which is frequently used to model the cement hydration (Lin & Meyer, 2009; Oksri-Nelfia et al., 2016):

$$\alpha = \frac{1.031 * \frac{w}{c}}{0.194 + \frac{w}{c}} \quad \text{(III.3)}$$

As mentioned before, 0.29 unit of $Ca(OH)_2$ and 0.23-0.25 unit of non-evaporable water are released for an unit of fully hydrated Portland cement (CEM I type), whereas for blended cement, the use of SCMs makes it difficult to estimate the amount of ultimate non-evaporable water due to the unknown stoichiometries and SCMs type (Deboucha et al., 2020). In fact, $Ca(OH)_2$ is easily influenced by the type of cement, carbonation and the supplementary cementing materials (Papadakis, 1999a, 1999b), while non-evaporable water is much less sensitive to these factors (Chidiac & Shafikhani, 2019; Pane & Hansen, 2005). Thus, non-evaporable water content (C_{water}) was more suitable to calculate the unhydrated cement content of RCA manufactured by blended cement, instead of portlandite ($Ca(OH)_2$) content used by Oksri-Nelfia et al. (2016).

To implement this methodology to blended cement, the SCMs are considered as the equivalent Portland cement by the *k*-value concept (Deboucha et al., 2020; NF EN 206-1, 2004; Papadakis et al., 2002), so the unknown released non-evaporable water for blended cement can be considered as the same as the Portland cement (0.23-0.25 gram). This concept makes it possible to simply quantify the contributions of SCMs on the hydration of blended cements, which can be used to evaluate unhydrated cement content of all kinds of cement (Portland cement or blended cement). Table III.2 summarizes the *k* values for different types of SCMs. The equivalent binder content (C_{binder}) can be expressed as:

$$C_{binder} = C_{cement} + k * C_{SCMs} \quad \text{(III.4)}$$

Then, Equation (III.2) can be substituted by:

$$C_{water} = 0.24 \times \alpha \times C_{binder} \quad \text{(III.5)}$$

Finally, the unhydrated binder content ($C_{unhydrated}$) of NRCA can be determined as follows:

$$C_{unhydrated} = (1-\alpha) \times C_{binder} \quad \text{(III.6)}$$

It should be mentioned that the carbonation of concrete can decrease the calculated C_{binder} and $C_{unhydrated}$ by decreasing the non-evaporable water content. However, the influence of carbonation was not considered in this study as the high pH value of NRCA (13.07) suggested that carbonation of NRCA is negligible.

Table III.2. *k* values for different types of supplementary cementing materials.

Additive	Limestone filler	Blast furnace slag	Silica fume	Fly ash	
				CEM I 32.5	≥ CEM I 42.5
k value	0.25	0.9	2	0.2	0.4

III.3.2 Results

To calculate potential unhydrated binder content of NRCA, Table III.3 summaries the weight loss (%) of NRCA and ORCA before using (curing 0 day) under different temperature ranges, as well as C_{CH}, C_{water} and C_{CaCO3} calculated on the basis of TG curves (Figure II.8) and Equations (II.4), (II.5) and (II.6). It can be observed that C_{water} of NRCA (4.30%) is much higher than that of ORCA (2.66%), caused by the high degree of carbonation of ORCA after long-term storage. For NRCA, C_{CH} is 2.04%. Since ORCA exhibits no DTG peak between 430 °C and 490 °C, C_{CH} of ORCA was considered as 0, which is in good agreement with pH value.

As for the $CaCO_3$ content, ORCA has a much higher C_{CaCO3} (30.09%) than that of NRCA (14.92%), which is believed to be caused by the high degree of carbonation after long term of storage. However, a part of $CaCO_3$ could also come from the original natural aggregates, although an effort was made to eliminate the influence of original natural aggregates by limiting the maximum particle size (2 mm). Note that the carbonation of NRCA and its influence on the decrease of C_{CH} is ignored since the pH value of NRCA is close to 13.

Besides, C_{CaCO3} calculated by TGA, 14.92% (NRCA) and 30.09% (ORCA), were also compared with the values obtained with calcimeter method (Table III.1), 14.7% (NRCA) and

29.97% (ORCA), presented also in Table III.3. It indicates that two calculation methods have obtained almost the same results, showing the reliability of TGA results.

Table III.3. Selected components of NRCA and ORCA without curing.

Materials	Weight loss/%			Non-evaporable water C_{water}/%	$Ca(OH)_2$ content C_{CH}/%	$CaCO_3$ content C_{CaCO3}/%	C_{CaCO3}-calcimeter method/%
	105-*550* °C (C_{water})	*430-490* °C ($Ca(OH)_2$)	*550-850* °C ($CaCO_3$)				
NRCA	4.30	0.50	6. 56	4.30	2.04	14.92	14.7
ORCA	2.66	None	13.23	2.66	None	30.09	29.97

Subsequently, the potential equivalent binder content (C_{binder}) and potential unhydrated binder content ($C_{unhydrated}$) can be calculated based on the C_{CH} and C_{water} (Equations (III.1), (III.5) and (III.6)). Since ORCA were stored for a long term before using (without curing), the partial unhydrated cement has already hydrated, resulting in a much higher ultimate degree of cement hydration α, which can not be calculated by Equation (III.3). Thus, only C_{cement} of NRCA could be calculated in this study.

Figure III.2 presents the potential C_{binder} and $C_{unhydrated}$ of NRCA with varying initial water-cement ratio *w/c*, due to the unknown initial *w/c* of original composition of concrete structure after long-term service, calculated by non-evaporable water content (C_{water}) and $Ca(OH)_2$ content (C_{CH}). Generally, the typical *w/c* ratio for conventional concrete ranges from 0.4 to 0.5 (Shi et al., 2015). The typical equivalent binder content, global concrete with full size aggregates, is between 15.5% and 21.3% at this specified *w/c* ratio (0.4-0.5), according to the hundreds of concrete mixture proportions collected from the literature (Ahmad et al., 2021). It appears that within the typical *w/c* ratio (0.4-0.5), the potential C_{binder} of NRCA fine aggregates (0-2 mm) calculated by C_{water} (24.1%-25.8%) is slightly higher than the typical equivalent binder content (15.5%-21.3%). This is due to the fact that the tested fine aggregates (0-2 mm) have higher mortar content than the global concrete (Juan & Gutierrez, 2009), resulting in a higher C_{binder} of NRCA than the typical concrete.

However, it can be observed that the potential C_{binder} of NRCA fine aggregates (0-2 mm) calculated by C_{CH} (9.46%-10.12%) is the lowest, even lower than the typical equivalent binder content of global concrete (15.5%-21.3%). As mentioned above, $Ca(OH)_2$ is easily influenced by the type of cement, carbonation and the supplementary cementing materials (Papadakis, 1999a, 1999b), while non-evaporable water is much less sensitive to these factors (Chidiac &

Shafikhani, 2019; Pane & Hansen, 2005). Thus, non-evaporable water content (C_{water}) was more suitable to calculate the unhydrated cement content of RCA, instead of portlandite ($Ca(OH)_2$). Within the typical *w/c* (0.4-0.5), the potential unhydrated binder content of NRCA (0-2 mm) is between 6.2% and 7.9% (calculated by C_{water}).

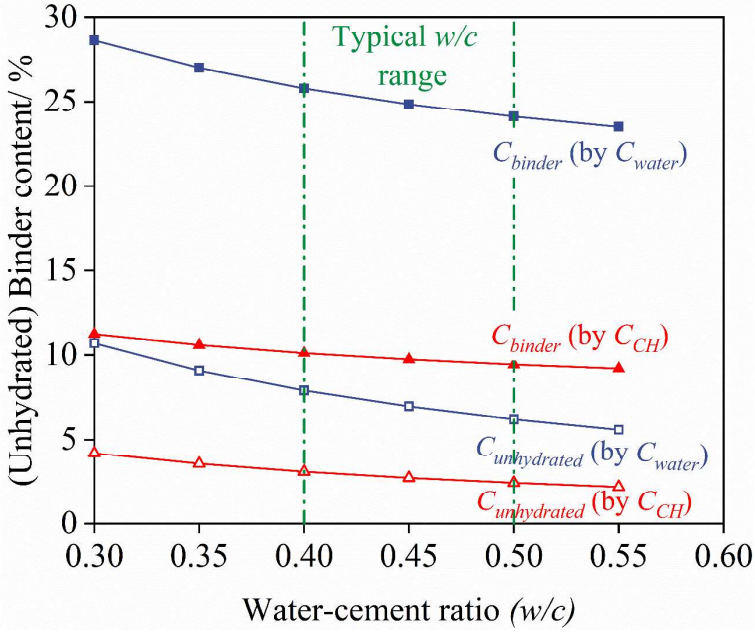

Figure III.2. Potential binder content and unhydrated binder content of NRCA calculated by non-evaporable water content (C_{water}) and $Ca(OH)_2$ (C_{CH}) with different w/c.

III.4 Hydration of unhydrated cement

It is known that the unhydrated cement, primary cause of self-cementing properties, will hydrate after mixing with water, increasing strength and stiffness of unbound pavement layers built with RCA materials after construction. To study the hydration of unhydrated cement after pavement construction, the fine aggregates of NRCA and ORCA (0-2mm), extracted from the cured samples (curing for 360 days and 720 days), were also subjected to TGA. The comparison of TG-DTG curves of NRCA and ORCA without curing and curing for 360 and 720 days are presented in Figure III.3 and Figure III.4. In the DTG curve of NRCA after curing for 720 days, the peak of $CaSO_4 \cdot 2H_2O$ (around 150 °C) disappeared, and the intensity of $Ca(OH)_2$ peak (around 450 °C) is reduced, indicating a decrease of $CaSO_4 \cdot 2H_2O$ and $Ca(OH)_2$ content in NRCA after curing for 720 days, which could be attributed to the sulfate attack. On the contrary, for ORCA, the DTG and TG curves remain the same after curing for 0 and 360 days, in agreement with the negligible self-cementing properties of RCA indicated by low pH value and

total released heat (calorimeter test). Note that ORCA curing for 720 days was not subjected to TGA due to the negligible self-cementing properties.

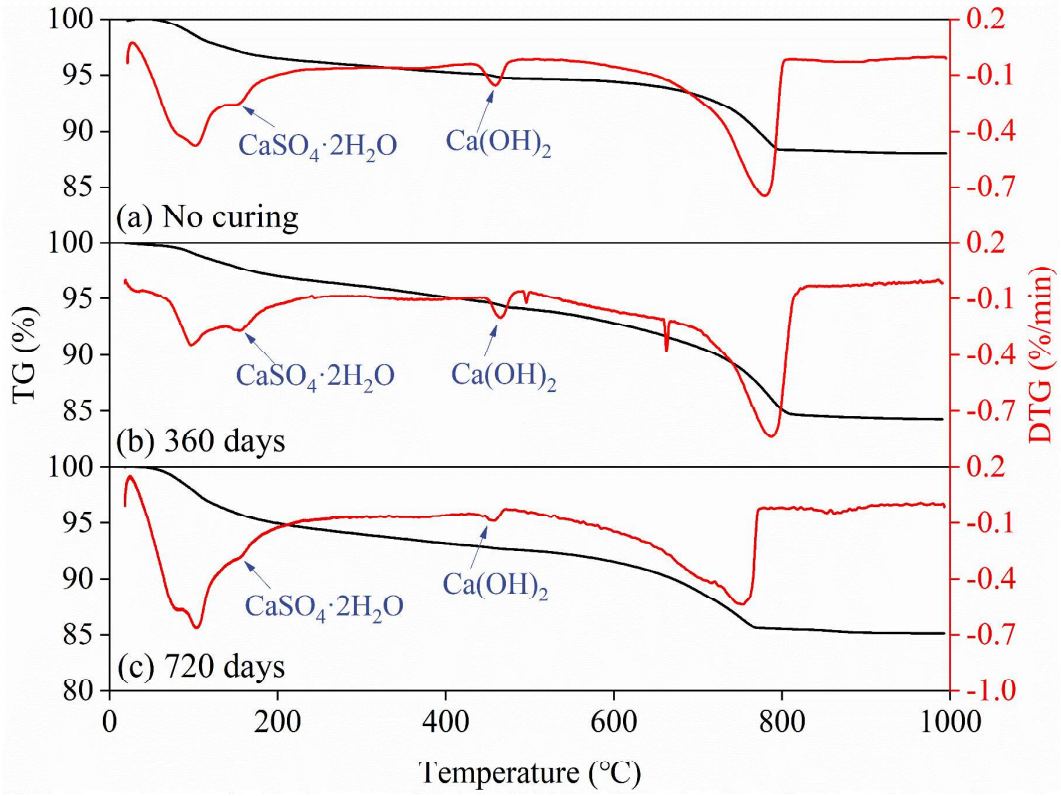

Figure III.3. Comparison of TG-DTG curves of NRCA without curing and curing for 360 and 720 days: (a) without curing; (b) 360 days and (c) 720 days.

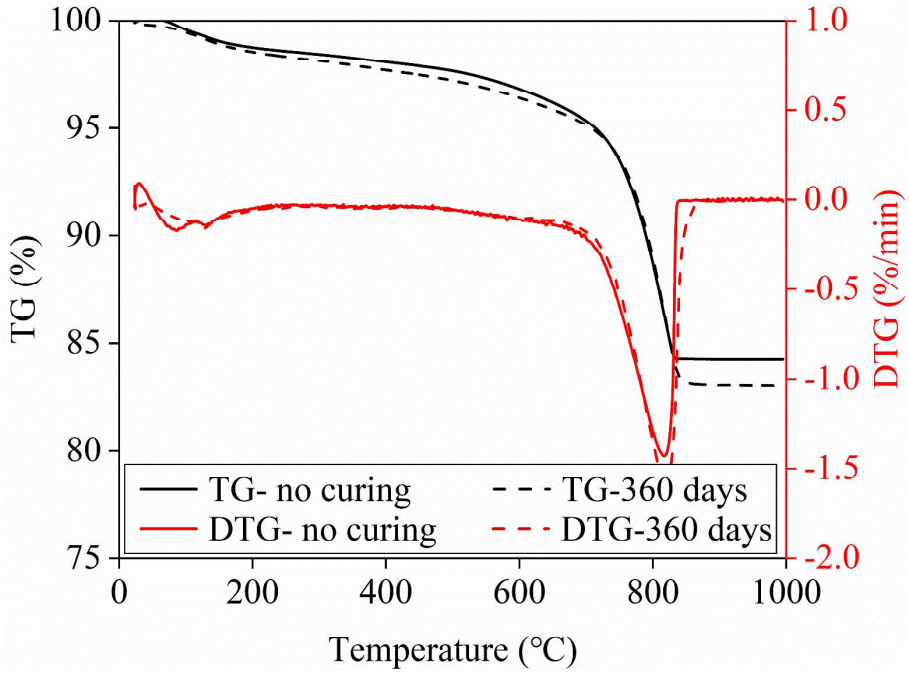

Figure III.4 Comparison of TG-DTG curves of ORCA without curing and 360 days curing.

To further study the hydration of unhydrated cement, Table III.4 summarizes the mass loss of NRCA and ORCA curing for different times at different temperature ranges, corresponding to the non-evaporable water (between 105 and 550 °C) and free water content (between 25 and 70/90 °C), and also the decomposition of $Ca(OH)_2$ (between 430 and 490 °C), $CaCO_3$ (between 550 and 850 °C), ettringite (between 70/90 and 120 °C) and gypsum $CaSO_4 \cdot 2H_2O$ (between 140 and 170 °C). The corresponding decomposition temperatures were chosen carefully according to the slope of the DTG curves, to improve the accuracy of quantification. Since no obvious variations of mass loss at different temperature ranges are observed for ORCA, only the evolutions of mass losses for NRCA in different temperature ranges are presented in Figure III.5.

It can be observed that a significant increase of non-evaporable water content of NRCA after curing for 360 days can be observed, from 4.3% to 5.34%, which is believed to be related to the hydration of unhydrated cement, and then reaches a constant value (5.37%). Consequently, the amount of unhydrated binder that was hydrated during curing phase of 360 and 720 days, named hydrated binder content, can be calculated by Equations (III.5) (α equals to 1), according to the variation of non-evaporable water content (1.04% and 1.07% for curing 360 and 720 days). It appears that some unhydrated binder (around 4.3%) in NRCA fine aggregates (0-2 mm) are hydrated after curing for 360 days, and then the hydrations are almost stopped.

Table III.4. Mass losses of NRCA and ORCA curing for different times.

Weight loss/%	Temperature range/°C	NRCA			ORCA	
		0	360	720	0	360
Non-evaporable water	105-550	4.30	5.34	5.37	2.66	2.54
$Ca(OH)_2$	430-490	0.50	0.71	0.39		
$CaCO_3$	550-850	6.56	9.06	6.76	13.23	13.75
Ettringite	70/90-120	1.20	1.12	1.58		
Gypsum	140-170	0.66	0.66	None		
Free water	25-70/90	2.57	1.43	3.17	0.68	0.45

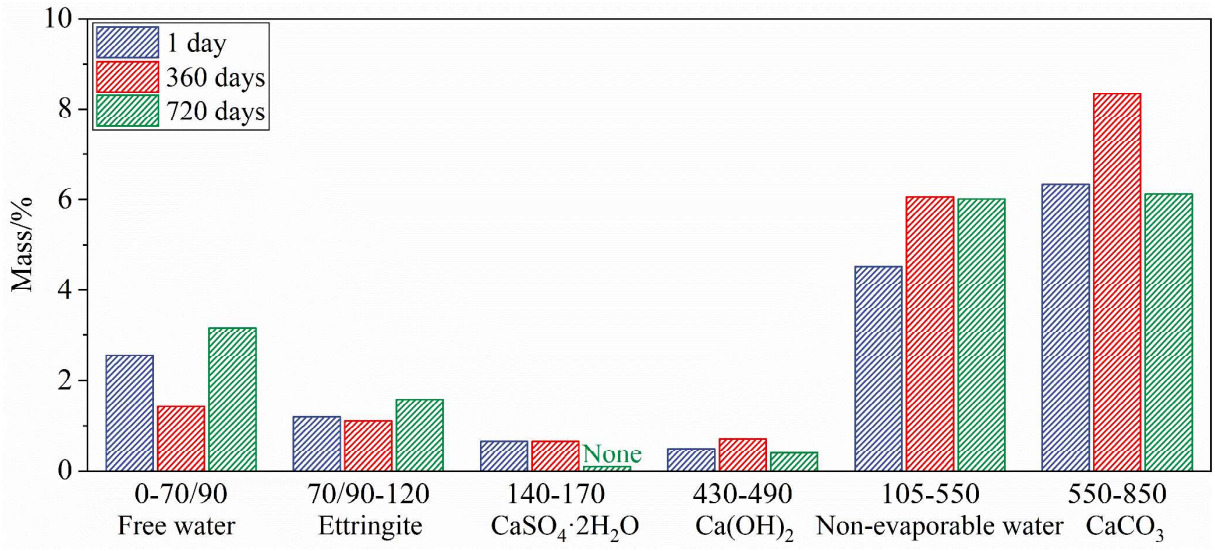

Figure III.5 The evolution of mass loss for NRCA in different temperature ranges.

As a result, the mass loss corresponding to the $Ca(OH)_2$ increases after curing for 360 days, from 0.5% to 0.71%. However, a decrease of $Ca(OH)_2$ content can be observed after curing for 720 days. Besides, $CaSO_4 \cdot 2H_2O$ content also decreases while ettringite content increases after curing for 720 days. This can be attributed to the sulfate attack product, ettringite, by the reactions between $CaSO_4 \cdot 2H_2O$, $Ca(OH)_2$ and cement hydration products (Rajasekaran, 2005). Note that the ettringite can absorb a large amount of water and has a large volume, filling the voids between particles and improving the microstructure and mechanical behaviour of RCA specimen, which could also lead to the self-cementing properties of RCA.

Figure III.5 also reveals that $CaCO_3$ content of NRCA increases after curing 360 days, which could be attributed to the carbonation of RCA. Note that the air-dry NRCA after curing 360 days was not subjected to TGA immediately, instead it was stored in another plastic bag without good seal for another month. Thus, the carbonation could occur during the storage phase after curing, or occur on the surface of specimen during the long-term curing. It should be pointed out that the carbonation on the surface of specimen during curing stage could have potential to increase the strength and stiffness of RCA specimens (Terzis & Laloui, 2019; Zadeh et al., 2021), which could also lead to the observed self-cementing properties of RCA. However, the effect of carbonation on self-cementing properties could be negligible.

In comparison to the total unhydrated binder content of NRCA (0-2 mm) without curing (between 6.2% and 7.9%), between 55% to 70% of the total unhydrated binder (4.3%) were hydrated after curing 360 days, and this hydration appears to be stopped after curing for 360

days, according to TGA results. However, the formation of ettringite, sulfate attack products, was observed between curing for 360 days and 720 days, which could also lead to the self-cementing properties of RCA. In other words, almost all the effective unhydrated binder would hydrate in the first year after the construction of pavement. Then, the sulfate attack continue to increase the strength and stiffness of RCA specimen, which is in good agreement with Arm (2001). This phenomenon is also observed in several field tests (Korkiala-Tanttu et al., 2014; Lancieri et al., 2006; Wang et al., 2016) where the strength and stiffness of RCA base and subbase layers increase faster in the first few years, and a continuous increase was observed even up to 10 years after construction.

III.5 Microstructural characteristics

III.5.1 Scanning electron microscopic analysis (SEM)

The microstructure of NRCA curing for 1 and 360 days observed by SEM under different magnification (300×, 2400×, 4000×) are presented in Figure III.6-Figure III.8. Because the self-cementing properties of ORCA are negligible, only the microstructure of NRCA was studied. As shown in Figure III.6 (a), Figure III.7 (a) and Figure III.8 (a), NRCA specimen curing 1 day exhibits a relatively open type of microstructure, with numerous fine particles assembled between coarse aggregates, exhibiting many different sizes of voids.

The SEM images of NRCA curing for 360 days show the influence of self-cementing properties on the microstructures of RCA specimens, as observed in Figure III.6 (b), Figure III.7 (b) and Figure III.8 (b). There are two different kinds of pores for typical unbound granular materials: micro-pores (within aggregates) and macro-pores (between aggregates), with a limit diameter around 0.65 μm for micro- and macro-pores for compacted soil (particle size less than 3.2 mm) reported by Su et al. (2022b). It appears that the number and size of macro-pores (width less than 3 μm and higher than 0.65 μm) decrease after curing 360 days (Figure III.8 (b)), as the bonds were formed between particles instead of within particles. While for the big void (width larger than 3 μm), the influence of self-cementing properties on the microstructures is limited, as there are still some big voids as can be seen in Figure III.8 (b). The microstructure of NRCA after curing 360 days is much tighter than that curing for 1 day.

Figure III.7 (b) and Figure III.8 (b) also show that the amount of fine aggregates decreases after curing 360 days, which could be attributed to the hydration of unhydrated cement in fine

aggregates. It also indicates that the unhydrated cement in fine aggregates are responsible for the self-cementing properties of RCA, in good agreement with Poon et al. (2006).

The hydration products of unhydrated cement in fine aggregates not only act as bonds between particles, but also fill the voids between particles (macro-pores). However, for large pores (larger than 3 μm), the low amount of hydration production limits the bonding and filling effects. As a result, the small macro-pores (width less than 3 μm and higher than 0.65 μm) were filled by the hydration products, and the open type of structure (curing 1 day) gradually turns to a rigid tight skeleton structure (curing 360 days), increasing the strength and stiffness of RCA and may change unbound pavement layers to bound layers.

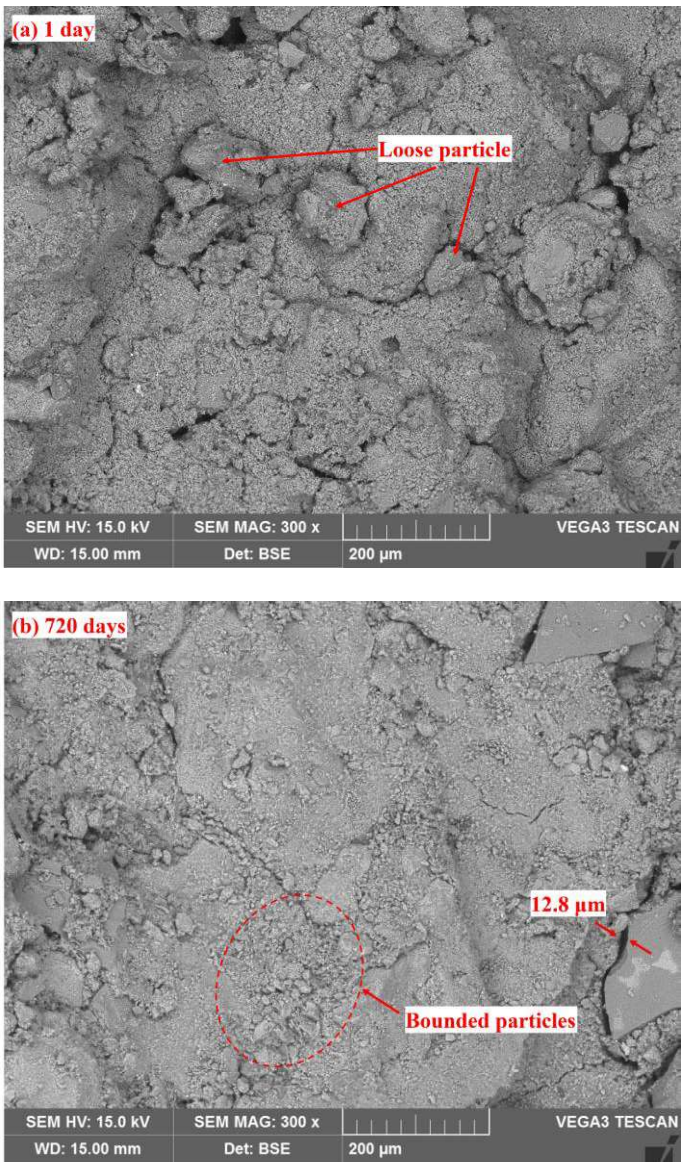

Figure III.6. SEM images of NRCA curing for 1 and 360 days (300×): (a) 1 day (unbound); (b) 360 days (bound).

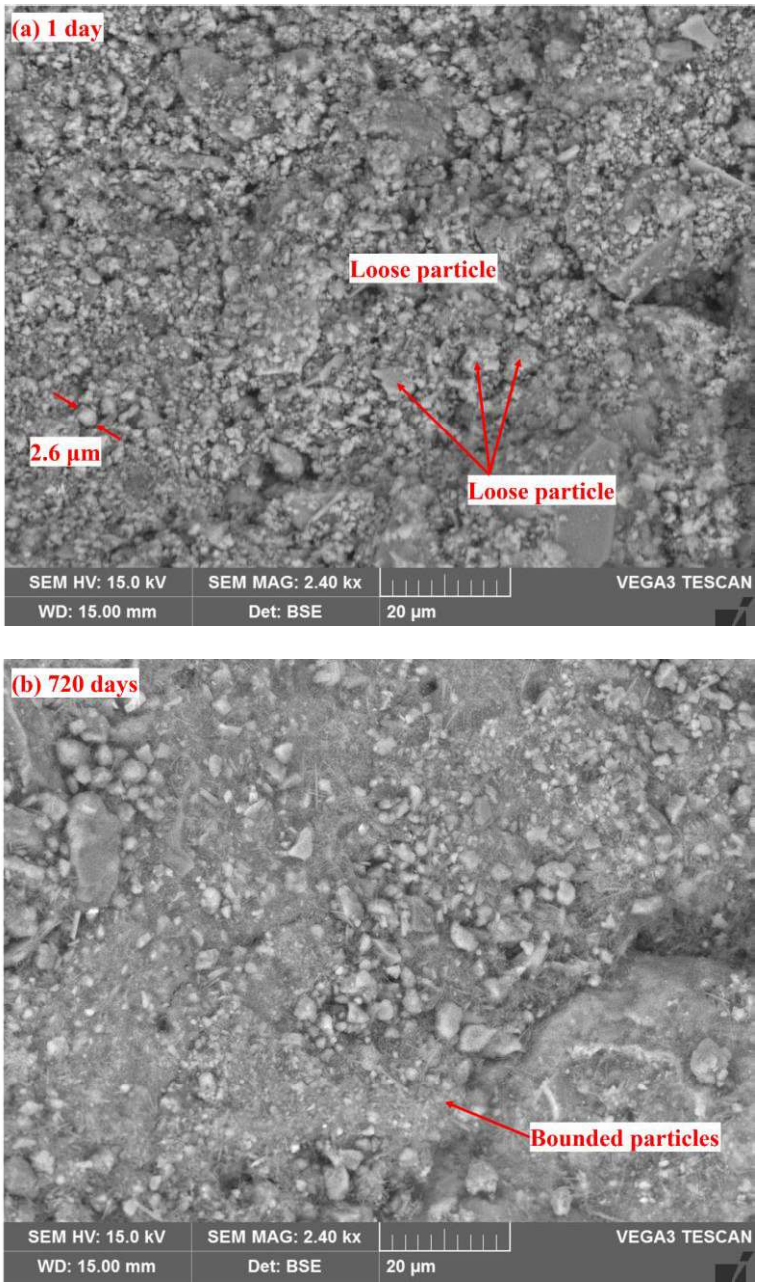

Figure III.7. SEM images of NRCA curing for 1 and 360 days (2400×): (a) 1 day (unbound); (b) 360 days (bound).

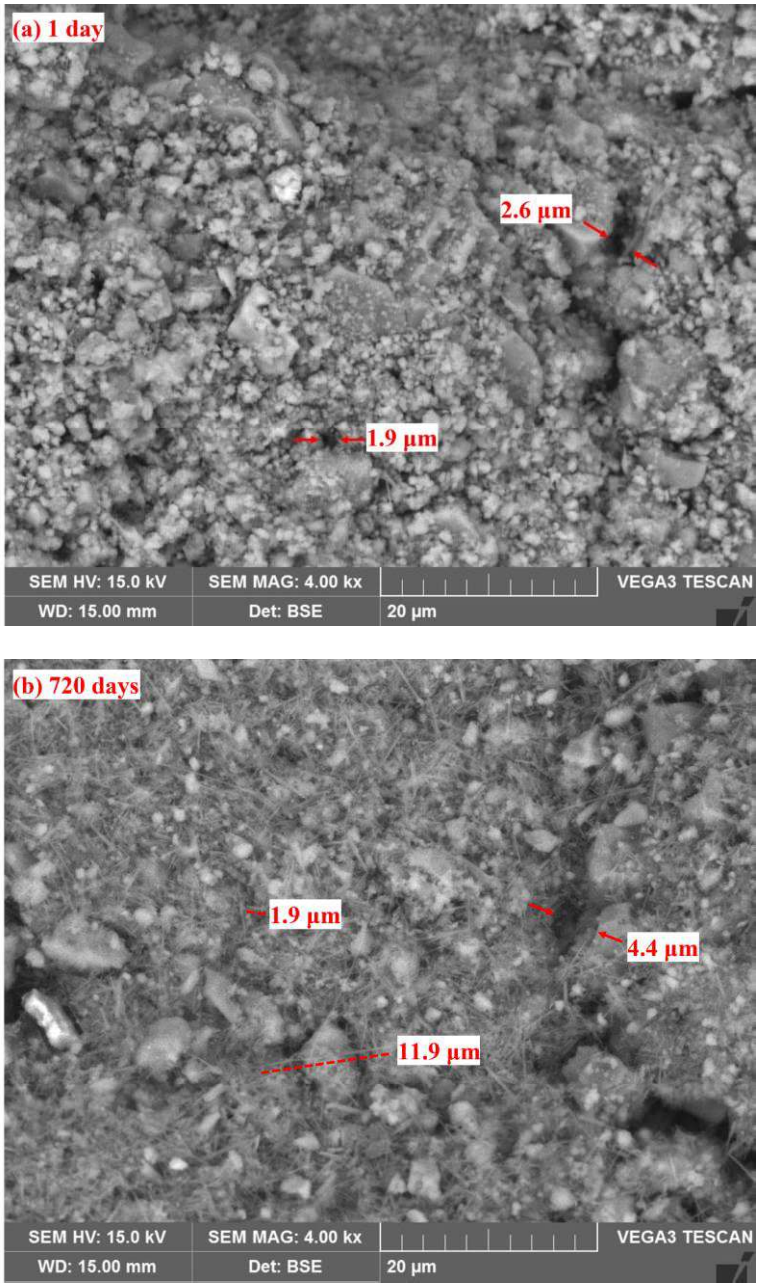

Figure III.8. SEM images of NRCA curing for 1 and 360 days (4000×): (a) 1 day (unbound); (b) 360 days (bound).

Among these hydration products, it can be observed that the numerous needle-shape hydration products, ettringite, between few and ten µm long, are formed after curing 360 days, followed with the decreasing number of fine particles as can be seen in Figure III.8 (b). This is in good agreement with the observation from TGA. These ettringite ($Ca_6Al_2(OH)_{12}\cdot(SO_4)_3\cdot 26H_2O$) absorb a large amount of water and has a large volume, filling the small macro-pores (width less than 3 µm). Furthermore, it can be observed that most of these ettringite are small ettringite (less than 10 µm long), only very few long ettringite can be observed. In general, there are two

types of ettringite: large ettringite (10-100 μm long) and small ettringite (typically 1-2 μm long) (Mehta, 1983). One explanation is that these small needle-shape ettringite are formed by the reactions between sulfate and cement hydration products (Hewlett & Liska, 2019; Kampala et al., 2021), such as hydrated calcium aluminates. The low water-soluble sulfate content of NRCA (0.23%) limits the growth and the size of ettringite. However, the hydration of unhydrated cement can also form the ettringite.

Although the water-soluble sulfate content of NRCA (0.23%) is much less than the limitation of standard (0.7%) as mentioned above, many small ettringite were still formed. It should be mentioned that once the voids are fully filled by the hydration products, such as hydration products of unhydrated cement and ettringite, the continuous formations of ettringite can lead to the cracks of structure, known as sulfate attack for concrete (Mehta, 1983), decreasing the strength and stiffness of RCA base and subbase layer, although this phenomenon has not been observed yet in this study. Thus, the sulfate content of RCA should be strictly limited when RCA are used in unbound or bound pavement layers.

Among those SEM images (Figure III.6-Figure III.8), a few cracks can be observed for NRCA curing for both 1 and 360 days (such as Figure III.8), which could due to the oven-drying method although the low drying temperature was used to avoid the shrinkage of drying. For soil samples, freeze-drying method is considered to be the most appropriate method than oven-drying method, as it makes no damage to microporosity structure (Su et al., 2022b; Zhang & Li, 2010). However, due to the limitation of the device, oven-drying method was used in this study.

III.5.2 Mercury intrusion porosimetry (MIP) tests

Figure III.9 and Figure III.10 depict the pore size distribution and cumulative intrusion void ratio e_M of fine NRCA soil curing 1 and 360 days. It was known that the microstructure of UGM is highly non-uniform. To improve the reliability of MIP results, each test was repeated 3 times under 3 specimens.

The pore size distribution curves of fine NRCA soil curing 1 day show a trimodal feature, which is a one mode mainly in the pore radius ranges from 0.1 to 3 μm and another mainly in the range from 3 to 100 μm. While for NRCA curing 360 days, only a bimodal distribution was observed, with pore radius less than 1 μm. For compacted UGM, there are two different kinds of pores: micro-pores and macro-pores (Delage et al., 1996; Su et al., 2022b; Zhang & Li, 2010). The micro-pores were generally within aggregates (intra-aggregate pores), while the macro-pores

were between aggregates (inter-aggregate pores), also known as skeleton void which could be used to interpret the mechanical behaviour of UGM (Zhang & Li, 2010). Su et al. (2022b) observed the boundary radius is around 0.65 μm for micro-pores and macro-pores for compacted soil without coarse aggregates (particle size less than 3.2 mm). In other words, the number of macro-pores (radius above 1 μm and less than 20 μm) decreased after curing 360 days due to the self-cementing properties of RCA. This was also supported by the SEM observations as mentioned above. Besides, it appears that the macro-pores larger than 20 μm, especially for NRCA curing for 360 days, tend to increase, probably due to the oven-drying method, which is in agreement with the SEM observations.

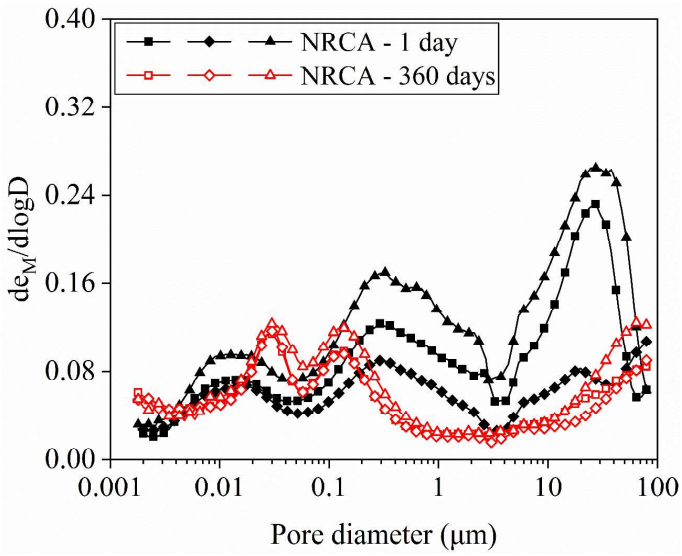

Figure III.9. Pore size distributions of fine NRCA soil curing 1 and 360 days.

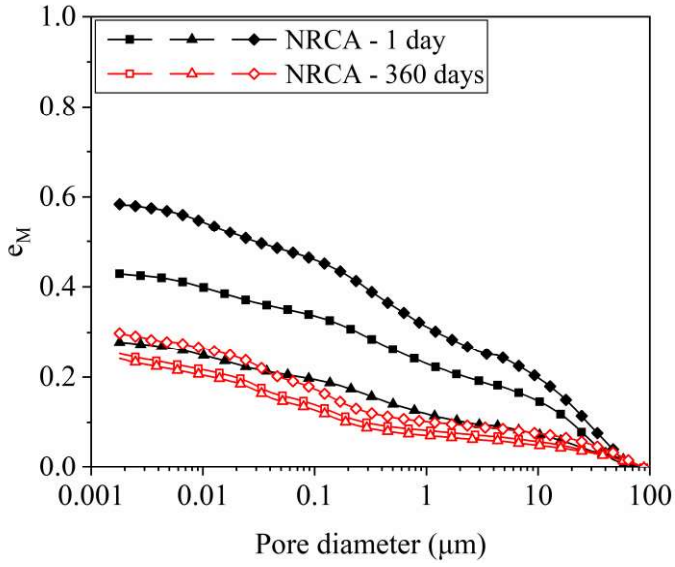

Figure III.10. Cumulative intrusion void ratio e_M of fine NRCA soil curing 1 and 360 days.

Since the volume of macro-pores (radius above 1 μm) decreased after curing 360 days, a decrease of maximum intrusion void ratio e_M after curing can be observed, as shown in Figure III.10, indicating a tighter microstructure after curing 360 days, observed also from SEM observation. For NRCA curing 1 day, the average e_M of three specimens is 0.43, decreasing to 0.26 after curing 360 days.

Another interesting observation is that the uniformity of microstructure is improved after curing 360 days (Figure III.10). For NRCA curing 1 day, both pore size distribution and e_M of three specimens vary significantly due to the non-uniformity of UGM. However, after curing 360 days, pore size distribution and e_M of three specimens are quite similar. As can be seen in Figure III.9, the primary cause of non-uniform microstructure of UGM is due to the non-uniformity of macro-pores, which is observed also by Su et al. (2021). However, since hydration productions fill the macro-pores, the number of macro-pores decreases, improving the uniformity of microstructure.

III.6 Mechanism of self-cementing properties

These results reveal that the mechanism of self-cementing properties is complex. On one hand, almost all the effective unhydrated cement, especially in fine aggregates, hydrate with moisture in the first year, as indicated by TGA. Besides, the sulfate in the RCA can also lead to the self-cementing properties of RCA, by forming ettringite. The hydration products and sulfate attack products not only form bonds between particles, but also fill the small macro-pores (width less than 3 μm), turning loose open type structure to the rigid tight skeleton structure (Figure III.6 (b), Figure III.7 (b) and Figure III.8 (b)).

On the other hand, the consumption of moisture due to the hydration process decreases the free water content, around 1% indicated by the increased non-evaporable water content , which can also improve the mechanical behaviours of RCA specimens (Gaillard et al., 2019; Jing et al., 2019). Besides, the improved tighter microstructure and decreased free water content can also lead to the increase of matric suction, which can also improve the mechanical behaviours of RCA specimens. However, the effect of suction after curing needs to be studied in a further study.

III.7 Conclusions

In this chapter, the self-cementing properties of NRCA and ORCA were investigated firstly by pH value measurement and calorimeter test. To evaluate unhydrated cement content, a method was proposed based on the non-evaporable water content measured by thermogravimetric analysis (TGA). The hydration of unhydrated cement and the improvement of microstructure of RCA specimens due to the self-cementing properties was investigated by TGA, scanning electron microscopic analysis (SEM) and mercury intrusion porosimetry (MIP) tests. Finally, the mechanism of the self-cementing properties was demonstrated based on these observations.

The evaluation of self-cementing properties shows that NRCA exhibits strong self-cementing properties while those of ORCA and RCAP are negligible. The pH value of NRCA (13.07) is much higher than that of ORCA (10.53) and RCAP (9.48). Besides, the average heat released by NRCA, due to the hydration of unhydrated cement, is 14.7 J, which is much higher than that released by ORCA (1.97 J). The calcite content of ORCA (29.97%) is much higher than that of NRCA (14.7%) and RCAP (11.67%), showing a high degree of carbonation of ORCA after long-term storage outside.

The calculation of unhydrated cement content based on TGA shows that the non-evaporable water is more suitable to be used to quantify unhydrated cement content than portlandite ($Ca(OH)_2$). The potential unhydrated cement content of NRCA fine aggregates (0-2 mm) is between 6.2% and 7.9%.

After curing 360 days, the non-evaporable water content of NRCA increased by 1%, while for ORCA, it is almost constant. The greatest influence of self-cementing properties on the RCA mechanical behavior is in the first year. For NRCA, between 55% to 70% of the total unhydrated binder (4.3%) were hydrated after curing 360 days, and this hydration appears to be stopped after curing for 360 days. However, the formation of ettringite, sulfate attack products, was observed between curing for 360 days and 720 days, which could also lead to the self-cementing properties of RCA.

SEM observation indicates that the hydration products not only form bonds between particles, but also fill the small macro-pores between particles (radius less than 3 μm and higher than 0.65 μm). For the big macro-pores (radius larger than 3 μm), the filling effect is limited. The open type of structure (curing 1 day) turns to rigid tight skeleton structure after curing 360 days.

MIP tests show that the volume of macro-pores (radius above 1 μm and less than 20 μm) decreases significantly after curing 360 days. As a result, the average intrusion void ratio e_M

decreases from 0.43 (curing 1 day) to 0.26 (curing 360 days). The decreased volume of macro-pores also improve the uniformity of RCA specimen.

The mechanism of self-cementing properties is complex. The hydration products and sulfate attack products not only form bonds between particles, but also fill the small macro-pores, improving the microstructure of RCA specimen. Besides, the hydration of unhydrated cement also decreases the free water content. Consequently, the improved microstructure and decreased free water content can increase the matric suction, which further improve the mechanical behaviour of RCA specimen.

Chapter IV. Mechanical behaviour of RCA in repeated load triaxial tests

The gradual accumulation of permanent deformation could lead to rutting, while the too large resilient deformation could lead to fatigue cracking of the overlying bound layers, resulting in the failure of the pavement. As a result, permanent deformation and resilient deformation determined by repeated load triaxial tests (RLTT) are two important parameters for pavement design.

The engineering properties of RCA materials from different sources could be totally different due to the different strength and quality of concrete structures, while the self-cementing properties can improve the mechanical behavior of RCA. However, little studies and experimental data could be found in the literature in terms of the study of permanent deformation and resilient deformation behavior of RCA.

In this chapter, the effect of RCA source and self-cementing properties on the permanent deformation and resilient deformation has been studied by repeated load triaxial tests. Three different RCA materials, sourced from demolished buildings (NRCA and ORCA) and pavement (RCAP), after different curing times (1, 180, 360 and 720 days), were subjected to repeated load triaxial test. For analytical modelling, the widely used model proposed by Hornych (1993) for unbound granular materials (UGM) was adopted to simulate the permanent axial deformations. The resilient modulus was modelled by k-θ model and Uzan model, while resilient deviatoric strain and volumetric strain were modelled by modified Boyce model and DBGSP model (Chapter I). The study can lead to a better understanding of the short-term and the long-term mechanical behaviors of RCA materials.

IV.1 Methods

The sample preparation procedures were same with the monotonic triaxial tests. The mixtures were mixed with water to the targeted water content, and sealed in plastic bags for 24h for moisture homogenization. Thereafter, each sample, with a diameter of 150mm and a height of 285mm, was compacted in a split mould to the targeted dry density, by vibrating hammer in 7 layers. To better compare the permanent deformation and resilient deformation behaviors of these RCA materials, all the RCA specimens are prepared to have the same testing parameters,

such as particle size distribution, water content (OMC-1%) and dry density (maximum dry density at the targeted water content).

The RLTT is the most representative method to investigate permanent and resilient behaviors of UGM under traffic loads. In this study, RLTTs were carried out following the procedure of the European Standard NF EN 13286-7 (2004), which consist of a conditioning phase (permanent deformation test) followed by a resilient phase (resilient deformation test).

To study the permanent deformation (conditioning phase), the specimens were subjected to repeated load triaxial tests under constant confining pressure (CCP, σ_3=70 kPa) and a cyclic axial load (Δq=340 kPa) at the frequency of 1 Hz for 20000 loading cycles, to stabilize permanent deformation.

After the permanent deformation test, the same specimen was subjected to RLTT, under constant confining pressure (CCP) or variable confining pressure (VCP), at the frequency of 0.1 Hz for 100 loading cycles, to study the resilient behavior of RCA materials. Stress paths for the resilient test (CCP loading and VCP loading) are provided in Table II.4 and Table II.5.

The resilient deformation behavior was presented in terms of resilient modulus (M_r), resilient deviatoric strain (ε_q^r) and volumetric strain (ε_v^r) (see section I.2.2). The widely used k-θ model (Seed et al., 1967) and Uzan model (Uzan, 1985) were used to analyze the M_r:

$$M_r = K_1 \theta^{K_2} \tag{IV.1}$$

$$M_r = K_3 \left(\frac{\theta}{p_a}\right)^{K_4} \left(\frac{q}{p_a}\right)^{K_5} \tag{IV.2}$$

where θ is the bulk stress ($\sigma_1+\sigma_2+\sigma_3$), q is the deviator stress, p_a is the atmospheric pressure (100 kPa), and K_1, K_2, K_3 K_4, and K_5 are model parameters determined by regression analyses.

Resilient deviatoric strain (ε_q^r) and volumetric strain (ε_v^r) give a different approach to characterize the stress-strain relationship of granular materials. It is well known that unbound granular materials show a nonlinear resilient deformation behavior and exhibit an anisotropy behavior. Thus, ε_q^r and ε_v^r were modelled by a nonlinear elastic model proposed by Boyce (1980) and improved by Hornych et al. (1998) by introducing a coefficient of anisotropy γ:

$$\varepsilon_q^{\ r} = \frac{2}{3} * \frac{p^{*n_1}}{p_a^{\ n_1-1}} \left[\frac{\gamma-1}{3K_a} + \frac{n_1-1}{18G_a}(\gamma-1)\left(\frac{q^*}{p^*}\right)^2 + \frac{2\gamma+1}{6G_a} * \frac{q^*}{p^*} \right] \tag{IV.3}$$

$$\varepsilon_v^{\ r} = \frac{p^{*n_1}}{p_a^{\ n_1-1}}\left[\frac{\gamma+2}{3K_a} + \frac{n_1-1}{18G_a}(\gamma+2)\left(\frac{q^*}{p^*}\right)^2 + \frac{\gamma-1}{3G_a} * \frac{q^*}{p^*}\right] \quad \text{(IV.4)}$$

where p_a is the atmospheric pressure (100 kPa), K_a, G_a, γ and n_1 are model parameters. K_a and G_a are related to the bulk and shear moduli and γ is the anisotropy coefficient. p^* and q^* are modified mean normal stress and deviator stress, and can be redefined as follows:

$$p^* = \frac{\gamma\sigma_1 + 2\sigma_3}{3} \quad \text{(IV.5)}$$

$$q^* = \gamma\sigma_1 - \sigma_3,\ 0 < \gamma < 1 \quad \text{(IV.6)}$$

Recently, Ezaoui et al. (2006) and Ezaoui and Di Benedetto (2008) have proposed another anisotropic model, the DBGSP model, to describe the anisotropic resilient behavior of UGM. According to the assumption of a transverse isotropic elastic behaviour, the strain increment and stress increment can be expressed as:

$$\Delta\varepsilon_1 = \frac{P_{ref}^{\ n_2}}{\alpha \cdot \sigma_z^{\ n_2}}\left[\Delta\sigma_z - \nu_0\left(1 + \beta\frac{\sigma_z^{\ n_2}}{\sigma_r^{\ n_2}}\right)\Delta\sigma_r\right] \quad \text{(IV.7)}$$

$$\Delta\varepsilon_3 = \frac{P_{ref}^{\ n_2}}{\alpha}\left[\frac{\beta(1-\nu_{rr})}{\sigma_r^{\ n_2}}\Delta\sigma_r - \frac{\nu_0\left(1+\beta\frac{\sigma_z^{\ n_2}}{\sigma_r^{\ n_2}}\right)}{2\sigma_z^{\ n_2}}\Delta\sigma_z\right] \quad \text{(IV.8)}$$

where P_{ref} is a constant equal to 1MPa, α, β, n_2, v_0 and v_{rr} are model parameters. α is related to the Young modulus, β is the anisotropy coefficient, v_0 and v_{rr} are related to the Poisson ratio. Consequently, volumetric strain ε_v and the deviatoric strain ε_q can be obtained from $\Delta\varepsilon_1$ and $\Delta\varepsilon_3$.

To better classify and rank all the RCA materials, the characteristic resilient modulus E_c, defined as the resilient modulus determined for the stress states p=250 kPa and q=500 kPa, can be calculated by:

$$E_c = \frac{q}{\varepsilon_1^{\ r}} \quad \text{(IV.9)}$$

where q is the deviator stress (500 kPa), $\varepsilon_1^{\ r}$ is the resilient axial strain under stress state p=250 kPa and q=500 kPa, calculated by modified Boyce model and DBGSP model.

IV.2 Effect of RCA sources

The engineering properties of RCA materials from different sources could be totally different due to the different strength and quality of concrete structures. To study the mechanical behavior of RCA from different sources, three different RCA materials, sourced from demolished buildings (NRCA and ORCA) and demolished pavement (RCAP), were obtained and were subjected to RLTT with same testing parameters, such as water content, dry density, sample preparation and curing time (1 day). The differences of physical properties between these RCA materials are presented in Chapter II, Section II.1.

IV.2.1 Permanent deformation behavior

Figure IV.1 and Figure IV.2 present the evolution of the permanent axial strains ε_1^p and permanent radial strains ε_3^p of all RCA materials, with the number of cycles. For both RCA materials, ε_1^p increases rapidly in the first cycles, and then a predominant stabilisation phase is noticed except for RCAP. Indeed, since all the testing parameters are the same for NRCA and ORCA, they present a similar evolution of ε_1^p and ε_3^p, as shown in Figure IV.1 (a) and Figure IV.2 (a).

To classify these RCA materials, Table IV.1 summarizes the average ε_1^p after loading 20000 cycles, the average permanent strain rate $\Delta\varepsilon_1^p/\Delta N$ over the last hundred cycles and the characteristic permanent strain ε_1^c for all RCA materials. The classification of RCA will be illustrated after. The characteristic permanent strain ε_1^c is defined by (NF EN 13286-7, 2004):

$$\varepsilon_1^c = \varepsilon_1^p(20000) - \varepsilon_1^p(100) \quad \text{(IV.10)}$$

where ε_1^p *(100)* and ε_1^p *(20000)* are ε_1^p after 100 cycles and 20000 cycles.

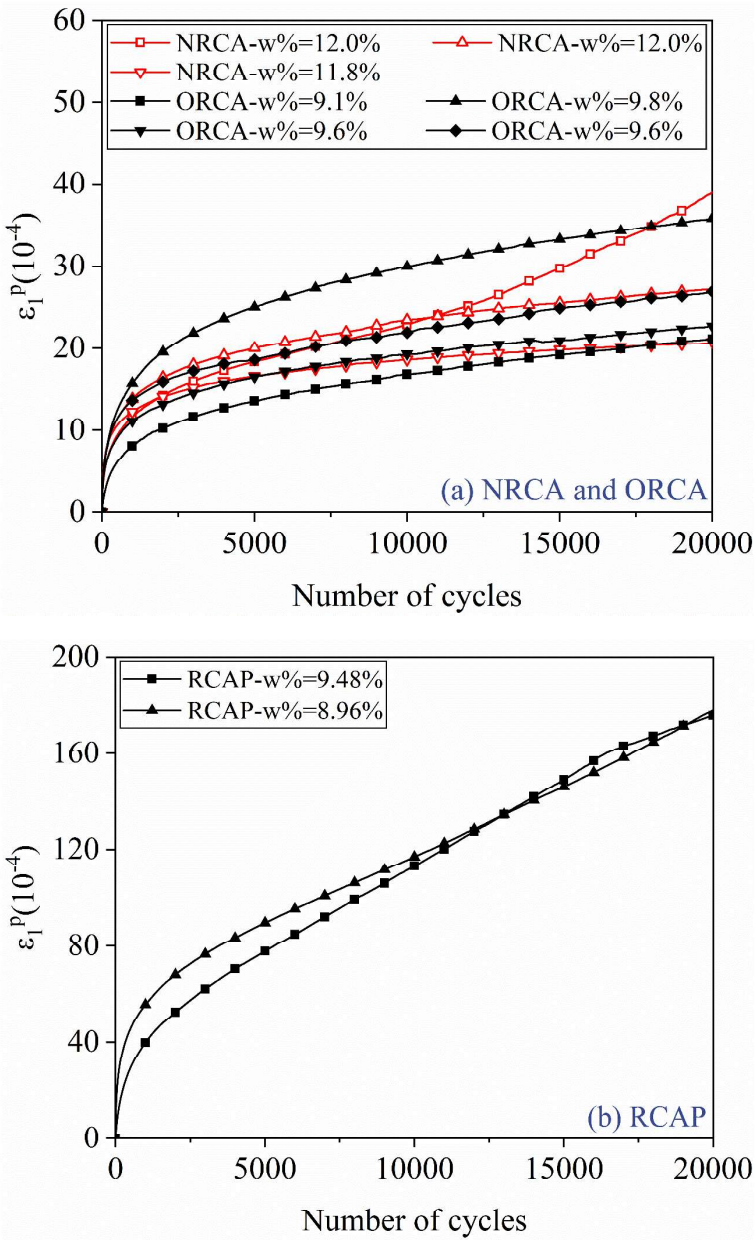

Figure IV.1. Permanent axial deformations of all RCAs (curing for 1 day): (a) NRCA and ORCA; (b) RCAP.

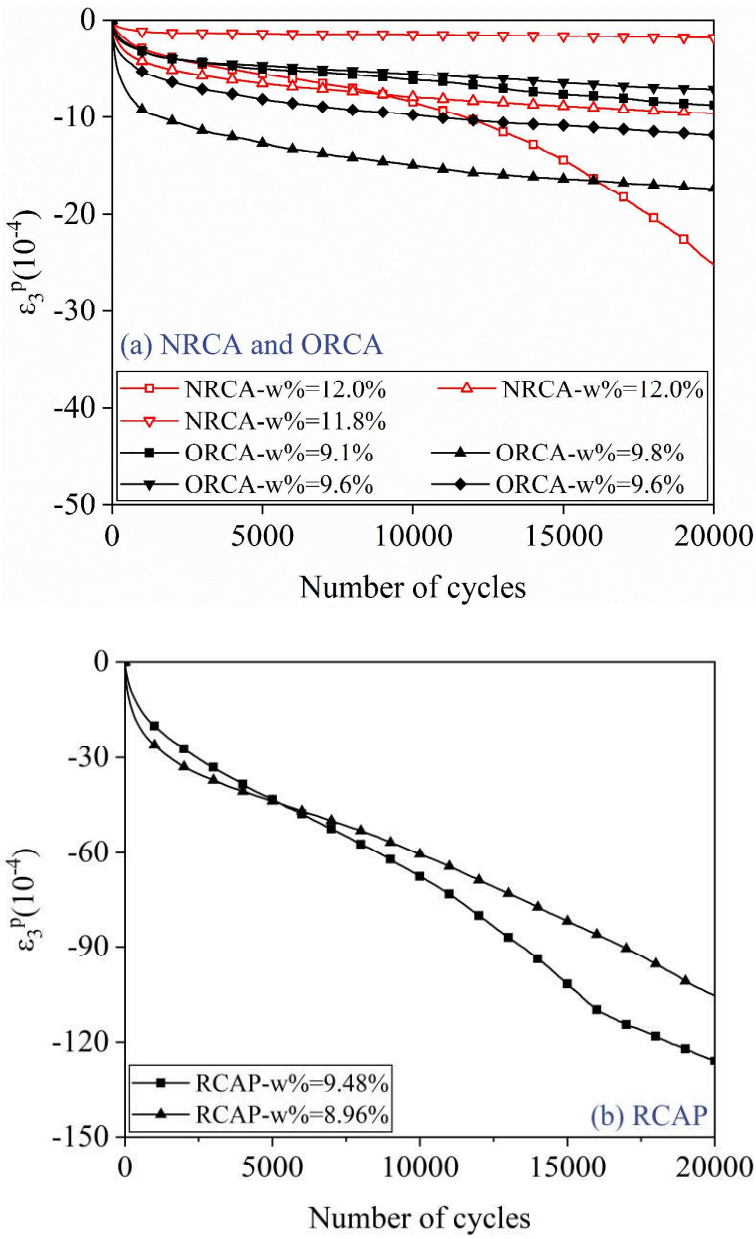

Figure IV.2. Permanent radial deformations of all RCAs (curing for 1 day): (a) NRCA and ORCA; (b) RCAP.

Table IV.1. Average permanent deformation of NRCA, ORCA and RCAP.

Materials	ε_1^p (10^{-4})	$\Delta\varepsilon_1^p/\Delta N$ (10^{-7})	ε_1^c (10^{-3})
NRCA	28.9	1.04	2.39
ORCA	26.7	0.68	2.14
RCAP	176.9	5.71	15.73

It can be observed that the permanent deformation behavior depends strongly on the RCA source, with RCAP, sourced from demolished concrete pavement, generating much larger ε_1^p and ε_3^p than these of NRCA and ORCA, sourced from demolished buildings. Besides, the value of $\Delta\varepsilon_1^p/\Delta N$ of RCAP is higher than 10^{-7}, indicating that ε_1^p has not achieved the shakedown state after 20000 cycles (Jing et al., 2018; NF EN 13286-7, 2004). More loading cycles could be carried out to confirm the shakedown behavior of RCAP. This high increasing rate of ε_1^p induced by traffic loads could lead to failure or excessive rutting of pavement. Although the main physical properties of RCAP, such as fine content, the resistance of aggregates to fragmentation and wear and sulfate content, were within the specified limits (see Section II.1), the RCAP appears to be unsuitable for use in base or subbase layers.

Thereafter, the permanent deformation behavior of these RCA materials were compared with that of unbound granular materials (UGM). Alnedawi et al. (2021) and Jing et al. (2020) conducted RLTT on different UGM, with similar test conditions as in this study. The results indicated that the tested UGM presented much higher ε_1^p values, varying between 50×10^{-4} and 200×10^{-4} after 20000 cycles, than the NRCA and ORCA materials. Gaillard et al. (2019) also determined the ε_1^p values of reclaimed asphalt pavement (RAP) used as UGM. The results showed that the ε_1^p values of RAP are around 200×10^{-4}, under the same test conditions. This suggests that the performance of most RCA materials (NRCA and ORCA) in terms of permanent deformations are similar or better than that of natural UGM, while the performance of RCAP was worse than most of UGM, as shown in Table IV.1.

It should be recalled that RCAP presented a much higher percentage of rounded particles (15.1%) than those of NRCA (4.1%) and ORCA (1.1%) (see Section II.1). Besides, the water absorption of RCAP aggregates, between 2.56% and 7%, is lower than that of NRCA and ORCA, between 4.30% and 10.86%. RCAP also has a higher fine content (5.3%) and lower optimum moisture content (10.9%), and the dry density is sensitive to the water content (Figure II.3). This can be attributed to the high amount of rounded aggregates and low strength of parent concrete of RCAP. Due to the crushing process, the attached mortar can separate from the rounded particles, leading to a smaller mortar content and a high amount of rounded aggregates in RCAP. Indeed, the design compressive strength of concrete for pavements in France is generally smaller than that for buildings.

Some researchers (Kwon et al., 2017; Lekarp et al., 2000b; Pan et al., 2006; Tutumluer & Pan, 2008) have indicated that aggregates with higher percentage of angular particles (RCAB1 and

RCAB2) can resist to the permanent deformation accumulation and have higher resilient modulus, compared to the aggregates with rounded particles which have higher permanent deformation. This indicates that the high permanent deformation of RCAP was highly attributed to the high rounded particles content. On the other hand, the lower design strength of concrete for pavement and rounded particles could lead to a lower bond strength between original NA and surrounding mortar, which could break during the conditioning phase, leading to a higher ε_1^p and ε_3^p of RCAP.

IV.2.2 Resilient deformation behavior under CCP loading

Resilient modulus

Figure IV.3 depicts resilient modulus M_r and k-θ model predictions of three RCA materials, NRCA, ORCA and RCAP, as well as the M_r of typical unbound granular materials (UGM) reported in Corradini et al. (2021). The testing parameters of presented UGM, such as particle size (0-20 mm), water content (OMC) and dry density (MDD), were similar to our study. Both RCA materials, NRCA, ORCA, RCAP, show a high degree of dependence on the mean normal stress q for the resilient modulus M_r, in good agreement with unbound granular materials (Lekarp et al., 2000a). Furthermore, the resilient moduli M_r of NRCA and ORCA, both sourced from demolished buildings, are similar with those of UGM, but higher than those of RCAP, sourced from demolished concrete pavement, especially under high stress state.

The parameters of k-θ model and Uzan model for NRCA, ORCA and RCAP, as well as traditional UGM (Corradini et al., 2021; Stolle et al., 2009), were summarized in Table IV.2. A very good fit can be obtained as all the coefficient of determinations are higher than 0.90, except RCAP. Besides, it appears that Uzan model is more accurate than k-θ model, after accounting for the effect of shear stress q, indicated by a higher R^2.

Another significant observation is that the parameters K_1 and K_3 of RCAP are higher or similar to these of NRCA and ORCA, while the parameters K_2, K_4 and K_5 (absolute value) are much lower than these of NRCA and ORCA, showing a less stress dependency of RCAP caused by high amount of rounded particles. When we compared these parameters with the UGM, reported by Corradini et al. (2021) and Stolle et al. (2009), it can be observed that these RCA materials have lower K_1 and K_3, while higher K_2, K_4 and K_5 (absolute value) (except RCAP), than those of UGM. This suggests that RCA materials have lower resilient modulus than most

of UGM under low stress state. However, the stress dependencies of NRCA and ORCA are higher than RCAP and most UGM.

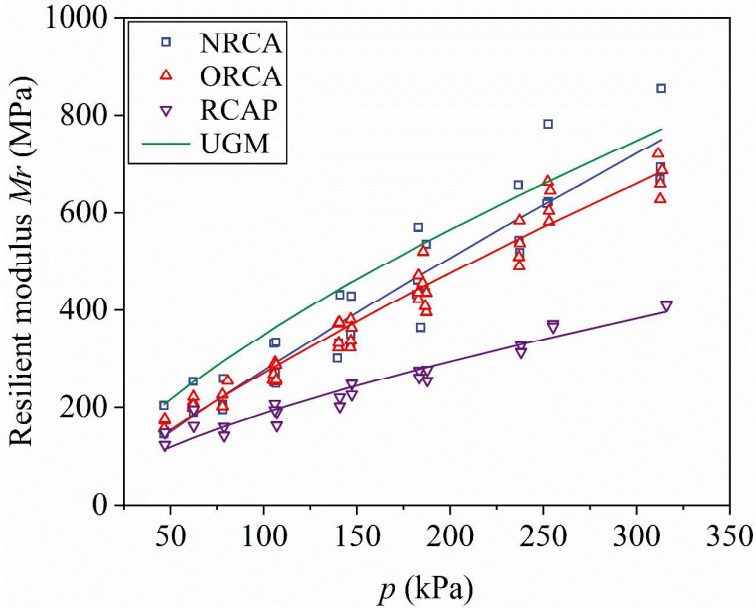

Figure IV.3. Test results and k-θ model predictions of M_r for NRCA, ORCA, RCAP (curing for 1 day) and UGM (Corradini et al., 2021) under CCP loading.

Table IV.2. Summary of k-θ model and Uzan model parameters for NRCA, ORCA, RCAP and UGM.

Materials	k-θ			Uzan			
	K_1	K_2	R^2	K_3	K_4	K_5	R^2
NRCA	1.91	0.87	0.903	95.35	1.12	-0.29	0.912
ORCA	2.69	0.81	0.959	100.32	1.05	-0.29	0.970
RCAP	4.76	0.65	0.817	90.49	0.70	-0.07	0.818
UGM	5.41-14.45[a]	0.64-0.71[a]		40-260[b]	0-0.9[b]	-0.45-0.6[b]	

Note: data from [a]Corradini et al. (2021), [b]Stolle et al. (2009).

Resilient deviatoric strain and volumetric strain

Figure IV.4 and Figure IV.5 depict the experimental and modelling results (Boyce and DBGSP model) of resilient deviatoric strain ε_q^r and volumetric strain ε_v^r of NRCA, ORCA and RCAP,

under different constant confining pressures (20, 35, 50, 70, 100 and 150 kPa). As observed in resilient modulus, NRCA and ORCA have a similar ε_q^r under different confining pressures, while it is much lower than those of RCAP. As for the ε_v^r, NRCA exhibits a contractant behavior under these confining pressures, while ORCA and RCAP show a dilatant behavior. In particular, the ε_v^r of RCAP are much higher than those of NRCA and ORCA.

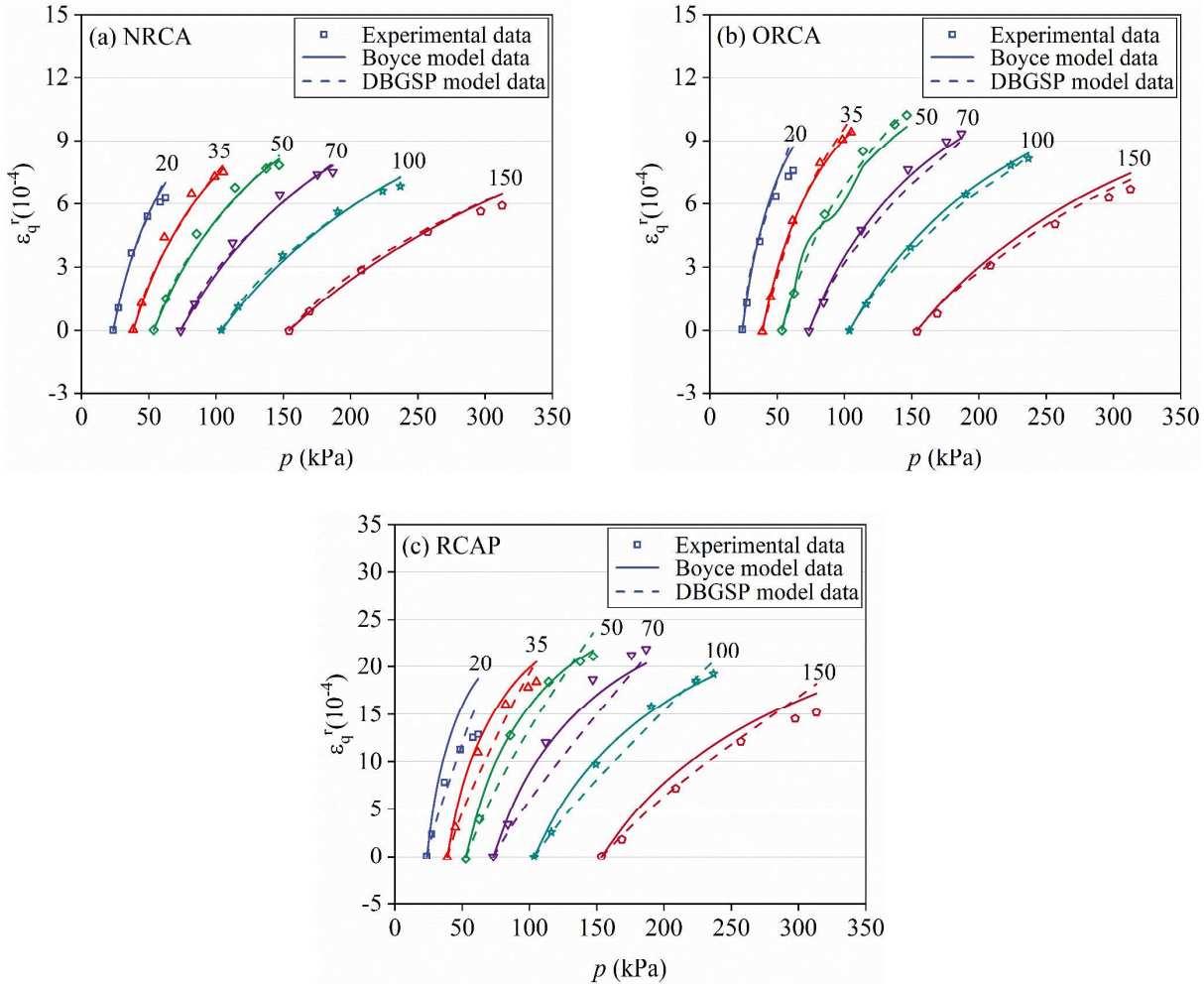

Figure IV.4. Resilient deviatoric strain ε_q^r of RCA materials (curing for 1 day) under different constant confining pressures (σ_3=20/35/50/70/100/150 kPa): (a) NRCA; (b) ORCA and (c) RCAP.

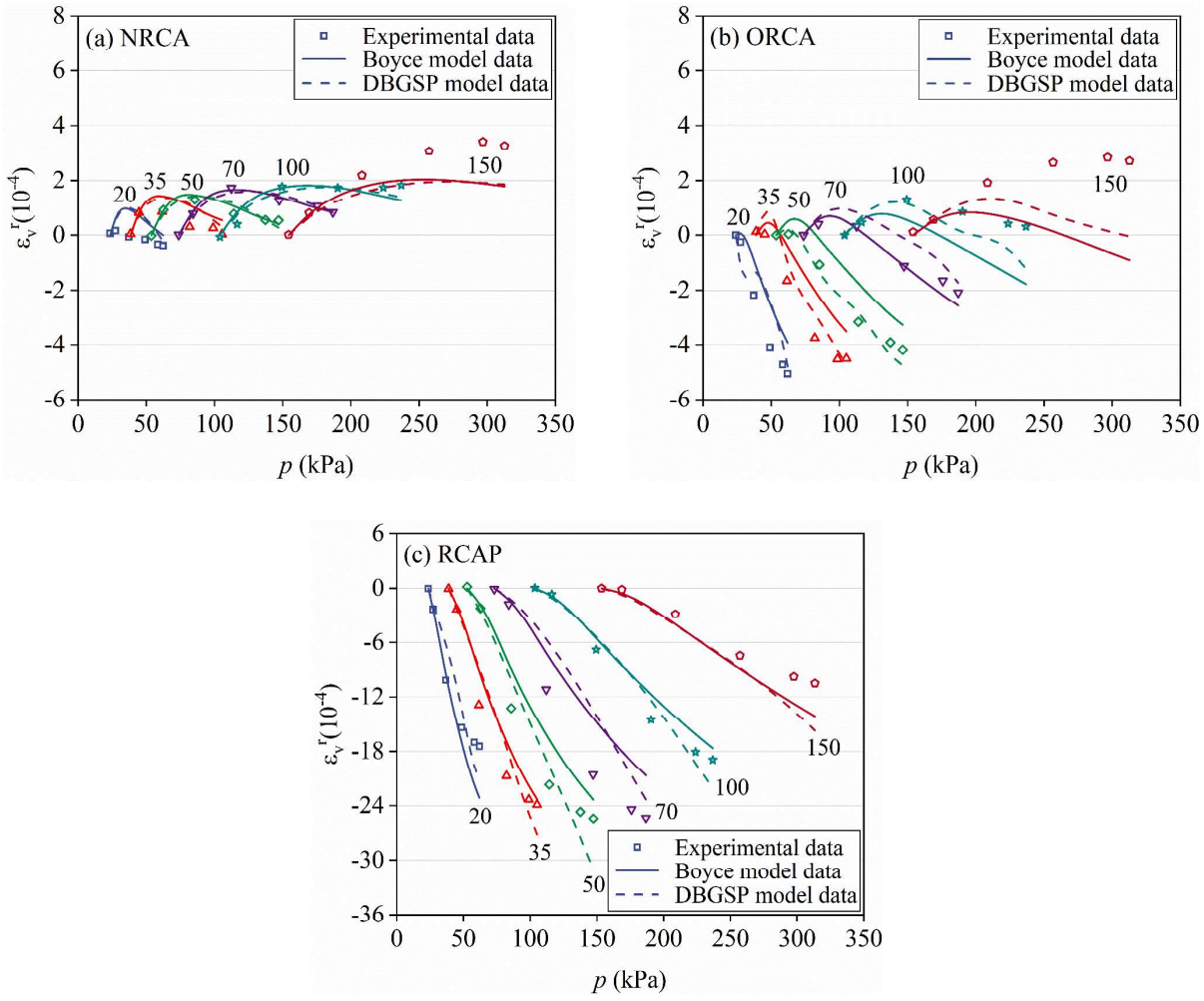

Figure IV.5. Resilient volumetric strain ε_v^r of RCA materials (curing for 1 day) under different constant confining pressures (σ_3=20/35/50/70/100/150 kPa): (a) NRCA; (b) ORCA and (c) RCAP.

Table IV.3 and Table IV.4 summarize the modified Boyce and DBGSP model parameters of NRCA, ORCA and RCAP, under these constant confining pressures. It can be observed that these models can predict ε_q^r and ε_v^r very well (Figure IV.4 and Figure IV.5), with the same accuracy, as all the coefficient of determination (R^2) are higher than 0.9. The parameters *Ka* and *Ga* are related to the bulk and shear moduli, while parameter α is related to the Young modulus. As observed in experimental results, NRCA and ORCA have obtained similar parameters *Ka*, *Ga* and α, which are higher than those of RCAP, indicating a better resilient performance of NRCA and ORCA. Note that these parameters can only be used to predict ε_q^r and ε_v^r under CCP loading, as only experimental data under CCP loading was used to optimise these parameters.

Table IV.3. Modified Boyce model parameters of NRCA, ORCA and RCAP, under constant confining pressure.

Materials	K_a/MPa	G_a/MPa	n_1	γ	R^2
NRCA	1.54	49.81	0.03	0.59	0.97
ORCA	1.15	42.36	0.02	0.55	0.94
RCAP	0.10	31.06	0.00	0.97	0.97

Table IV.4. DBGSP model parameters of NRCA, ORCA and RCAP, under constant confining pressure.

Materials	α/MPa	β	n_2	ν_0	R^2
NRCA	2027.32	1.22	0.96	0.30	0.965
ORCA	1915.14	29.86	0.98	0.01	0.958
RCAP	781.25	62.72	0.70	0.02	0.978

IV.2.3 Resilient deformation behavior under VCP loading

After CCP loading, the same specimens were also subjected to VCP loading, where both confining pressure and axial load are cycled in phase, as VCP loading is considered to better simulate the stress paths in pavements subjected to rolling loads than CCP loading. Figure IV.6 and Figure IV.7 present comparisons between the experimental values of ε_q^r and ε_v^r obtained under different stress paths, and the predictions of the modified Boyce model and DBGSP model, for the three RCA materials. It can be observed that the resilient behaviour of RCA is very similar to that of UGM, whose resilient behaviour is strongly non-linear, and depends on the stress path $\Delta q/\Delta p$ (Ho et al., 2014; Jing et al., 2017). Besides, ε_q^r increases while ε_v^r decreases with increasing stress ratio $\Delta q/\Delta p$, for all RCAs.

For ε_v^r, it is positive (contraction) for all the RCAs, for all the stress paths except for RCAP, which presents negative volumetric strains (dilation) for the stress path $\Delta q/\Delta p$=2.5, as can be seen in Figure IV.7 (c). Furthermore, the ε_q^r and ε_v^r (absolute value) of RCAP under different stress paths are slightly higher than those of NRCA and ORCA. However, the resilient strains of all the RCAs are of the same order of magnitude, unlike permanent deformations and resilient deformations under CCP loading.

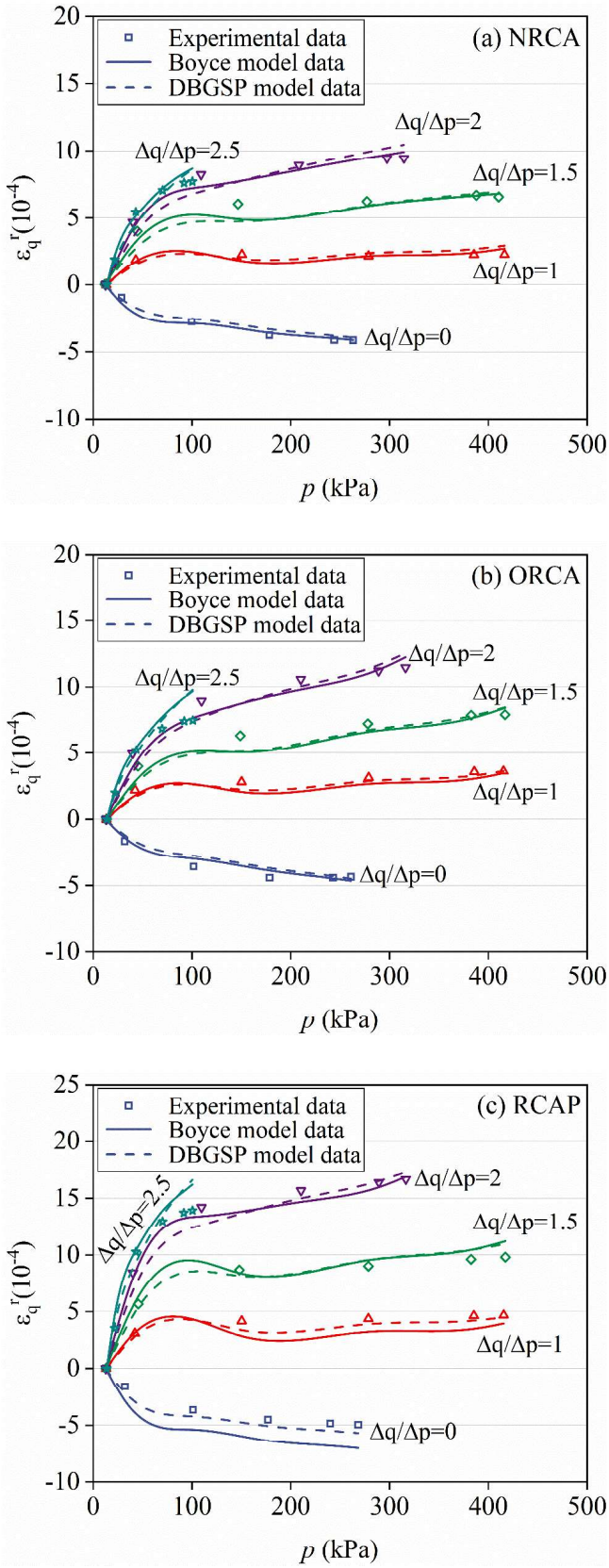

Figure IV.6. Resilient deviatoric strain ε_q^r of RCA materials (curing for 1 day) under different stress paths (Δq/Δp=0/1/1.5/2/2.5): (a) NRCA; (b) ORCA and (c) RCAP.

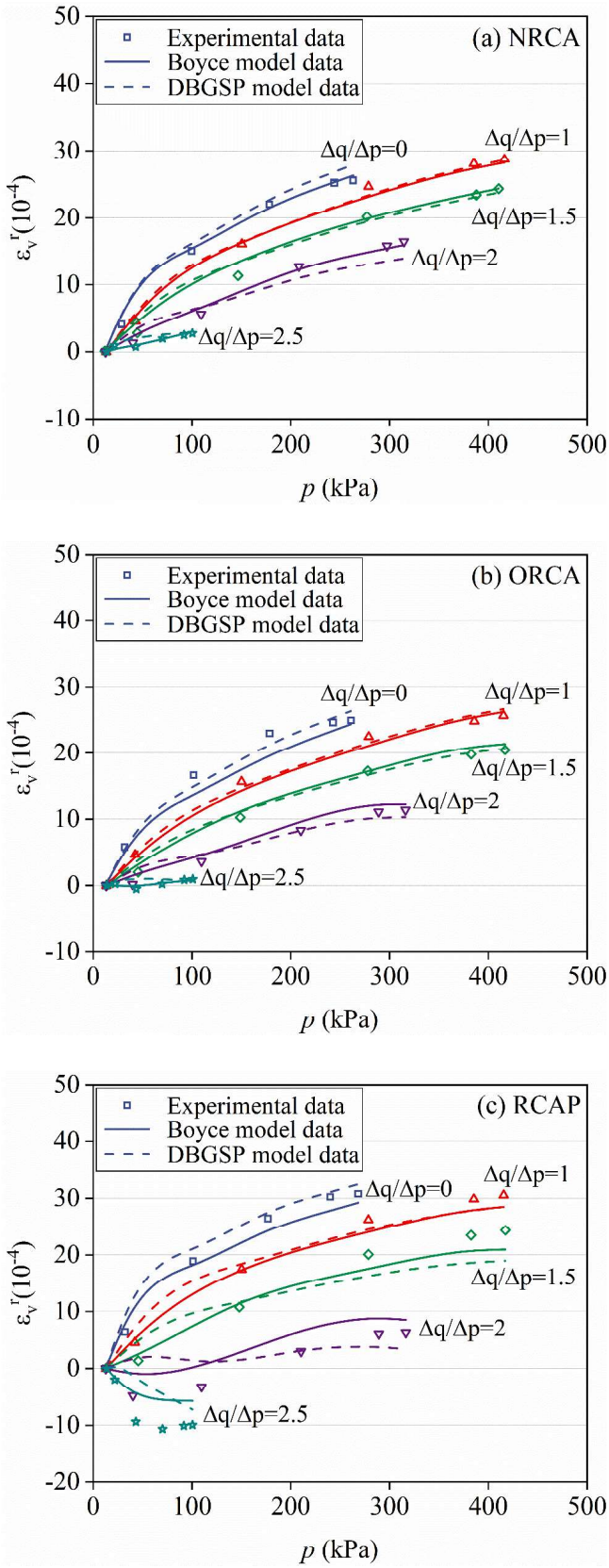

Figure IV.7. Resilient volumetric strain ε_v^r of RCA materials (curing for 1 day) under different stress paths (Δq/Δp=0/1/1.5/2/2.5): (a) NRCA; (b) ORCA and (c) RCAP.

The modified Boyce and DBGSP model parameters of NRCA, ORCA and RCAP, under different stress paths (Δq/Δp=0/1/1.5/2/2.5), are summarized in Table IV.5 and Table IV.7. The modified Boyce model parameters of unbound granular materials (UGM) and reclaimed asphalt pavement (RAP) aggregates reported by other researchers (Gaillard, 2019; Hornych et al., 2009; Jing & Chazallon, 2020) were also summarized in Table IV.5. Note that the original natural aggregates of all RCA and RAP were all sourced from Strasbourg and Gonesse, France, and have the similar mineralogical compositions, while the two UGM were both sourced from Nantes, France. All the testing parameters in these studies, such as particle size distribution (0-20mm), water content (OMC-1% or 2%), dry density (97%-99% of MDD), frequency (0.1Hz-2Hz), are similar for all materials, as summarized in Table IV.6.

Table IV.5. Modified Boyce model parameters of NRCA, ORCA and RCAP, under variable confining pressure.

Materials	K_a/MPa	G_a/MPa	n_1	γ	CC
NRCA	41.37	55.55	0.35	0.78	0.88
ORCA	39.80	48.61	0.44	0.71	0.84
RCAP	20.41	24.66	0.29	0.62	0.809
UGM[a]	16.77	38.47	0.27	0.80	0.799
UGM[b]	36.58	57.87	0.49	0.92	0.682
RAP[c]	23.81	58.84	0.31	0.68	0.776

Note: data from [a]Jing and Chazallon (2020), [b]Hornych et al. (2009) and [c]Gaillard (2019).

Table IV.6. Testing parameters of UGM and RCAP.

Materials	Grading/mm	Water content/%	Dry density/ Mg/m^3	Frequency/Hz
UGM[a]	0/20	OMC-2%	96% MDD	0.05
UGM[b]	0/14	OMC-1%	Void content of 15%	2
RAP[c]	0/20	OMC-1%	97% MDD	0.1

Table IV.7. DBGSP model parameters of NRCA, ORCA and RCAP, under variable confining pressure.

Materials	α/MPa	β	n_2	ν_0	ν_{rr}	CC
NRCA	1117.84	1.26	0.68	0.25	0.1	0.856
ORCA	902.43	1.39	0.61	0.24	0.1	0.839
RCAP	1131.64	1.47	0.86	0.28	0.1	0.789

It can be observed that both models describe the resilient behavior quite well, with the same accuracy, for all three RCA under different stress paths, as all the correlation coefficients (CC) are higher than 0.8. Regarding the modified Boyce model parameters, NRCA and ORCA have higher bulk modulus K_a and shear modulus G_a than RCAP, indicating a better performance of NRCA and ORCA. The parameters K_a and G_a of the three RCA materials are of the same order of magnitude compared with UGM (Hornych et al., 2009; Jing & Chazallon, 2020) and RAP (Gaillard, 2019). By contrast, the parameter n_1 of NRCA and ORCA, representing the stress dependency of materials, are higher than that of UGM[a], UGM[b] and RCAP, indicating a high stress dependency of NRCA and ORCA, which is observed also in resilient modulus. Besides, the coefficients of anisotropy γ of RCA materials are slightly smaller than those obtained for UGM, determined by Hornych et al. (2009) and Jing and Chazallon (2020), indicating a more pronounced anisotropic behavior of RCAs.

To better classify and rank all the RCA materials, the characteristic resilient modulus E_c, defined as the resilient modulus determined for the stress states p=250 kPa and q=500 kPa, was then calculated with the modified Boyce model and with the DBGSP model. The E_c values of the tested RCAs and UGM as well as RAP, calculated with the modified Boyce model and DBGSP model parameters, are also summarized in Table IV.8. It appears that NRCA and ORCA present a better performance than RCAP, indicated by the much higher E_c. Since the dry densities of presented two UGM materials and RAP (96-97% MDD) were slightly lower than those of studied RCA (optimum dry density at the targeted water content), E_c of NRCA and ORCA are much higher than those of UGM, showing a good performance of NRCA and ORCA. On the other hand, the *Ec* values calculated by two models are similar for these RCA materials, which is consistent with the accuracy of the two models.

European Standard NF EN 13286-7 (2004) proposed a simple ranking of UGM, based on the values of E_c and characteristic permanent strain ε_1^c (see Chapter IV.2.1), into 3 performance

categories, named C1, C2 and C3, as presented in Table IV.9. Based on this classification, three RCA materials can be ranked based on the permanent and resilient deformation behavior, as presented in Table IV.10. The results indicate that materials NRCA and ORCA are classified in category C2, which corresponds to a satisfactory behavior for use in pavement base layers, while RCAP is classified C3, which means that it is not suitable, according to this classification, for pavement base layers, which is in good agreement with the permanent deformation behavior.

Table IV.8. Characteristic resilient modulus E_c of RCA materials (NRCA, ORCA and RCAP), UGM and RAP.

Models	NRCA	ORCA	RCAP	UGM[a]	UGM[b]	RAP[c]
Boyce	302.8	299.6	233.8	176	207	342
DBGSP	343.2	322.3	280.3	No	No	No

Note: data from [a]Jing and Chazallon (2020), [b]Hornych et al. (2009) and [c]Gaillard (2019).

Table IV.9. Classification of unbound granular materials based on E_c and ε_1^c.

Class	E_c/MPa	$\varepsilon_1^c/10^{-3}$
C1	$500 \leq E_c$	$\varepsilon_1^c \leq 2.5$
C2	$500 \leq E_c$	$2.5 < \varepsilon_1^c \leq 6$
	$250 \leq E_c < 500$	$\varepsilon_1^c \leq 6$
C3	$250 \leq E_c$	$6 < \varepsilon_1^c$

Table IV.10. Classification of RCA materials.

Materials	E_c (Boyce)/MPa	E_c (DBGSP)/MPa	$\varepsilon_1^c/10^{-3}$	Class
NRCA	302.8	343.2	2.39	C2
ORCA	299.6	322.3	2.14	C2
RCAP	233.8	280.3	15.73	C3

IV.2.4 Discussion

RCA is composed of original natural aggregates (NA) and attached mortar surrounding the natural particles. Generally, the presence of mortar leads to a decrease of density and strength compared to that of NA (Belin et al., 2014), which limits the application of RCA in pavements. On the contrary, attached mortar also increases the angularity and roughness of RCA aggregates, increasing the permanent and resilient deformation behavior of RCA materials as an unbound

granular material (UGM). As a result, most of RCA materials has a comparable performance than that of traditional natural UGM.

However, in this study, it appears that RCAP, sourced from demolished concrete pavement, contains very high amount of rounded particles, which can be attributed to the high amount of rounded particles and low strength of original parent concrete. Thus, under the same traffic loading, permanent deformation of RCAP ($176.9*10^{-4}$) is much higher than that of NRCA ($28.9*10^{-4}$) and ORCA ($26.7*10^{-4}$), and the resilient deformation behavior of RCAP is also higher than that of NRCA and ORCA. The ranking of these materials according to the RLTT results shows that RCAP is not suitable for the use in pavement base and subbase layers. As a result, the application of RCA, containing high amount of rounded particles and with low strength of parent concrete, as an unbound granular material, should be limited.

Another significant observation is that RCAP has a lower parameters K_2, K_4 and K_5 (resilient modulus modelling), as well as parameter n_1 (resilient deviatoric and volumetric strain modelling with Boyce model), than those of NRCA and ORCA. In particular, these parameters of NRCA and ORCA were even higher than most of UGM. These results indicate that the mechanical behavior of RCA materials (except RCAP with high amount of rounded particles) is generally more stress dependent than most of UGM, which can be attributed to the attached mortar. On the one hand, the higher porosity of attached mortar leads to the higher compressibility of RCA than that of natural aggregates. Besides, high angularity and roughness of RCA aggregates due to attached mortar increase the difficulty of compaction, may lead to a higher void ratio than UGM.

IV.3 Effect of self-cementing properties

The strength and stiffness of pavement built with RCA increases with time, known as self-cementing properties. To study the effect of self-cementing properties on the mechanical behavior of RCA under repeated load triaxial test, two RCA materials, NRCA and ORCA, both sourced from demolished buildings, were subjected to repeated load triaxial tests (RLTT), after curing 1, 180, 360 and 720 days. Only two RCA materials, NRCA and ORCA, were tested, since the permanent deformation, resilient deformation behavior and self-cementing properties of another RCA material (RCAP) are worse than NRCA and ORCA, and it was not suitable for the use in pavement construction. Note that ORCA specimens were cured until 360 days due to the negligible self-cementing properties.

The weight of each RCA specimens after curing and after RLTT were measured to check that no water evaporation during the curing stage and test stage.

IV.3.1 Permanent deformation

Experimental results

Figure IV.8 (a) and (b) show the permanent axial deformation ε_1^p and the water content of each NRCA and ORCA specimen, after different curing times. Table IV.11 summaries the repeated load triaxial test (RLTT) results, such as average value of ε_1^p, permanent strain rate $\Delta\varepsilon/\Delta N$ at the end of the test and characteristic permanent strain ε_1^c, as well as their standard error, for NRCA and ORCA after different curing times. For both specimens, ε_1^p increases at a fast speed at the early loading stage owing to the particles rearrangement, and then reaches an equilibrium state as all the $\Delta\varepsilon/\Delta N$ are less than 10^{-7} per cycle at the end of test (NF EN 13286-7, 2004).

To better show the effect of self-cementing properties on permanent deformation, Figure IV.9 plots the final ε_1^p of NRCA and ORCA after 20000 loading cycles versus curing times. For NRCA, crushed recently, showing strong self-cementing properties indicated by high pH value and heat of hydration, the results show ε_1^p decreases quickly after curing few months (180 days), then the influence of self-cementing properties on ε_1^p is diminished as ε_1^p reaches to a constant value. Abu-Farsakh et al. (2015) observed that the ε_1^p of soil decrease largely when treated with a little amount of cement (0.5%), compared with that of untreated soil. Afterwards, increasing cement content has a reduced influence on the decrease of ε_1^p, which is in good agreement with the evolution of ε_1^p of NRCA. The characteristic permanent strain ε_1^c, difference of ε_1^p between 100 loading cycle and 20000 cycle, depicted in the Figure IV.10, shows the same tendency as ε_1^p, where ε_1^c decreases quickly after curing and then reaches to a constant value.

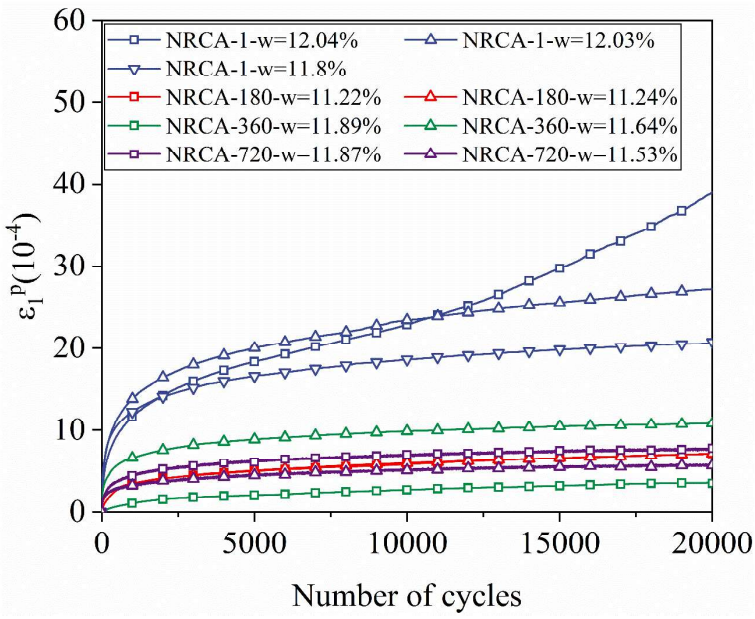

(a) NRCA

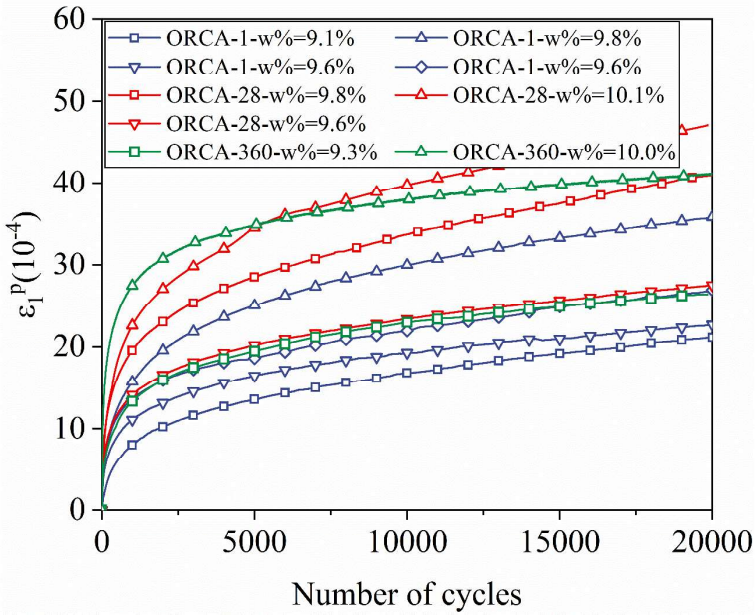

(b) ORCA

Figure IV.8. Permanent axial deformation ε_1^p of NRCA and ORCA after varying curing times: (a) NRCA; (b) ORCA.

Table IV.11. RLTT results of NRCA and ORCA after different curing times.

Results	NRCA				ORCA		
	1 day	180 days	360 days	720 days	1 day	28 days	360 days
ε_1^p (10^{-4})	28.9±5.3	7.1±0.03	7.2±3.7	6.7±1.0	26.7±3.3	38.5±5.8	34.3±6.8
$\Delta\varepsilon/\Delta N$ (10^{-7})	1.07±0.7	0.09±0.01	0.1±0.01	0.06±0.03	0.68±0.2	0.6±0.14	0.21±0.12
ε_1^c (10^{-3})	3.39±1.3	0.55±0.05	0.88±0.23	0.45±0.13	2.14±0.56	2.94±0.84	2.3±0.32

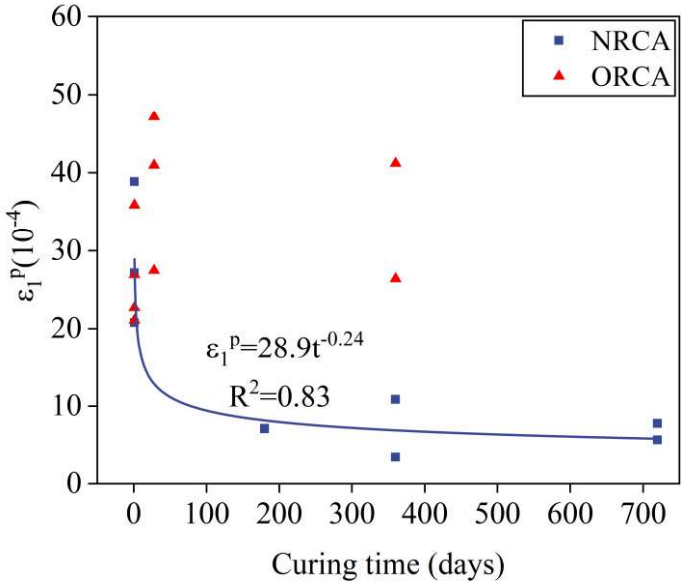

Figure IV.9. Final permanent axial deformation of NRCA and ORCA after 20000 cycles at different curing time.

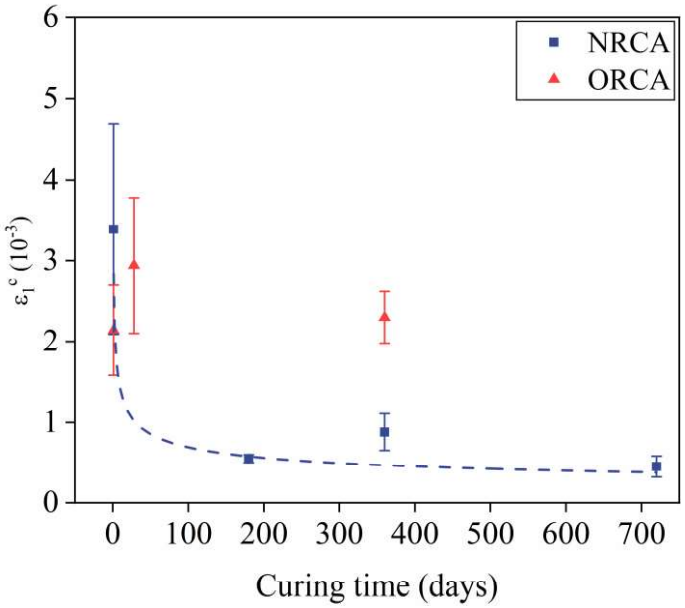

Figure IV.10. Characteristic permanent strain ε_1^c of NRCA and ORCA after different curing times.

Furthermore, as observed in Table IV.11, the ε_1^p of NRCA after curing (180, 360 and 720 days) are somehow negligible, less than $10*10^{-4}$, which can be attributed to the strong self-cementing properties of NRCA, observed also for other lightly cementitious treated materials (Ardah et al., 2017; Senanayake et al., 2022), while for traditional unbound granular materials, with similar test conditions, the ε_1^p are higher than 50×10^{-4} after 20000 cycles (Alnedawi et al., 2021; Jing & Chazallon, 2020). The results indicate that the permanent deformation behavior of NRCA after curing (at least 180 days) is equivalent to that of bound materials.

As for ORCA, stored for a long time, with negligible self-cementing properties, ε_1^p is influenced by water content as other unbound granular materials (Jing et al., 2018; Soliman & Shalaby, 2015), instead of self-cementing properties, as can be seen in Figure IV.8 (b). However, ε_1^p of ORCA are still less than 50×10^{-4} after 20000 cycles, indicating a better performance than the most of traditional unbound granular materials.

Modelling of permanent deformation behavior

Various empirical models were proposed to predict the permanent axial deformation of unbound granular materials based on the repeated load triaxial test (Barksdale, 1972; Hornych, 1993; Jing et al., 2018; Lekarp & Dawson, 1998; Sweere, 1992). However, to the authors′ knowledge, no relationship, taking into account the effect of curing time *t* on the permanent deformation, has been proposed for RCA showing self-cementing properties. Since the curing time has no influence on ε_1^p of ORCA due to the negligible self-cementing properties, only the results of NRCA were used to model the permanent deformation behavior.

To develop the model, the widely used model proposed by Hornych (1993) for unbound granular materials was adopted to simulate the permanent axial deformation with the number of cycles N:

$$\varepsilon_1^p = A\ (1-(\frac{N}{N_0})^B) \tag{IV.11}$$

where ε_1^p is the permanent strain (10^{-4}) after N_0 cycles, N_0 is the number of cycles before the first measurement (N_0=100 in this study), parameter A represents the final permanent axial deformation and parameter B controls the evolution of permanent deformation with increasing N.

According to the test results presented in Figure IV.9, a power relationship can be obtained between final permanent axial deformation A and curing time t. The expression can be expressed as follows:

$$A = a\ (\frac{t}{t_0})^b \tag{IV.12}$$

where a and b are parameters, t is the curing time after t_0 days (t_0=1).

The evolution of permanent deformation with N was controlled by another parameter B, becoming flatter when B increases (absolute value). According to the Figure IV.8, the permanent deformation is flatter with increasing curing time t. Based on these results, the exponential function is adopted to describe the relationship:

$$B = c\ e^{\frac{t}{t_0 d}} + B_0 \tag{IV.13}$$

where c, d and B_0 are constant parameters.

Substituting Equations (IV.12) and (IV.13) into (IV.11), the proposed model, accounting for the effect of curing time t, can be obtained:

$$\varepsilon_1^p = a\ (\frac{t}{t_0})^b \left(1 - \left(\frac{N}{N_0}\right)^{c \cdot e^{\frac{t}{t_0 d}} + B_0}\right) \tag{IV.14}$$

The average permanent deformations under each different curing times are used to determine the parameters, summarized in Table IV.12. Figure IV.11 presents a comparison between measured data and the proposed model data. It appears that the proposed model can fit the experimental data very well with the global correlation of determination R^2 above 0.95, which can be used to predict the permanent deformation behavior of RCA at different curing times.

Table IV.12. Parameters of the proposed model for NRCA based on curing times.

RCA	a	b	c	d	B_0	R^2
NRCA	28.874	-0.243	0.169	-386.117	-0.479	0.960

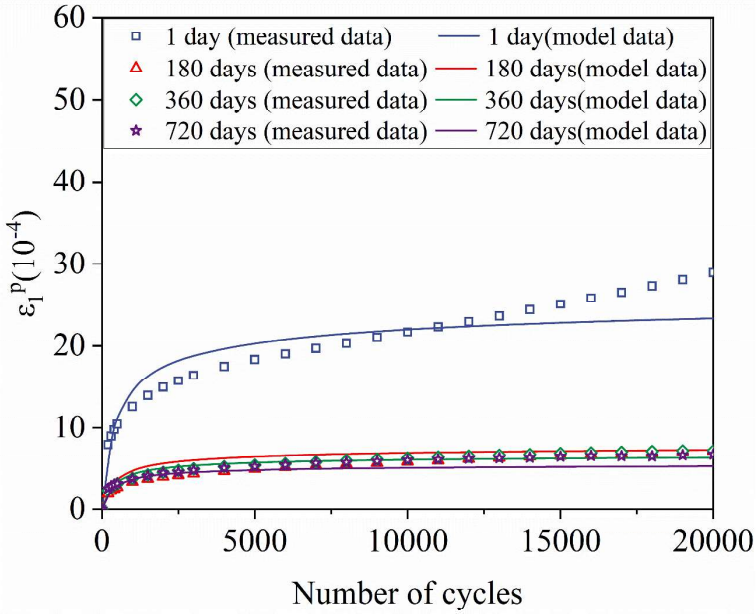

Figure IV.11. Average test results and the model prediction of ε_1^p for NRCA at different curing times.

Resilient modulus during permanent deformation test

Resilient modulus M_r is a key input parameter in pavement design. During permanent deformation test, resilient modulus, defined by the ratio between deviator stress q and resilient axial strain ε_1^r, can also be obtained.

Figure IV.12 plots the resilient modulus M_r of NRCA and ORCA, during permanent deformation test, after different curing times, and Table IV.13 summarizes the average final resilient modulus M_r, at the end of permanent deformation test. A clear increase of M_r for NRCA with curing time can be observed due to the self-cementing properties. After curing for 180, 360 and 720 days, the final M_r of NRCA at last cycle is 1.6, 2.3 and 4.3 times, respectively, larger than that curing for 1 day. By contrast, the final M_r of ORCA is constant, which is consistent with the evolution of permanent deformation.

Figure IV.12 also shows that an increase of M_r during the first load cycles can be observed, and then gradually reaches to a constant value, for both NRCA and ORCA after different curing times except the NRCA specimens curing 360 and 720 days. This behavior is due to the particle rearrangement and consolidation during the conditioning phase, which is observed also for unbound granular materials (UGM) in a shakedown state by other researchers (Jing et al., 2019; Xiao et al., 2018; Yang et al., 2008).

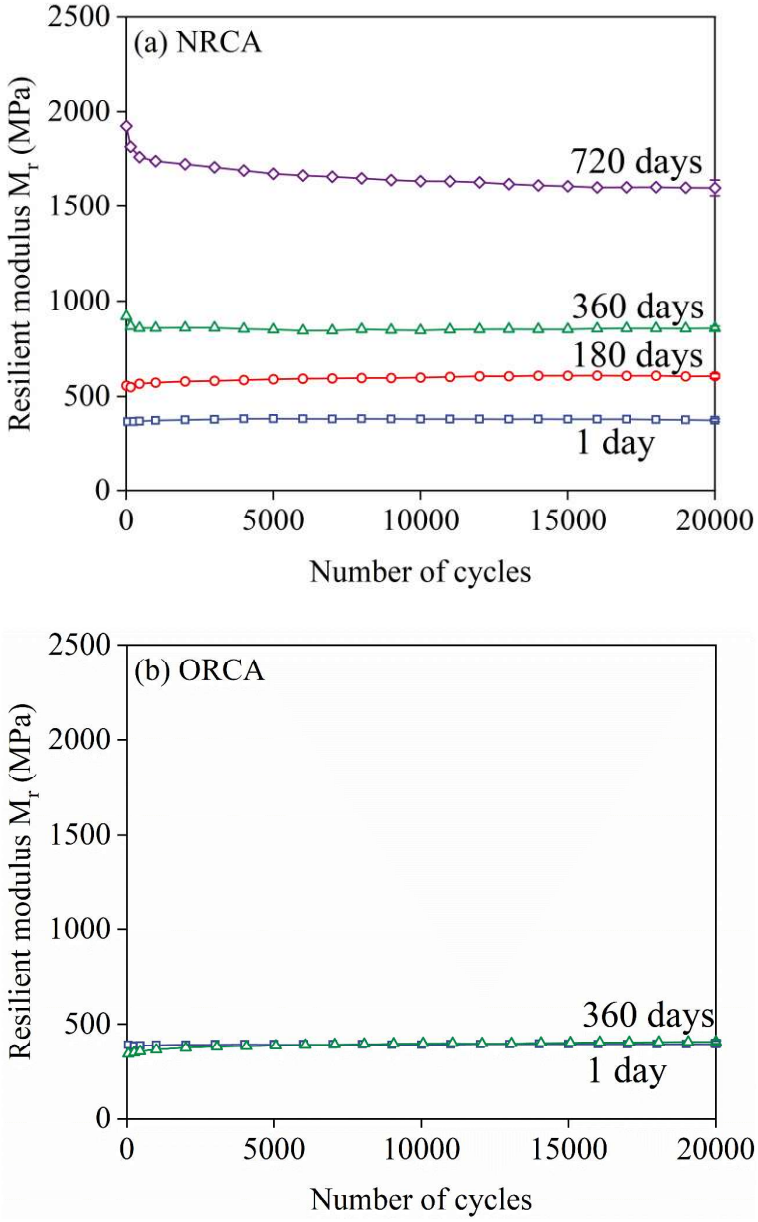

Figure IV.12. Resilient modulus of NRCA and ORCA at different curing times: (a) NRCA; (b) ORCA.

Table IV.13. Average and standard error of final resilient modulus M_r of NRCA and ORCA.

Results	NRCA				ORCA		
	1 day	180 days	360 days	720 days	1 day	28 days	360 days
M_r (MPa)	370.9 ±7.6	606.7 ±12.3	857.6 ±10.4	1598.7 ±41.8	395.3 ±8.4	406.9 ±1.1	408.9 ±7.5

Interestingly, for NRCA specimens after curing 360 and 720 days, a decrease of M_r during the first loading cycles can be observed, especially for NRCA curing 720 days. Recall that the hydration of unhydrated cement in RCA fine aggregates forms bonds between particles, increasing both strength and stiffness of RCA specimens. However, some weak bonds could break under the traffic loadings, decreasing resilient modulus during the permanent deformation test. These findings were consistent with cement treated materials reported by others (Rabbi et al., 2011; Rios et al., 2014; Vranna & Tika, 2020).

To predict the M_r, Figure IV.13 shows the evolution of final resilient modulus of NRCA and ORCA with curing time. It can be observed that the M_r of NRCA increases with curing time till the studied curing time due to the self-cementing properties, which can be described by an exponential function. In addition, unlike permanent deformation whose decreasing rate decreases with curing time, the increasing rate of M_r increases with curing time. For example, M_r increases 741 MPa from curing 360 to 720 days, while the increased M_r is only 487 MPa from curing 1 to 360 days. However, it should be pointed out that this observation was confirmed only for the studied material (NRCA) till curing 720 days. As the curing time increases, the hydration of unhydrated cement stops and M_r will reach to a constant value, which needs to be confirmed with longer curing time.

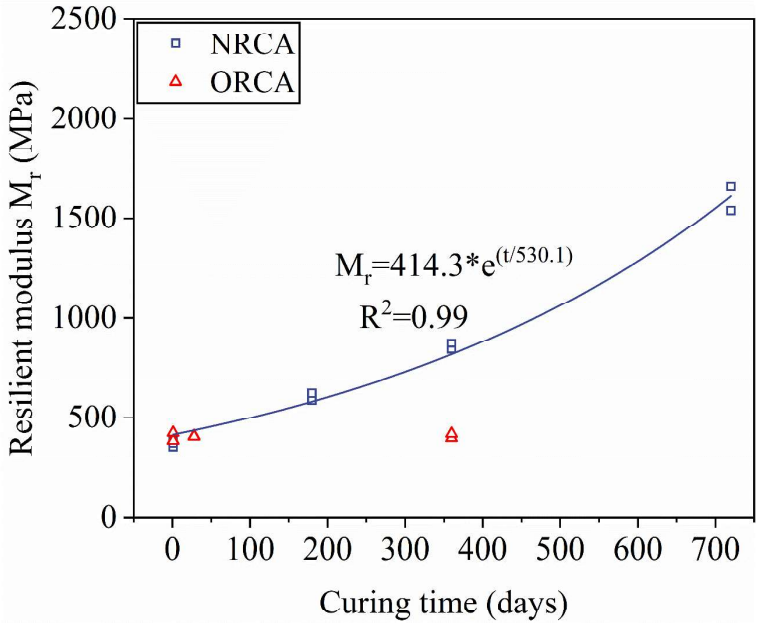

Figure IV.13. Evolution of final resilient modulus M_r of NRCA and ORCA with curing time.

IV.3.2 Resilient deformation behavior under CCP loading

Resilient modulus

Figure IV.14 (a) and (b) show the experimental data and k-θ model predictions of resilient modulus M_r for NRCA and ORCA after different curing times, under CCP loading. The average resilient modulus of NRCA and ORCA, curing for different times, under different stress paths and stress levels are summarized in Table IV.14. A significant influence of self-cementing properties on the M_r of NRCA can be observed (Figure IV.14 (a)), as M_r increases with curing time, under a same stress state, in accordance with previous studies (Arm, 2001; Jitsangiam et al., 2015). Another interesting observation is that the increasing rate of M_r increases with curing time, until the tested curing time (720 days). For example, under the highest stress level (σ_3=150 kPa, high stress level), M_r increases 0.3 (180 days), 0.8 (360 days) and 2.2 (720 days) times compared to the 1 day curing specimens. However, the curing time has no influence on the M_r of ORCA (Figure IV.14 (b)), in good agreement with the self-cementing properties.

Then, all the experiment data of NRCA and ORCA were fitted with k-θ model and Uzan model, the parameters are summarized in Table IV.15 and Table IV.16. Figure IV.14 also depicts the fitted results by k-θ model, for NRCA and ORCA. A very good fit can be obtained as all the coefficient of determinations are higher than 0.90, except that of NRCA curing 720 days (R^2=0.761). The scattered tested data of NRCA curing 720 days, as observed also by Jitsangiam et al. (2015), are attributed to the low resilient deformation under the tested stress state (high stiffness). Table IV.16 summaries the Uzan model parameters for NRCA and ORCA after different curing times. It can be observed that the Uzan model is more accurate than k-θ model after accounting for the effect of shear stress, indicated by a higher R^2.

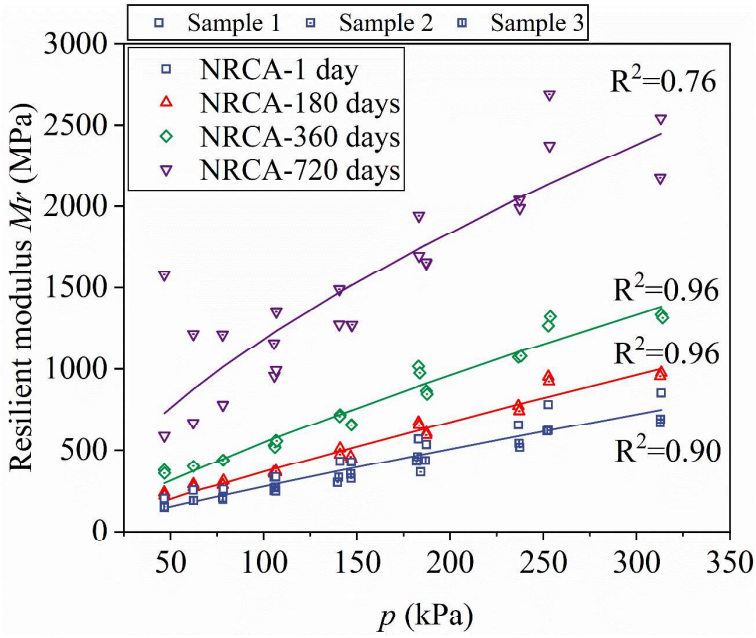

(a) NRCA

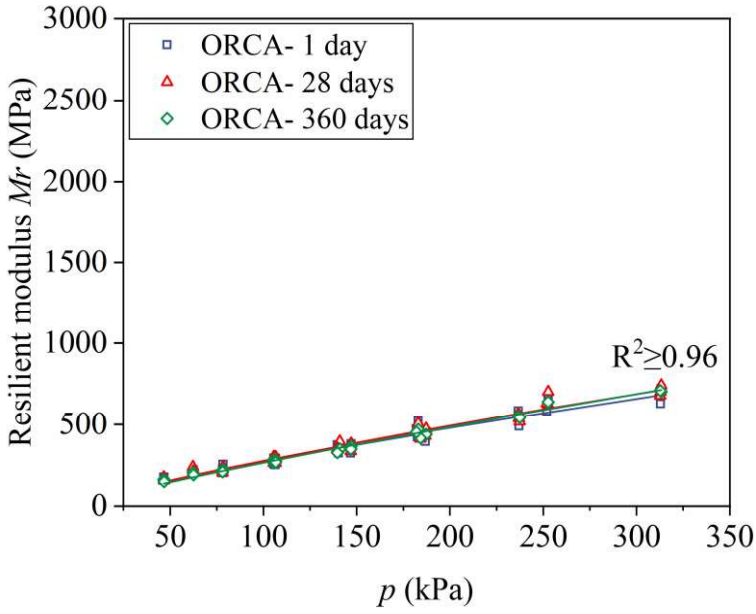

(b) ORCA

Figure IV.14. Test results and k-θ model predictions of M_r for NRCA and ORCA after varying curing times: (a) NRCA; (b) ORCA.

Table IV.14. Average M_r of NRCA and ORCA at different curing times.

Confining pressure (kPa)	Stress level	NRCA				ORCA		
		1 day	180 days	360 days	720 days	1 day	28 days	360 days
20	Low	167	230	367	1084	166	167	157
	High	211	281	401	944	209	219	199
35	Low	220	299	438	997	222	221	217
	High	284	358	524	1059	277	284	274
50	Low	285	366	559	1174	273	281	274
	High	369	453	658	1273	352	359	356
70	Low	355	493	715	1382	351	365	338
	High	445	600	856	1654	424	438	428
100	Low	487	665	996	1820	462	474	462
	High	573	759	1076	2013	530	541	548
150	Low	675	938	1296	2534	624	653	640
	High	739	967	1326	2360	674	708	707

Table IV.15. Summary of k-θ model parameters for NRCA and ORCA.

Parameters	NRCA				ORCA		
	1 day	180 days	360 days	720 days	1 day	28 days	360 days
K_1	1.91	2.40	5.39	31.69	2.69	2.49	1.90
K_2	0.87	0.88	0.81	0.64	0.81	0.83	0.87
R^2	0.903	0.963	0.958	0.761	0.959	0.965	0.984

Table IV.16. Summary of Uzan model parameters for NRCA and ORCA.

Parameters	NRCA				ORCA		
	1 day	180 days	360 days	720 days	1 day	28 days	360 days
K_3	95.35	116.68	187.26	471.36	100.32	99.71	93.08
K_4	1.12	1.28	1.22	1.14	1.05	1.09	1.08
K_5	-0.29	-0.47	-0.48	-0.59	-0.29	-0.31	-0.25
R^2	0.912	0.989	0.989	0.818	0.970	0.978	0.992

To better understand the effect of self-cementing properties on the resilient modulus, Figure IV.15 and Figure IV.16 depict the evolution of k-θ model parameters, K_1 and K_2, and Uzan model parameters, K_3, K_4 and K_5, for NRCA. Given that the self-cementing properties of ORCA are negligible, only the parameters of NRCA were presented. Parameter K_1 is an indicator of the resilient modulus magnitude, while K_2 represents the stress dependency of materials. It can be observed that K_1 increases while K_2 decreases with increasing curing time, indicating the improvement of stiffness and the reduce of stress dependency of NRCA as curing time increases, as observed also by other researchers (Arm, 2001; Corradini et al., 2021; Jitsangiam et al., 2015). Furthermore, the variations of K_1 and K_2 are more pronounced with increasing curing time, which is in good agreement with the improvement of M_r. However, this observation is contrary to the field test results reported by Arm (2001), who found that the growth of stiffness is largest in the first few months and then diminishes. This could be attributed to the traffic loadings after pavement construction, increasing the density and stiffness of unbound base and subbase layers, which is not considered in this study.

Figure IV.16 depicts the evolution of Uzan model parameters K_3, K_4 and K_5 of NRCA with curing time. Similarly, parameter K_3 increases with curing time due to the self-cementing properties, and this increasing rate also increases with curing time. However, it seems that the curing time has no influence on K_4, indicating that the sensitivity of M_r to bulk stress has no change with increasing curing time. Furthermore, the absolute value of K_5 (negative value) increases with curing time, from 0.29 to 0.59. It indicates that the influence of deviatoric stress on M_r increases with curing time and a more strain softening behavior after curing can be observed. Note that the resilient deformation behavior of unbound granular materials is primarily governed by confining pressure, while the influence of deviatoric stress can be

neglected which leads to the well-known *k-θ* model (Stolle et al., 2009). By contrast, the bound materials have an improved relationship between the strength, maximum deviator stress, and stiffness than unbound materials, observed also by other researchers (Kang et al., 2017; Miller et al., 2021).

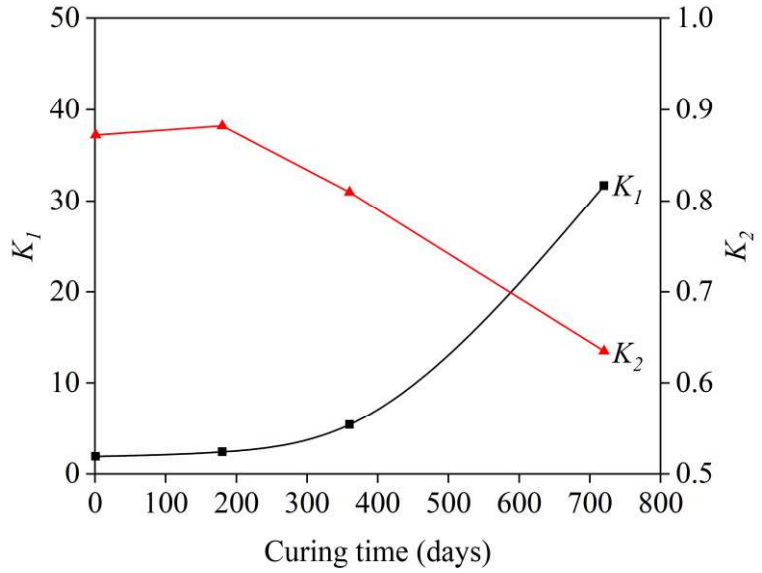

Figure IV.15. Evolution of k-θ model parameters K_1 and K_2 of NRCA with curing time.

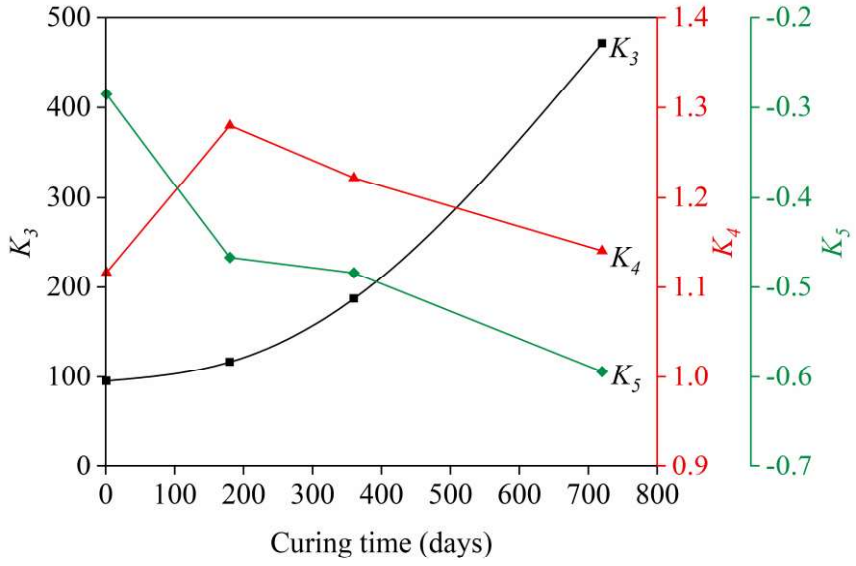

Figure IV.16. Evolution of Uzan model parameters K_3, K_4 and K_5 of NRCA with curing time.

Parameters K_1 and K_3 can be considered as good indicators of the influence of self-cementing properties on M_r, while parameters K_2, K_4 and K_5 reveal the evolution of the stress dependency of M_r. A comparison of M_r between NRCA (curing 1 and 720 days), UGM (Corradini et al., 2021; Stolle et al., 2009), and bound materials (soils stabilized with lime, fly ash and cement

kiln dust) (Corradini et al., 2021; Solanki et al., 2010) is presented in Table IV.17, containing the parameter ranges of k-θ and Uzan model. It can be observed that the parameters K_1 and K_3 of NRCA curing 720 days are greater than those of UGM, and these values are similar to those of bound materials. In general, UGM has a stress dependency property of resilient behavior, while it is not a property of bound materials. As a result, it appears that bound materials have lower K_2, K_4 and K_5 than UGM. However, only a decrease of K_2 and K_5 was observed for NRCA after curing 720 days. The results also indicate that the unbound NRCA specimen turns to (partially) bound specimen after curing 720 days.

Table IV.17. Synthesis of model parameters for bound and unbound materials.

Model		NRCA		UGM		Bound materials	
		1 day	720 days	Min	Max	Min	Max
k-θ	K_1	1.91	31.69	5.41[a]	14.45	32.48[a]	55.16
	K_2	0.87	0.64	0.71	0.78	0.43	0.52
Uzan	K_3	95.35	471.36	40[b]	260	123.5[c]	2239.9
	K_4	1.12	1.14	0	0.9	-0.05	0.40
	K_5	-0.29	-0.59	-0.45	0.6	-0.64	0.03

Note: data from [a]Corradini et al. (2021), [b]Stolle et al. (2009) and [c]Solanki et al. (2010).

Resilient deviatoric and volumetric strains

Figure IV.17-Figure IV.20 depict the experimental and modelling results of resilient deviatoric ε_q^r and volumetric strain ε_v^r, under different confining pressures, for NRCA and ORCA after different curing times. Note that only the results of ε_q^r and ε_v^r under high stress level are presented. It can be observed that ε_q^r of NRCA decreases with increasing curing time under both confining pressures, as shown in Figure IV.17. For instance, under confining pressure 150 kPa, ε_q^r is 5.9, 4.2, 2.5 and 1.6×10^{-4} after curing 1, 180, 360 and 720 days, respectively. Besides, under low confining pressure (20 kPa), the dilatant behavior (negative ε_v^r) turns to contractant behavior after curing 180, 360 and 720 days (Figure IV.18 (a)). While under high confining pressures (150 kPa), ε_v^r is slightly decreased after curing 720 days. Same tendency was observed for ORCA, especially the evolution of ε_v^r. In general, the influence of curing time on

ε_q^r and ε_v^r of ORCA is negligible compared to these of NRCA due to the negligible self-cementing properties of ORCA.

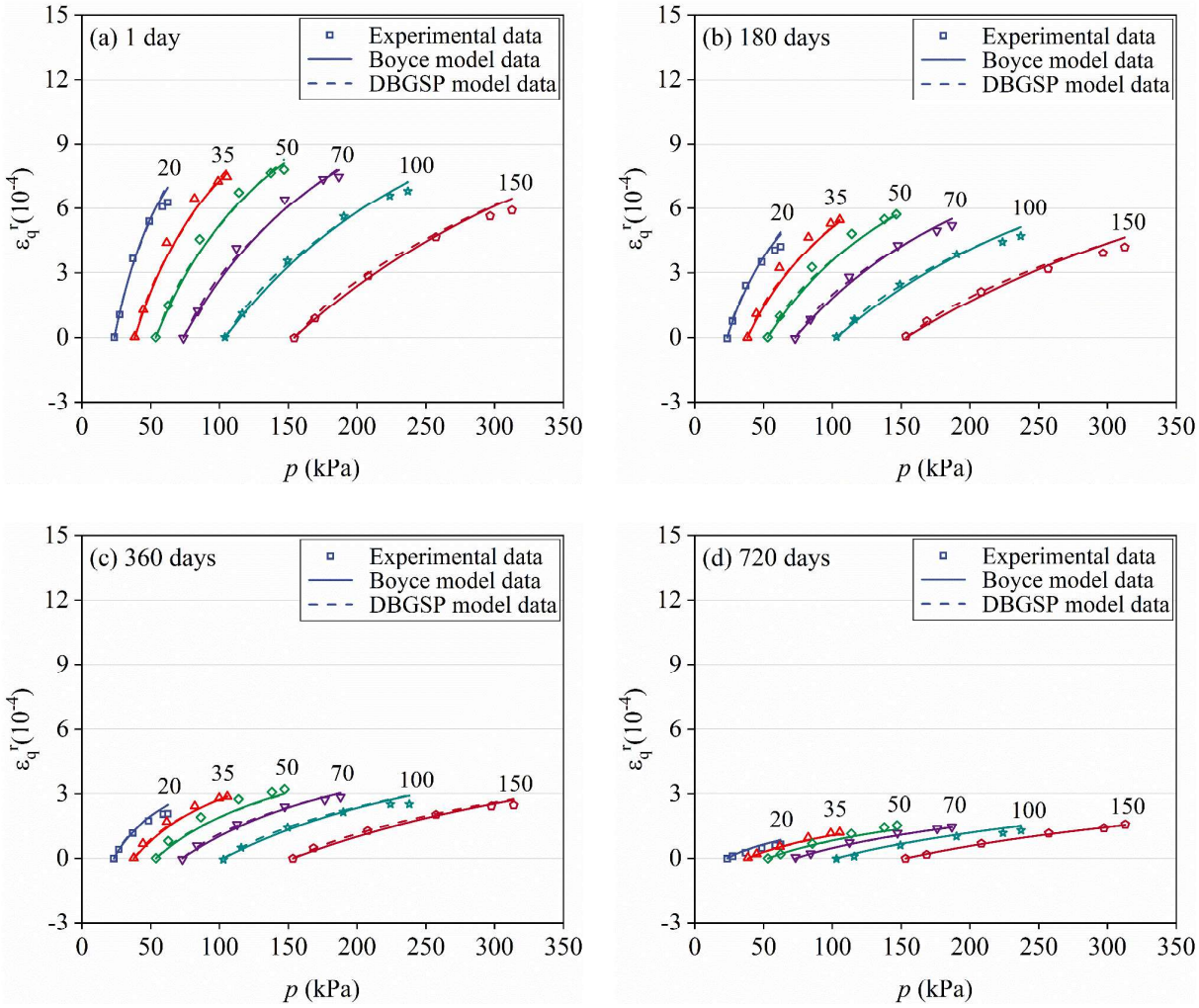

Figure IV.17. Resilient deviatoric strain ε_q^r of NRCA after different curing times under different constant confining pressures (σ_3=20/35/50/70/100/150 kPa): (a) curing 1 day; (b) curing 180 days; (c) curing 360 days and (d) curing 720 days.

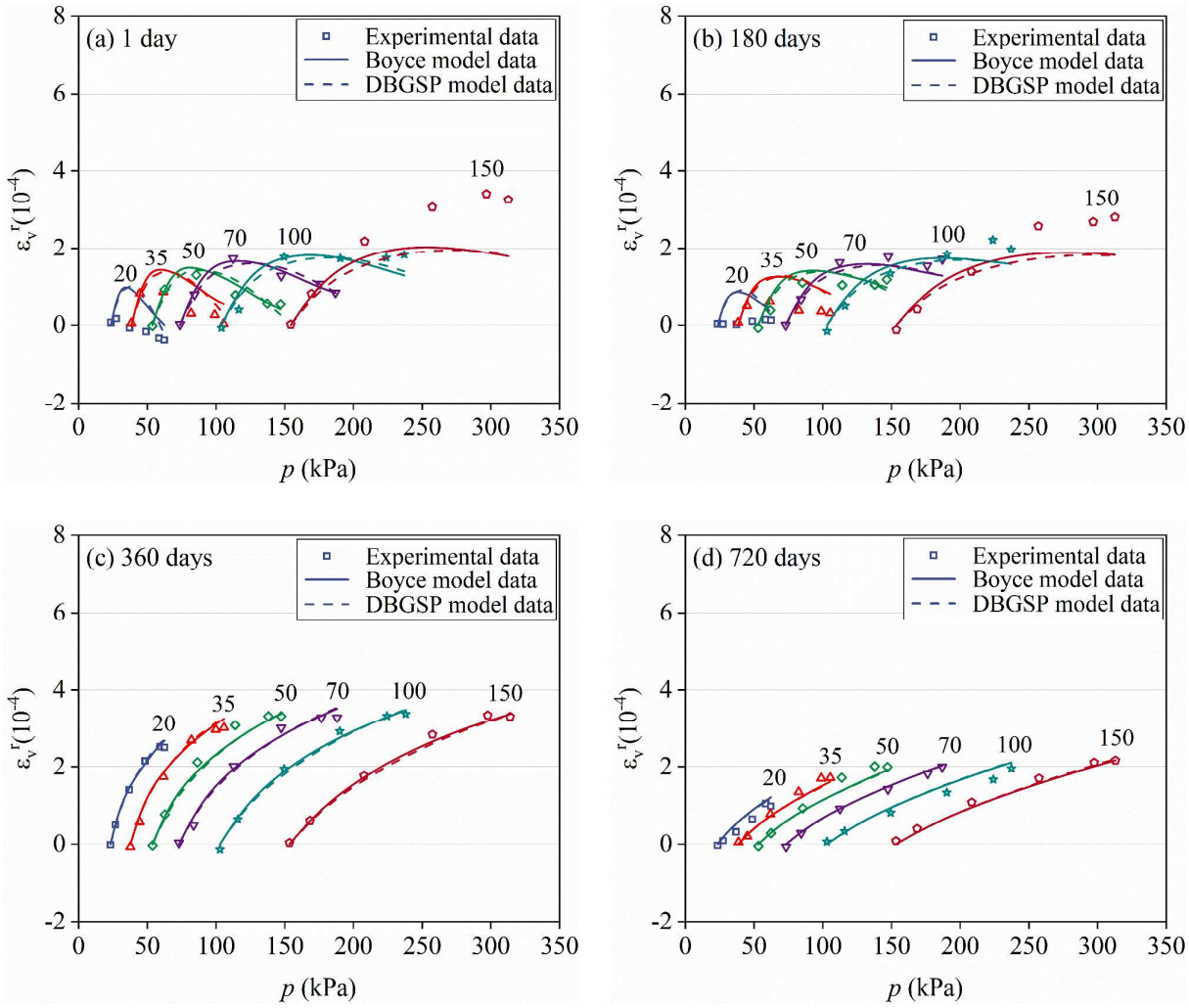

Figure IV.18. Resilient volumetric strain ε_v^r of NRCA after different curing times under different constant confining pressures (σ_3=20/35/50/70/100/150 kPa): (a) curing 1 day; (b) curing 180 days; (c) curing 360 days and (d) curing 720 days.

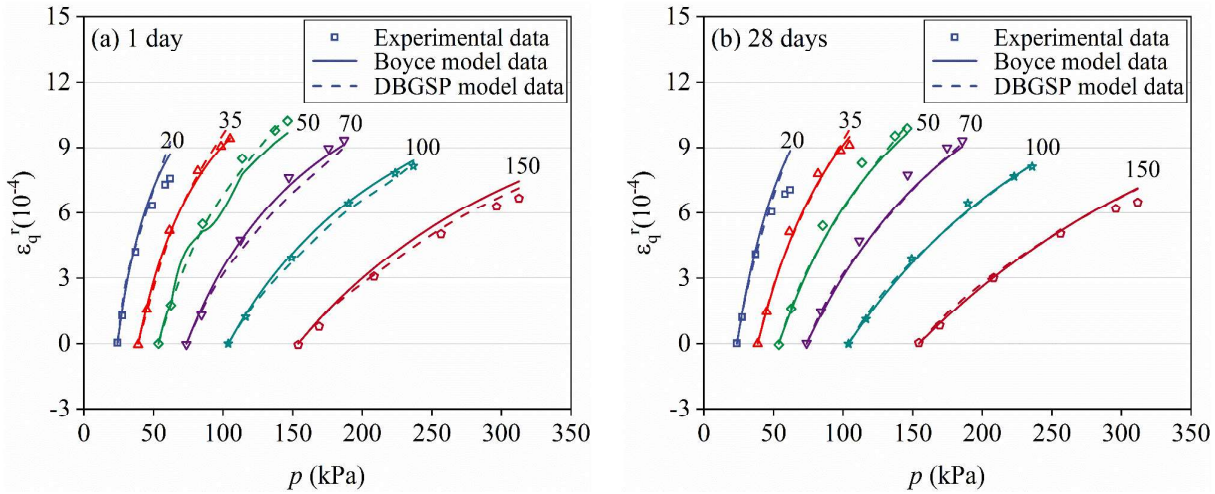

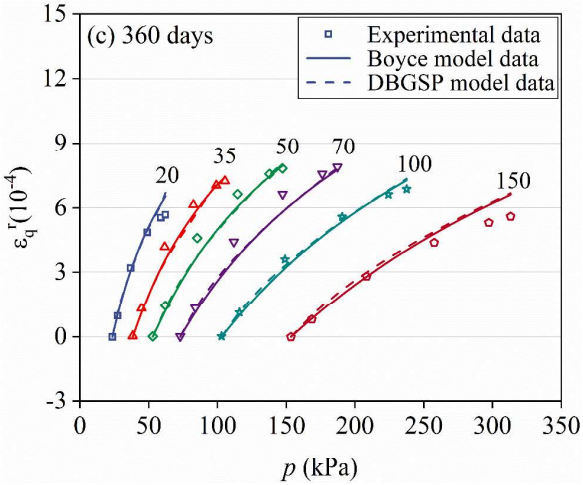

Figure IV.19. Resilient deviatoric strain ε_q^r of ORCA after different curing times under different constant confining pressures (σ_3=20/35/50/70/100/150 kPa): (a) curing 1 day; (b) curing 28 days; (c) curing 360 days.

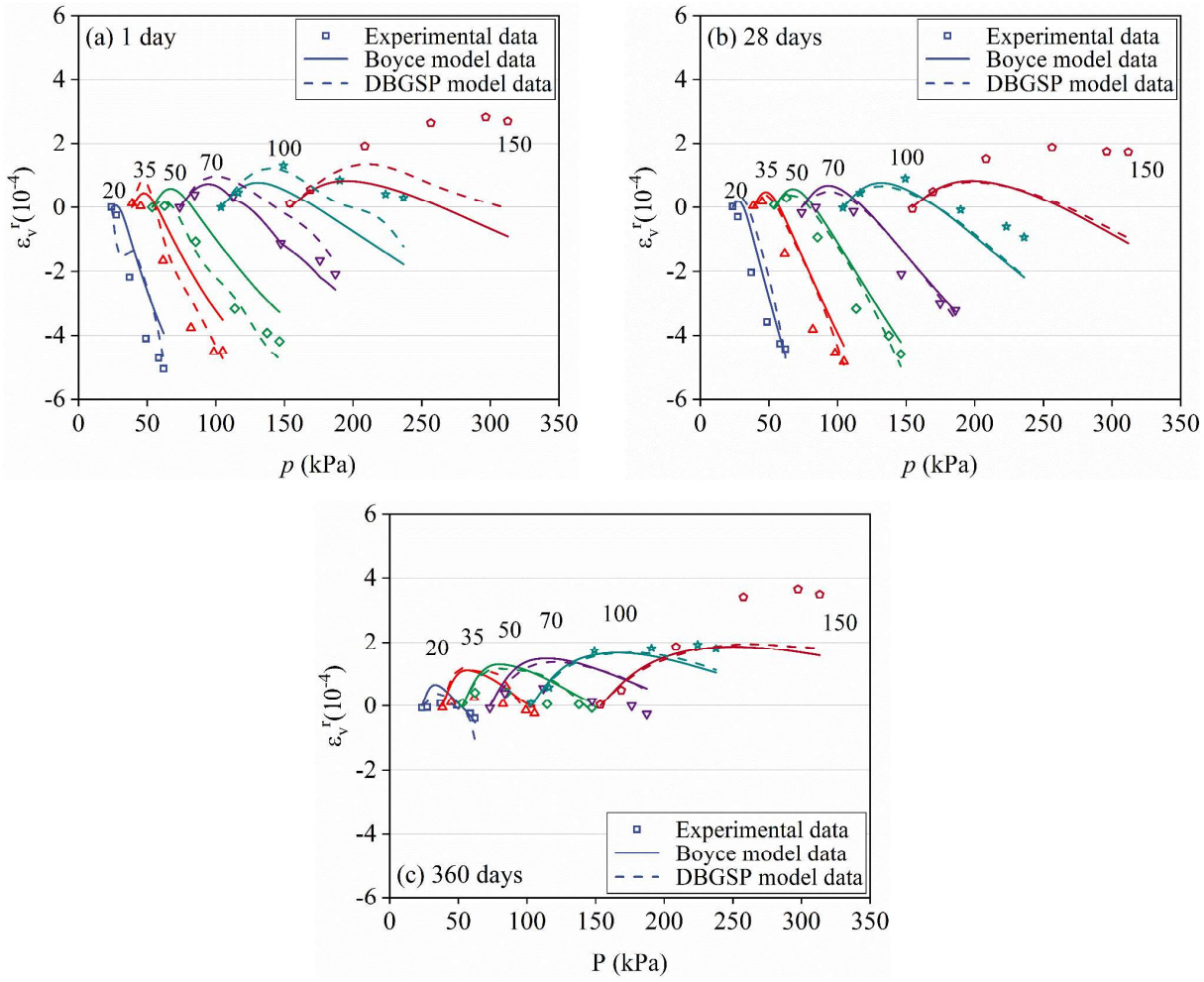

Figure IV.20. Resilient volumetric strain ε_v^r of ORCA after different curing times under different constant confining pressures (σ_3=20/35/50/70/100/150 kPa): (a) curing 1 day; (b) curing 28 days; (c) curing 360 days.

The modified Boyce model and DBGSP model parameters of NRCA and ORCA after different curing times are summarized in Table IV.18 and Table IV.19, and the modelling results are also presented in Figure IV.17-Figure IV.20. It can be seen that both the modified Boyce model and DBGSP model describe both ε_q^r and ε_v^r quite well for both RCA materials, after different curing times, as indicated by the good R^2.

Table IV.18. Modified Boyce model parameters of NRCA and ORCA after different curing times (CCP loading).

Materials	Curing days	K_a/MPa	G_a/MPa	n_1	γ	R^2
NRCA	1	1.54	49.81	0.03	0.59	0.97
	180	7.62	46.55	0.17	0.41	0.94
	360	17.24	116.49	0.21	0.57	0.98
	720	85.86	477.46	0.27	1.00	0.94
ORCA	1	1.15	42.36	0.02	0.55	0.94
	180	1.66	41.35	0.03	0.50	0.96
	360	7.30	46.39	0.14	0.53	0.96

Table IV.19. DBGSP model parameters of NRCA and ORCA after different curing times (CCP loading).

Materials	Curing days	α/MPa	β	n_2	ν_0	ν_{rr}	R^2
NRCA	1	2027.3	1.22	0.96	0.30	0.3	0.97
	180	2282.6	2.88	0.89	0.09	0.3	0.93
	360	2863.9	9.64	0.81	0.01	0.2	0.97
	720	4665.3	1	0.72	0.04	0.3	0.96
ORCA	1	1915.1	29.9	0.98	0.01	0.3	0.96
	180	2006.6	12.4	0.96	0.05	0.2	0.96
	360	1584.1	14.7	0.85	0.06	0.2	0.96

Figure IV.21 depicts the evolution of parameters K_a, G_a and α, relating to the bulk moduli, shear moduli and Young modulus, for NRCA with varying curing times. It can be observed that both K_a, G_a and α increase with curing times, showing a significant improvement of self-cementing properties on ε_q^r and ε_v^r. Furthermore, the increasing rate of parameters K_a, G_a and α also increase with curing time, until the studied curing time (720 days), in good agreement with the evolution of resilient modulus (Figure IV.15 and Figure IV.16).

Furthermore, nonlinear coefficients, parameters n_1 and n_2 of NRCA, are depicted in Figure IV.22. Results show that n_1 increases with curing times, from 0.03 to 0.27 after curing 720 days. It indicates that the relationship between resilient behavior and mean normal stress p becomes more linear after curing, in good agreement with the evolution of ε_v^r with curing times (Figure IV.18), while n_2 decreases with curing times, from 0.96 to 0.72 after curing 720 days, indicating the increased influence of axial principal stress.

For ORCA, only the slight increases of K_a and n_1 were observed, relating to the improvement of ε_v^r. However, owing to the weak self-cementing properties, the increased K_a and n_1 of ORCA curing 360 days are similar to these of NRCA curing 180 days.

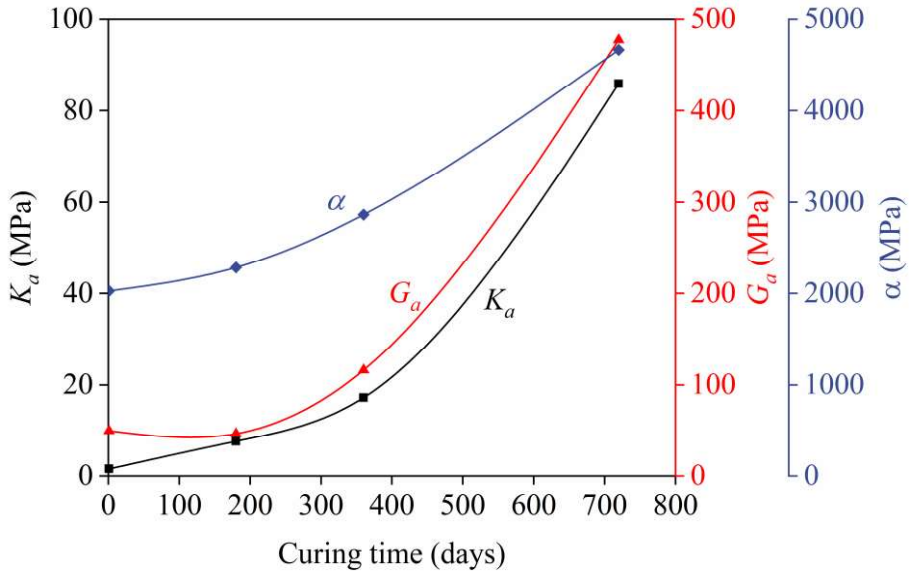

Figure IV.21. Evolution of parameters K_a, G_a and α of NRCA with curing time.

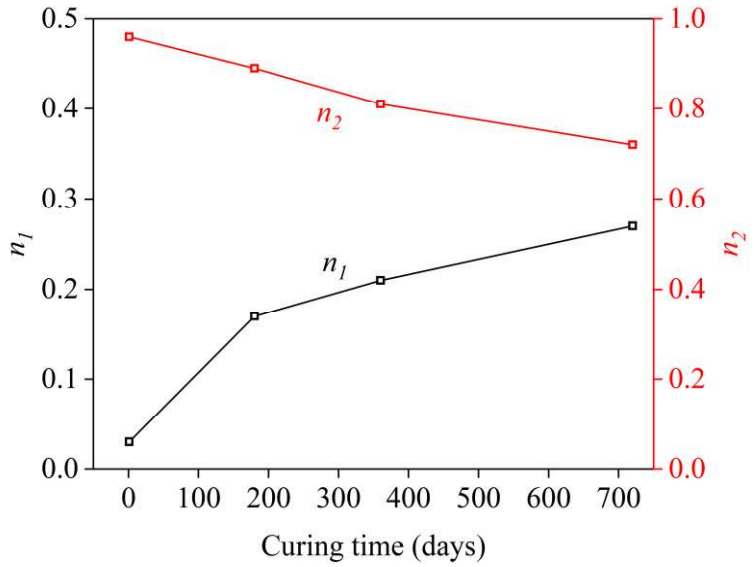

Figure IV.22. Evolution of n_1 and n_2 of NRCA with curing time.

IV.3.3 Resilient deformation behavior under VCP loading

Experimental results

Figure IV.23-Figure IV.26 present comparisons between the experimental values of ε_q^r and ε_v^r obtained under different stress paths ($\Delta q/\Delta p$=0/1/1.5/2/2.5), and the predictions of the modified Boyce model and DBGSP model, for NRCA and ORCA, after different curing times (1, 180, 360 and 720 days). It is known that the resilient behavior of UGM is strongly non-linear and depends on the stress path $\Delta q/\Delta p$. However, as curing time increases, ε_q^r and ε_v^r of NRCA become linear and less depend on the stress path, which is the behavior of bound materials. This was also supported by the observation from CCP loading.

In particular, it can be observed that the resilient deformation behavior of NRCA after curing 360 days (linear and less stress dependency) are different from those before curing 360 days (non-linear and stress dependency), showing the unbound NRCA specimens gradually turn to bound specimens after curing 360 days. It has to mention that this observation is confirmed by the resilient modulus during permanent deformation test (Figure IV.12), whose resilient modulus decreases during the first loading cycles, indicating the bonding breakage introduced by the mechanical loading.

As for the ORCA, it appears that the negligible self-cementing properties has no influence on the resilient deformation behavior under VCP loading, as observed also in permanent deformation and resilient deformation under CCP loading.

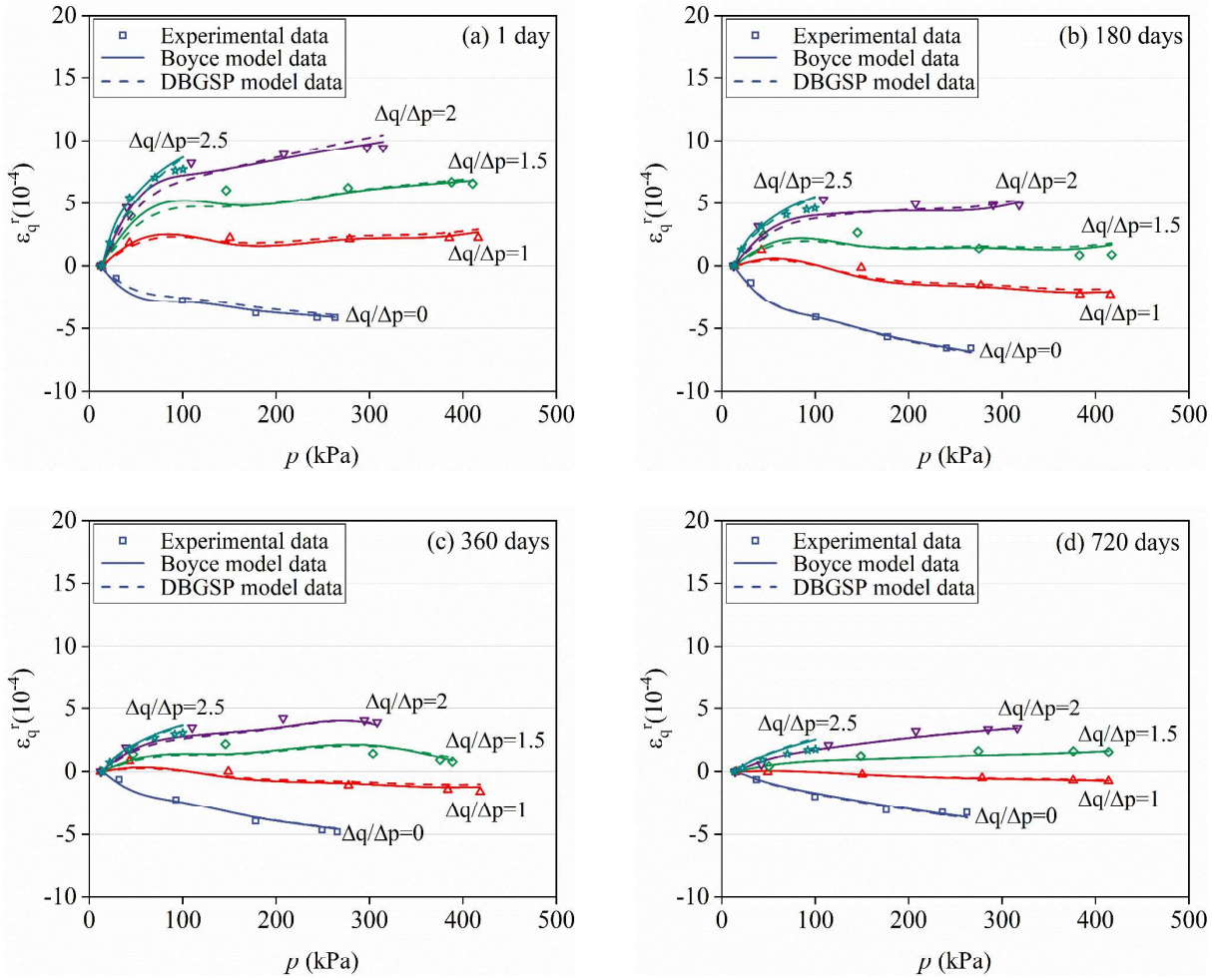

Figure IV.23. Resilient deviatoric strain ε_q^r of NRCA after different curing times under different stress path (Δq/Δp=0/1/1.5/2/2.5): (a) curing 1 day; (b) curing 180 days; (c) curing 360 days and (d) curing 720 days.

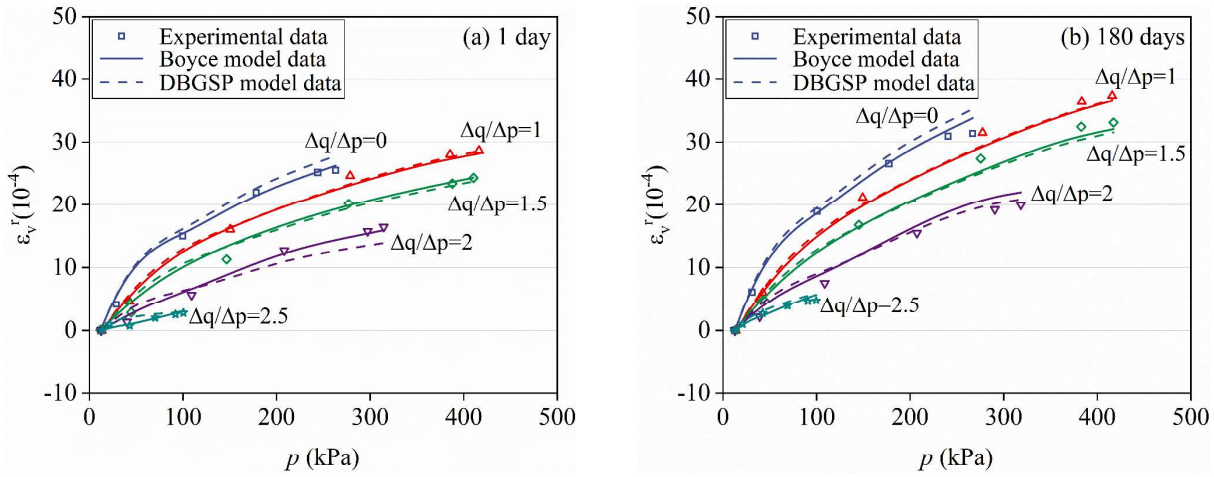

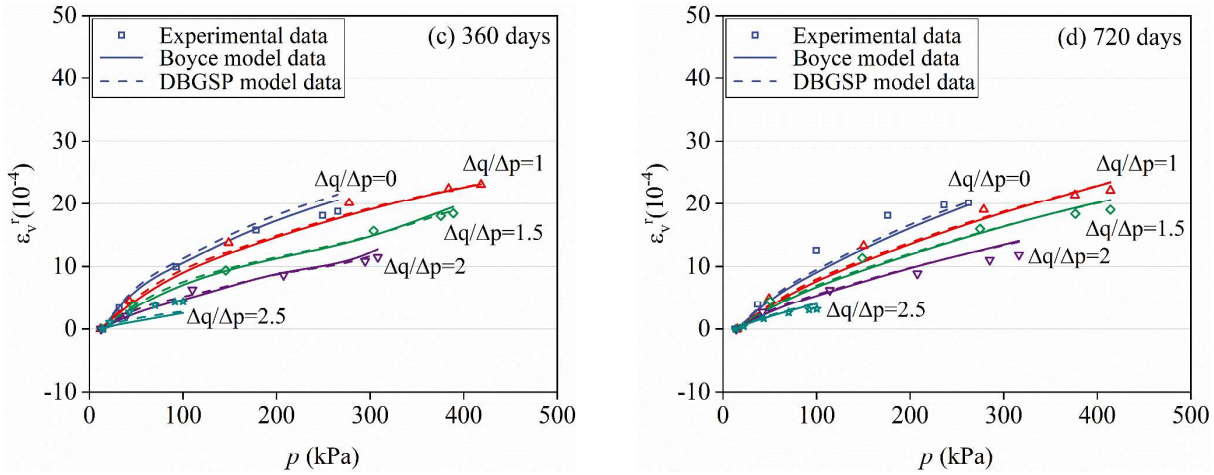

Figure IV.24. Resilient volumetric strain ε_v^r of NRCA after different curing times under different stress path (Δq/Δp=0/1/1.5/2/2.5): (a) curing 1 day; (b) curing 180 days; (c) curing 360 days and (d) curing 720 days.

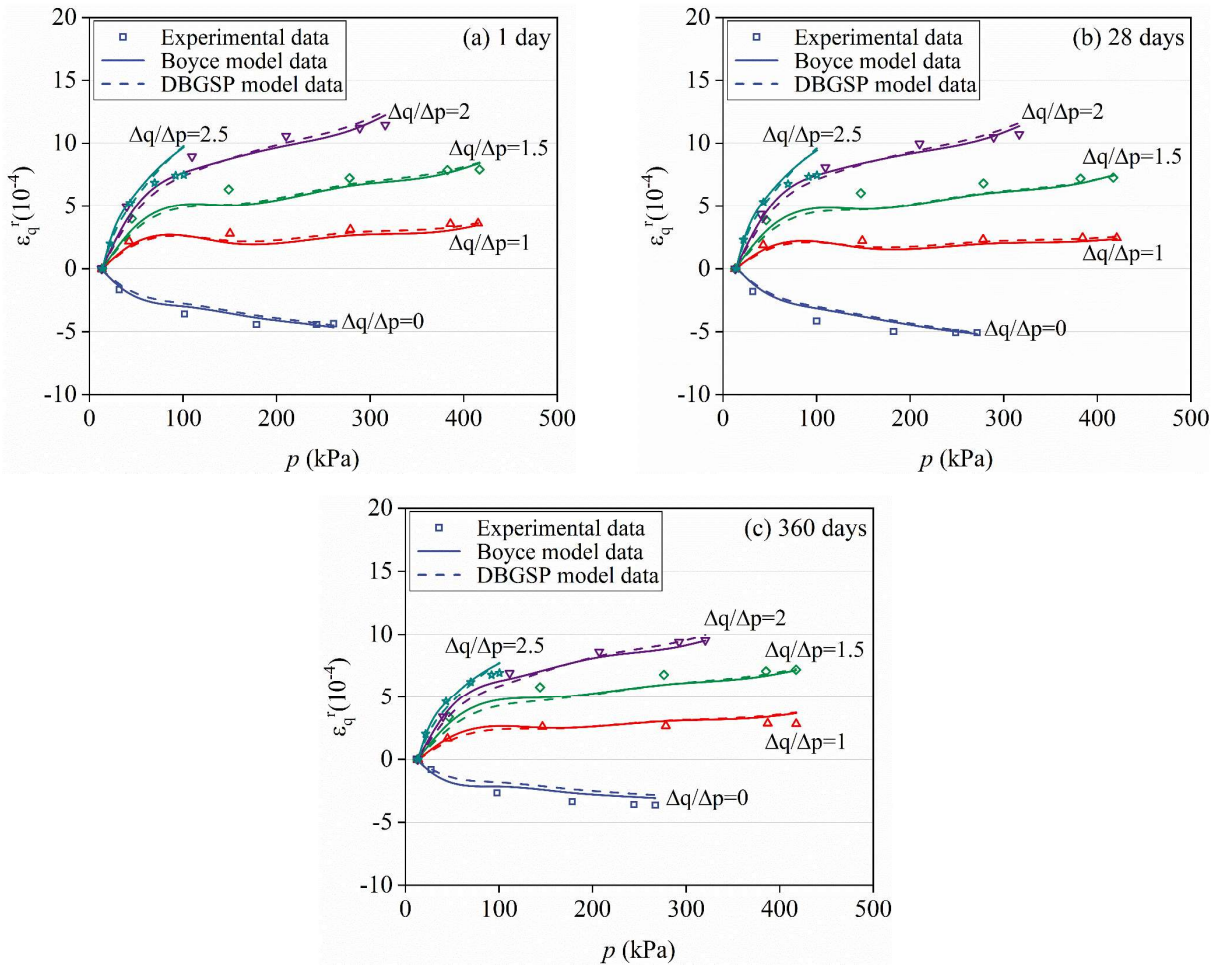

Figure IV.25. Resilient deviatoric strain ε_q^r of ORCA after different curing times under different stress path (Δq/Δp=0/1/1.5/2/2.5): (a) curing 1 day; (b) curing 28 days; (c) curing 360 days.

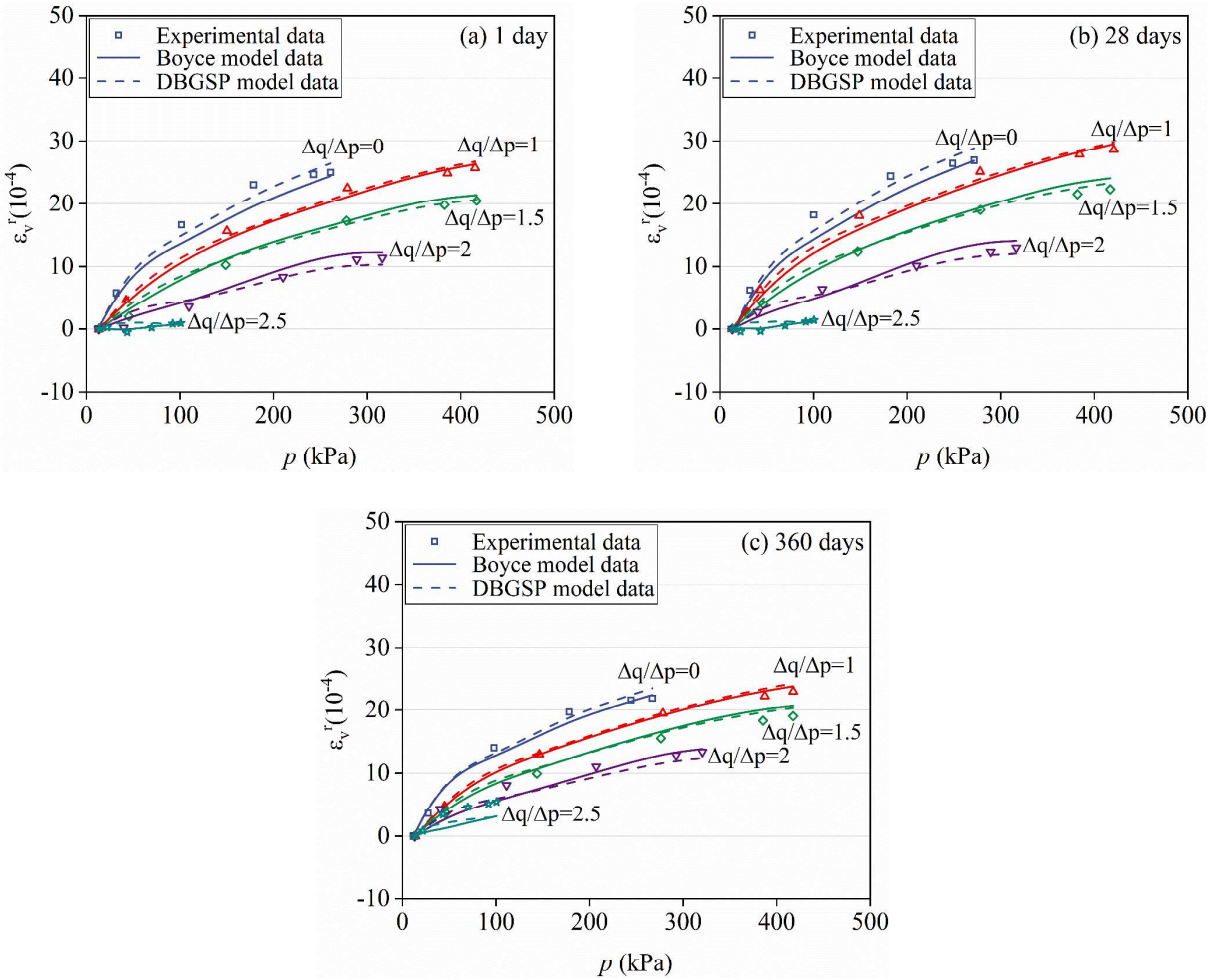

Figure IV.26. Resilient volumetric strain ε_v^r of ORCA after different curing times under different stress path (Δq/Δp=0/1/1.5/2/2.5): (a) curing 1 day; (b) curing 28 days; (c) curing 360 days.

Modelling results

Table IV.20 and Table IV.21 summarize the modified Boyce model parameters of NRCA and ORCA after different curing times, and the modelling results are also presented in Figure IV.23-Figure IV.26. It can be seen that both modified Boyce model and DBGSP describes both ε_q^r and ε_v^r quite well for both RCA materials, under VCP loading, after different curing times, as indicated by the good correlation coefficient CC. Recall that parameters K_a, G_a and α are related to the bulk moduli, shear moduli and Young modulus, n_1 and n_2 are the nonlinear coefficients, while γ and β are the coefficients of anisotropy.

Table IV.20. Modified Boyce model parameters of NRCA and ORCA after different curing times (VCP loading).

Materials	Curing days	K_a/MPa	G_a/MPa	n_1	γ	CC
NRCA	1	31.06	49.49	0.35	0.69	0.89
	180	26.98	52.22	0.41	0.58	0.87
	360	50.82	99.41	0.45	0.68	0.86
	720	51.79	102.91	0.53	0.54	0.83
ORCA	1	39.80	48.61	0.44	0.71	0.84
	180	31.44	45.62	0.36	0.68	0.88
	360	34.16	54.12	0.39	0.71	0.86
UGM[a]	1	16.77	38.47	0.27	0.80	0.799
UGM[b]	1	36.58	57.87	0.49	0.92	0.682
RAP[c]	1	23.81	58.84	0.31	0.68	0.776

Note: data from [a]Jing and Chazallon (2020), [b]Hornych et al. (2009) and [c]Gaillard (2019).

Table IV.21. DBGSP model parameters of NRCA and ORCA after different curing times (VCP loading).

Materials	Curing days	α/MPa	β	n_2	v_0	v_{rr}	CC
NRCA	1	1117.8	1.26	0.68	0.25	0.1	0.856
	180	1195.8	2.22	0.64	0.12	0.2	0.865
	360	1564.6	1.90	0.58	0.12	0.2	0.850
	720	1783.4	3.16	0.50	0.07	0.3	0.827
ORCA	1	902.4	1.39	0.61	0.24	0.1	0.839
	180	1051.6	1.29	0.69	0.24	0.1	0.858
	360	1017.5	1.48	0.63	0.20	0.1	0.850

Figure IV.27 depicts the evolution of parameters K_a and G_a, for NRCA and ORCA, with curing time. For NRCA, it can be observed that K_a and G_a increase with curing time, as observed also under CCP loading, indicating the improvement of resilient behavior due to the self-cementing properties. In particular, a large increase of K_a and G_a after curing 360 days were observed, and then reaches an almost constant value. A similar tendency can be observed for parameter α, as shown in Figure IV.29. The parameters K_a and G_a of NRCA after curing 360 days are much larger than those of UGM and reclaimed asphalt pavement (RAP) aggregates reported by other researchers (Gaillard, 2019; Hornych et al., 2009; Jing & Chazallon, 2020), showing a very good resilient deformation behaviour of NRCA after curing. As for ORCA, these parameters are similar after curing different times.

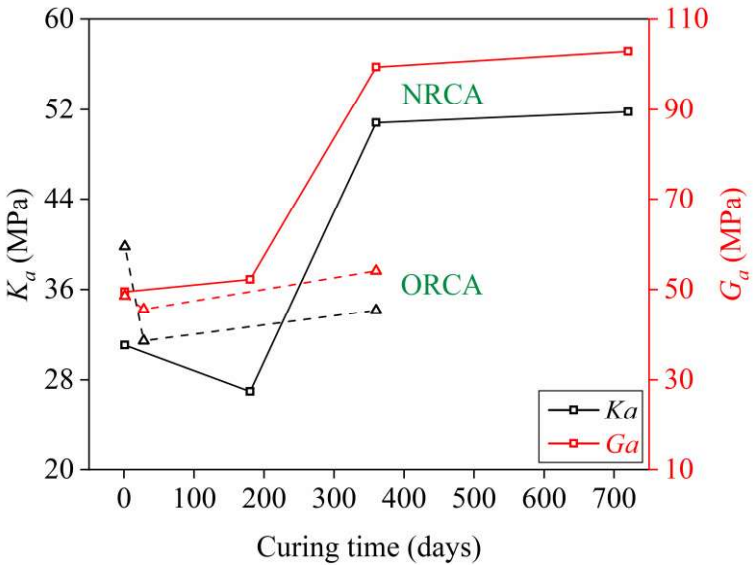

Figure IV.27. Evolution of modified Boyce model parameters K_a and G_a of NRCA and ORCA with curing time.

Figure IV.28 and Figure IV.29 show the evolution of parameters n_1 and n_2 of NRCA and ORCA with curing time. As observed from the results under CCP loading (Figure IV.22), parameter n_1 of NRCA increases with curing times and higher than these of UGM and RAP, suggesting a linear relationship between resilient behavior and mean normal stress p, while n_2 decreases with curing times, indicating the increased influence of axial principal stress.

As for the coefficients of anisotropy γ and β, it appears anisotropy behavior of NRCA is slightly improved after curing, since γ decreased while β increased after curing. As observed from microstructure observation (Section III.5), only small macro-pores (radius above 1 µm and less than 20 µm) were filled by the hydration products of unhydrated cement. Since the anisotropy

behavior of UGM due to the conditioning and compaction, the number and size of macro-pores in axial direction are higher than these in radial direction, resulting in a higher axial stiffness than radial stiffness. Thus, the cementing effect in axial direction could be more significant.

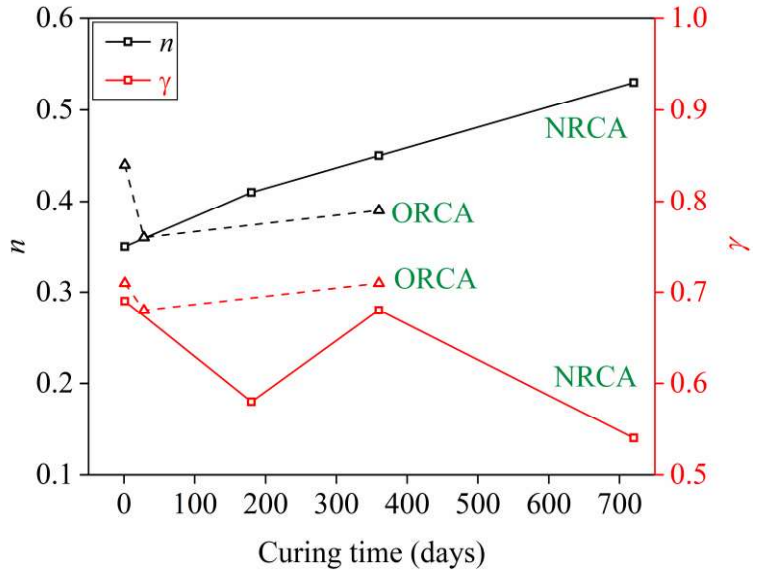

Figure IV.28. Evolution of modified Boyce model parameters n_1 and γ of NRCA and ORCA with curing time.

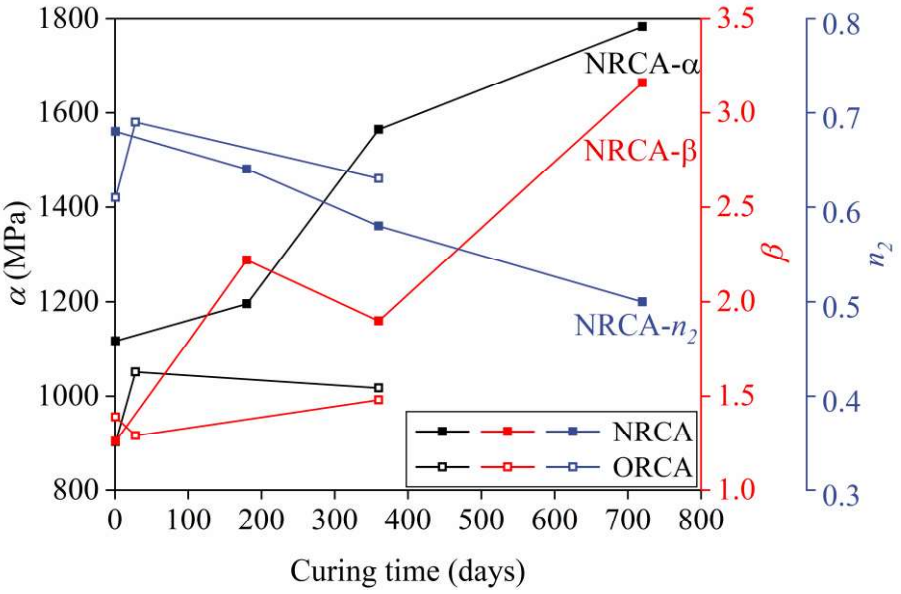

Figure IV.29. Evolution of DBGSP model parameters α, β and n_2 of NRCA and ORCA with curing time.

Classification

Subsequently, the characteristic resilient modulus E_c, defined as the resilient modulus determined for the stress states p=250 kPa and q=500 kPa, was calculated with the modified Boyce model and DBGSP model. Table IV.22 summarizes E_c and characteristic permanent strain ε_1^c (Table IV.11), as well as classification of these RCA materials after different curing time based on the classification of unbound granular materials proposed in European Standard NF EN 13286-7 (2004) (Table IV.10). A similar E_c was obtained between modified Boyce model and DBGSP model. Besides, a clear increase of E_c and a decrease of ε_1^c with increasing curing time, for NRCA, can be observed due to the strong self-cementing properties of NRCA, improving the performance of NRCA. As a result, NRCA can be classified in category C1 after curing 360 days, representing the highest performance level in unbound granular materials.

Table IV.22. Classification of RCA materials after different curing times.

Results	NRCA				ORCA		
	1 day	180 days	360 days	720 days	1 day	28 days	360 days
E_c (Boyce)/MPa	328.6	403	589.2	803.1	322.5	319.8	337.7
E_c (DBGSP)/MPa	343.2	383.8	549.3	699.9	322.3	319.4	337.9
$\varepsilon_1^c/10^{-3}$	3.39	0.55	0.88	0.45	2.14	2.94	2.30
Class	C2	C2	C1	C1	C2	C2	C2

IV.3.4 Discussion

In the present study, it appears that the permanent deformation of NRCA decreases quickly to a constant low value (Figure IV.9), while the resilient modulus increases continuously and this increasing rate increases with curing time (Figure IV.13). Similar observation was made by Barbieri et al. (2022), who studied the effect of curing and freeze-thaw cycles on the permanent deformation and resilient modulus of cement treated materials. They reported that the permanent deformation of cement treated materials is constant while the resilient modulus increases after curing 180 days and 10 freeze-thaw cycles due to the curing effect.

Chapter III.6 revealed the mechanisms of self-cementing properties of RCA on the mechanical behaviors: the hydration of unhydrated cement and the formation of ettringite form interparticle bonds and hydration products fill the pores among coarse aggregates, turning open type of soil

structure to the rigid tight skeleton structure. This was confirmed by the evolution of resilient modulus of NRCA after curing 360 and 720 days (Figure IV.12), whose resilient modulus decreases during the first loading cycles due to the breakage of bonds.

Furthermore, the reaction between unhydrated cement and water also decreases free water content of RCA specimens, indicated by the increasing non-evaporable water content of NRCA (Chapter III.4). Thus, the water content of NRCA after curing were lower than those curing 1 day (Figure IV.8 (a)). Recall that the non-evaporable water of NRCA (Chapter III.4), corresponding to the hydration of cement, measured by thermogravimetric analysis (TGA), increases 1% after curing 360 days, indicating the decrease of 1% free water, in good agreement with this study. However, the decrease of water content of NRCA after curing is believed to have been related to the reactions between unhydrated cement and water, instead of water evaporation during the curing stage, as the weight of specimen after curing was measured before RLTT. Besides, the decrease of water content of ORCA specimens was not observed under the same curing state. It should be noted that the decreasing water content of NRCA after curing (Figure IV.8 (a)) could also decrease the ε_1^p. However, this needs to be confirmed in the future study.

For unbound granular materials, the deformation is governed by the consolidation, distortion and attrition of particles (Lekarp et al., 2000a). However, since the bonds between particles are formed and the water content decreases, the consolidation, distortion and attrition of particles are limited, decreasing the permanent deformation immediately. Thereafter, as the curing time increases, the further hydration of unhydrated cement and the formation of ettringite have a limited effect on the decreasing of permanent deformation. As a result, the permanent deformation of NRCA gradually decreases to a constant value after curing 180 days.

On the contrary, as the curing time increases, the increase number of bonds and the amount of hydration products increase the particle contact numbers, decreasing the contact stress of particles. Thus, resilient modulus of NRCA increases continuously with curing time, until the end of the hydration of unhydrated cement and the formation of ettringite.

Recall that the hydration of unhydrated cement attain to stop after curing for 360 days, although the continued formation of sulfate attack products, ettringite, was observed, as observed from TGA results (Section III.4). Interestingly, however, the increasing rate of resilient modulus increases with curing time till the studied curing time (720 days), showing the important effect of sulfate attack products, ettringite, on the resilient modulus. Since the ettringite can absorb a large amount of water and has a large volume, the voids between particles can be filled largely

by ettringite and the void ratio can be reduced largely. Besides, the improved microstructures of unbound RCA specimen, from open type of soil structure to the rigid tight skeleton structure, further decreases the average contact stress of per particle. As a result, the increasing rate of resilient modulus increases with curing time till the studied curing time (720 days).

IV.4 Conclusions

In this chapter, the influence of RCA source (three different RCA materials: NRCA, ORCA and RCAP) and self-cementing properties (two different RCA materials: NRCA and ORCA) on the permanent deformation and resilient deformation behaviour of RCA was investigated by repeated load triaxial test.

Effect of RCA sources

RCAP, with a larger amount of rounded particles, presents much larger permanent strains and permanent strain rate than those of NRCA and ORCA, indicating a plastic creep behavior of RCAP. Besides, RCAP has a lower resilient modulus and higher resilient deviatoric strain ε_q^r and volumetric strain ε_v^r, while the values of NRCA and ORCA are similar to those of UGMs. These results indicate that RCA with high amounts of rounded particles and low strength of the parent concrete may lead to poor mechanical properties, and thus may not be suitable for use in pavement layers. However, the performance of the other RCA (NRCA and ORCA) is comparable to that of NA and they can be used as unbound pavement layers.

The modelling results showed that the resilient behaviour of RCA materials (except RCAP with high amount of rounded particles) is generally more stress dependent than that of most of UGMs, which can be attributed to the high angularity and roughness of RCA aggregates. According to the classification of UGM, NRCA and ORCA can be classified as C2, while RCAP is classified as C3, which is not suitable for use in pavement layers.

Effect of self-cementing properties

The permanent deformation of NRCA, with strong self-cementing properties, decreases quickly after curing 180 days, then reaches to a constant and very low value, less than $10*10^{-4}$, which is equivalent to that of bound materials. While the permanent deformation of ORCA is influenced by water content instead of its negligible self-cementing properties.

During conditioning, the resilient modulus of NRCA curing 1 and 180 days increase with loading cycles, due to the particle rearrangement and consolidation, while after curing 360 and

720 days, the resilient modulus decreases first in the first loading cycles, to a constant value, since some weak bonds break under the traffic loadings, indicating unbound granular NRCA specimens gradually turn to bound specimens.

The resilient modulus of NRCA increases with curing time. However, unlike the permanent deformation, the increasing rate also increases with curing time till the studied curing time (720 days). After curing 720 days, the resilient modulus of NRCA is much higher than that of UGM, and similar to that of lightly treated materials. Besides, the stress dependency of NRCA decreases with the increasing curing time, while for ORCA, curing time has no influence on the resilient modulus.

The resilient deviatoric strain ε_q^r and volumetric strain ε_v^r of NRCA decrease with increasing curing time. Besides, both experimental and modelling results show that ε_q^r and ε_v^r of NRCA also become linear and less depend on the stress path, which is the behaviour of bound materials. The self-cementing properties also improved anisotropy behavior of NRCA slightly, while for ORCA, curing time has no significant influence on the ε_q^r and ε_v^r.

After curing 720 days, ε_q^r and ε_v^r of NRCA are smaller than these of UGM. According to the classification of UGM, NRCA can be classified as C1 after curing 360 days, which can be used in the high-level pavement.

Chapter V. Mechanical behaviour of RCA in monotonic triaxial tests

Although shear strength parameters, determined by monotonic triaxial tests, are not direct input parameters for pavement design, monotonic triaxial tests can still provide important information related to the potential rutting of pavements, according to the stress ratio $q_{max}/q_{failure}$, in which q_{max} is the applied maximum deviatoric stress and $q_{failure}$ is the failure deviatoric stress.

In the previous chapter, the effect of self-cementing properties on the mechanical behaviour has been studied by repeated load triaxial tests. In this chapter, the influence of self-cementing properties on the shear behaviour of RCA was studied by conducting a series of monotonic triaxial tests on NRCA and ORCA specimens. The effects of curing times (1, 28 and 360 days) and confining pressures (20 kPa, 40 kPa and 70 kPa) were considered. Moreover, different models were developed to predict the development of strength, stiffness and cohesion with curing time, allowing to predict the influence of self-cementing properties on the long-term mechanical behavior of RCA.

V.1 Methods

Only two RCA materials, NRCA and ORCA, were tested in this study as the self-cementing properties of RCAP are negligible, as indicated by the very low pH value (9.48). The compacted NRCA and ORCA specimens, after curing for different times (1, 28, 360 days), were subjected to monotonic triaxial tests under three different confining pressures (20 kPa, 40 kPa and 70 kPa).

The tests were performed in drained conditions at a displacement rate of 0.3 mm/min until failure. Note that all the testing parameters were the same for the two materials, such as particle size distribution, water content (OMC-1%) and dry density (optimum dry density at the targeted water content), to allow a better comparison of the mechanical behaviour of the two RCA materials. The weight of each RCA specimen was measured after curing and after RLTT, to make sure that there was no water loss during the curing and testing stage.

V.2 Development of strength with curing time

The stress-strain curves of NRCA and ORCA, after curing for 1, 28 and 360 days under different confining pressures are shown in Figure V.1 and Figure V.2. These curves show the

deviatoric stress q as a function of axial strain ε_1. Note that monotonic triaxial tests were not performed on ORCA after curing for 28 days, because of the negligible self-cementing properties of ORCA. As expected, NRCA and ORCA curing for 1 day have similar stress-strain curves, owing to the same testing parameters, such as particle size distribution, water content (OMC-1%), dry density and sample preparation procedures.

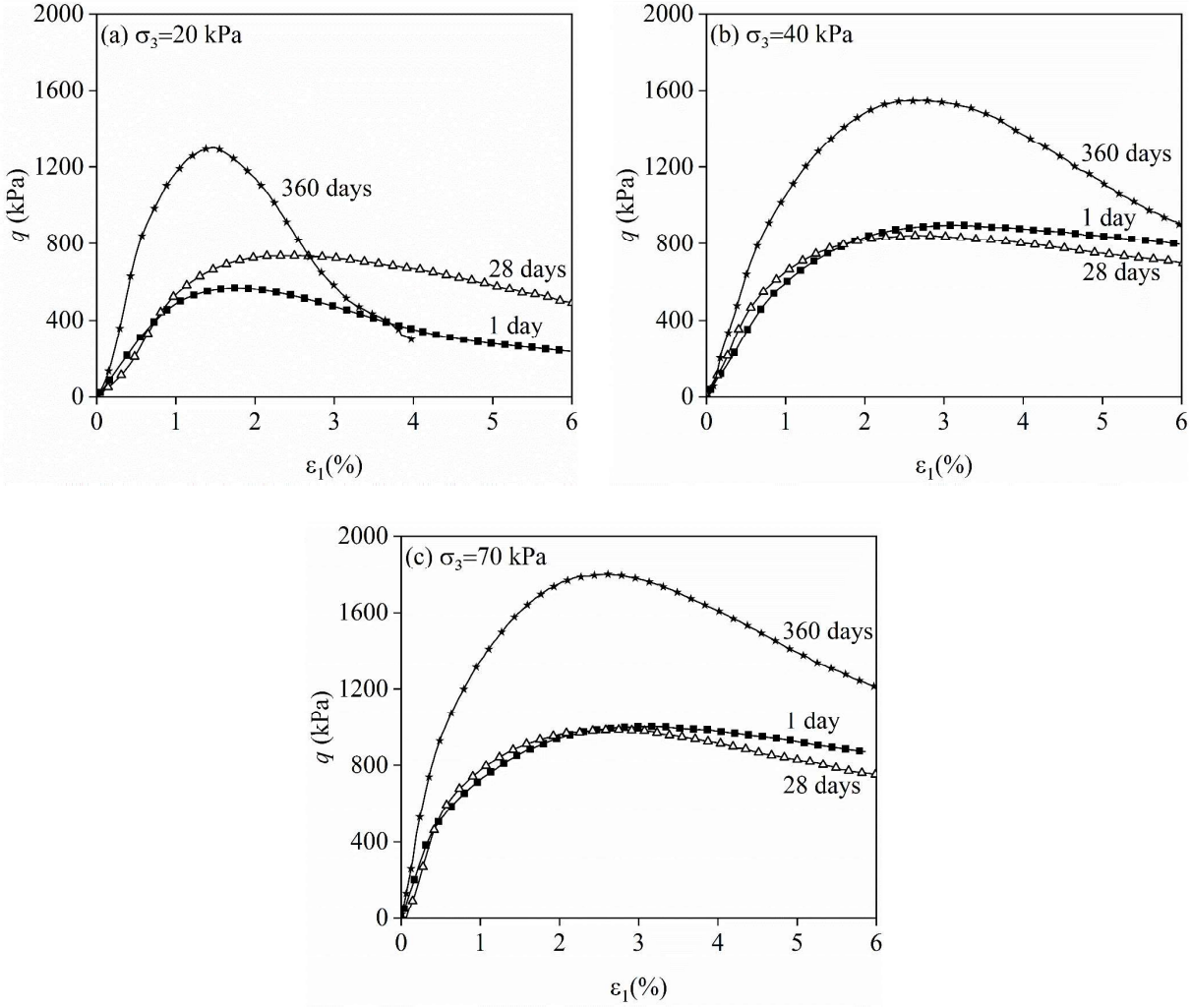

Figure V.1. Stress-strain curves of NRCA under different confining pressures after different curing times: (a) 20 kPa; (b) 40 kPa and (c) 70 kPa.

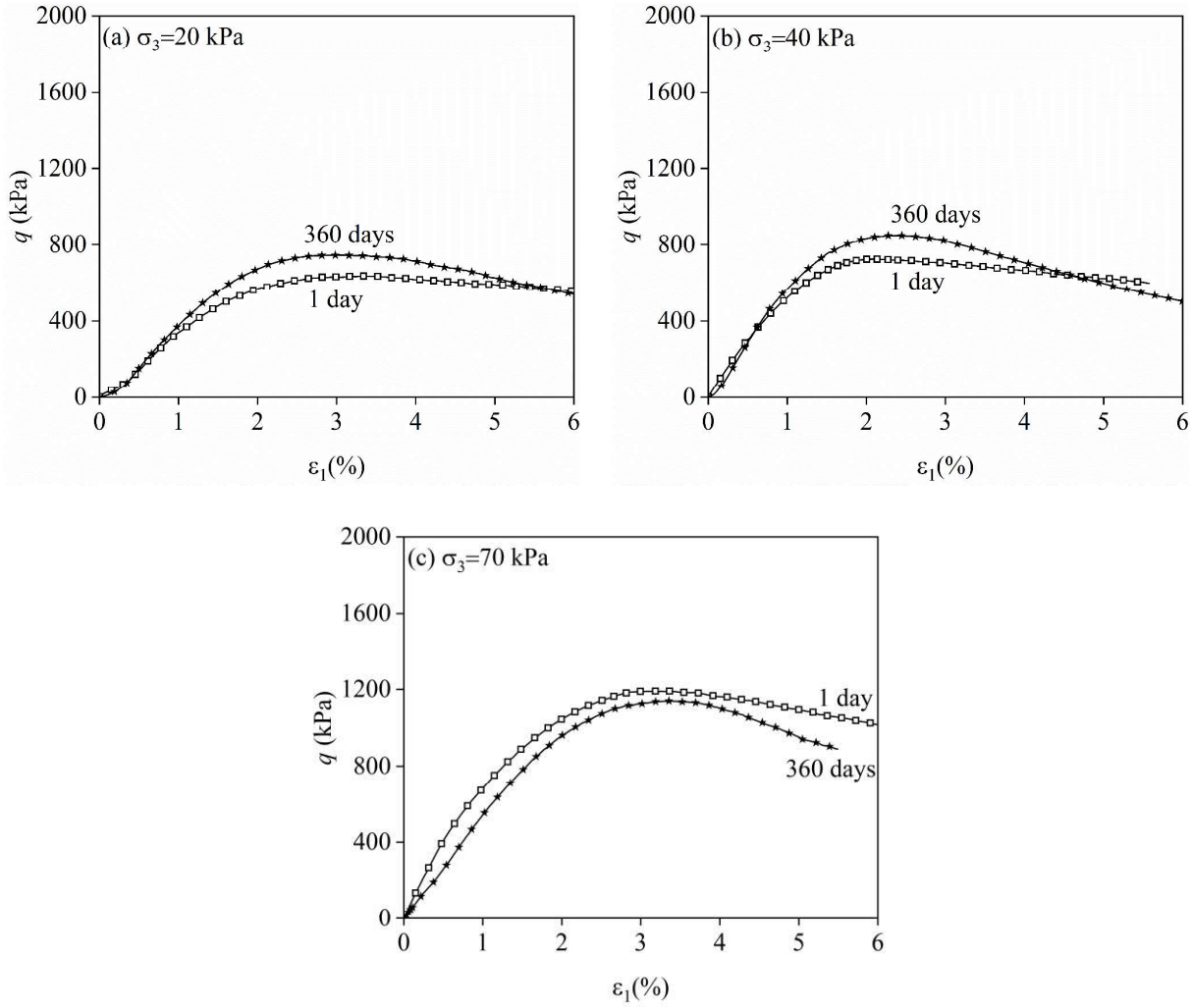

Figure V.2. Stress-strain curves of ORCA under different confining pressures after different curing times: (a) 20 kPa; (b) 40 kPa and (c) 70 kPa.

To better study the development of strength of RCA, the evolutions of the peak deviatoric stress q_{max} under different confining pressures for NRCA and ORCA are shown in Figure V.3. The q_{max} of NRCA, exhibiting strong self-cementing properties, indicated by the pH value, calorimeter test and TGA test, increases with curing time under all confining pressures, showing a clear cementation effect. However, this increase is not observed for ORCA, which self-cementing properties are negligible.

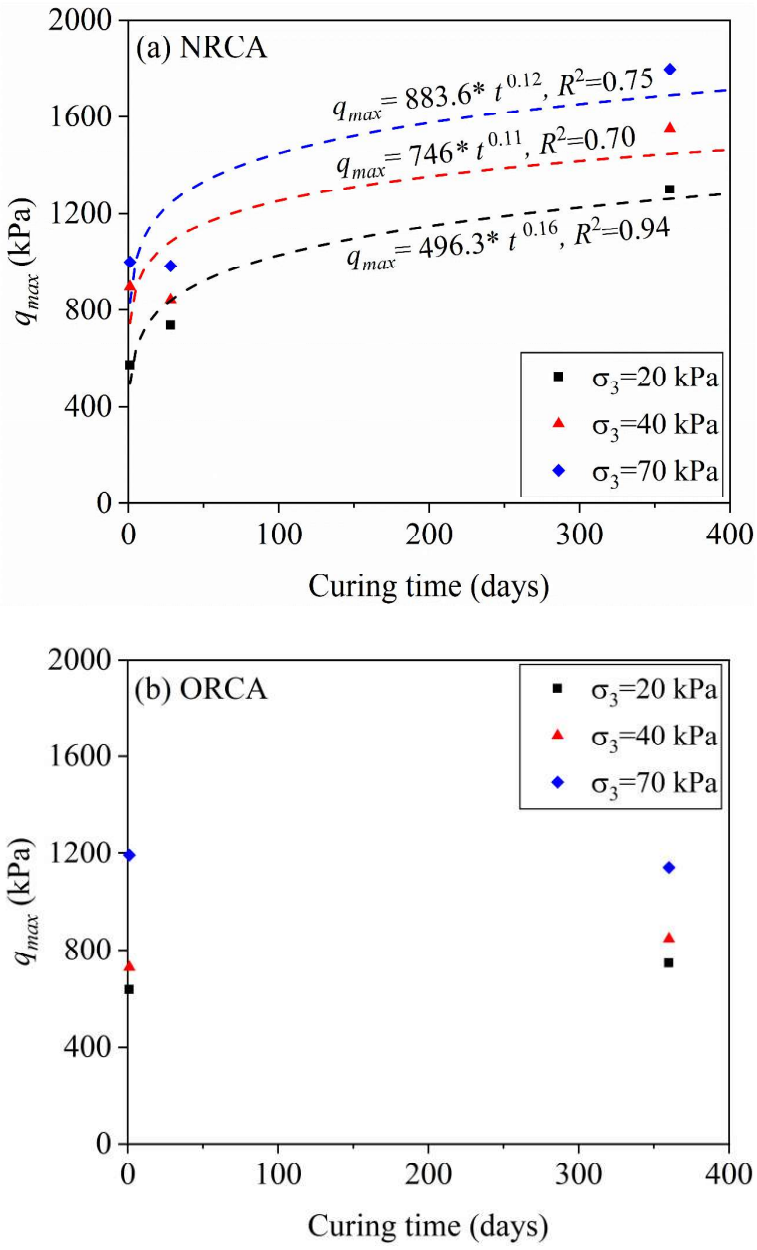

Figure V.3. Evolution of peak deviatoric stress q_{max}: (a) NRCA and (b) ORCA.

The different evolutions of q_{max} of the two RCA materials, under different confining pressures, are in good accordance with their self-cementing properties. For NRCA, after curing for 360 days, the increase of q_{max} under the lowest confining pressure of 20 kPa (2.3 times) is larger than those under the higher confining pressures of 40 kPa (1.7 times) and 70 kPa (1.8 times), indicating that the strength increase is more important under low confining pressure.

Furthermore, the strength of NRCA after long-term curing is much higher than that of unbound granular materials (UGM) used in pavement unbound layers. For example, under similar confining pressures (40±10 kPa) and testing parameters (particle size distribution, water content

and dry density), the peak deviatoric stress q_{max} of NRCA curing for 360 days is 1550 kPa, much higher than that of the UGM tested by Jing and Chazallon (2020) (q_{max}=792 kPa) and by Su et al. (2020) (q_{max}=707 kPa). However, the strength of NRCA after 360 days of curing remains lower than that of the light cement-bound granular mixtures, whose unconfined compressive strength is higher than 1 MPa (Crucho et al., 2021).

In order to better describe the effect of cementation on the development of strength of RCA, a power model, used to describe the evolution of resilient modulus and unconfined compression strength for chemically stabilized soils (typically treated with cement, lime, fly ash, etc.) (Miller et al., 2021; Xiu et al., 2021), was adopted for NRCA. The q_{max} can be expressed as:

$$q = q_0 \times t^a \tag{V.1}$$

where q_0 is the parameter related to the initial value of q_{max} without curing, and the parameter a describes the effect of self-cementing properties on the development of q_{max}, t is the curing time (t>0).

As shown in Figure V.3 (a), there is a good agreement between the experimental results and predicted q_{max} for the low confining pressure σ_3=20 kPa (R^2=0.94). Moreover, the parameter a obtained for σ_3=20 kPa (a=0.16) is higher than those obtained for under σ_3=40 kPa and 70 kPa (a=0.11 and 0.12), also indicating a more significant increase of q_{max} under low confining pressures, which is in good agreement with Xiu et al. (2021).

During the curing phase, bonds between particles developed with the hydration of residual unhydrated cement, increasing the cohesion as well as the strength and stiffness of unbound base and subbase layers built with RCA. When the confining pressure is low, cohesion has a dominating effect on the mechanical behavior of RCA. When the confining pressure increases, the friction between particles, which is slightly influenced by cementation effects, dominates the failure resistance instead of cohesion (Consoli et al., 2012; Jafari et al., 2021). On the other hand, bonds can be damaged during isotropic consolidation under higher confining stress, as observed also in other cemented materials (Jafari et al., 2021; Rabbi et al., 2011; Rios et al., 2014; Vranna & Tika, 2020). As a result, the influence of self-cementing properties on mechanical behaviors is more pronounced under low confining pressure.

With increasing curing time, the unbound base and subbase layers gradually turn into (partially) bound layers. This leads to a significant decrease of the deviatoric stress q after the peak deviatoric stress q_{max}, under 20 kPa confining pressure (Figure V.1 (a)), indicating that the ductile response observed at early age gradually turns into a stiff brittle behavior under low

confining pressure, which could potentially result in pavement cracking. This brittle behavior in the post peak region increases with the increasing degree of cementation and decreases as confining pressure increases, as observed also by other researchers for cement treated materials (Consoli et al., 2012; Feng & Montoya, 2016; Jafari et al., 2021). In addition, the ultimate state, where the deviatoric stress reaches a constant value, does not appear to be influenced by the curing time, as observed also by other researchers for cement treated materials (Schnaid et al., 2001).

V.3 Development of stiffness with curing time

In this study, the stiffness, secant modulus E_{50}, defined as the ratio of the deviatoric stress q to the axial strain ε_1 at a stress level equal to 50% of the peak deviatoric stress q_{max}, was used to study the effect of self-cementing properties on the development of stiffness with curing time, under different confining pressures, as shown in Figure V.4. It appears that for NRCA, E_{50} increases with curing time, while for ORCA, it is constant even after curing for 360 days, which is consistent with the evolution of q_{max} for the two RCA materials. After curing for 360 days, the E_{50} of NRCA is 2.6, 1.9 and 1.8 times larger than that after curing for 1 day at σ_3=20, 40 and 70 kPa respectively, this is similar to the increase of q_{max}.

For NRCA, a linear relationship between E_{50} and curing time is observed in this study, till the considered curing times (360 days in this study), which was also observed by other researchers (Niroshan et al., 2017; Rios et al., 2017) for chemically treated soils in the early curing stage (less than 90 days). E_{50} can be expressed as:

$$E_{50}=b+k*t \tag{V.2}$$

where b and k are parameters related to the initial E_{50} and the effect of self-cementing properties on E_{50}, t is the curing time. It is pointed out that Equation (V.2) was confirmed only for the studied material (NRCA) curing till 360 days, which was not valid for very long curing time since the hydration of unhydrated cement gradually stopped after curing for 360 days, as indicated by TGA (Section III.4). It also indicates that the hydration of unhydrated cement in RCA is slower than that of chemically treated soils and that a longer curing time is needed for unbound RCA specimens to harden significantly.

To compare the cementation effect of unhydrated cement inside RCA with that of cement treated materials, the slope k was compared with those of cement treated materials. Values of parameter k extracted from Niroshan et al. (2017) show that the cementation effect of the

studied NRCA (k=0.14 to 0.27), which unhydrated cement content contained in fine NRCA (0 to 2 mm) is between 6.2% and 7.9% according to the TGA, is not as effective as that of backfill treated with 2% cement and curing for 56 days (k=1.17), since only unhydrated cement contained in fine NRCA is effective as mentioned before.

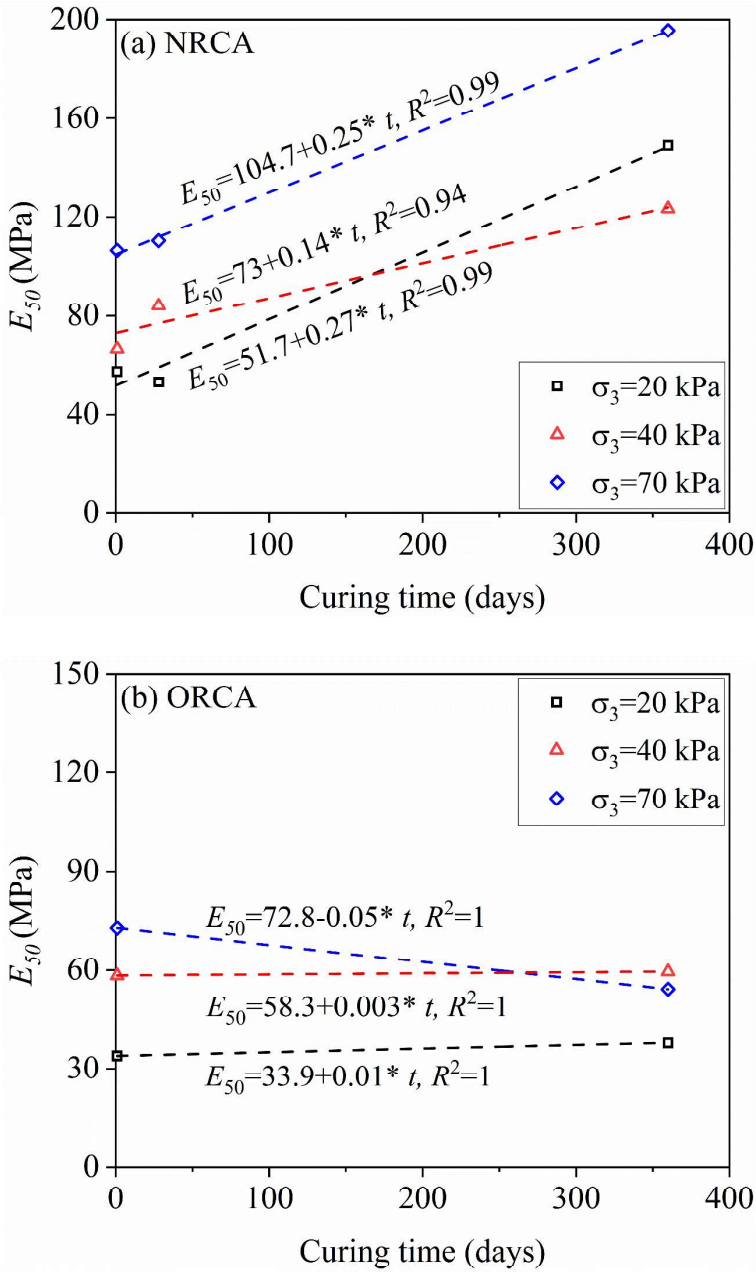

Figure V.4. Evolution of secant modulus E_{50}: (a) NRCA and (b) ORCA.

V.4 Relationship between q_{max} and E_{50}

Based on the results of monotonic triaxial tests, a linear relationship between q_{max} (kPa) and E_{50} (MPa), under different confining pressures (20/40/70 kPa) and curing times (1/28/360 days),

can be obtained (Miller et al., 2021; Niroshan et al., 2017), as shown in Figure V.5. It can be observed that the relationship for NRCA (R^2=0.84) is better than that for ORCA (R^2=0.48), as observed also by Miller et al. (2021) for chemically treated and untreated soils. Since the self-cementing property of ORCA is negligible, the mechanical behavior of ORCA, even after long-term curing, is similar to that of unbound granular materials, which is highly related to the confining pressure. As a result, q_{max} is not well correlated with E_{50} for ORCA. While for NRCA, with significant self-cementing properties, the cementation effect increases both strength (q_{max}) and stiffness (E_{50}), and leads to a linear relationship between them.

Similarly, the slopes of the regression lines were compared with those obtained for other cement treated materials. For cemented paste backfill, mixed with 2% to 6% of cement, the slopes are between 0.15 and 0.35 (Niroshan et al., 2017). For other chemically treated materials (typically treated with cement, lime, fly ash, etc.), the slopes are widely distributed, between 0.03 and 1 (Kang et al., 2017), highly depending on the soil type, amount and type of additives, etc. It can be observed that the slopes of the studied RCA (0.099 and 0.059 in this study), after long-term curing, are lower than those of most cement treated materials, even with a similar dosage of unhydrated cement, revealing that the cementation effect of RCA is not as effective as cement treated materials, which is in good agreement with the increase of the secant modulus E_{50} observed in Figure V.4.

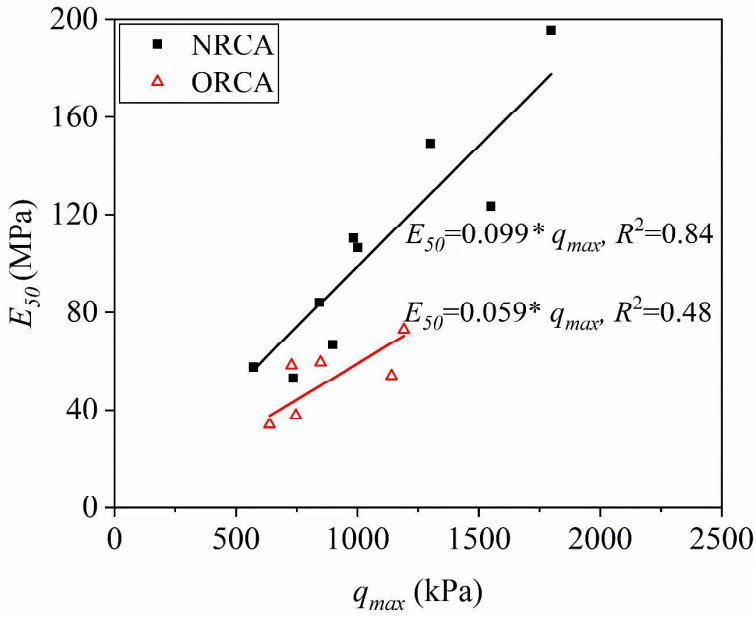

Figure V.5. Relationship between q_{max} and E_{50} for NRCA and ORCA, under different confining pressures (20/40/70 kPa) and curing times (1/28/360 days).

V.5 Development of strength parameters

From the values of peak deviatoric stress q_{max} and peak mean normal stress p_{max}, the failure lines of NRCA and ORCA, after different curing times, can be obtained, as shown in Figure V.6. The failure line can be defined by the equation:

$$q = k_0 \cdot p + b \tag{V.3}$$

Then, the peak friction angle φ_{peak} and cohesion c at failure can be determined from failure lines:

$$\varphi_{peak} = \arcsin(\frac{3k_0}{6 + k_0}) \tag{V.4}$$

$$c = \frac{3 - \sin(\varphi_{peak})}{6\cos(\varphi_{peak})} b \tag{V.5}$$

It can be observed that NRCA and ORCA specimens have similar failure lines, after curing for 1 day, since all the testing parameters are the same. The increase of curing time improves the resistance to failure for NRCA specimens. However, after short-term curing (28 days), the failure lines remain similar.

The failure line can be used to determine. Figure V.7 represents the φ_{peak} of NRCA and ORCA as a function of curing time. As indicated in Figure V.7, there is no clear correlation between φ_{peak}, varying from 50° to 57°, and curing time for both RCA materials. For cement treated materials, there is no consensus on how cementation affects the friction angle φ. Some researchers have found that cementation has a negligible effect on the friction angle (Fernandez & Santamarina, 2001; Jafari et al., 2021), in accordance with our observations. Other researchers have observed that the cementation can increase the friction angle (Feng & Montoya, 2016; Vranna & Tika, 2020) because of bonded particles and increased roughness of particle surfaces caused by the cementation effect (Wang & Leung, 2008).

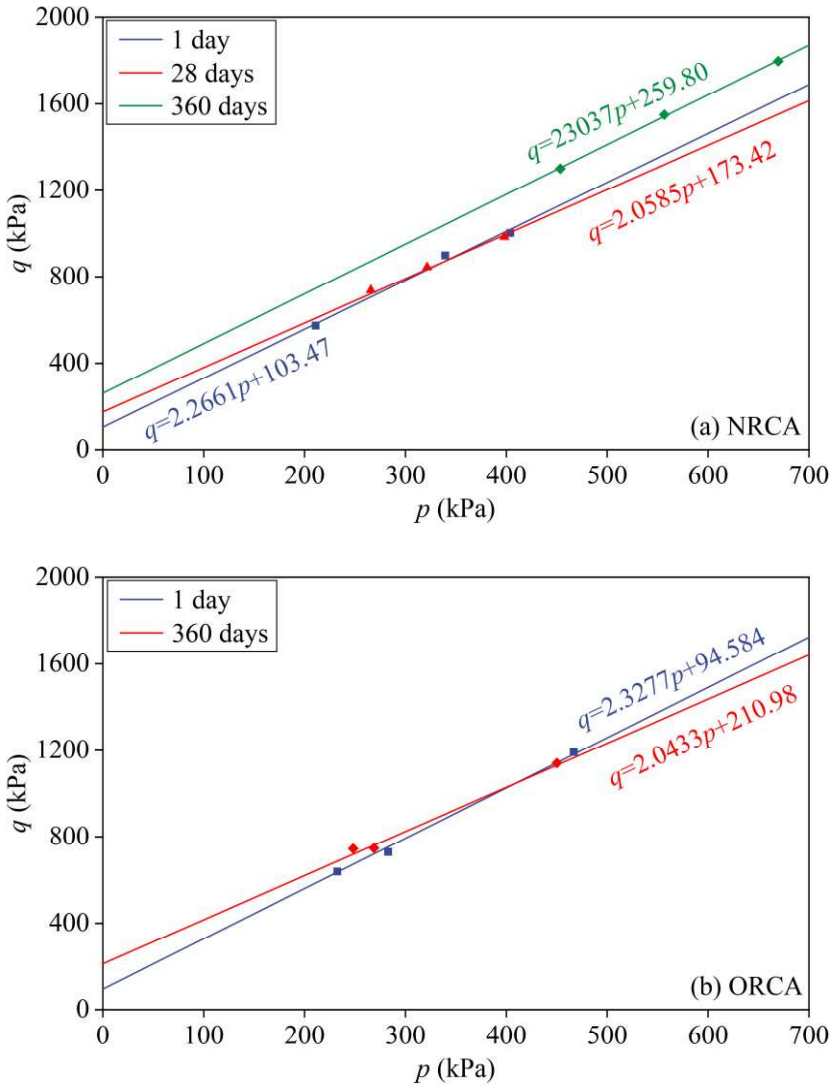

Figure V.6. Failure lines of RCA materials after curing for 1, 28 and 360 days: (a) NRCA and (b) ORCA.

Figure V.8 shows the evolution of cohesion c with curing time, and the fitted linear relationships, for the two RCA materials. It appears that c increases with curing time and this behavior is also influenced by the self-cementing properties of RCA. The cohesion c of NRCA increases by a factor of approximately 2.6 after 360 days of curing, which is higher than that of ORCA (1.9 times). A linear relationship exists between c and the logarithm of the curing time t for both RCA materials, as observed also for cemented paste backfill by Jafari et al. (2021). The relationship between cohesion c and curing time t ($t \geq 1$) can be established as:

$$c = k_1 + k_2 * \ln(t) \tag{V.6}$$

in which c and t are the cohesion (kPa) and curing time (days), k_1 and k_2 are parameters related to the initial cohesion and the influence of self-cementing properties of RCA, respectively. A

good agreement between the experimental results and predicted values is obtained with this equation, as all the R^2 values are higher than 0.9.

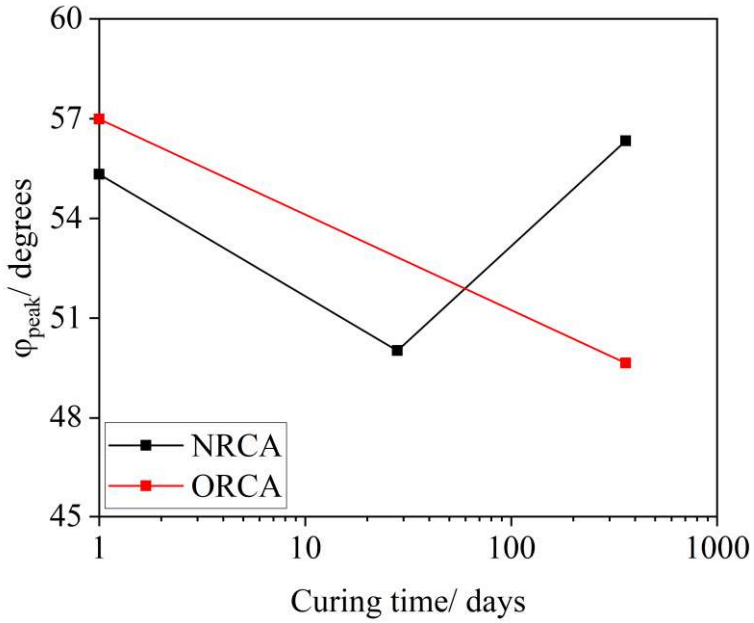

Figure V.7. Evolution of peak friction angle at failure for NRCA and ORCA.

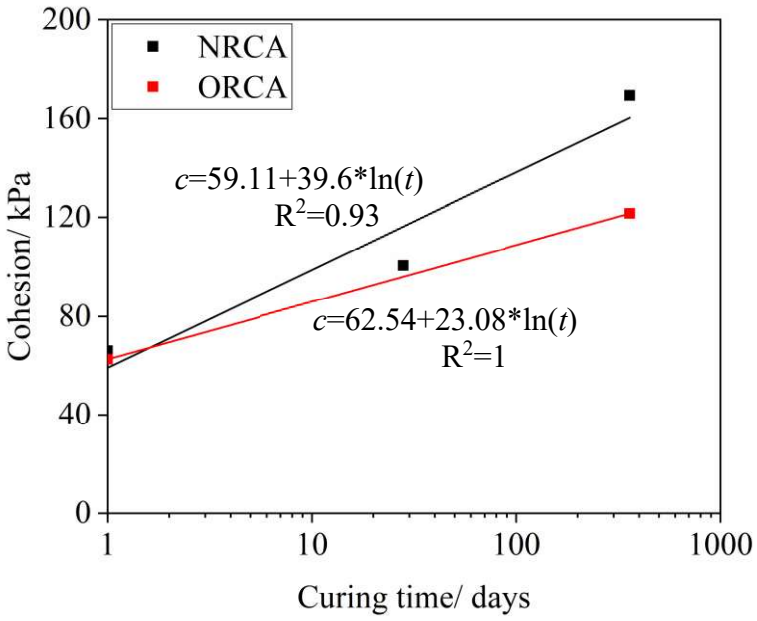

Figure V.8. Evolution of cohesion at failure for NRCA and ORCA

V.6 Conclusions

This chapter investigates the influence of self-cementing properties on the shear behavior of RCA, by conducting a series of monotonic triaxial tests on NRCA and ORCA specimens, after different curing times (1, 28 and 360 days), under different confining pressures (20, 40 and 70 kPa).

The results show that the peak deviatoric stress q_{max}, secant modulus E_{50} and cohesion increase with curing time, and this behavior is influenced by the self-cementing properties of RCA and confining pressure. The increase of q_{max} and E_{50} is more pronounced for RCA which has significant self-cementing properties (NRCA) and under smaller confining pressure. A power model can be used to estimate the evolution of q_{max} as for other cemented materials.

The mechanical behavior of NRCA after long-term curing is similar to that of cement treated materials, as ductile stress-strain response gradually turns to stiff brittle behavior under low confining pressures after long-term curing (360 days), and a linear relationship between E_{50} and q_{max} is also observed. This shows that for unbound pavement base and subbase layers built with RCA, with strong self-cementing properties, a significant gains of mechanical properties can be obtained with time.

The parameters of the models used to predict performance, increasing with curing time, were compared with those of other cement treated materials. The results show that the cementation effect of RCA is not as effective as that of new cement treated materials with similar unhydrated cement content, since only unhydrated cement contained in fine RCA can lead to an increase of strength and stiffness.

Conclusions and perspectives

The use of recycled crushed concrete aggregates (RCA) as a substitution to natural aggregates (NA) in pavement unbound base and subbase layers has become more popular in recent years. However, the mechanical behaviour and self-cementing properties of RCA are not fully understood. In this study, three different RCA materials were obtained from different sources: demolished buildings (NRCA and ORCA) and demolished concrete highway pavement (RCAP). The physical properties, self-cementing properties, microstructure and mechanical behaviours of these RCA materials under monotonic and repeated load triaxial loading were investigated.

Physical properties

The physical properties of the three RCA materials show that RCAP has a higher fines content before compaction and rounded particle content, while a lower water absorption, optimum moisture content, LA and MDE, than those of NRCA and ORCA, indicating the high amount of rounded aggregates and low strength of the parent concrete of RCAP. However, these properties fulfil the requirements of RCA for a pavement base course.

The water absorption kinetics of the three RCA materials show that a degree of saturation higher than 95% can be obtained for all three RCA mixtures, after saturation for 24 hours, confirming the suitability of the standard specimen preparation method for RCA.

Self-cementing properties

The evaluation of self-cementing properties shows that NRCA exhibits strong self-cementing properties while those of ORCA and RCAP are negligible. The pH value of NRCA (13.07) is much higher than that of ORCA (10.53) and RCAP (9.48). Besides, the average heat released by NRCA, due to the hydration of unhydrated cement, is 14.7 J, which is much higher than that released by ORCA (1.97 J).

The calculation of the unhydrated cement content based on TGA shows that non-evaporable water is more suitable to quantify the unhydrated cement content than portlandite ($Ca(OH)_2$). The potential unhydrated cement content of NRCA fine aggregates (0-2 mm) was evaluate between 6.2% and 7.9%. After curing for 360 days, the non-evaporable water content of NRCA increased by 1.04%, while for ORCA, it remained almost constant.

Not only the unhydrated cement can lead to the self-cementing properties, the sulfate attack products, ettringite, can also lead to the self-cementing properties. The greatest influence of self-cementing properties on the mechanical behavior of RCA is in the first year, as almost all the effective unhydrated cement was hydrated.

Microstructure observation

SEM observations indicate that the hydration products not only form bonds between particles, but also fill the small macro-pores between particles (radius less than 3 μm and higher than 0.65 μm), while for big macro-pores (radius larger than 3 μm), the filling effect is limited. The open type of structure (curing for 1 day) turns to rigid tight skeleton structure after curing 360 days.

MIP tests show that the volume of macro-pores (radius above 1 μm and less than 20 μm) decreases significantly after curing for 360 days. As a result, the average intrusion void ratio e_M decreases from 0.43 (curing for 1 day) to 0.26 (curing for 360 days). The decreased number of macro-pores also improves the homogeneity of the RCA specimen.

The mechanism of self-cementing is complex. The hydration products and sulfate attack products not only form bonds between particles, but also fill the small macro-pores, improving the microstructure of RCA specimen. Besides, the hydration of unhydrated cement also decreases the free water content. Consequently, the improved microstructure and decreased free water content can increase the matric suction, further improving the mechanical behaviour of RCA specimen.

Mechanical behaviour in repeated load triaxial tests

The laboratory test program has shown that RCA with high amounts of rounded particles and low strength of the parent concrete (RCAP) can lead to poor mechanical properties: larger permanent strain and permanent strain rate, larger resilient deviatoric strain ε_q^r and volumetric strain ε_v^r, leading to a lower resilient modulus, and thus not be suitable for use in pavement layers.

Besides, RCA materials (except RCA with high amount of rounded particles) is generally more stress dependent than most UGMs, which can be attributed to the attached mortar. However, high angularity and roughness of RCA aggregates improve the mechanical behaviour of RCA. Thus, the performance of most RCA (NRCA and ORCA) is comparable or even better to that of UGMs.

The permanent deformations of NRCA, with strong self-cementing properties, decrease quickly after curing for 180 days, and then reach a constant and very low value. However, traffic loading can reduce the effect of self-cementing properties by damaging the formed bonds between particles. For the ORCA, with negligible self-cementing properties, the permanent deformations remain is constant.

The resilient modulus of NRCA increases, while ε_q^r and ε_v^r decrease with increasing curing time. However, unlike for permanent deformations, the evolutions continue during the studied curing time (720 days). Besides, the resilient behaviour of NRCA also becomes more linear and less stress dependent, and its anisotropy increases. After curing for 720 days, the classification of NRCA improves from C2 to C1, according to the French standard for unbound granular materials, while ORCA is still ranked as C2, due to the lack of self-cementing properties.

Mechanical behaviour in monotonic triaxial tests

The monotonic triaxial test results show that the peak deviatoric stress q_{max}, secant modulus E_{50} and cohesion increase with curing time, and this behaviour is influenced by the self-cementing properties of RCA and confining pressure. The increase of q_{max} and E_{50} is more pronounced with RCA which has significant self-cementing properties (NRCA) and under smaller confining pressure. A power model can be used to estimate the evolution of q_{max}, as for other cemented materials.

The mechanical behaviour of NRCA after long-term curing is similar to that of cement treated materials: the ductile stress-strain response gradually changes to stiff brittle behavior under low confining pressures after long-term curing (360 days), and a linear relationship between E_{50} and q_{max} is also observed. The unbound pavement base and subbase layers built with RCA can gradually evolve into (partially) bound layers.

The parameters of the relationships used to predict mechanical properties were compared with those obtained for other cement treated materials. The study shows that the cementation effect of RCA is not as effective as the effect obtained with cement treated materials with similar unhydrated cement content. This can be explained by the fact that only unhydrated cement contained in fine RCA particles can lead to the increase of strength and stiffness.

Perspectives

The investigation allows the better understanding of the self-cementing properties and the short-term and long-term mechanical performance of RCA, which encourages the application of RCA in pavement. However, there are still some studies which can be continued:

As shown in previous study, unhydrated cement in fine aggregates domains the self-cementing properties of RCA. Besides, a good soil structure would improve the effect of cementation. As a result, the fine content and particle size distribution could have an influence on the long-term performance of RCA.

As the curing time increases, the unbound RCA specimen can gradually evolve into (partially) bound RCA specimen. Monotonic triaxial tests and repeated load triaxial tests show that the formed bonds can be damaged under high stress level. Thus, the effect of stress level on permanent deformation (multi-stage permanent deformation test) and resilient modulus could be studied. Models used to describe the effects of curing time and stress state on the permanent and resilient deformation behaviour could also be developed.

At the end, treatment methods to improve the properties of RCA can also be investigated, such as thermal treatment to reactive the hydrated cement, removal of attached mortar, RCA treated with cement or pozzolanic materials.

References

Abu-Farsakh, M., Dhakal, S., & Chen, Q. M. (2015). Laboratory characterization of cementitiously treated/stabilized very weak subgrade soil under cyclic loading. *Soils Found.*, *55*(3), 504-516. https://doi.org/10.1016/j.sandf.2015.04.003

AFNOR. (1995). NF P98-235-1—Test relating to pavements. Unbound granular materials. Part 1: Repeated Loading Triaxial Test.

Ahmad, A., Farooq, F., Niewiadomski, P., Ostrowski, K., Akbar, A., Aslam, F., & Alyousef, R. (2021). Prediction of Compressive Strength of Fly Ash Based Concrete Using Individual and Ensemble Algorithm. *Mater.*, *14*(4), Article 794. https://doi.org/10.3390/ma14040794

Akbarnezhad, A., Ong, K. C. G., Zhang, M. H., & Tam, C. T. (2013). Acid Treatment Technique for Determining the Mortar Content of Recycled Concrete Aggregates. *Journal of Testing and Evaluation*, *41*(3), 441-450. https://doi.org/10.1520/jte20120026

Allen, J. J., & Thompson, M. R. J. T. R. R. (1974). Resilient response of granular materials subjected to time-dependent lateral stresses. (510).

Alnedawi, A., Kafle, B., Ullah, S., & Kerr, W. (2021). Investigation of non-standard unbound granular materials under cyclic loads: experimental and regression analyses. *Int. J. Pavement Eng.* https://doi.org/10.1080/10298436.2021.1877291

Amin, A., Hasnat, A., Khan, A. H., & Ashiquzzaman, M. (2016). Residual Cementing Property in Recycled Fines and Coarse Aggregates: Occurrence and Quantification. *J. Mater. Civ. Eng.*, *28*(4), Article 04015174. https://doi.org/10.1061/(asce)mt.1943-5533.0001472

Ardah, A., Chen, Q. M., & Abu-Farsakh, M. (2017). Evaluating the performance of very weak subgrade soils treated/stabilized with cementitious materials for sustainable pavements. *Transp. Geotech.*, *11*, 107-119. https://doi.org/10.1016/j.trgeo.2017.05.002

Arm, M. (2001). Self-cementing properties of crushed demolished concrete in unbound layers: results from triaxial tests and field tests. *Waste Manage.*, *21*(3), 235-239. https://doi.org/10.1016/s0956-053x(00)00095-7

Arulrajah, A., Disfani, M. M., Horpibulsuk, S., Suksiripattanapong, C., & Prongmanee, N. (2014). Physical properties and shear strength responses of recycled construction and demolition materials in unbound pavement base/subbase applications. *Constr. Build. Mater.*, *58*, 245-257. https://doi.org/10.1016/j.conbuildmat.2014.02.025

Arulrajah, A., Piratheepan, J., Ali, M. M. Y., & Bo, M. W. (2012). Geotechnical Properties of Recycled Concrete Aggregate in Pavement Sub-Base Applications. *Geotechnical Testing Journal*, *35*(5), 743-751. <Go to ISI>://WOS:000309574000007

Arulrajah, A., Piratheepan, J., Disfani, M. M., & Bo, M. W. (2013). Resilient Moduli Response of Recycled Construction and Demolition Materials in Pavement Subbase Applications. *J. Mater. Civ. Eng.*, *25*(12), 1920-1928. https://doi.org/10.1061/(asce)mt.1943-5533.0000766

Azam, A. M., & Cameron, D. A. (2013). Geotechnical Properties of Blends of Recycled Clay Masonry and Recycled Concrete Aggregates in Unbound Pavement Construction. *J. Mater. Civ. Eng.*, *25*(6), 788-798. https://doi.org/10.1061/(asce)mt.1943-5533.0000634

Barbieri, D. M., Lou, B. W., Dyke, R. J., Wang, X. T., Chen, H., Shu, B. A., Gazder, U., Horpibulsuk, S., Tingle, J. S., & Hoff, I. (2022). Design and sustainability analyses of road base layers stabilized with traditional and nontraditional additives. *J. Cleaner Prod.*, *372*, Article 133752. https://doi.org/10.1016/j.jclepro.2022.133752

Barksdale, R. D. (1972, 1972). Laboratory evaluation of rutting in base course materials. (Ed.),^(Eds.). Third International Conference on the Structural Design of Asphalt Pavements, Grosvenor House, Park Lane, London, England.

Batmunkh, N., Siripun, K., Jitsangiam, P., & Nikraz, H. (2010). Sustainable use of crushed concrete waste as a road base material. (Ed.),^(Eds.). Proceedings of the 4th International Conference on Sustainability Engineering and Science.

Belin, P., Habert, G., Thiery, M., & Roussel, N. (2014). Cement paste content and water absorption of recycled concrete coarse aggregates. *Mater. Struct.*, *47*(9), 1451-1465. https://doi.org/10.1617/s11527-013-0128-z

Bestgen, J. O., Hatipoglu, M., Cetin, B., & Aydilek, A. H. (2016). Mechanical and Environmental Suitability of Recycled Concrete Aggregate as a Highway Base Material. *J. Mater. Civ. Eng.*, *28*(9), Article 04016067. https://doi.org/10.1061/(asce)mt.1943-5533.0001564

Bhatty, J. I. (1986). Hydration versus strength in a portland cement developed from domestic mineral wastes—A comparative study. *Thermochim. Acta*, *106*, 93-103. https://doi.org/10.1016/0040-6031(86)85120-6

Biarez, J. (1962). *Contribution à l'étude des propriétés mécaniques des sols et des matériaux pulvérulents*, Faculte des Sciences de Grenoble].

Blankenagel, B. J., Guthrie, W. S., & Trb. (2006). Laboratory characterization of recycled concrete for use as pavement base material (*Geomaterials 2006* (Vol. 1952, pp. 21-27). https://doi.org/10.3141/1952-03

Bordy, A., Younsi, A., Aggoun, S., & Fiorio, B. (2017). Cement substitution by a recycled cement paste fine: Role of the residual anhydrous clinker. *Constr. Build. Mater.*, *132*, 1-8. https://doi.org/10.1016/j.conbuildmat.2016.11.080

Boyce, H. (1980). A nonlinear model for the elastic behaviour of granular materials under repeated loading. (Ed.),^(Eds.). In Proceedings of the International Symposium on Soils under Cyclic and Transient Loading, Swansea.

Brown, S., & Hyde, A. (1975). Significance of cyclic confining stress in repeated-load triaxial testing of granular material. *Transp. Res. Rec.*(537).

Brown, S., & Selig, E. (1991). The design of pavement and rail track foundations. (Ed.),^(Eds.). Cyclic loading of soils: from theory to design.

Brown, S. F., & Pappin, J. (1985). *Modeling of granular materials in pavements*.

BS 1377-3. (2018). Methods of test for soils for civil engineering purposes. Part 3: chemical and electro-chemical testing.

Cardoso, R., Silva, R. V., de Brito, J., & Dhir, R. (2016). Use of recycled aggregates from construction and demolition waste in geotechnical applications: A literature review. *Waste Manage.*, *49*, 131-145. https://doi.org/10.1016/j.wasman.2015.12.021

CETE de l'Est. (2009). *Guides d'utilisation des matériaux lorrains en technique routière - Guide matériaux de démolition*. http://materrio.construction/mediatheque/media/35-guide_materiaux_de_demolition.pdf.

Chan, F. W. K. (1990). *Permanent deformation resistance of granular layers in pavements*, University of Nottingham].

Chang, C. F., & Chen, J. W. (2006). The experimental investigation of concrete carbonation depth. *Cem. Concr. Res.*, *36*(9), 1760-1767. https://doi.org/10.1016/j.cemconres.2004.07.025

Chidiac, S. E., & Shafikhani, M. (2019). Cement degree of hydration in mortar and concrete. *J. Therm. Anal. Calorim.*, *138*(3), 2305-2313. https://doi.org/10.1007/s10973-019-08800-w

Consoli, N. C., Cruz, R. C., da Fonseca, A. V., & Coop, M. R. (2012). Influence of Cement-Voids Ratio on Stress-Dilatancy Behavior of Artificially Cemented Sand. *J. Geotech. Geoenviron. Eng.*, *138*(1), 100-109. https://doi.org/10.1061/(asce)gt.1943-5606.0000565

Cook, C. S., Tanyu, B. F., & Yavuz, A. B. (2017). Effect of Particle Shape on Durability and Performance of Unbound Aggregate Base. *J. Mater. Civ. Eng.*, *29*(2), Article 04016221. https://doi.org/10.1061/(asce)mt.1943-5533.0001752

Corradini, A., Cerni, G., & Porceddu, P. R. (2021). Comparative study on resilient modulus of natural and post-quake recycled aggregates in bound and unbound pavement subbase applications. *Constr. Build. Mater.*, *297*, Article 123717. https://doi.org/10.1016/j.conbuildmat.2021.123717

Crucho, J., Picado-Santos, L., & Neves, J. (2021). Cement-treated pavement layers incorporating construction and demolition waste and coconut fibres: a review. *Int. J. Pavement Eng.* https://doi.org/10.1080/10298436.2021.1984475

Cui, Y. J. (2018). Mechanical behaviour of coarse grains/fines mixture under monotonic and cyclic loadings. *Transp. Geotech.*, *17*, 91-97. https://doi.org/10.1016/j.trgeo.2018.09.016

Dawson, A., Thom, N., & Paute, J. (1996). *Mechanical characteristics of unbound granular materials as a function of condition*. Gomes Correia, Balkema, Rotterdam.

Debnath, B., & Sarkar, P. P. (2020). Pervious concrete as an alternative pavement strategy: a state-of-the-art review. *Int. J. Pavement Eng.*, *21*(12), 1516-1531. https://doi.org/10.1080/10298436.2018.1554217

Deboucha, W., Leklou, N., & Khelidj, A. (2020). Combination effect of limestone filler and slag on hydration reactions in ternary cements. *Eur. J. Environ. Civ. Eng.* https://doi.org/10.1080/19648189.2020.1825233

Delage, P., Audiguier, M., Cui, Y. J., & Howat, M. D. (1996). Microstructure of a compacted silt. *Canadian Geotechnical Journal*, *33*(1), 150-158. https://doi.org/10.1139/t96-030

Deodonne, K. (2015). *Etudes des caractéristiques physico-chimiques de bétons de granulats recyclés et de leur impact environnemental*, Université de Strasbourg].

Dunlap, W. A. (1963). *A report on a mathematical model describing the deformation characteristics of granular materials*. Texas Transportation Institute, Texas A & M University.

Duong, T. V., Tang, A. M., Cui, Y.-J., Trinh, V. N., Dupla, J.-C., Calon, N., Canou, J., Robinet, A. J. S., & foundations. (2013). Effects of fines and water contents on the mechanical behavior of interlayer soil in ancient railway sub-structure. *53*(6), 868-878.

El Hannani, M. (1991). *Modèlisation et simulation numérique des Chaussées Souples*, Nantes].

Elliott, R. P., & David, L. J. T. R. R. (1989). Improved characterization model for granular bases. (1227).

Ezaoui, A., & Di Benedetto, H. (2008, Aug 25-27). Measurements and modelling of anisotropic elastic behaviour of unbound granular materials. (Ed.),^(Eds.). 1st International Conference on Transportation Geotechnics, Nottingham, ENGLAND.

Ezaoui, A., Di Benedetto, H., & Van Bang, D. P. (2006, Mar 16-17). Anisotropic behaviour of sand in the small strain domain. Experimental measurements and modelling. (Ed.),^(Eds.), *Solid Mechanics and its Applications*. Geotechnical Symposium held to Celebrate the 60th Birthday of Fumio Tatsuko, Univ Rome La Sapienza, Rome, ITALY.

Feng, K., & Montoya, B. M. (2016). Influence of Confinement and Cementation Level on the Behavior of Microbial-Induced Calcite Precipitated Sands under Monotonic Drained Loading. *J. Geotech. Geoenviron. Eng.*, *142*(1). https://doi.org/10.1061/(asce)gt.1943-5606.0001379

Fernandez, A. L., & Santamarina, J. C. (2001). Effect of cementation on the small-strain parameters of sands. *Canadian Geotechnical Journal*, *38*(1), 191-199. https://doi.org/10.1139/cgj-38-1-191

Gabr, A., Mills, K., & Cameron, D. (2013). Repeated load triaxial testing of recycled concrete aggregate for pavement base construction. *Geotechnical*

Geological Engineering, *31*(1), 119-132.

Gabr, A. R., & Cameron, D. A. (2012). Properties of Recycled Concrete Aggregate for Unbound Pavement Construction. *J. Mater. Civ. Eng.*, *24*(6), 754-764. https://doi.org/10.1061/(asce)mt.1943-5533.0000447

Gaillard, L. (2019). *Comportement thermo-hydro-mécanique des agrégats d'enrobés compactés non saturés*, Université de Strasbourg].

Gaillard, L., Chazallon, C., Hornych, P., Quezada, J. C., & Raab, C. (2019). Thermo-hydro-mechanical behaviour of cold reclaimed asphalt aggregates without binder addition. *Road Mater. Pavement Des.*, *20*, S49-S63. https://doi.org/10.1080/14680629.2019.1587490

Gidel, G., Hornych, P., Breysse, D., & Denis, A. (2001). A new approach for investigating the permanent deformation behaviour of unbound granular material using the repeated loading triaxial apparatus. *Bulletin des laboratoires des Ponts et Chaussées*(233).

Han-Cheng, D., Lin-Hua, H., & Lian-Heng, Z. (2020). Experimental investigation on the resilient response of unbound graded aggregate materials by using large-scale dynamic triaxial tests. *Road Mater. Pavement Des.*, *21*(2), 434-451. https://doi.org/10.1080/14680629.2018.1500300

Hewlett, P., & Liska, M. (2019). *Lea's chemistry of cement and concrete*. Butterworth-Heinemann.

Hick, R., & Monismith, C. (1971). Factors influencing the resilient response of granular materials. *Highway Research Record*, *345*, 15-31.

Hicks, R. G. (1970). *Factors influencing the resilient properties of granular materials*. University of California, Berkeley.

Ho, X. N., Nowamooz, H., Chazallon, C., & Migault, B. (2014). Influence of fine content and water content on the resilient behaviour of a natural compacted sand. *Road Mater. Pavement Des.*, *15*(3), 606-621. https://doi.org/10.1080/14680629.2014.908136

Hornych, P. (1993). Étude des déformations permanentes sous chargements répétés de trois graves non traitées. (184).

Hornych, P., Gaudefroy, V., Geffard, J. L., & Goyer, S. (2009, May 27-29). Study of the mechanical behaviour of gravel-emulsions using triaxial tests. (Ed.),^(Eds.). 7th International RILEM Symposium on Advanced Testing and Characterisation of Bituminous Materials, Rhodes, Greece.

Hornych, P., Kazai, A., & Piau, J. M. (1998). *Study of the resilient behaviour of unbound granular materials*. In Proceedings of the 5th Conference on Bearing Capacity of Roads and Airfields, Trondheim, Norway.

Jafari, M., Shahsavari, M., & Grabinsky, M. (2021). Drained Triaxial Compressive Shear Response of Cemented Paste Backfill (CPB). *Rock Mechanics and Rock Engineering*, *54*(6), 3309-3325. https://doi.org/10.1007/s00603-021-02464-5

Janoo, V., Bayer, J. J., & Benda, C. C. (2004). Effect of aggregate angularity on base material properties. *J. Mater. Civ. Eng.*, *16*(6), 614-622. https://doi.org/10.1061/(asce)0899-1561(2004)16:6(614)

Jayakody, S., Gallage, C., & Ramanujam, J. (2019). Performance characteristics of recycled concrete aggregate as an unbound pavement material. *Heliyon*, *5*(9), Article e02494. https://doi.org/10.1016/j.heliyon.2019.e02494

Jing, P., & Chazallon, C. (2020). Hydro-Mechanical Behaviour of an Unbound Granular Base Course Material Used in Low Traffic Pavements. *Mater.*, *13*(4), Article 852. https://doi.org/10.3390/ma13040852

Jing, P., Nowamooz, H., & Chazallon, C. (2018). Permanent deformation behaviour of a granular material used in low-traffic pavements. *Road Mater. Pavement Des.*, *19*(2), 289-314. https://doi.org/10.1080/14680629.2016.1259123

Jing, P., Nowamooz, H., & Chazallon, C. (2019). Unsaturated mechanical behaviour of a granular material. *Road Mater. Pavement Des.*, *20*(6), 1429-1451. https://doi.org/10.1080/14680629.2018.1447506

Jitsangiam, P., Boonserm, K., Phenrat, T., Chummuneerat, S., Chindaprasirt, P., & Nikraz, H. (2015). Recycled Concrete Aggregates in Roadways: Laboratory Examination of Self-Cementing Characteristics. *J. Mater. Civ. Eng.*, *27*(10), Article 04014270. https://doi.org/10.1061/(asce)mt.1943-5533.0001245

Johnson, T., Berg, R. L., & Dimillio, A. (1986). *Frost action predictive techniques: an overview of research results*.

Jorenby, B. N., & Hicks, R. G. (1986). *Base course contamination limits*.

Juan, M. S. D., & Gutierrez, P. A. (2009). Study on the influence of attached mortar content on the properties of recycled concrete aggregate. *Constr. Build. Mater.*, *23*(2), 872-877. https://doi.org/10.1016/j.conbuildmat.2008.04.012

Kalinowska-Wichrowska, K., Kosior-Kazberuk, M., & Pawluczuk, E. (2020). The Properties of Composites with Recycled Cement Mortar Used as a Supplementary Cementitious Material. *Mater.*, *13*(1), Article 64. https://doi.org/10.3390/ma13010064

Kampala, A., Jitsangiam, P., Pimraksa, K., & Chindaprasirt, P. (2021). An investigation of sulfate effects on compaction characteristics and strength development of cement-treated sulfate bearing clay subgrade. *Road Mater. Pavement Des.*, *22*(10), 2396-2409. https://doi.org/10.1080/14680629.2020.1753564

Kang, G., Tsuchida, T., & Kim, Y. (2017). Strength and stiffness of cement-treated marine dredged clay at various curing stages. *Constr. Build. Mater.*, *132*, 71-84. https://doi.org/10.1016/j.conbuildmat.2016.11.124

Khedr, S. (1985). Deformation characteristics of granular base course in flexible pavements. *Transp. Res. Rec.*, *1043*, 131-138.

Kim, J., Nam, B., Behring, Z., & Al Muhit, B. (2014). Evaluation of Recementation Reactivity of Recycled Concrete Aggregate Fines. *Transp. Res. Rec.*(2401), 44-51. https://doi.org/10.3141/2401-05

Korkiala-Tanttu, L., Dettenborn, T., & Forsman, J. (2014). Long-term behavior of crushed concrete in road structure. (Ed.),^(Eds.). 23rd European Young Geotechnical Engineers Conference, August 2014.

Kuo, S. S., Mahgoub, H. S., & Nazef, A. (2002). Investigation of recycled concrete made with limestone aggregate for a base course in flexible pavement. *Transp. Res. Rec.*, *1787*, 99-108. <Go to ISI>://WOS:000179620300011

Kwon, J., Kim, S. H., Tutumluer, E., & Wayne, M. H. (2017). Characterisation of unbound aggregate materials considering physical and morphological properties. *Int. J. Pavement Eng.*, *18*(4), 303-308. https://doi.org/10.1080/10298436.2015.1065997

Lancieri, F., Marradi, A., & Mannucci, S. (2006, Jun). C&D waste for road construction: long time performance of roads constructed using recycled aggregate for unbound pavement layers. (Ed.),^(Eds.), *WIT Transactions on Ecology and the Environment*. 3rd International Conference on Waste Management and the Environment, Malta.

Lekarp, F., & Dawson, A. (1998). Modelling permanent deformation behaviour of unbound granular materials. *Constr. Build. Mater.*, *12*(1), 9-18. https://doi.org/10.1016/s0950-0618(97)00078-0

Lekarp, F., Isacsson, U., & Dawson, A. (2000a). State of the art. I: Resilient response of unbound aggregates. *Journal of Transportation Engineering-Asce*, *126*(1), 66-75. https://doi.org/10.1061/(asce)0733-947x(2000)126:1(66)

Lekarp, F., Isacsson, U., & Dawson, A. (2000b). State of the art. II: Permanent strain response of unbound aggregates. *Journal of Transportation Engineering-Asce*, *126*(1), 76-83. https://doi.org/10.1061/(asce)0733-947x(2000)126:1(76)

Lin, F., & Meyer, C. (2009). Hydration kinetics modeling of Portland cement considering the effects of curing temperature and applied pressure. *Cem. Concr. Res.*, *39*(4), 255-265. https://doi.org/10.1016/j.cemconres.2009.01.014

Lu, C., Chen, J. Y., Gu, C., Wang, J., Cai, Y. Q., Zhang, T. T., & Lin, G. (2021). Resilient and permanent deformation behaviors of construction and demolition wastes in unbound pavement base and subbase applications. *Transp. Geotech.*, *28*, Article 100541. https://doi.org/10.1016/j.trgeo.2021.100541

Luong, M. (1982). Mechanical aspects and thermal effects of cohesionless soils under cyclic and transient loading.

Mathias, V., Sedran, T., & de Larrard, F. (2009). Modelling of Mechanical Properties of Cement Concrete Incorporating Reclaimed Asphalt Pavement. *Road Mater. Pavement Des.*, *10*(1), 63-82. https://doi.org/10.3166/rmpd.10.63-82

Mayhew, H. (1983). *Resilient properties of unbound roadbase under repeated triaxial loading* (

Mefteh, H., Kebaili, O., Oucief, H., Berredjem, L., & Arabi, N. (2013). Influence of moisture conditioning of recycled aggregates on the properties of fresh and hardened concrete. *J. Cleaner Prod.*, *54*, 282-288. https://doi.org/10.1016/j.jclepro.2013.05.009

Mehta, P. K. (1983). Mechanism of sulfate attack on portland cement concrete—Another look. *Cem. Concr. Res.*, *13*(3), 401-406. https://doi.org/10.1016/0008-8846(83)90040-6

Miller, G. A., Cerato, A. B., Snethen, D. R., Holderby, E., & Boodagh, P. (2021). Empirical method for predicting time-dependent strength and resilient modulus of chemically treated soil. *Transp. Geotech.*, *29*, Article 100551. https://doi.org/10.1016/j.trgeo.2021.100551

Mills, R. H. (1966). Factors influencing cessation of hydration in water cured cement pastes. *Highway Research Board*(90).

Mishra, D., & Tutumluer, E. (2012). Aggregate Physical Properties Affecting Modulus and Deformation Characteristics of Unsurfaced Pavements. *J. Mater. Civ. Eng.*, *24*(9), 1144-1152. https://doi.org/10.1061/(asce)mt.1943-5533.0000498

Morgan, J. (1966). *The response of granular materials to repeated loading*. Australian Road Research Board Proc.

Mounanga, P., Khelidj, A., Loukili, A., & Baroghel-Bouny, W. (2004). Predicting $Ca(OH)_2$ content and chemical shrinkage of hydrating cement pastes using analytical approach. *Cem. Concr. Res.*, *34*(2), 255-265. https://doi.org/10.1016/j.cemconres.2003.07.006

NF EN 196-9. (2010). Methods of testing cement — Part 9: Heat of hydration — Semi-adiabatic method (Vol. 9).

NF EN 206-1. (2004). Concrete — Part 1: Specification, performance, production and conformity

NF EN 933-1. (2012). Tests for geometrical properties of aggregates — Part 1: Determination of particle size distribution —Sieving method

NF EN 933-5. (1998). Tests for geometrical propertiesof aggregates — Part 5 : Determination of percentage of crushedand broken surfaces in coarse aggregate particles.

NF EN 1097-1. (2011). Tests for mechanical and physical properties of aggregates - Part 1: Determination of the resistance to wear (micro-Deval).

NF EN 1097-2. (2020). Tests for mechanical and physical properties of aggregates - Part 2 : methods for the determination of resistance to fragmentation.

NF EN 1097-6. (2014). Tests for mechanical and physical propertiesof aggregates — Part 6: Determination of particle density and water absorption.

NF EN 1744-1. (2014). Tests for chemical properties of aggregates — Part 1: Chemical analysis

NF EN 13285. (2018). Unbound mixtures - Specifications.

NF EN 13286-7. (2004). Unbound and hydraulically bound mixtures – Part 7: Triaxial test under cyclic loading for unbound mixtures.

NF ISO 10693. (1995). Soil quality---determination of carbonate content---volumetric method. Association Française de Normalisation ed Paris.

Niroshan, N., Sivakugan, N., & Veenstra, R. L. (2017). Laboratory Study on Strength Development in Cemented Paste Backfills. *J. Mater. Civ. Eng.*, *29*(7). https://doi.org/10.1061/(asce)mt.1943-5533.0001848

Nowamooz, H., Chazallon, C., Arsenie, M. I., Hornych, P., & Masrouri, F. (2011). Unsaturated resilient behavior of a natural compacted sand. *Computers and Geotechnics*, *38*(4), 491-503. https://doi.org/10.1016/j.compgeo.2011.02.013

Nwakaire, C. M., Yap, S. P., Onn, C. C., Yuen, C. W., & Ibrahim, H. A. (2020). Utilisation of recycled concrete aggregates for sustainable highway pavement applications; a review. *Constr. Build. Mater.*, *235*, Article 117444. https://doi.org/10.1016/j.conbuildmat.2019.117444

Oksri-Nelfia, L., Mahieux, P. Y., Amiri, O., Turcry, P., & Lux, J. (2016). Reuse of recycled crushed concrete fines as mineral addition in cementitious materials. *Mater. Struct.*, *49*(8), 3239-3251. https://doi.org/10.1617/s11527-015-0716-1

Paige-Green, P. (2010, 16 - 19 August 2010). *Preliminary evaluation of the reuse of cementitious materials*. 29th Annual Southern African Transport Conference, Pretoria, South Africa.

Pan, T. Y., Tutumluer, E., Anochie-Boateng, J., & Trb. (2006). Aggregate morphology affecting resilient behavior of unbound granular materials. *Transp. Res. Rec.*, *1952*, 12-20. https://doi.org/10.3141/1952-02

Pane, I., & Hansen, W. (2005). Investigation of blended cement hydration by isothermal calorimetry and thermal analysis. *Cem. Concr. Res.*, *35*(6), 1155-1164. https://doi.org/10.1016/j.cemconres.2004.10.027

Papadakis, V. G. (1999a). Effect of fly ash on Portland cement systems Part I. Low-calcium fly ash. *Cem. Concr. Res.*, *29*(11), 1727-1736. https://doi.org/10.1016/s0008-8846(99)00153-2

Papadakis, V. G. (1999b). Experimental investigation and theoretical modeling of silica fume activity in concrete. *Cem. Concr. Res.*, *29*(1), 79-86. https://doi.org/10.1016/s0008-8846(98)00171-9

Papadakis, V. G. (2000). Effect of supplementary cementing materials on concrete resistance against carbonation and chloride ingress. *Cem. Concr. Res.*, *30*(2), 291-299. https://doi.org/10.1016/s0008-8846(99)00249-5

Papadakis, V. G., Antiohos, S., & Tsimas, S. (2002). Supplementary cementing materials in concrete - Part II: A fundamental estimation of the efficiency factor. *Cem. Concr. Res.*, *32*(10), 1533-1538, Article Pii s0008-8846(02)00829-3. https://doi.org/10.1016/s0008-8846(02)00829-3

Pereira, C. G., Castro-Gomes, J., & de Oliveira, L. P. (2009). Influence of natural coarse aggregate size, mineralogy and water content on the permeability of structural concrete. *Constr. Build. Mater.*, *23*(2), 602-608. https://doi.org/10.1016/j.conbuildmat.2008.04.009

Pezo, R. F. (1993). A general method of reporting resilient modulus tests of soils, a pavement engineer's point of view. (Ed.),^(Eds.). 72nd Annual Meeting of the TRB.

Poon, C. S., Qiao, X. C., & Chan, D. X. (2006). The cause and influence of self-cementing properties of fine recycled concrete aggregates on the properties of unbound sub-base. *Waste Manage.*, *26*(10), 1166-1172. https://doi.org/10.1016/j.wasman.2005.12.013

Poon, C. S., Shui, Z. H., Lam, L., Fok, H., & Kou, S. C. (2004). Influence of moisture states of natural and recycled aggregates on the slump and compressive strength of concrete. *Cem. Concr. Res.*, *34*(1), 31-36. https://doi.org/10.1016/s0008-8846(03)00186-8

Prosek, Z., Trejbal, J., Nezerka, V., Golias, V., Faltus, M., & Tesarek, P. (2020). Recovery of residual anhydrous clinker in finely ground recycled concrete. *Resources Conservation and Recycling*, *155*, Article 104640. https://doi.org/10.1016/j.resconrec.2019.104640

Qoku, E., Bier, T. A., & Westphal, T. (2017). Phase assemblage in ettringite-forming cement pastes: A X-ray diffraction and thermal analysis characterization. *J. Build. Eng.*, *12*, 37-50. https://doi.org/10.1016/j.jobe.2017.05.005

Rabbi, A. M. Z., Kuwano, J., Deng, J. L., & Boon, T. W. (2011). Effect of curing stress and period on the mechanical properties of cement-mixed sand. *Soils Found.*, *51*(4), 651-661. https://doi.org/10.3208/sandf.51.651

Rajasekaran, G. (2005). Sulphate attack and ettringite formation in the lime and cement stabilized marine clays. *Ocean Eng.*, *32*(8-9), 1133-1159. https://doi.org/10.1016/j.oceaneng.2004.08.012

Ramachandran, V. S., Paroli, R. M., Beaudoin, J. J., & Delgado, A. H. (2002). *Handbook of thermal analysis of construction materials*. William Andrew.

Rios, S., Cristelo, N., da Fonseca, A. V., & Ferreira, C. (2017). Stiffness Behavior of Soil Stabilized with Alkali-Activated Fly Ash from Small to Large Strains. *International Journal of Geomechanics*, *17*(3), Article 04016087. https://doi.org/10.1061/(asce)gm.1943-5622.0000783

Rios, S., da Fonseca, A. V., & Baudet, B. A. (2014). On the shearing behaviour of an artificially cemented soil. *Acta Geotech.*, *9*(2), 215-226. https://doi.org/10.1007/s11440-013-0242-7

Rudman, C. (2019). *Aspects of self-cementation of recycled concrete aggregate when applied in roads*, Stellenbosch University].

Saberian, M., Li, J., Nguyen, B., & Wang, G. (2018). Permanent deformation behaviour of pavement base and subbase containing recycle concrete aggregate, coarse and fine crumb rubber. *Constr. Build. Mater.*, *178*, 51-58. https://doi.org/10.1016/j.conbuildmat.2018.05.107

Schnaid, F., Prietto, P. D. M., & Consoli, N. C. (2001). Characterization of cemented sand in triaxial compression. *J. Geotech. Geoenviron. Eng.*, *127*(10), 857-868. https://doi.org/10.1061/(asce)1090-0241(2001)127:10(857)

Seed, H., Mitry, F., Monismith, C., & Chan, C. (1967). Prediction of flexible pavement deflections from laboratory repeated-load tests. *NCHRP report*(35).

Selvam, M., Debbarma, S., Singh, S., & Shi, X. J. (2022). Utilization of alternative aggregates for roller compacted concrete pavements - A state-of-the-art review. *Constr. Build. Mater.*, *317*, Article 125838. https://doi.org/10.1016/j.conbuildmat.2021.125838

Senanayake, M., Arulrajah, A., Maghool, F., & Horpibulsuk, S. (2022). Evaluation of rutting resistance and geotechnical properties of cement stabilized recycled glass, brick and concrete triple blends. *Transp. Geotech.*, *34*, Article 100755. https://doi.org/10.1016/j.trgeo.2022.100755

Shi, C. J., Wu, Z. M., Xiao, J. F., Wang, D. H., Huang, Z. Y., & Fang, Z. (2015). A review on ultra high performance concrete: Part I. Raw materials and mixture design. *Constr. Build. Mater.*, *101*, 741-751. https://doi.org/10.1016/j.conbuildmat.2015.10.088

Sobhan, K., Gonzalez, L., & Reddy, D. V. (2016). Durability of a pavement foundation made from recycled aggregate concrete subjected to cyclic wet-dry exposure and fatigue loading. *Mater. Struct.*, *49*(6), 2271-2284. https://doi.org/10.1617/s11527-015-0648-9

Solanki, P., Zaman, M. M., & Dean, J. (2010). Resilient Modulus of Clay Subgrades Stabilized with Lime, Class C Fly Ash, and Cement Kiln Dust for Pavement Design. *Transp. Res. Rec.*(2186), 101-110. https://doi.org/10.3141/2186-11

Soleimanbeigi, A., Shedivy, R. F., Tinjum, J. M., & Edil, T. B. (2015). Climatic effect on resilient modulus of recycled unbound aggregates. *Road Mater. Pavement Des.*, *16*(4), 836-853. https://doi.org/10.1080/14680629.2015.1060250

Soliman, H., & Shalaby, A. (2015). Permanent deformation behavior of unbound granular base materials with varying moisture and fines content. *Transp. Geotech.*, *4*, 1-12. https://doi.org/10.1016/j.trgeo.2015.06.001

Solyman, M. (2005). *Classification of recycled sands and their applications as fine aggregates for concrete and bituminous mixtures*].

Stolle, D., Guo, P. J., & Liu, Y. (2009). Resilient modulus properties of granular highway materials. *Canadian Journal of Civil Engineering*, *36*(4), 639-654. https://doi.org/10.1139/l08-141

Su, Y., Cui, Y.-J., Dupla, J.-C., & Canou, J. (2022a). Effect of water content on permanent deformation of fine/coarse soil mixtures with varying coarse grain contents and subjected to multi-stage cyclic loading. *Acta Geotech.*, 1-10.

Su, Y., Cui, Y. J., Dupla, J. C., & Canou, J. (2020). Investigation of the effect of water content on the mechanical behavior of track-bed materials under various coarse grain contents. *Constr. Build. Mater.*, *263*, Article 120206. https://doi.org/10.1016/j.conbuildmat.2020.120206

Su, Y., Cui, Y. J., Dupla, J. C., & Canou, J. (2021). Effect of water content on resilient modulus and damping ratio of fine/coarse soil mixtures with varying coarse grain contents. *Transp. Geotech.*, *26*, Article 100452. https://doi.org/10.1016/j.trgeo.2020.100452

Su, Y., Cui, Y. J., Dupla, J. C., & Canou, J. (2022b). Soil-water retention behaviour of fine/coarse soil mixture with varying coarse grain contents and fine soil dry densities. *Canadian Geotechnical Journal*, *59*(2), 291-299. https://doi.org/10.1139/cgj-2021-0054

Su, Y., Cui, Y. J., Dupla, J. C., Canou, J., & Qi, S. (2021). Developing a Sample Preparation Approach to Study the Mechanical Behavior of Unsaturated Fine/Coarse Soil Mixture. *Geotechnical Testing Journal*, *44*(4), 912-928. https://doi.org/10.1520/gtj20190450

Sweere, G. T. (1992). *Unbound granular bases for roads*, Delft University of Technology].

Tam, V. W. Y., Gao, X. F., Tam, C. M., & Chan, C. H. (2008). New approach in measuring water absorption of recycled aggregates. *Constr. Build. Mater.*, *22*(3), 364-369. https://doi.org/10.1016/j.conbuildmat.2006.08.009

Tam, W., & Brown, S. (1988). Use of the falling weight deflectometer for insitu evaluation of granular materials in pavements. (Ed.),^(Eds.). Australian Road Research Board (ARRB) Conference, 14th, 1988, Canberra.

Taylor, H. F. (1997). *Cement chemistry* (Vol. 2). Thomas Telford London.

Tegguer, A. D. (2012). Determining the water absorption of recycled aggregates utilizing hydrostatic weighing approach. *Constr. Build. Mater.*, *27*(1), 112-116. https://doi.org/10.1016/j.conbuildmat.2011.08.018

Terzis, D., & Laloui, L. (2019). A decade of progress and turning points in the understanding of bio-improved soils: A review. *Geomechanics for Energy and the Environment*, *19*. https://doi.org/10.1016/j.gete.2019.03.001

Thom, N., & Brown, S. (1988). The effect of grading and density on the mechanical properties of a crushed dolomitic limestone. (Ed.),^(Eds.). Australian Road Research Board (ARRB) Conference, 14th, 1988, Canberra.

Thom, N., & Brown, S. F. (1987). *Effect of moisture on the structural performance of a crushed-limestone road base*.

Trinh, V. N., Tang, A. M., Cui, Y.-J., Dupla, J.-C., Canou, J., Calon, N., Lambert, L., Robinet, A., & Schoen, O. (2012). Mechanical characterisation of the fouled ballast in ancient railway track substructure by large-scale triaxial tests. *Soils foundations*, *52*(3), 511-523.

Trollope, D. H., Lee, I., & Morris, J. (1962). Stresses and deformation in two layer pavement structures under slow repeated loading. (Ed.),^(Eds.). Australian Road Research Board (ARRB) Conference, 1st, 1962, Canberra.

Tutumluer, E., & Pan, T. Y. (2008). Aggregate morphology affecting strength and permanent deformation behavior of unbound aggregate materials. *J. Mater. Civ. Eng.*, *20*(9), 617-627. https://doi.org/10.1061/(asce)0899-1561(2008)20:9(617)

UNICEM IDF. (2003). *Guide technique pour l'utilisation des materiaux regionaux d'Île-de-France*. http://materrio.construction/mediatheque/media/22-_IDF_Betons_produits_demol(2).pdf.

Uzan, J. (1985). Characterization of granular material. *Transp. Res. Rec.*, *1022*(1), 52-59.

Van Niekerk, A. A. (2002). *Mechanical behavior and performance of granular bases and sub-bases in pavements*, Delft University of Technology].

Vranna, A., & Tika, T. (2020). Undrained Monotonic and Cyclic Response of Weakly Cemented Sand. *J. Geotech. Geoenviron. Eng.*, *146*(5), Article 04020018. https://doi.org/10.1061/(asce)gt.1943-5606.0002246

Wang, C., Chazallon, C., Hornych, P., & Braymand, S. (2022). Permanent and resilient deformation behaviour of recycled concrete aggregates from different sources, in pavement base and subbase. *Road Mater. Pavement Des.* https://doi.org/10.1080/14680629.2022.2134048

Wang, J. J., Mu, M. L., & Liu, Y. L. (2018). Recycled cement. *Constr. Build. Mater.*, *190*, 1124-1132. https://doi.org/10.1016/j.conbuildmat.2018.09.181

Wang, Y. H., Hung, T., Zhao, K. C., & Sheng, Y. (2016, Jul 16-18). Re-cementation of Recycled Concrete Aggregate in Pavement Base or Sub-base. (Ed.),^(Eds.). 1st International Conference on Transportation Infrastructure and Materials (ICTIM), Xian, PEOPLES R CHINA.

Wang, Y. H., & Leung, S. C. (2008). Characterization of cemented sand by experimental and numerical investigations. *J. Geotech. Geoenviron. Eng.*, *134*(7), 992-1004. https://doi.org/10.1061/(asce)1090-0241(2008)134:7(992)

Werkmeister, S., Dawson, A. R., & Wellner, F. (2001). Permanent deformation behavior of granular materials and the shakedown concept. *Transp. Res. Rec.*, *1757*(1), 75-81.

Xiao, Y. J., Zheng, K. Y., Chen, L. X., & Mao, J. F. (2018). Shakedown analysis of cyclic plastic deformation characteristics of unbound granular materials under moving wheel loads. *Constr. Build. Mater.*, *167*, 457-472. https://doi.org/10.1016/j.conbuildmat.2018.02.064

Xiu, Z. G., Wang, S. H., Ji, Y. C., Wang, F. L., Ren, F. Y., & Wang, P. Y. (2021). An analytical model for the triaxial compressive Stress-strain relationships of Cemented Pasted Backfill (CPB) with different curing time. *Constr. Build. Mater.*, *313*, Article 125554. https://doi.org/10.1016/j.conbuildmat.2021.125554

Yaghoubi, E., Disfani, M. M., Arulrajah, A., & Kodikara, J. (2018). Impact of compaction method on mechanical characteristics of unbound granular recycled materials. *Road Mater. Pavement Des.*, *19*(4), 912-934. https://doi.org/10.1080/14680629.2017.1283354

Yang, S. R., Huang, W. H., & Liao, C. C. (2008). Correlation Between Resilient Modulus and Plastic Deformation for Cohesive Subgrade Soil Under Repeated Loading. *Transp. Res. Rec.*(2053), 72-79. https://doi.org/10.3141/2053-09

Zadeh, A. H., Mamirov, M., Kim, S., & Hu, J. (2021). CO2-treatment of recycled concrete aggregates to improve mechanical and environmental properties for unbound applications. *Constr. Build. Mater.*, *275*, Article 122180. https://doi.org/10.1016/j.conbuildmat.2020.122180

Zega, C. J., Villagran-Zaccardi, Y. A., & Di Maio, A. A. (2010). Effect of natural coarse aggregate type on the physical and mechanical properties of recycled coarse aggregates. *Mater. Struct.*, *43*(1-2), 195-202. https://doi.org/10.1617/s11527-009-9480-4

Zhang, L. M., & Li, X. (2010). Microporosity Structure of Coarse Granular Soils. *J. Geotech. Geoenviron. Eng.*, *136*(10), 1425-1436. https://doi.org/10.1061/(asce)gt.1943-5606.0000348

Zhao, Z. (2014). *Valorisation des sables de béton recyclé pour la fabrication de mortiers*, Ecole des mines de Douai et l'université Lille 1].

Zhao, Z., Remond, S., Damidot, D., & Xu, W. (2013). Influence of hardened cement paste content on the water absorption of fine recycled concrete aggregates. *Journal of Sustainable Cement-Based Materials*, *2*(3-4), 186-203.

Étude des propriétés de prise et du comportement mécanique des granulats de béton recyclé

Doctorant: Chong WANG

Directeur de Thèse: Cyrille CHAZALLON

Co-directeur de Thèse: Pierre HORNYCH

Laboratoire: Laboratoire des sciences de l'ingénieur, de l'informatique et de l'imagerie (ICube, UMR 7357, CNRS), INSA de Strasbourg, 67084, Strasbourg Cedex, France

Résumé

La réutilisation des agrégats de béton recyclé (RCA) en remplacement des agrégats naturels (NA) dans les couches de base et de fondation des chaussées est devenue plus populaire ces dernières années. Parfois, une croissance de la rigidité et de la résistance dans les couches de base et de fondation non liées construites avec RCA peut être observée, ce qui est connu sous le nom de propriétés de prise résiduelle des RCA. Cependant, les propriétés de prise résiduelle et le comportement mécanique des RCA ne sont toujours pas étayés par les données d'essai. Cette thèse présente une étude sur les propriétés de la prise résiduelle, la microstructure et le comportement mécanique des RCA sous essai triaxial monotone et à charge répétée.

Les propriétés de prise résiduelle sont évaluées par mesure de la valeur du pH et essais calorimétriques. Les résultats montrent que les NRCA présentent de fortes propriétés de prise résiduelle alors que celles des ORCA et des RCAP sont négligeables. La valeur du pH et la chaleur libérée des NRCA (13.07 et 14.7 J, respectivement) sont beaucoup plus élevées que celles des ORCA (10.53 et 1.97 J) et des RCAP (9.48). En outre, pour calculer la teneur en ciment non hydraté des RCA, principale cause des propriétés de prise résiduelle, une méthode

de calcul a été proposée sur la base de l'analyse thermogravimétrique (TGA). Les résultats montrent que la teneur potentielle en ciment non hydraté des granulats fins de NRCA (0-2 mm) se situe entre 6.2% and 7.9%. Après séchage pendant 360 jours, entre 55% et 70% du liant non hydraté total (4.3%) ont été hydratés, et cette hydratation semble être arrêtée après le durcissement pendant 360 jours. Cependant, la formation d'ettringite, produits d'attaque de sulfate, a été observée entre le durcissement pendant 360 jours et 720 jours, ce qui pourrait également conduire aux propriétés autocimentantes de RCA.

L'amélioration de la microstructure des RCA due aux propriétés de prise résiduelle a été étudiée par analyse microscopique électronique à balayage (SEM) et porosimétrie d'intrusion de mercure (MIP). Les résultats montrent que les produits d'hydratation non seulement forment des liaisons entre les particules, mais remplissent également les petits macro-pores entre les particules (rayon supérieur à 1 μm et inférieur à 20 μm). Alors que pour les grands macro-pores (rayon supérieur à 20 μm), l'effet de remplissage est limité. En conséquence, le taux moyen de vide mesuré avec un essai MIP (intrusion porosimétrique au mercure) diminue de 0.43 (durcissement 1 jour) à 0.26 (durcissement 360 jours). La diminution du nombre de macropores améliore également l'uniformité de l'échantillon RCA. Le type de structure ouverte (durcissement 1 jour) se transforme en structure rigide et serrée après 360 jours de murissement.

Les effets des propriétés de prise résiduelle sur la déformation permanente et le comportement résilient des RCA ont été étudiés par des essais triaxiaux à chargements répétés. Les résultats indiquent que la déformation permanente des NRCA, avec de fortes propriétés de prise résiduelle, diminue rapidement après 180 jours de murissement, puis atteint une valeur constante et très faible. En ce qui concerne le comportement résilient, le module de résilience des NRCA augmente, tandis que ε_q^r et ε_v^r diminuent avec l'augmentation du temps de murissement. En outre, les évolutions de ε_q^r et ε_v^r, avec la pression p de confinement, deviennent également linéaires et dépendent moins de l'état de contrainte, et le paramètre d'anisotropie s'est légèrement amélioré (matériau moins anisotrope). Après un durcissement de 720 jours, la classification des NRCA peut être améliorée de C2 à C1, ce qui peut être utilisé dans les chaussées ayant les meilleurs performances. Alors que pour ORCA, les propriétés de prise résiduelle sont négligeables et n'ont aucune influence sur la déformation permanente et la déformation résiliente.

En outre, la déformation permanente et le comportement résilient des RCA obtenus à partir de différentes sources ont également été étudiés. Les résultats montrent que les RCA avec de grandes quantités de particules arrondies et une faible résistance du béton parent (RCAP) peut

entraîner de mauvaises propriétés mécaniques: indiquées par les déformations permanentes plus grandes, la vitesse de déformation permanente, la déformation déviatoire résiliente ε_q^r et la déformation volumétrique ε_v^r, tout en réduisant le module de résilience, et ne convient donc pas à une utilisation dans les couches de chaussée. En outre, les matériaux RCA (à l'exception du RCA avec une grande quantité de particules arrondies) sont généralement plus dépendants des contraintes que la plupart des UGM, ce qui peut être attribué à la forte angularité et rugosité des agrégats RCA.

L'effet des propriétés de prise résiduelle sur le comportement au cisaillement des RCA a été étudié par essai triaxial monotone. Les résultats montrent que la contrainte déviatoire maximale q_{max}, le module sécant E_{50} et la cohésion des RCA augmentent avec le temps de murissement. Cet effet croissant avec le temps est influencé par les propriétés de prise résiduelle des RCA (NRCA > ORCA) et la pression de confinement (effet sous faible pression de confinement > effet sous pression de confinement élevée).

s

Mots-clés: granulats de béton recyclé, matériaux granulaires non liés, propriétés autocimentantes, essai triaxial à charge répétée, déformation permanente, déformation résiliente, essai triaxial monotone, microstructure.

Abstract

The reuse of recycled concrete aggregates (RCA) as a substitution to natural aggregates (NA) in pavement base and subbase layers has become more popular in recent years. Occasionally, a growth of stiffness and strength in unbound base and subbase layers built with RCA can be observed, which is known as self-cementing properties of RCA. However, the self-cementing properties and mechanical behaviour of RCA still lack the support of test data. This dissertation presents an investigation on self-cementing properties, microstructure and mechanical behaviour of RCA under monotonic and repeated load triaxial tests.

The self-cementing properties of RCA were evaluated by pH value measurement and calorimeter tests. Results show that NRCA exhibits strong self-cementing properties while those of ORCA and RCAP are negligible. The pH value and released heat of NRCA (13.07 and 14.7 J, respectively) is much higher than those of ORCA (10.53 and 1.97 J) and RCAP (9.48). Besides, to calculate unhydrated cement content of RCA, the cause of self-cementing properties, a calculation method was proposed based on the thermogravimetric analysis (TGA). Results show that the potential unhydrated cement content of NRCA fine aggregates (0-2 mm) is between 6.2% and 7.9%. After curing for 360 days, between 55% to 70% of the total unhydrated binder (4.3%) were hydrated, and this hydration appears to be stopped after curing for 360 days. However, the formation of ettringite, sulfate attack products, was observed between curing for 360 days and 720 days, which could also lead to the self-cementing properties of RCA.

The improvement of RCA microstructure due to self-cementing properties was studied by scanning electron microscopic analysis (SEM) and mercury intrusion porosimetry (MIP) tests. Results show that the hydration products not only form bonds between bonds, but also fill the small macro-pores between particles (radius above 1 μm and less than 20 μm). While for big macro-pores (radius larger than 20 μm), the filling effect is limited. As a result, the average intrusion void ratio decreases from 0.43 (curing 1 day) to 0.26 (curing 360 days). The decreased number of macro-pores also improve the uniformity of RCA specimen. The open type of structure (curing 1 day) turns to rigid tight skeleton structure after curing 360 days.

The effect of self-cementing properties on the permanent deformation and resilient deformation behaviour of RCA was also investigated by repeated load triaxial tests. Results indicate that the permanent deformation of NRCA, with strong self-cementing properties, decreases quickly after curing 180 days, then reaches a constant and very low value. As for the resilient deformation behaviour, the resilient modulus of NRCA increases, while ε_q^r and ε_v^r decrease

with increasing curing time. Besides, ε_q^r and ε_v^r evolution with pressure also become more linear and less dependent on the stress level, and anisotropy behavior is slightly improved. After curing 720 days, the ranking of NRCA can be improved from C2 to C1, which can be used in high-level pavement. While for ORCA, the negligible self-cementing properties have no influence on the permanent deformation and resilient deformation.

Besides, the permanent deformation and resilient deformation behaviour of RCA obtained from different sources were also studied. The results show that RCA with high amounts of rounded particles and low strength of parent concrete (RCAP) can lead to poor mechanical properties: indicated by the larger permanent strains, permanent strain rate, resilient deviatoric strain ε_q^r and volumetric strain ε_v^r, while lower resilient modulus, and thus is not suitable for use in pavement layers. Besides, RCA materials (except RCA with high amount of rounded particles) is generally more stress dependent than most of UGM, which can be attributed to the high angularity and roughness of RCA aggregates.

The effect of self-cementing properties on the shear behaviour of RCA was studied by monotonic triaxial test. The results show that the peak deviatoric stress q_{max}, secant modulus E_{50} and cohesion of RCA increase with curing time. This increasing effect is influenced by self-cementing properties of RCA (NRCA>ORCA) and confining pressure (larger influence with low confining pressure compared to high confining pressure).

Keywords: recycled concrete aggregates, unbound granular materials, self-cementing properties, repeated load triaxial test, permanent deformation, resilient deformation, monotonic triaxial test, microstructure.

List of publications

Journal papers:

1. Wang, C., Chazallon, C., Hornych, P., & Braymand, S. (2022). Permanent and resilient deformation behaviour of recycled concrete aggregates from different sources, in pavement base and subbase. Road Materials and Pavement Design, 1-18.

2. Wang, C., Chazallon, C., Braymand, S., & Hornych, P. (2023). Influence of self-cementing properties on the mechanical behaviour of recycled concrete aggregates under monotonic loading. Construction and Building Materials, 367, 130259.

3. Wang, C., Chazallon, C., Braymand, S., & Hornych, P. (2023). Investigation of self-cementation of recycled concrete aggregates used in unbound pavement layers. Under review in Journal of Materials in Civil Engineering.

4. Wang, C., Chazallon, C., Hornych, P., & Jing P. (2023). Effect of self-cementing properties on the mechanical behaviour of recycled concrete aggregates in unbound pavement layers. Under review in Transportation Geotechnics.

5. Wang, C., Chazallon, C., Hornych, P., & Jing P. (2023). Effect of self-cementing properties on the resilient behaviour of recycled concrete aggregates used in base and subbase. Plan to submit to Road Materials and Pavement Design.

6. Wang, C., Chazallon, C., Hornych, P., & Jing P. (2023). Long-term performance of recycled concrete aggregates in unbound layer under cyclic loading. Plan to submit to Construction and Building Materials.

Conference papers:

1. Wang, C., Chazallon, C., Mouhoubi, S., Hornych, P., & Jing, P. (2022). Study of the mechanical behaviour and self-cementing properties of recycled crushed concrete aggregates. In Eleventh International Conference on the Bearing Capacity of Roads, Railways and Airfields, Volume 3 (pp. 398-406).

2. Wang, C., Chazallon, C., Hornych, P., Jing, P., & Mouhoubi, S. (2023). Study of mechanical behavior and self-cementing properties of recycled concrete aggregates under repeated loading. The 13th International Conference on Road and Airfield Pavement Technology (accepted).

APPENDIX A. Mathematical expressions for permanent deformation

Table A. 1 Mathematical expressions for permanent deformation.

Expression	Eq.	Reference
$\varepsilon_1^{\,p} = a + b\log(N)$	(1)	(Barksdale, 1972)
$\frac{\varepsilon_1^{\,p}}{N} = A \times N^{-b}$	(2)	(Khedr, 1985)
$\log(\varepsilon_1^{\,p}(N) = a + b\log(N)$	(3)	(Sweere, 1992)
$\varepsilon_1^{\,p} = A(1-(\frac{N}{N_0})^B)$	(4)	(Hornych, 1993)
$\varepsilon_1^{\,p} = f(N) \bullet g(p_{\max}, q_{\max})$ $g(p_{\max}, q_{\max}) = \varepsilon_1^{\,p_0} \bullet \left(\frac{L_{\max}}{p_a}\right)^n \bullet \frac{1}{m + \frac{s_b}{p_{\max}} - \frac{q_{\max}}{p_{\max}}}$	(5)	(Gidel et al., 2001)
$\varepsilon_1^{\,p} = f(N) \bullet t(w, \Delta q_{\max})$ $t(w, \Delta q_{\max}) = \varepsilon_1^{\,p_0}(w+a)(\frac{\Delta q_{\max}}{p_a})^{\alpha}$	(6)	(Trinh et al., 2012)

$\varepsilon_1^{\,p}$	= permanent deformation	N	= number of load cycles
A, B, a, b, $\varepsilon_1^{\,p0}$, α	= regression parameters	N_0	= number of cycles before the first measurement
f(N)	= Hornych model (Eq. (4))	*m, s_b*	= parameters of failure line
p_a	= atmospheric pressure (100 kPa)	p_{max}, q_{max}	= maximum mean stress and the maximum deviator stress
L_{max}	$= \sqrt{p_{\max}^{\,2} + q_{\max}^{\,2}}$	*w*	= water content

APPENDIX B. Mathematical expressions for resilient deformation

Table B. 1 Mathematical expressions for resilient modulus.

Expression	Eq.	Reference
$M_r = k_1\sigma_3^{k_2}$ <or> $M_r = k_1(\frac{\sigma_3^{k_2}}{p_a})$	(1)	Dunlap (1963)
$M_r = k_1(\frac{\theta}{p_a})^{k_2}$ <or> $M_r = k_1\theta^{k_2}$	(2)	Seed et al. (1967)
$M_r = k_1\left(\frac{\theta}{p_a}\right)^{k_2}\left(\frac{q}{p_a}\right)^{k_3}$ <or> $M_r = k_1\left(\frac{\theta}{p_a}\right)^{k_2}\left(\frac{\tau_{oct}}{p_a}\right)^{k_3}$	(3)	Uzan (1985)
$M_r = k_1\left(\frac{J_2}{\tau_{oct}}\right)^{k_2}$	(4)	Johnson et al. (1986)
$M_r = k_1\left(\frac{p}{q}\right)^{k_2}$	(5)	Tam and Brown (1988)
$M_r = k_1\frac{\theta^{k_2}}{10^{A_1}}$	(6)	Elliott and David (1989)
$M_r = k_1 q^{k_2}\sigma_3^{k_3}$	(7)	Pezo (1993)

M_r	= resilient modulus	τ_{oct}	= octahedral shear stress = $(2^{0.5}/3)q$
σ_3	= confining pressure	p_a	= atmospheric pressure (100 kPa)
q	= deviatoric stress = $\sigma_1-\sigma_3$	k_1, k_2 and k_3	= model parameters
p	= mean normal stress =$(\sigma_1+2\sigma_3)/3$	J_2	= first stress invariant = $\sigma_1\sigma_2+\sigma_2\sigma_3+\sigma_3\sigma_1$
θ	= bulk stress=$3p$	A_1	= mR^3

Table B. 2 Mathematical expressions for volumetric and deviatoric strain.

Expression	Eq.	Reference
$\begin{cases} \varepsilon_v = \dfrac{p^n}{K_a}\left[1+\dfrac{(n-1)\bullet K_a}{6G_a}\left(\dfrac{q}{p}\right)^2\right] \\ \varepsilon_q = \dfrac{p^n}{3G_a}\bullet\dfrac{q}{p} \end{cases}$	(1)	Boyce (1980)
$\begin{cases} \varepsilon_v = \delta\left[\left(\dfrac{p}{A}\right)^B\left(1-C\left(\dfrac{q}{p}\right)^2\right)\right] \\ \varepsilon_q = D\delta\left[\dfrac{q}{p+E}\right]\left[\dfrac{\sqrt{p_r{}^2+q_r{}^2}}{p_m}\right]^F \end{cases}$	(2)	Brown and Pappin (1985)
$\begin{cases} \varepsilon_v = p^A\dfrac{1}{K_1}\left(1-C\dfrac{q^2}{p^2}\right) \\ \varepsilon_q = p^B\dfrac{1}{3G_1}\left(\dfrac{q}{p}\right) \end{cases}$	(3)	Mayhew (1983)
$\begin{cases} \varepsilon_v = A\left(\delta\ln p\right)^B\left(\delta p\right)^C - D\left[\delta\left(\ln\dfrac{\sigma_1}{\sigma_3}\right)^2\right]^E \\ \varepsilon_q = E\left[\delta\left(\ln\dfrac{\sigma_1}{\sigma_3}\right)^2\right]^F\left(\delta\tau+\dfrac{\delta S}{3}\right)^G \end{cases}$	(4)	Thom and Brown (1988)
$\begin{cases} \varepsilon_v = p_a{}^{1-B}p^B\left[\dfrac{1}{A}-\dfrac{(1-B)}{6C}\left(\dfrac{q}{p}\right)^2-\dfrac{B}{D}\left(\dfrac{q}{p}\right)\right] \\ \varepsilon_q = p_a{}^{1-B}p^B\left[\dfrac{1}{3C}\left(\dfrac{q}{p}\right)-\dfrac{1}{D}\right] \end{cases}$	(5)	El Hannani (1991)
$\begin{cases} \varepsilon_v = \dfrac{p^{*n}}{p_a{}^{n-1}}\left[\dfrac{\gamma+2}{3K_a}+\dfrac{n-1}{18G_a}(\gamma+2)\left(\dfrac{q^*}{p^*}\right)^2+\dfrac{\gamma-1}{3G_a}*\dfrac{q^*}{p^*}\right] \\ \varepsilon_q = \dfrac{2}{3}*\dfrac{p^{*n}}{p_a{}^{n-1}}\left[\dfrac{\gamma-1}{3K_a}+\dfrac{n-1}{18G_a}(\gamma-1)\left(\dfrac{q^*}{p^*}\right)^2+\dfrac{2\gamma+1}{6G_a}*\dfrac{q^*}{p^*}\right] \end{cases}$	(6)	Hornych et al. (1998)

σ_1, σ_2 and σ_3 = principal stresses | δ = change in

q	= deviatoric stress	p	= mean normal stress
p_r	= p_{max} - p_{min}	q_r	= q_{max} - q_{min}
τ	= shear stress in Mohr circle	S	= normal stress in Mohr circle
p^*	= $(\gamma\sigma_1 + 2\sigma_3)/3$	q^*	= $\gamma\sigma_1 - \sigma_3$
A-G, K_1, G_1, K_a, G_a, γ, n	= model parameters		

Chong WANG

Étude des propriétés de prise et du comportement mécanique des granulats de béton recyclé

Résumé

1000 caractères maximum

La réutilisation des agrégats de béton recyclé (RCA) en remplacement des agrégats naturels (NA) dans les couches de base et de fondation des chaussées est devenue plus populaire ces dernières années. Parfois, une croissance de la rigidité et de la résistance dans les couches de base et de fondation non liées construites avec RCA peut être observée, ce qui est connu sous le nom de propriétés de prise résiduelle des RCA. Cependant, les propriétés de prise résiduelle et le comportement mécanique des RCA ne sont toujours pas étayés par les données d'essai. Cette thèse présente une étude sur les propriétés de la prise résiduelle, la microstructure et le comportement mécanique des RCA sous essai triaxial monotone et à charge répétée.

Mots clés :

granulats de béton recyclé, matériaux granulaires non liés, propriétés autocimentantes, essai triaxial à charge répétée, déformation permanente, déformation résiliente, essai triaxial monotone, microstructure.

Résumé en anglais

The reuse of recycled concrete aggregates (RCA) as a substitution to natural aggregates (NA) in pavement base and subbase layers has become more popular in recent years. Occasionally, a growth of stiffness and strength in unbound base and subbase layers built with RCA can be observed, which is known as self-cementing properties of RCA. However, the self-cementing properties and mechanical behaviour of RCA still lack the support of test data. This dissertation presents an investigation on self-cementing properties, microstructure and mechanical behaviour of RCA under monotonic and repeated load triaxial tests.

Keywords :

recycled concrete aggregates, unbound granular materials, self-cementing properties, repeated load triaxial test, permanent deformation, resilient deformation, monotonic triaxial test, microstructure.